HYDRAULIC INTERACTION BETWEEN THE ABOVE AND BELOW GROUND DRAINAGE SYSTEMS VIA GULLY INLETS

A thesis submitted in part fulfilment of the requirements for the degree of Doctor of Philosophy

By Nuridah Sabtu

The University of Sheffield

Department of Civil and Structural Engineering

March 2015

ACKNOWLEDGEMENT

My utmost gratitude goes to Professor Adrian Saul, for whom without his supervision and tutelage, this would not have been possible. Much appreciation also goes to Darren Unwin and Gavin Sailor for ideas and help in bringing about the laboratory design and the accumulation of data.

To my family – my pillar of strength, for their unconditional love, unwavering faith and constant support throughout the completion of the study. Many thanks to friends and colleagues, who have been supportive and comforting throughout the years.

Also to a special group of people, who are very dear to me, for never failing to provide comfort and laughter through the years.

Special acknowledgement also goes to our collaborators on the FRMRC project, from the University of Exeter.

Finally, to the Malaysian Government namely the Ministry of Higher Education of Malaysia and the University of Science, Malaysia (USM) for the given opportunity and monetary support.

Thank you.

ABSTRACT

The primary objective of this study was to complete an experimental programme to better understand the hydraulic performance of typical individual types of gully inlets and systems used in practice by analysing the interaction of flow into and from typical gully systems by determining the head-discharge relationship of each system. Therefore, a full scale laboratory system comprising of a testing platform with an inlet tank and an outlet tank on both ends of the platform has been designed to mimic the hydraulic interaction between the above and below ground drainage system via gully inlets and the designated catchment area. Longitudinal slope was later incorporated onto the initially flat testing platform to represent different road conditions. Tests were completed with the flow in one direction to the gulley (intermediate tests) and from both tanks such that the flow to the gulley is in two directions (terminal tests). Surcharged condition was also tested where two flows were released into the system – a primary flow coming from the primary inlet and a secondary flow coming from an alternative inlet straight into the gully system itself. A gully pot manufactured by Milton Precast with a diameter of 375mm and 750mm nominal depth was used for this study and was tested over a range of flowrates of 0 – 50 *l/s*. Another variable studied was two different longitudinal slopes (S_L). Two different types of grates with BS EN 124 loading class of C250 representing different hydraulic characteristics were also used and were tested for a range of surcharged and non-surcharged flow conditions. The interaction – expressed in terms of head-discharge relationship, was determined for the different gully systems and flow conditions tested. Based on the head-discharge relationship, a range of coefficient of discharge, C_d was established. C_d is known to be a function of many parameters and hence to examine how C_d changes, a dimensional analysis approach has been used. This is followed by a review of the application of different types of equations in an attempt to link the dimensionless terms and hence define a universal equation that describes the performance of the system for a range of conditions. This analysis has resulted in a number of significant findings, which have formed the conclusions to the thesis and may be used to inform the way in which these coefficients are represented in water industry standard software.

CONTENTS

CHAPTER 3

CHAPTER 4

CHAPTER 6

LIST OF FIGURES

LIST OF TABLES

LIST OF EQUATIONS

NOMENCLATURE AND ABBREVIATIONS

η	grating efficiency
ξ	effective weir length
ρ	density
ν	kinematic viscosity
γ	surface tension
2minM5	rainfall depth (mm) occurring at the site in a period of 2 minutes with an average return period of 5 years
A	total grating area used
A_a	actual area
A_{dr}	area of the road drained by an intermediate gully for a rainfall intensity of 50mm/h,
A_w	total waterway area of the grates
AP	all-purpose
ARI	average recurrence interval
ASHCC	Allowable Street Hydraulic Conveyance Capacity
A, B	characteristic parameters related to the grate geometry
B	permitted width of kerb flow
B_o	Bond number
BOD	Biological Oxygen Demand
BS	British Standard
C_d	Coefficient of discharge
CFD	Computational Fluid Dynamics
CPU	Central Processing Unit
d	water depth by the kerb (m)
d_{50}	aggregate size (medium diameter 50 mm)
D	gully spacing
DEM	Digital Elevation Model
DMRB	Design Manual for Road and Bridges
E	grate depth
F_r	Froude number

FRMRC	Flood Risk Management Research Consortium
g	gravitational velocity, 9.82 ms^{-2}
G_d	grating parameter
GIS	Geographic Information System
H	water depth against the kerb/Head of water
h	average head of the weir
h_D	downstream water level
h_G	water level in the gully
h_U	upstream water level
i (subscript)	lateral street slope (m/m)
I	design rainfall intensity
K	Submergence coefficient
k_n	roughness and grating efficiency factor
K_r	grating coefficient
L	length
LAN	Local Area Network
m	maintenance factor
MLE	Multiple Linking Element
n	Manning's coefficient
PAC	Programmable Automation Controller
Q	flowrate (m^3/s),
Q_a	approaching flow (m^3/s)
Q_b	bypass flow (m^3/s)
$Q_{int/}$ Q_i	intercepted flow
QUDM	Queensland Urban Drainage Manual
R^2	coefficient of determination/ correlation coefficient
R_e	Reynolds number
S	road gradient
S_c	crossfall
S_L	longitudinal slope
S_p	design spacing
SHCC	Street Hydraulic Conveyance Capacity

SLE	Single-Linking-Element
T	critical storm duration
t_s	time taken for water to travel from the furthest point on the road surface to the kerb (s),
t_g	and the time along the kerb to the gully (s)
TSS	Total Suspended Solid
V	hydraulic velocity
VPN	Virtual Private Network
w	width
W_e	effective catchment area
Y	hydraulic depth upstream to the grate
z_{crest}	crest elevation

CHAPTER 1
INTRODUCTION

1.1 INTRODUCTION

In the summer of 2007, 13 people lost their lives and about 48,000 houses and 7000 businesses were flooded in the UK. The rainfall that occurred during June and July 2007 was unprecedented and records from rainfall and river levels shows that the rainfall was extreme with only a 1 in 150 years probability of occurring (Pitt, 2007). River flows in many areas exceeded the design limits of many flood alleviation schemes which led to urban drainage systems being overwhelmed resulting in devastating floods which affected tens of thousands of people, businesses, livestock and also lead to the loss of essential services as well as disruption to the social infrastructure, including health and social care services. Although records showed that the May to July period was the wettest ever since national records began in 1766, much of the flooding occurred in the month of June and July.

Meteorological Office records showed that a total cumulative average of 395.1mm rainfall fell across England and Wales between the months of May, June and July 2007, which amounts to well over double the usual levels. Total river outflows for England and Wales during June and July were well over three times the long-term average and nearly twice the previous maximum in the year 1968. The additional rain which fell from May to July was 31,140 million cubic metres, which was more than four times the amount of water in all the lakes in England and Wales combined (Pitt, 2007). The concentration of excessive river runoff into several major basins caused extensive flooding but around two-thirds affected urban areas were inundated by pluvial flooding (flash flooding).

Table 1.0 shows the total rainfalls for both England and Wales for the month of May – July 2007 whilst Figure 1.0 shows the precipitation level for England and Wales between 24 -25 June and 19 – 20 July which has been chosen to represent the summer 2007 flood event.

Table 1.0 – Total rainfalls for England and Wales (May – July) (Pitt, 2007)

Area	May – July 2007 rainfall	May – July 1971 – 2000 average	Previous wettest May – July in series	Additional information
NE England	379 mm	170 mm	Wettest since records began	Previous wettest was 308mm in 1879
NW England & North Wales	387 mm	198 mm	Wettest since records began	Previous wettest was 354mm in 1920
Central England	364 mm	154 mm	Wettest since records began	Previous wettest was 297mm in 1879
SE England	315 mm	153 mm	Wettest since records began	Previous wettest was 293mm in 1903
SW England & South Wales	422 mm	178 mm	Wettest since records began	Previous wettest was 345mm in 1879
England & Wales	414 mm	186 mm	Wettest since records began	Previous wettest was 349mm in 1789

Note: England and Wales record starts in 1766, other regions in 1873.

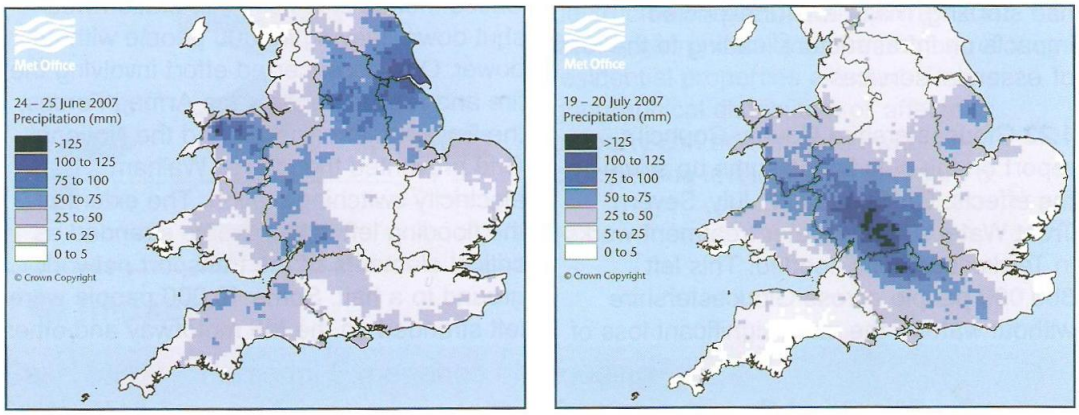

Figure 1.0 - Precipitation levels for England and Wales (24-25 June and 19-20 July) (Pitt, 2007)

The Pitt Review of the summer 2007 floods recommended that the Environment Agency, supported by local authorities and water companies, should urgently identify the areas that are at highest risk from surface water flooding (www.defra.gov.uk).

The flooding event in 2007 and again in 2012 has brought a national outcry for the betterment of not just flood mitigation measures, defences, and awareness but also of flood prediction methods as well as flood maps. This consequently brought forth the idea of the importance of knowledge of storm frequency, gutter flow and inlet capacity

and surcharge conditions for the purpose of a good design of surface drainage systems. Without an adequate regard for the surface drainage system, implementation of expansive hydraulic structures might not be able to function optimally because the intended flow did not get into the network (Gomez et. al., 2006).

Linking the hydraulic performance of a drainage system with the frequency of flooding demands a clear definition of flooding and a distinction from the state – or different stages – of surcharge (Schmitt et. al., 2004). According to BS 752, flooding is a condition where wastewater and/or surface water escapes from or cannot enter a drain system and either remains on the surface or enters buildings. Surcharge on the other hand is described as a condition in which wastewater and/or surface water is held under pressure within a gravity drain or sewer system, but does not escape to the surface to cause flooding.

Extended surcharge conditions may eventually lead to a rise in the water level above surface where water either escapes from the sewer system or prevents surface water from entering the system (Schmitt et. al., 2004). The occurrence and possible effects of surface flooding depend much more on local constraints and surface characteristics such as street gradient, sidewalks, as well as kerb heights. These characteristics however are much more difficult to describe physically and the data are not available in practice. This urban runoff process is also described to be a two-phase phenomenon, incorporating a surface phase with an underground phase (Kidd and Helliwell, 1977; Gomez et. al., 2011). Existing simulation models are not fully adequate to simulate the relevant hydraulic phenomena associated with surface flooding especially in representing the relationship between inlet capacity, inlet efficiency and surcharge conditions of different types of gully systems commonly used in practice. The shortfall in this knowledge could produce unreliable simulations from stormwater management models (Russo et. al, 2005; Gomez et. al, 2011). This study was therefore proposed to address the lack of knowledge between the two phases of the urban runoff process and to give an insight of this complicated relationship with the hope that the outcome is of use to further develop the existing flood prediction models. Due to the expansive nature

of the study that could be carried out, this study will focus only on one structure, which is the gully system.

An essential feature of a highway drainage system is that it should provide a route for stormwater to flow along from the highway to a suitable discharge point known as the outfall. However, before reaching an outfall, stormwater from the catchment is transferred to the sewer drainage network via gully system, which comprises of gully inlets/grates and gully pots. As have been previously mentioned, there is a lack of understanding on how inlets perform hence leading to a need for further research to improve on the shortfall in knowledge. The importance of this knowledge is that it ultimately determines and regulates the extent and the damage due to flooding on the surface network caused by sewer surcharge (Leandro, 2008).

A study (Argue and Pezzaniti, 1996) of a 0.4 scale model and a full sized models of a stormwater inlet was compared in a laboratory study and it was found that significant differences of up to 40% were observed in flow captured with the small scale values capturing the lesser amount of flow. This has led to the use of a full-scale laboratory rig for this study.

This research is also an attempt to continue the previous work conducted by Leandro (2008) under the Flood Risk Management Research Consortium (FRMRC 1) – a consortium set up as part of the UK government to address issues relating to flooding. Leandro (2008) in his work highlighted the fact that most inundation models focuses on the above ground linking elements namely inlet type, gully efficiency and surface flow hence overlooking the importance of below ground linking elements. Linking elements – defined as features responsible for regulating flow from sub-surface to the surface and vice versa includes not only the surface inlet but also the geometry of the inlet below ground such as pipe inlets and its connections. The outcome of the research was a theoretical linkage-model (Multiple Linking Element, MLE) of interaction between the sewer system and the surface system addressing this issue.

In an intermediate stage to reach the full MLE, a Single-Linking-Element (SLE) is established to outline all the control sections that restricts the flowrate and a set of equations have been derived for each control section [section 1.3.2]. Previous studies simplify these connections by using the weir or orifice equation without providing guidance for which parameter values to use in each equation. By doing this, the number of inlets associated, its characteristics as well as the discharge pattern of different inlet components and how they are related to each other are neglected (Leandro, 2008). Therefore, the next stage is to establish the different discharge coefficients experimentally for these sets of equations. This thesis describes one such study.

1.2 OBJECTIVES

- A primary objective of this study was to construct, instrument, calibrate and test an experimental facility that contained a single gully inlet.

Specific objectives

- To test the hydraulic performance (head-discharge relationships) of this system with different grate configurations, longitudinal bedslopes and different flows.

- To analyse the interaction of flow into and from typical existing gully systems.

- To establish a better design criteria for the inlet and gully systems by comparing the hydraulic efficiency of the inlets and gully under different flow conditions.

1.3 SCOPE OF WORK

The scope of this study primarily focuses on how different variables affect the hydraulic performance of a single full scale gully with flow conditions typical of those found in practice in the range of 0 – 50 *l*/s. For the purpose of this study, the variables that were tested included slope, geometry of gully grates and flow outlets from gully pot:

- **Slope.**

  Three longitudinal slopes (S_L), horizontal, 1 in 100 and 1 in 30 were used to represent different road conditions.

- **Types of gully grating.**

  Two grates that conform to BS EN 124, with a loading class of C250 were used for this study. The types of gully gratings used are further explained in Section 3.1.3. A summary of the properties of the grates are as listed below:

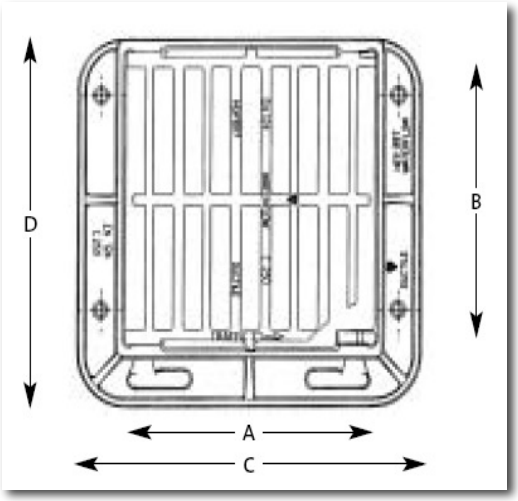

Figure 1.1 – Representation of a gully grate

Clear opening [A x B] (mm)	**Waterway (cm^2)**
325 x 437	933
400 x 432	1128

The scope of the study was to test the changes in the hydraulic performance of the system for the different geometries.

- **Gully pot**

  A typical gully pot has 2 different outlets as shown in Figure 1.2. These are further explained in Section 2.2.

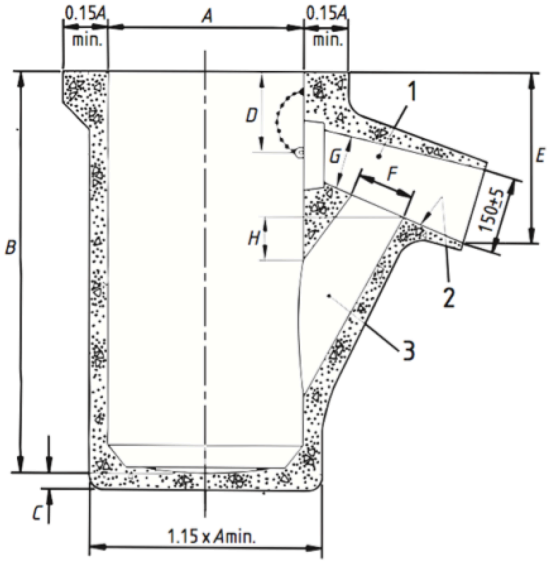

Figure 1.2 – Gully pot

Test were completed with both outlets open, the system is termed **'unplugged'** and with one outlet plugged by sealing the top outlet, termed **'plugged system'**.

- **Flow conditions used in the study.**

  Two flow conditions were used in the tests. These were termed **'terminal'** and **'intermediate'**. Intermediate gully systems are systems which intercept only a portion of the approaching flow (Q_a) whilst permitting some portion of the flow to be picked up by the next downstream gully whereas terminal gully systems all of the flow enters the gully. Both systems are defined and further explained in Section 2.2.

- **Hydraulic conditions tested**.

  Test were completed with a free surface flow to the gully grate, termed '**free flow'** and with a backflow from the gully pot onto the surface, termed '**surcharged'** tests.

- **Test programme**

  A total of 486 tests were completed over an experimental programme that was completed over a 3-year period. Full details of these tests and the test methodology are presented in Chapter 3 and 4.

CHAPTER 2
LITERATURE REVIEW

2.1 INTRODUCTION

An essential feature of a highway drainage system is that it should provide a route for stormwater to flow along from the highway to a suitable discharge point known as the outfall (Watson, 1994). However, before reaching an outfall, stormwater from the catchment is transferred to the sewer drainage network via gully systems.

According to BS EN 124:1994, the definition of a gully is an assembly to receive surface water for discharge into a drainage system. A gully system consists of a frame and grates which is positioned over the gully pot. The gully frame is fixed on to the gully pot to support the grates and has to have the capacity to withstand loadings from vehicles and traffic whereas the gully pot on the other hand acts as a trap for silts and debris. Gully grates are an important feature of the gully system since it permits the passage of water into the gully pot and hence the drainage system. The grates used in a gully system are an important factor in determining the overall efficiency of the system.

Gullies are always placed at low points, on the high side of junctions and pedestrian crossings and at changes of super-elevation. Other gullies are then placed at spacing determined by the use of an appropriate spacing method (Davis et. al., 1996). The maximum flow capacity that can be accepted by a gully pot without surcharge is about 10 *l/s* for gully pot with a 100mm diameter outlet and 15 *l/s* for gully pot with a 150mm diameter outlet (HA 102/00).

Gully pots are the first entry point to road runoff into an urban drainage network and are extensively used to trap solids from runoff in order to minimise the problem associated with sediment deposition in downstream drainage structures and receiving waters (Memon and Butler, 2002). Gully pots can bring both benefit and hazardous impact on water quality of the receiving watercourse. Its main benefit is to trap potentially contaminated pollutants during normal rainfall events prior to discharge to receiving

watercourse (HA 33/06). However, gully pots are more effective at trapping coarse sediments since its principle is to reduce the amount of coarse sediments that enters the drainage system. This is important since the presence of coarse sediment in the drainage system reduces the flow velocity and ultimately causes blockages. Gully pots also provide a good first line of defence against accidental spillages. It is also said that the conventional gully pot is effective at retaining some 90% of sediment of d_{50} = 0.8mm. This efficiency however drops to around 25% if the sediment level approaches the maximum level before blockage of the outlet occurs (HA105/04).

Although conventional gully pots are generally effective at trapping sediments, poor maintenance practices can lead to generation of polluting materials, which puts the receiving watercourse at a risk. These pollutants are a result of the degradation of organic materials within the sediments and debris by bacteria thus creating a high Biological Oxygen Demand (BOD) in the liquor. This liquor, once released into the receiving watercourse has the tendency to remove oxygen and the higher the BOD level, the more detrimental it is to health (HA105/04). There are numerous studies with regards to the efficiency of roadside gully pots conducted which includes (Ellis and Harrop, 1984; Pratt, 1984; Pratt and Adams, 1984; Ellis et. al., 1986; Grottker, 1990; Butler and Karunaratne, 1995; Butler and Memon, 1999; Deletic et. al., 2000; Memon and Butler, 2002). In this thesis, no account was taken of the qualitative performance of the gully system and focuses only on the hydraulic aspects of the system.

2.2 TYPES OF GULLIES

Gullies can be classified according to its hydraulic operation, design or the position of the gully system itself. British Standard (BS 5911:2004) has identified two main types of gullies according to its design. The more common type is the trapped gully, as used in this study, which consists of a hollow cylinder concrete with a base with an outlet designed to form a water seal and a rodding eye – which is an outlet to facilitate the connection of a pipeline [Figure 2.1]. The less common gully system [Figure 2.2]– which is the untrapped gully, is similar to the trapped gully but lacks the water seal outlet.

In a less significant way, gullies can also be classified according to the design of the final outlet. The gullies highlighted in Figure 2.1 and 2.2 show a similar outlet type, which is the spigot outlet, whereas Figure 2.3 highlights a gully with a socket outlet. In this study, the gully type shown in Figure 2.1 was used.

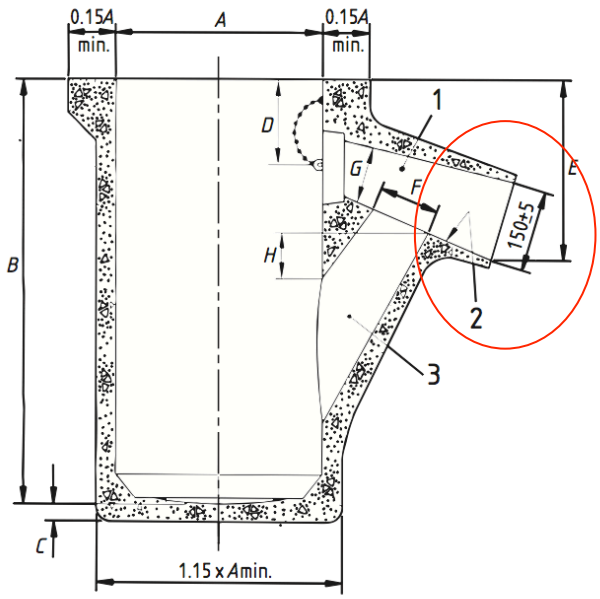

Key

1	Rodding eye
2	Minimum slope 1 in 10
3	Riser
A	Internal manufacturing diameter
B	Internal manufacturing depth
C	Minimum thickness of base
D	Maximum inside depth to centre of outlet
E	Maximum outside depth of outlet
F	Minimum dimension of riser (for trapped gullies)
G	Minimum internal diameter of rodding eye (for trapped gullies)
H	Minimum depth of water seal (for trapped gullies)

Figure 2.1 – Typical trapped gully with spigot

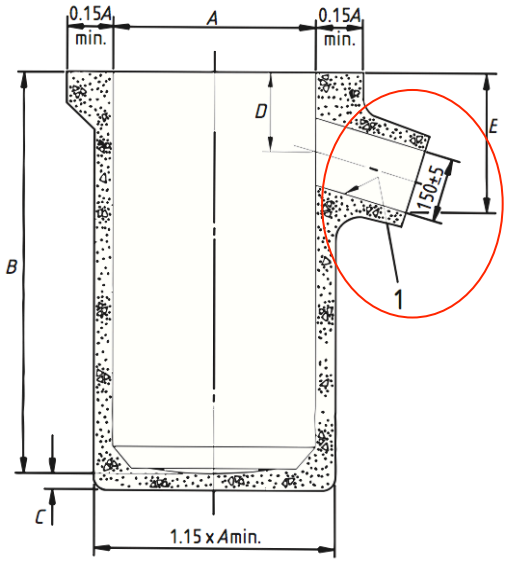

Key

1	Minimum slope 1 in 10
A	Internal manufacturing diameter
B	Internal manufacturing depth
C	Minimum thickness of base
D	Maximum inside depth to centre of outlet
E	Maximum outside depth of outlet

Figure 2.2 – Untrapped gully with spigot outlet

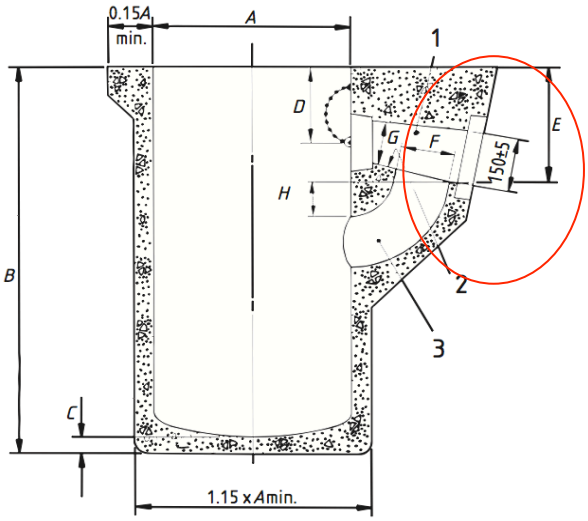

Key

1	Rodding eye
2	Minimum slope 1 in 10
3	Riser
A	Internal manufacturing diameter
B	Internal manufacturing depth
C	Minimum thickness of base
D	Maximum inside depth to centre of outlet
E	Maximum outside depth of outlet
F	Minimum dimension of riser (for trapped gullies)
G	Minimum internal diameter of rodding eye (for trapped gullies)
H	Minimum depth of water seal (for trapped gullies)

Figure 2.3 – Trapped gully with socket outlet (BS 5911:2004)

The trapped gully [full specifications are highlighted in Appendix 1] with spigot outlet was chosen for the purpose of this study since it is the most commonly used and will be the best choice to represent the gully frequently found in practice. Elaborated details regarding the proposed gully are mentioned in Chapter 3. Both modes of hydraulic operation – intermediate and terminal gullies were tested in order to obtain a better understanding of the hydraulic interaction of both systems.

The trapped outlet has the advantage in that it reduces the risk of debris being washed into the connection and the carrier drain. As oils floats on water, the provision of the trap helps to retain oils within the pot and prevent them from being washed into the drain. Trapped gullies are essential especially for combined sewers since it has the ability to prevent smells from being transmitted from the sewers through the gullies (Watson, 1994). The less common form of gully, which has no trap, will not have the capability to retain oil but will help in retaining most of the coarser materials from being washed into the drain (HA 105/04).

Another classification made by Design Manual for Road and Bridges (DMRB) classifies gullies into 2 modes based on its hydraulic operation. Based on this classification, the design of gully spacing is made simpler. The gullies are classified as (HA 102/00):

(i) Intermediate gullies – gullies that permit some portion of the approaching flow to pass and are picked up by the next downstream gully.

(ii) Terminal gullies – gullies with no significant portion of flow to pass through it possibly due to the inexistence of another downstream gully or due to the interference to traffic/pedestrian if allowed.

There are various sizes in terms of diameter or width and length allowable for gullies according to (BS 5911-6: 2004), Table 2.1 shows the nominal dimensions allowable for gullies. Based on this, one single round gully with an internal diameter of 375mm and 150mm outlet was chosen for this experimental programme based on a review of typical gullies found in practice.

Table 2.1 – Nominal sizes for typical gully (BS 5911-6:2004)

Nominal size of gully (see 3.7)			Limits of internal manufacturing section of gully (see 3.10)	Deviation of actual internal manufacturing depth (see 3.10)	Limits of internal manufacturing depth (see 3.10)	Deviation of actual internal depth from internal manufacturing depth	Minimum thickness of base	Maximum inside depth to centre of outlet (untrapped) or rodding eye (trapped)	Maximum outside depth of outlet (see 3.7)	Trapped gullies only			
										Minimum dimension of riser	Minimum cross sectional area of riser	Minimum internal diameter of rodding eye	Minimum depth of water seal
Nominal section		Nominal depth	A		B		C	D	E	F		G	H
Nominal diameter	Nominal width/ length		mm	mm	mm	mm	mm	mm	mm	mm	mm^2	mm	mm
375		750	365 to 385	6	740 to 760	25	50	300	400	90	8 000	100	85
		900			890 to 910								
450		750	435 to 465	9	740 to 760	25	50	300	400	90	8 000	100	85
		900			890 to 910								
		1 050			1 040 to 1 060								
		1 200			1 180 to 1 210								
	300/385	700	AW 290 to 310	6	690 to 710	25	50	335	430				
			AL 375 to 395										
	300/385	750	AW 290 to 310	6	740 to 760	25	50	335	430				
			AL 375 to 395										
	300/385	700	AW 290 to 310	6	690 to 710	25	50	195	290	N/A	8 000	100	80
			AL 375 to 395										
NOTE Typical arrangements for gullies and the dimensions A, B, C, D, E, F, G and H are shown in Figure 1, Figure 2, Figure 3 and Figure 4.													

Re-suspension of sediments happens frequently within the conventional gully pots due to high inflow rates and the subsequent discharge from the gully pot can result in a pollutant flush to the receiving sewer. The high inflow rates can also cause turbulence and mixing between the sediments and oils in the sump. This might pose a detrimental effect to the receiving watercourse. The best way to avoid re-suspension as suggested by the Design Manual for Road and Bridges (DMRB) is by ensuring that the gradient of the pipe leading to the gully is kept as shallow as possible yet consistent with adequate hydraulic performance. If this cannot be achieved, it is suggested that a sumpless gully should be used as an alternative (see below).

Another form of gully is the sumpless gully and is different from the conventional gully because of the position of its outlet. The sumpless gully is a means of directing flows to the drainage system via discrete entry points without the construction of a sump for the purpose of trapping debris, sediments and oils. Sumpless gullies can be divided into two distinct types – chutes and pots. Both have similar characteristic in terms of their outlet position but they differ geometrically. The outlet, as can be seen in Figure 2.4 and 2.5, is situated at the base of the gully pot hence not allowing it to have the ability to retain both oil and sediment. The base of the pot is designed in such a way that the flow of

water is allowed to be channelled to the outlet directly minimising sediment build up at the edge of the pot base (HA 105/04).

Chute type sumpless gully have similar plan area as its grates and frame but has a sloping face at the bottom end of the chute with a longitudinal outlet pipe incorporated into it. Pot type sumpless gully however, like its name has a cylindrical body with a rounded base shaped in such a way that all the flows are directed to the outlet. Chute type gullies are usually used on flat roads in low-lying areas where adequate pipeline gradients for drainage are difficult to obtain (HA 105/04). A more detailed description of sumpless gullies can be obtained from DMRB HA 105/04 – Sumpless gullies.

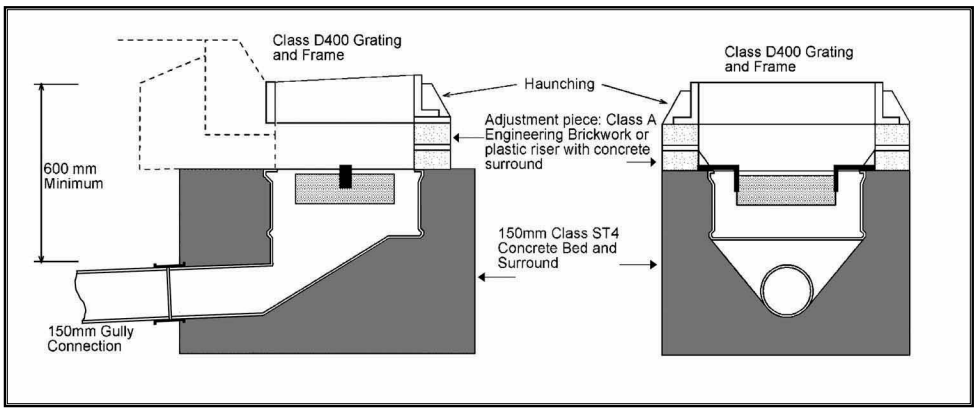

Figure 2.4 – Chute type sumpless gully (HA 105/04)

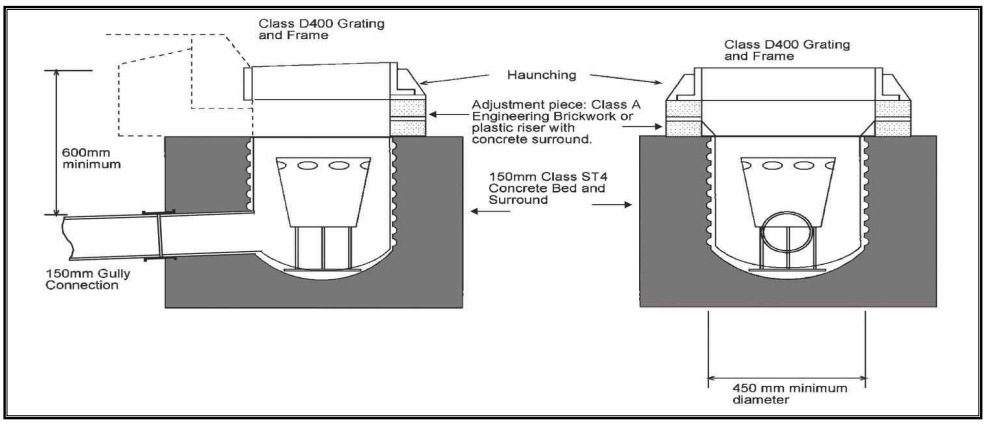

Figure 2.5 – Pot type sumpless gully (HA 105/04)

Conventional gullies pose a pollution risk with the flushing of polluting liquor from the gully sump particularly during dry weather. This however is not the case when sumpless gullies are used. Among the benefits of sumpless gullies are (HA105/04):

- Preventing contaminated silt and liquor accumulation;
- Eliminating 'foul flush' of heavily contaminated or polluted flow as the gully starts to operate;
- Reducing the overall need in terms of maintenance since there is only a minimal need to clean the pots hence reducing the risk of contaminated water being released into the receiving watercourse during the cleaning process.

It should be noted however that sumpless gullies are not suitable for use where the carriageway drains to a combined sewer. The downstream system also must be designed in such a way that the excess debris and sediments can be transported to prevent blockages from occurring. In this study however, sumpless gullies will not be taken into consideration.

2.3 STORMWATER INLET / GULLY GRATINGS

As mentioned previously, stormwater from a highway needs to pass through a gully system with an inlet configuration before being transferred to an outfall. A stormwater inlet is a structure for intercepting stormwater on the ground surface or in the roadway gutter.

Stormwater inlets or also known as gully grates are an important part of an urban drainage system, since its primary role is to control the amount of water conveyed from the ground surface to the sewer network. The capacity of the inlets therefore determines the efficiency and reliability of the whole storm drainage system. Inlet capacity defines the largest quantity of gutter/overland flow that can be captured by the inlet. This

definition assumes that the functionality of the inlet is not affected by conditions in manhole, pipe or any other device, or by backwater effects and surcharging (Despotovic et. al., 2005).

According to (Stephenson, 1981), there are two basic inlet configurations which are the vertical inlet or more commonly known as kerb inlet and horizontal screens or grated inlet. Kerb type inlets offers practical advantages to traffic but is less efficient hydraulically whereas horizontal screens are easily subjected to damage by heavy traffic. It should be noted that kerb type inlets however are not commonly used in the UK.

Figure 2.6 shows the difference between kerb type and grated inlet.

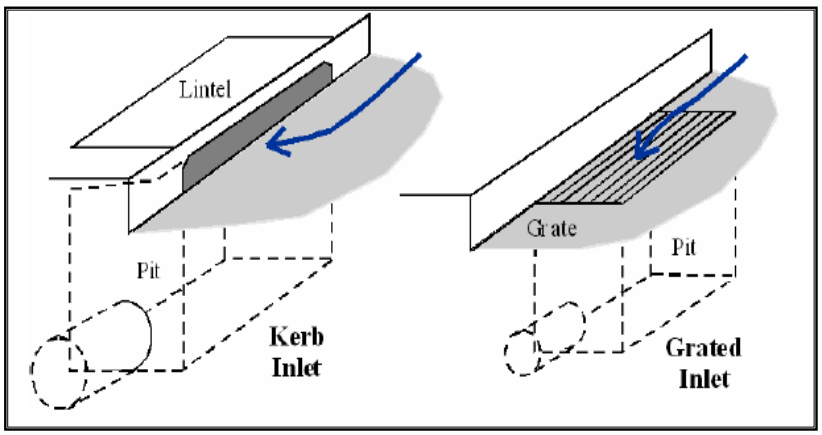

Figure 2.6 – Kerb inlet and grated inlet (Pezzaniti et al., 2005)

(Haestad and Durrans, 2003) however classifies inlet openings into four general types, which are grate inlets, kerb inlets, combination inlets, and slotted drain inlets as shown in Figure 2.7. Grate inlets consists of an opening in a gutter or swale and is covered with one or more grates whereas kerb inlets have vertical openings in the kerbs and is covered by a slab. Combination inlet, as the name goes, combines both grate and kerb inlets configuration. Slotted drain on the other hand consists of a grate opening oriented along the longitudinal axis of a pipe and is manufactured integrally with the pipe itself. For the purpose of this study, only grate type inlets will be used.

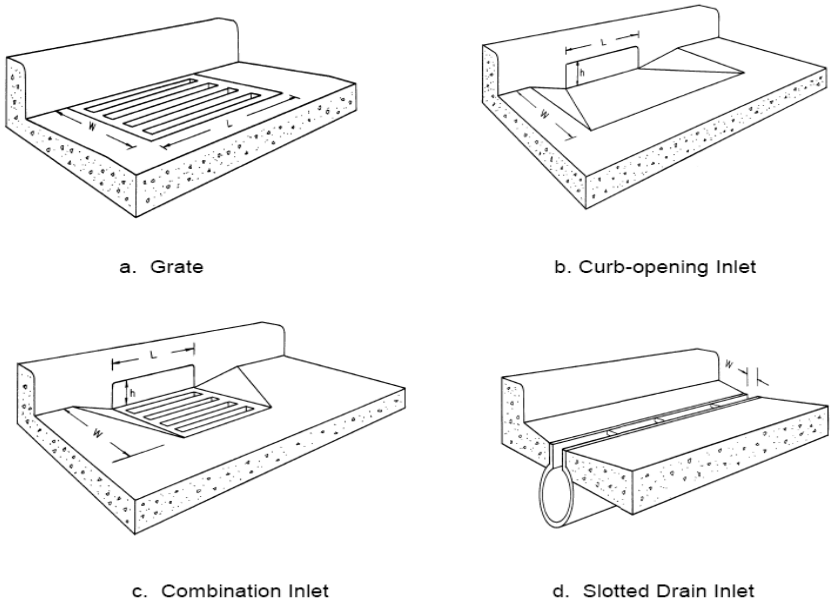

Figure 2.7 – Different types of stormwater inlet (HEC 22, 2001)

In terms of location, stormwater can be classified into – in-sag or on-grade inlets. This classification is similar when compared to the classification based on the hydraulic modes of gully systems since in-sag inlets acts as a terminal gully which does not permit any significant amount of flow to past through it whereas on-grade inlet acts as an intermediate gully which allows part of the flow that passes it to be captured by the downstream gully. Proper attention should be given to the conveyance of drainage water through sag inlets, because they frequently encounter water ponding which tends to increase the water spread over the pavement (Almedeij et. al., 2006).

There are many characteristics, which have to be taken into consideration while designing a stormwater inlet. Some of the factors include its hydraulic characteristics, loading class, hydraulic efficiency, orientation, dimensions, and road gradients as well as clogging factor. A more detailed review of these factors is elaborated in the following sections.

2.3.1 Hydraulic capacity

The hydraulic capacity or also known as the street hydraulic conveyance capacity (SHCC) of a storm drainage inlet depends on the geometry as well as the hydraulic characteristic flow into the system. Inlet capacity governs both the rate of removal from the road surface and the amount of stormwater that flows into the network (Russo et. al., 2006). The SHCC is the term used by the US Department of Transportation to ensure the roadway system is of acceptable level of service during storm events. The SHCC of any given highway should always be below the allowable street hydraulic conveyance capacity (ASHCC) as outlined in the Hydraulic Engineering Circular No-22 (HEC 22). Further reference with regards to SHCC can be found in the paper by (Guo, 2000).

The hydraulic performance of a gully is an important feature for the design of the gully. Hydraulic characteristics of the road surface are important for the design of a gully system and this are a function of the longitudinal (S_L) gradient and crossfall (S_c) of the road layout. Longitudinal gradient for an individual length drained by gully is defined as the average gradient of the road over a 3m distance upstream of the gully whereas the crossfall is measured 0.5m upstream of the leading edge of the gully. The hydraulic capacity of a gully grating also depends on its overall size, the number and orientation of the slots, and the total waterway area provided by the slots (HA 102/00).

The hydraulic characteristics of a gully grating can change since it can perform both as a weir and as an orifice depending on the depth of water against the kerb. Gully grates operate like a weir when the water depth is shallow and an orifice when it is submerged (Guo, 2000). According to HA 102/00, gully grates can be classified into Type P, Q, R, S and T according to its hydraulic characteristics with the capacity of the grates decreasing respectively. Details are shown in Table 2.2.

Due to the large possible designs that could be produced, characterisation based on hydraulic performance was made to give the advantage to manufacturers to classify the grates accordingly and designers the confidence that the selected grates conforms to a

certain hydraulic performance. This categorisation is usually predetermined through a series of hydraulic tests carried out by manufacturers.

Table 2.2 shows the classification of grate type based on its hydraulic characteristics and the corresponding design value for G_d.

Table 2.2 – Grating type and the design values for G_d (HA 102/00)

Grating type	P	Q	R	S	T
Range of G (s/m^2)	≤30	30.1 – 45	45.1 – 60	60.1 – 80	80.1 - 100
Design value G_d	30	45	60	80	100

This classification (Type P, Q, R, S and T) represents the range of grating parameter (G), which ultimately determines the design value for grating parameter (G_d) [Table 2.2]. This grating parameter is a significant parameter in estimating the efficiency of gully gratings. Since the efficiency of gully gratings is an elaborate subject on its own, it has been further explained in Section 2.3.3 [Equation 2.5]. The classification into which a grating falls is determined by calculation, based upon the geometric characteristics of the grates. The grating parameter, G (s/m^2) can be calculated using Equation 2.0 (HA 102/00):

$$G = \frac{69\ C_b}{A_g^{0.75}\sqrt{p}}$$

[Equation 2.0]

where,

C_b is the coefficient of grating bar pattern [Table 2.3],

A_g is the smallest rectangular area with two sides parallel to the kerb that contains all the slots in the grates (m^2), and

p is waterway area as a percentage of grating area.

Table 2.3 shows the coefficient of grating bar pattern.

Table 2.3 – Grating bar pattern (HA 102/00)

Grating bar pattern	C_b
Transverse bars	1.75
Other bar alignments – (i.e longitudinal, diagonal and bars curved in plan)	1.5

Two other important parameters that should also be taken into consideration during the design of the road gratings and kerb inlets for the determination of hydraulic capacity of gully grates are as listed below (HA 102/00):

- The flow of water parallel to the kerb should not exceed an allowable width (B) as in Figure 2.8. The maximum allowable flow width is 1.5m for the hard shoulder and 1.0m for the hard strip on trunk roads. This is for the 1 in 5 year storm.

- The grating of the gully or kerb inlet should be reasonably efficient in collecting the flow. The grating efficiency (η) should be kept as high as possible. For intermediate gullies, grating efficiency less than 80% should be redesigned by incorporating an improved grating type whereas for terminal gullies, grating efficiency less than 95% should be redesigned. If the required efficiency is still not achieved, it is proposed that the permitted width of kerb flow (B) is replaced with a lesser design width to reduce the design flow and hence increase the grating efficiency. This however, may require the use of an additional intermediate gully.

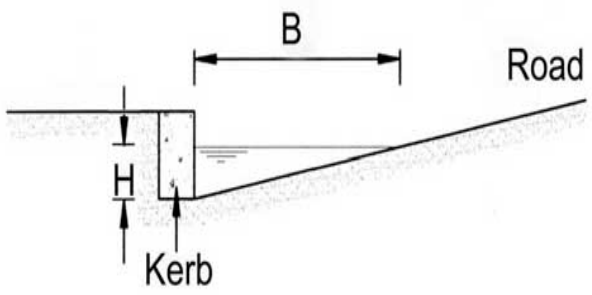

Figure 2.8 – Allowable width, B and depth, H of water against kerb (HA102/00)

(Despotovic et. al., 2005) highlights the same factors affecting the capacity of stormwater inlets on highways, which includes lateral slope or crossfall (S_c), longitudinal slope (S_L), but with an addition of road surface material as one of the contributing factors.

This is because road surface materials used or the pavement roughness is represented by different Manning's coefficient. Different surfaces have different values of Manning's coefficient and Table 2.4 compares some of the Manning coefficients quoted from different sources.

Table 2.4 – Manning's coefficient from various sources

Road surface material and condition		**Manning's coefficient**		
Material	**Condition**	**Davis et. al (1996)**	**HA 102/00 (2000)**	**Despatovic J. (2005)**
Concrete	Average	0.011	0.013	0.015
Concrete	Poor	0.014	0.016	0.025
Blacktop	Average	0.014	0.017	0.012
Blacktop	Poor	0.018	0.021	0.016

The relationship between longitudinal slope and lateral slope (crossfall) can be seen more clearly since the flow in the triangular cross-section of case (a) and (b) for Figure 2.9 can be determined using the Manning's equation. It should be noted however that for the determination of flow in these gutter cross-sections, it is assumed that all the streets have kerbs since it is more common for cities to have street kerbs than without. By assuming that the streets are all lined with kerbs, a boundary for stormwater flow can be assumed hence defining the cross section geometrically allowing Manning's equation to be used for the determination of flow.

For case (a) and (b), the flow can be calculated using Equation 2.1 (Despotovic et. al., 2005):

$$Q = \frac{0.315\, d^{8/3}\, S_L^{1/2}}{n \times i}$$

[Equation 2.1]

where,

Q is the flowrate (m^3/s),

d is the water depth by the kerb in m,

S_L is the longitudinal slope (m/m),

i is the lateral street slope (m/m), and

n is the Manning's coefficient.

Extensive flow concentration next to the kerb and non-uniform velocity field distribution makes Manning's formula not accurate enough in the above given form. The flow should then be calculated with an assumption that the hydraulic radius is constant laterally along the flow width. With such an assumption, the following formula is obtained (Despotovic et. al., 2005):

$$Q = \frac{0.375\, K_r\, d^{8/3} S_L^{1/2}}{n \times i}$$

[Equation 2.2]

where,

K_r is a coefficient with the following values (Clarke et. al., 1981): K_r=0.9–1 for cross sections as in Figure 2.9(b); K_r = 0.8 – 0.9 for cross sections as in Figure 2.9(a) and (c). Other notations are as described above.

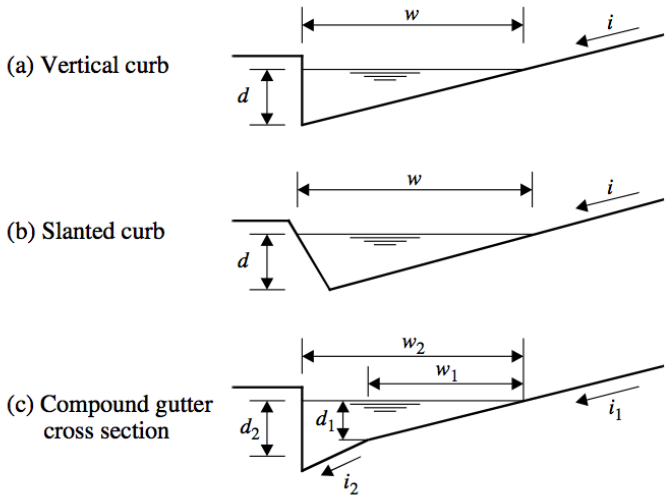

Figure 2.9 – Gutter cross sections (Despotovic et. al., 2005)

In another study made by (Gomez and Russo, 2007) on macro type inlets, it was found out that the hydraulic efficiency of grates depends on street geometry, the approaching flow and flow depth. It was also found that the efficiency of the grates increases as the transversal slope increases whilst reducing longitudinal slope. While considering the approaching flow, efficiency is higher for low circulating flows. The grates present a residual and almost constant efficiency for high longitudinal slopes and low transversal slope.

2.3.2 Loading class

Loading class of the gully grates is also an important criterion, which should be considered whilst selecting the appropriate gully grate for use. This is because the loading class of the gully grates determines the ability of the gully system to withstand the load of the pedestrians, cyclists, and more importantly heavy vehicles. In practice, although this criteria is insignificant hydraulically, it is however important that the correct loading class is chosen for the safety of users. BS EN 124:1994 has divided gully tops into 6 classes – class A15, B125, C250, D400, E600 and F900 with respect to the suitable place of installation. The division of classes and the suitable places for installation is as shown on Table 2.5:

Table 2.5 – Summary of minimum allowable loading class and place of installation for gully grates (BS EN 124:1994)

Group and minimum class	Place of installation
Group 1 (min class A15)	Areas which can only be used by pedestrians and pedal cyclists
Group 2 (min class B125)	Footways, pedestrian areas, car parks and car park decks
Group 3 (min class C250)	Areas which are of kerbside channels of roads which when measured extend a maximum of 0.5m into the carriageway and a maximum of 0.2 into the footway
Group 4 (min class D400)	Carriageways of roads, hard shoulders and parking areas for all types of vehicles
Group 5 (min class E600)	Areas imposing high wheel loads
Group 6 (min class F900)	Areas imposing particularly high wheel loads

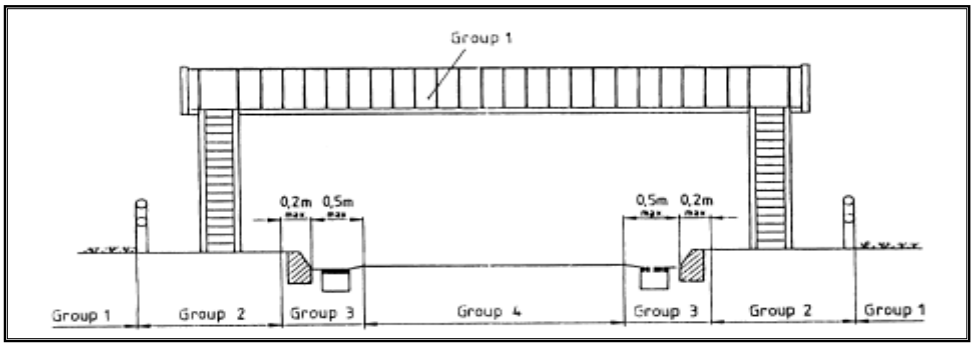

Figure 2.10– Typical highway cross-section showing the location of some installation group (BS EN 124:1994)

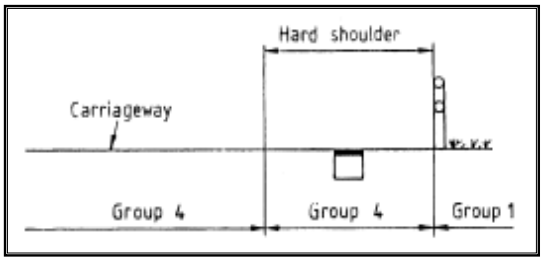

Figure 2.11 – Typical detail of a hard shoulder showing some of the locations of the installation groups (BS EN 124:1994)

These classes are also linearly linked to the allowable weight load that the material of the grate should withstand. Class C250 has been chosen for the purpose of this study since it is the best representation of the most commonly used grate. This selection is however quite insignificant in this study since there will be no loading tested for in the laboratory tests.

2.3.3 Efficiency of gully grates

The efficiency of gully grates is a function of the approaching flow, the captured flow as well as the intercepted flow. In circumstances where the approaching flow is smaller than inlet capacity, it is often assumed that the designated inlets are able to capture the whole approaching flow. In circumstances where the approaching flow is greater than inlet capacity however, the inlet captures only a portion of the approaching flow, while the remaining flow passes over the inlet and is then captured by the downstream inlet. This relationship is as seen in Figure 2.12 and is used to describe the efficiency of gully grates.

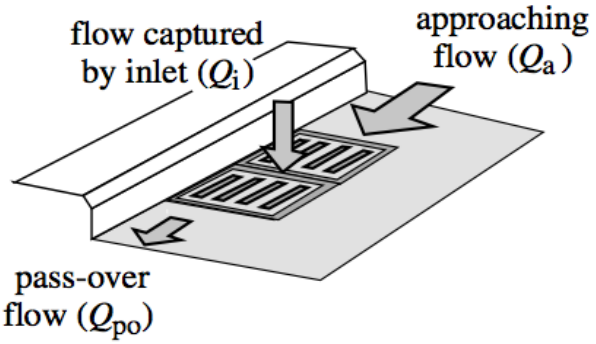

Figure 2.12 – Definition of flow components (Despotovic et. al., 2005)

The efficiency of an inlet (η) is the ratio of the intercepted flow against the approaching flow towards the gully system. In simple terms, the efficiency of an inlet is given as (Haestad and Durrans, 2003; Despotovic et. al., 2005; Valentin and Russo, 2007):

$$Efficiency\ (\eta) = \frac{Intercepted\ flow\ (Q_{int})}{Approaching\ flow\ (Q_a)}$$

[Equation 2.3]

Bypass flow (Q_b) or the discharge that has not been intercepted by the stormwater inlet can be defined as (Haestad and Durrans, 2003):

$$Q_b = Q - Q_{int}$$

[Equation 2.4]

According to Design Manual for Road and Bridges (HA 102/00) however, the efficiency of gully gratings, η (in %) can be determined using Equation 2.5:

$$Efficiency\ (\eta) = 100 - G_d \left(\frac{Q}{H}\right)$$

[Equation 2.5]

where,

G_d is the grating parameter with its values determined by the grating type [Table 2.2],

Q is the flowrate approaching the grate (m^3/s), and

H is the water depth against the kerb (m)

There are also circumstances when the inlets are unable to capture the whole approaching flow although it is less than the capacity of the inlet. This perhaps is due to malfunction, which often reduces the capacity of the inlets. Malfunction of inlets which reduces partially or completely the capacity of gully grates are often caused by (Despotovic et. al., 2005):

- inadequate position of the inlet in relation to the kerb or street other elements,
- deformation of the surrounding street pavement due to high temperatures and/or heavy traffic,
- clogging of the inlet grate openings by leaves or other debris,
- clogging of manholes, pipes or any other device downstream of the inlet.

Efficiency of gully grates is a crucial factor to be determined especially during the design phase for estimating gully spacing. Initial assumption regarding the efficiency of inlets should be made correctly to prevent from overestimating gully capacity hence its spacing. In instances where the inlet capacity is overestimated by assuming its full efficiency of 100%, then the distances between the inlets are also overestimated. This leaves a high probability for surplus storm runoff to remain on the street surface. Similarly, if an inlet is placed in an inadequate position that would contribute to the increased clogging, there will also be surplus of water on the surface (Despotovic et. al., 2005). Efficiency of gully grates therefore is an important criterion in ensuring a reliable and effective sewer drainage network.

In a paper by (Russo et al., 2006), it was reported that the Hydraulic Department of the Technical University of Catalonia (UPC), Barcelona with the help of Clavegueram de Barcelona S.A (CLABSA) – a company that manages the sewer system in Barcelona promoted a new line of research in the field of stormwater inlet efficiency. In line with the effort to promote the study, laboratory tests on commonly used grates in the city of Barcelona were conducted on a 2000m^2 platform that simulated the hydraulic behaviour of a road. The platform was designed to be able to simulate a roadway with transversal slope up to 4 and longitudinal slope up to 14% and a large range of flow rate ranging from 0 to 200 *l/s*. From that series of tests, along with studies made by HR Wallingford, a potential law expression was obtained and a reliable methodology concerning efficiency calculation was established:

$$Efficiency\ (\eta) = A \left(\frac{Q}{y}\right)^{-B}$$

[Equation 2.6]

where,

Q is the total flow approaching the inlet (*l/s*),

y is the hydraulic depth upstream to the grate (mm), and

A and B are two characteristic parameters related to the grate geometry (as described by equation 2.7 and 2.8).

The experimental data also exhibited a link between inlet efficiency and some particular geometric parameters of the grate such as the number of the longitudinal, transversal and diagonal bars, void area, length and width of the grates and et cetera. This link, termed as characteristic parameters (A and B) could be mathematically expressed as Equation 2.7 and 2.8 respectively:

$$A = \frac{0.39}{A_g^{-0.35} p^{-0.13}} (n_t + 1)^{0.01} (n_l + 1)^{0.11} (n_d + 1)^{0.03}$$

[Equation 2.7]

$$B = 0.36 \left(\frac{L}{W}\right)$$

[Equation 2.8]

where,

A_g is the area that includes the void area of the grate (A_H) (m^2),

p is the ratio of A_g to A_H,

n_t, n_l, n_d are respectively, the numbers of transversal, longitudinal and diagonal bars,

L is the length of the grate (m), and

W is the width of the grate (m).

Later, other grates were also experimented on to confirm this methodology and the resulting outcome indicated that the method could be theoretically applied to each grate with dimensions contained in the UPC tests range without previous experimental tests (Martinez and Gomez, 2000; Russo et. al., 2006). This study shows that the efficiency of grates are specific for each type of grates and are unique to its geometric conditions as well as the overall hydraulic characteristics related to the grates.

Existing data and understanding regarding specific grate types are still scarce. (Pezzaniti et. al., 2005) identifies some new needs with relations to the inlet capacity relationship which includes:

- Reliable inlet capacity relationship are not available for most of the inlet system types and configurations found in existing drainage systems and in many design situations,

- Most of the available relationships deal with relatively low, controllable flows not with higher flows occurring in the 100-year average recurrence interval, ARI storms.

Further study regarding the efficiency of gully grates should be promoted since it is an important criterion in ensuring a reliable and effective sewer drainage network.

2.3.4 Orientation of gully grates

The orientation of gully grates affects the hydraulic efficiency of a gully system. There have been numerous studies conducted to determine the extent of the effect of grates orientation to the hydraulic properties of the grates. (Eskenazi, 1984) established an experimental method to understand the influence of shape, disposition and interval of gully grating bars on stormwater absorption rate. It was found that the greater interval between the bars, the better efficiency of the grates. However, since there is a limit to intervals due to safety reasons, this parameter was not given much priority. It was also found that the longitudinal disposition of bar gives the best hydraulic results. Longitudinal bars however pose a threat to the safety of cyclists and cannot be considered safe for practice. Due to this, it was decided that the best solution was to use transversal bars and improve the draining rate as much as possible. It was found that grates profiled according to flow lines give the best result.

In the UK however, it is common practice to have the grates aligned between 45° and 90° to the kerb (HA 102/00). According to British Standard (BS EN 124:1994) on the other hand, the dimensions of slots for classes C250 to F900 should be dependent on the orientation of the longitudinal axis of the slots in relation to the direction of traffic and as in accordance to Table 2.6 and Figure 2.13:

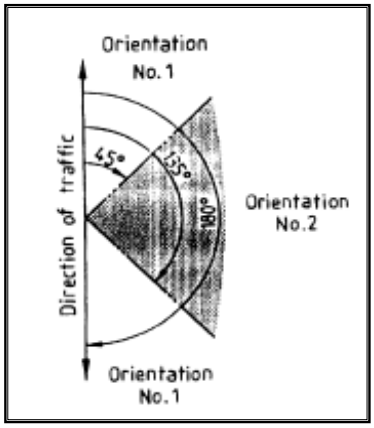

Figure 2.13– Orientation of slots (BS EN 124:1994)

Table 2.6 – Dimensions for classes C250 to F900

Orientation		Class (mm)	Width (mm)	Length (mm)
No.1	From 0º to 45º and from >135º to 180º	All classes	16 to 32	≤ 170
No.2	From 45º to 135º	C250	16 to 42	No limitations
		D400 to F900	20 to 42	No limitations

For the purpose of this study, grates aligned at 90° to the direction of traffic are used again to mimic common practice in the UK.

2.3.5 Dimension of gully grates

In the UK, all nominal widths of gratings and minimum areas of waterway should be in accordance to BS EN 124:1994 and BS 7903:1997. BS EN 124 specifies that the minimum waterway area should be 30% of the clear area of the gully grates. However, according to HA 104/02, a minimum 900cm^2 of waterway for any gully grates is usually used in practice here in the UK. If so, then the standard, which has been set by BS 124, is much lower than what is common practice in the UK.

According to BS 7903, it is the total waterway area with respect to the nominal widths, which is important instead of the clear area. Previous requirements in the UK have also always been stated in terms of minimum waterway area and the distribution of that area across the grating.

The minimum nominal widths and waterway areas of gully grates are as the Table 2.7:

Table 2.7 – Minimum nominal widths and waterway areas (BS 7903)

Minimal nominal width (mm)	Minimum area of waterway (cm^2)
325	650
450	900

The grates chosen for this study has the total waterway area of 933 cm^2 and 1128 cm^2 respectively and meets the minimum requirement set by both BS EN 124 and BS 7903.

2.3.6 Road gradients

Road gradients are important to establish outfall levels that are achievable and to ensure subgrade drainage can discharge above the design flood level of any outfall watercourses (HD 33/06). Road gradients determine the drainage flow path. Drainage flow path is defined by TA 80/99 as the maximum distance taken by runoff in reaching the edge of the carriageway channel or drainage system and is dependent on carriage width, crossfall, as well as longitudinal gradient. The UK standard minimum crossfall is 2.5% meanwhile 0.5% is the minimum standard for longitudinal gradient. This is one of the higher national standards and is intended to achieve efficient removal of water from carriageways (TA 80/99). The desirable maximum gradient for design should be 3%, 4% and 6% for motorways, AP dual carriageways and AP single carriageways respectively. However, in hilly terrain, steeper gradients are required particularly where traffic volumes are at the lower end of the range (HD 33/06).

On kerbed roads, a minimum 0.5% gradient should be maintained whenever possible to ensure effective drainage. In flatter areas however, the vertical alignment should not be manipulated by the introduction of vertical curvature simply to achieve adequate surface water drainage gradients (TD 9/93).

During the initial phases of this study, consideration was given to the longitudinal and transverse slopes as parameters to be tested. However, due to the nature of the laboratory rig, time and physical constraints associated with the necessary changes, it was only feasible to test the changes in the longitudinal bed slope. Three different slopes were used – horizontal, 1 in 100 and 1 in 30. The slopes are as listed in Table 2.8:

Table 2.8 – Gradients for laboratory tests

Longitudinal slope (S_L)
0
1/100
1/30

2.4 SPACING OF GULLIES

In order to minimize flooding on roads, it is imperative to install drainage inlets at the appropriate spacing to ensure the stormwater on the road surface are able to enter the underground sewer network. The inlet should be positioned under a ‘sump’ or a ‘continuous grade’ condition. The sump condition refers to a section of the roadway in which the longitudinal slope is level and its elevation is lower than the adjacent sections where ponding is likely to occur. The continuous grade condition on the other hand refers to an inlet that is located in such a way that the grade of the road has a continuous slope past the inlet (Wong and Moh, 1997).

(Davis et. al., 1996) points that the spacing of gullies in kerb and gully systems depends on the hydraulic capacity of the grating rather than that of the gully pot or the pipes in the drainage system. This is because the gully pot has been designed to cope with more water than the grating can deliver. It was also mentioned that the spacing is also determined by the allowable width of flow along the road edge since proper spacing will consequently minimise the nuisance to traffic.

As described previously, the spacing of road gullies is not independent of the hydraulic capacity as well as the efficiency of the grates. Overestimating inlet efficiency will result in overestimation of the spacing, hence increasing surplus storm runoff on the street surface. Similarly, if an inlet is placed in an inadequate position that would contribute to the increased clogging, there will also be surplus of water on the surface. Due to the above stated reasons, it is obvious that proper placing of inlets is very important if the drainage network is to be efficient and reliable (Despotovic et. al., 2005).

A general empirical spacing for gully systems according to Watson (1994) is at no more than 40m to 50m apart or one gully for every 200m^2 of impervious catchment (Bartlett, 1981; Pratt, 1984; Watson, 1994; Davis et. al., 1996). Gully spacing can also be calculated using Equation 2.7 (Watson, 1994; Davis et. al., 1996):

$$D = \frac{280\sqrt{S}}{W} \qquad or \qquad D = \frac{1000\sqrt{S}}{W}$$

[Equation 2.9]

where,
D is the gully spacing in m/ yards,
S is the gradient in percentage (%), and
W is the width of the paved area in m/ft.

Apart from using the formula above, some authorities determine the gully spacing based on the gradient of roadway. In cases where there is a false crown of d/m being introduced, the spacing between the gullies should be maintained at no more than d/2 m (Watson, 1994).

Gully spacing used by some UK highway authorities are according to Table 2.9:

Table 2.9 – Gully spacing used by highway authorities (Watson, 1994)

Gradient of carriageway	Area to drain into one gully (m^2)
1/200	160
1/150	160
1/100	167
1/80	180
1/60	200
1/40	240
1/30	275
1/20	330
1/15	330

However, based on Design Manual for Road and Bridges (HA 102) – the maximum design spacing (S_p) between adjacent intermediate gratings is given by:

$$S_p = \frac{A_a}{W_e}$$

[Equation 2.10]

where,

W_e is the effective catchment area, and

A_a is the actual area.

The actual area (A_a) that can be drained can be determined using Equation 2.11:

$$A_a = A_{dr}\left(\frac{50}{I}\right) m \times k_n$$

[Equation 2.11]

where,

A_{dr} is the area of the road that may be drained by an intermediate gully for a rainfall intensity of 50mm/h (m^2),

m, maintenance factor,

I, is the design rainfall intensity (mm/h), and

k_n is the roughness and grating efficiency factor.

The area of the road that may be drained (A_{dr}) can be obtained from Tables C2 to C6 [Appendix 2] and each of the table corresponds to the different classes of hydraulic capacities of gully gratings (Type P – T). It is reminded again that the area given is for an intermediate gully with a rainfall intensity of 50mm/h, with maintenance factor (m) of 1, and Manning's coefficient (n) of 0.0017. For other values of rainfall intensity, the area should be multiplied by (50/I). Additionally, for values of n other than 0.017, the flow should be multiplied by (0.017/n).

The maintenance factor that should be assumed can be determined using Table 2.10:

Table 2.10 – Maintenance factor (HA 102/00)

Maintenance factor (m)	Description
1.0	Well maintained urban roads
0.9	Roads subjected to less frequent maintenance
0.8	Roads subjected to substantial leaf falls/ vehicle spillages (e.g sharp roundabouts)
0.7	Sag points on road gradients

The roughness and grating efficiency factor, k_n can be found as in Equation 2.10:

$$k_n = \frac{\left(0.017/n\right) - \left(1 - \left(\eta/100\right)\right)\left(0.017/n\right)^2}{\eta/100}$$

[Equation 2.12]

The water flowing on the road surface can be classified as overland flow whereas water accumulating on the side of the road and kerb are known as gutter flow. From Figure 2.14, it can be seen that maximum discharge for an inlet is not necessarily fully intercepted by the designed gully. A portion of the flow bypasses the inlet into the adjacent gully. The maximum discharge, Q_m can then be described as:

$$Q_m = Q_i + Q_b$$

[Equation 2.13]

where,
Q_i is the intercepted flow, and
Q_b is the bypass flow.

For a given inlet under the partial interception condition, the intercepted flow is dependent on the maximum discharge, cross slope (S_c) and the longitudinal slope (S_L) of the road. These parameters are empirically related as (Wong, 1994; Wong and Moh, 1997):

$$Q_i = K {Q_m}^{k_1} {S_c}^{k_2} {S_L}^{k_3}$$

[Equation 2.14]

where,
K, k_1, k_2 and k_3 are constants. K is not always 1, except for when it is for small discharges (Wong and Moh, 1997). Based on experimental results by (Wong, 1994), under partial interception conditions ($Q_i < Q_m$), K has been found to be 3, for the range of grates (combination inlets) that were tested in Singapore.

In cases where there are only small discharges into the gully, then the maximum discharge for that gully can be intercepted fully and hence:

$$Q_i = Q_m$$

[Equation 2.15]

As can be seen from the cross section the maximum discharge is also a function of the maximum flood width, w. Assuming normal flow conditions and applying the Manning's formula to the vertical kerb section, Q_m (*l/s*) is related to was:

$$Q_m = \frac{315\, S_L^{1/2}\, w^{8/3}}{nz\left[\sqrt{(z^2+1)}+1\right]^{2/3}}$$

[Equation 2.16]

where,

z is the reciprocal of the cross slope of the roadway,

n is the Manning's roughness coefficient of the road surface.

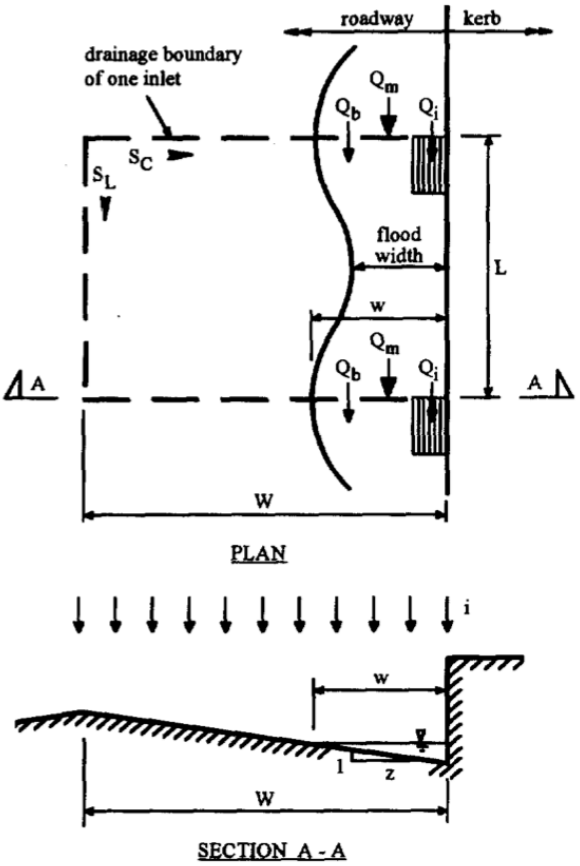

Figure 2.14 – Definition sketch of road drainage inlet system (Wong, 1994; Wong and Moh, 1997)

Whenever an inlet cannot capture the whole approaching flow, the excess flow is added to the amount of flow approaching the next inlet. On the streets where there are numerous inlets, this process will repeat from one inlet to another, increasing the by-pass flow and hence decreasing the efficiency of the downstream inlet. Therefore, the spacing between inlets should not be determined based on the subcatchment flow rate only. This has been proven in a study made by Despatović et. al., (2005) where it was proved that the next inlet was 'overloaded' if it has been placed with an assumption that it should only capture only the flow from its designated catchment. It was also found that another important feature of the bypassing flow, which also contributes to the surplus stormwater, is that it is not concentrated in the vicinity of the kerb, but it spreads laterally from the kerb. If the bypass flow from one inlet is added to the next downstream inlet, the lateral spreading also increases. Due to this assumption, there is also an over-estimation of the sewer size since it is assumed that all of the flow is captured into the sewer.

Although a general review has been conducted for the design of spacing for gullies, it is however not necessary when designing the laboratory system since only one inlet will be used throughout the entire study.

2.5 HYDROPLANING

Hydroplaning is a phenomenon, which occurs when a layer of water builds between the tyres of a vehicle and the road surface leading to the loss of traction, which then results in the loss of control of the vehicle function such as braking, accelerating, and even steering. Hydroplaning is primarily a function of water depth on a road surface and vehicle speed. The increase of the water depth along the road surface (spread) as well as the increase in the speed of the vehicle aggravates the problem of hydroplaning.

There are a number of factors that determines the depth of water on the pavement as identified by Hydraulic Engineering Circular (HEC 22). Factors that are the most significant are the length of the flow path, surface texture, surface slope, as well as

rainfall intensity. However, other factors influencing the hydroplaning phenomena include:

- ✓ Roadway geometrics
- ✓ Vehicle speed
- ✓ Tread depth
- ✓ The inflation pressure, and
- ✓ The conditions of the pavement surface

The factors that contribute to hydroplaning are often dependent on the attributes of the road drainage, which has been elaborated in the parts previously. Therefore, it is not repeated in this section.

2.6 DESIGN STORM

Design storm is an important factor to consider for the overall design of highway drainage. This is because proper design storm and spread are important factors in ensuring that the designed drainage are able to transfer and take the designated amount of runoff appropriately thus maintaining the safety on highways. Peak flows are generally adequate for the design of highway drainage. Peak flows or peak discharge is the maximum amount of runoff flowing out of a catchment area at one particular time. The most commonly used method to determine peak discharge is through the use of a Rational Method, for example the Wallingford Procedure (1981) and HEC 22. The Rational formula is of the form:

$$Q = \frac{CIA}{K_u}$$

[Equation 2.17]

where,

Q is the flow (m^3/s),

C is a dimensionless runoff coefficient [Table 2.11],

I is rainfall intensity (mm/h),

A is the drainage area (m^2), and
K_u is a unit conversion factor.

It should be noted that there are assumptions inherent in adopting the Rational Method. The accuracy of the Rational Method is limited to these assumptions. The assumptions are outlined as follows:

- Peak flow occurs when the entire catchment contributes to the flow, and that the catchment characteristics are homogenous.
- Rainfall intensity is the same over the entire drainage area.
- Rainfall intensity is uniform over time duration equal to the time of concentration, t_c. The time of concentration is the time required for water to travel from the hydraulically most remote point of the basin to the outlet.
- Frequency of the computed peak flow is the same as that of the rainfall intensity, i.e., the 10-year rainfall intensity is assumed to produce the 10-year peak flow.
- The coefficient of runoff is also the same for all storms of all recurrence probabilities.

The accuracy of Rational Formula decreases with the increase of the area due to these assumptions, therefore it is not recommended for drainage areas larger than 80 ha (200 ac).

The use of Rational Method is often extensively used in both in the US and the UK, however the determination of rainfall intensity is slightly different. The knowledge of the intensity of rainfall events is significant because it affects the selection of design frequency and spread (HEC22) and is one of the important parameters affecting peak discharge. The Rational Method that is opted by HEC 22 (US) obtains the rainfall intensity, duration, and frequency based on the regional IDF curves developed through frequency analysis of rainfall events for thousands of rainfall gauges for many jurisdictions throughout the United States. The IDF curve provides a summary of the respective site rainfall characteristics by relating storm duration and exceedence probability (frequency) to rainfall intensity (assumed constant over the duration). Figure 2.15 illustrates an example of an IDF curve.

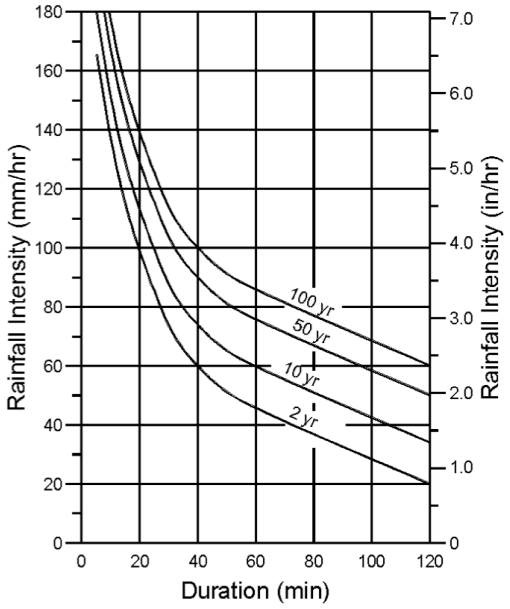

Figure 2.15 – An example of an IDF curve (HEC 22)

In the UK, the Wallingford Procedure (1983) gives full details on the design rainfall for use in urban drainage models, to derive the depth of rain in storms for the whole range of durations and return periods. These may be derived from two parameters: the depth of rain in 60 minutes for a return period of 5 years (M5-60 parameter) and the ratio between M5-60 and M5-2 day (r parameter). These parameters were plotted on maps for the whole of the UK and using these values for any location, the statistical relationships (growth factors) can be used to calculate rainfall depths for durations from 5 minutes to 48 hours, and for return periods from 1 year to 100 years. As a consequence, IDF curves may be produced for any location in the UK. In design, it is usual for the rainfall duration to equal the time of concentration for the catchment, which is the time taken for the rainfall to flow across the catchment surface plus the time it takes for the rainfall to travel through the drainage pipes to the downstream end of the catchment. Hence, for a selected return period, the rainfall intensity for the duration equal to the time of concentration may be estimated. This intensity is used together with an equation to predict the rainfall runoff, for example the rational method.

Note - Synthetic storm profiles may subsequently be derived but these profiles, together with the application of time series rainfall, are considered beyond the scope of this thesis, as only constant flowrates have been used in the experimental study.

When using the rational method it is necessary to select an appropriate runoff coefficient and typical runoff coefficients are given in Appendix 3.

Alternatively, the design rainfall intensity, I (mm/hr), for a storm with a return period of N years, as described in HA 37/97, can be determined using the following equation:

$$I = 32.7\ (N - 0.4)^{0.223}\ \frac{(T - 0.4)^{0.565}}{T}\ (2minM5)$$

[Equation 2.18]

where,

T is the critical storm duration (min), and

2minM5 is the rainfall depth (mm) occurring at the site in a period of 2 minutes with return period of 5 years [Appendix 4].

The critical storm (T) or inlet concentration time is defined as the length of time taken from the most hydraulically distant point of the catchment to the point of reference downstream (HEC12). This in mathematical terms can be determined by the sum of time taken for water to travel from the furthest point on the road surface to the kerb, t_s and the time along the kerb to the gully t_g as shown in the Equation 2.19. The critical storm duration usually taken as 5 minutes. This assumption however should be checked to ensure that it is valid for the shortest and longest drainage lengths between the gullies (HA 37/97). A value of 3 minutes is usually recommended for t_s (HA 102/00). To ensure that the correct rainfall intensity is used in the design phase, it is crucial that the critical storm is determined prior to estimating rainfall intensity.

$$T = t_s + t_g$$

[Equation 2.19]

Inlet concentration time is an important but difficult parameter to estimate. Current practice estimates inlet concentration time rather arbitrarily since there are various formulas, which can be adopted to determine the inlet concentration time. A study by (Akan, 1984) proposes a physics-based but simpler method to calculate inlet concentration times but the Design Manual for Road and Bridges adopts the method

mentioned above. The recommended storm return period for the use in the UK as recommended by (Watson, 1994) is mentioned in Table 2.11:

Table 2.11– Recommended storm periods to be used in the UK (Watson, 1994)

Nature of site	Return period
Sites with average ground slopes of > 1:100	1 years
Sites with average ground slopes of 1:100 or flatter	2 years
Sites where the consequences of flooding will be severe	5 years

2.7 INUNDATION MODELS

Flooding as defined by BS EN 752 is a condition where wastewater and/or surface water escapes from or cannot enter a drain or sewer system and either remains on the surface or enters buildings. On the other hand, surcharge has been defined as a condition in which wastewater and/or surface water is held under pressure within a gravity drain or sewer system but does not escape to the surface to cause flooding (Schmitt et. al., 2004). The phenomenon of urban flooding caused by the surcharged sewer systems in urban drainage systems leads to the necessity of an integrated model – dual drainage model.

The initial approach to urban drainage modelling was to establish the link between rainfall and observed flow whilst using a number of different non-physical parameters. Improvements were made to the first models and were incorporated into the model in smaller parts of the catchments down to the level of one sub-catchment. After careful calibration of the model on the basis of a single catchment with measured rainfalls and outflows, it was possible to estimate the sewer system response to a certain range of storms. However, the model accuracy for heavy storms is questionable and their lack of non-physical parameters gives only so much credibility to the model (Djordjević et. al., 1999).

To overcome this, the simulation of some physical processes – rainfall to runoff was introduced into the model. With the introduction of the physical processes, the modelling process was divided into two main phases (Djordjević et. al., 1999):

- Initial process in which it deals with the rainfall and its conversion into effective runoff from each sub-catchment whilst taking into consideration soil infiltration, retention capacities of the surface, land use, flow along the sub-catchment and others as input for the second process.
- The second process deals with the flow in the sewer system while looking into its interaction with the network of pipes, manholes, and control structures.

The links between the two processes are unidirectional. However, from this it has been pointed out that the lack of interaction between the surface and underground flow components as well as the coarse surface description is the two weakest point of existing flood models (Djordjević et. al., 1999).

The traditional one-phase sewerage-network model may be able to simulate the drainage system correctly until there is no overflow from the stormwater inlet or manhole. When overflow exists due to insufficient capacity of the drainage system, then reproducing the actual flooding extent using the traditional one-phase model would be difficult. The study by (Mark et. al., 2004) has looked into the potential and limitations of 1D modelling in further detail. On the other hand, the traditional 2D models that simulate surface flooding resulting from storm conditions usually does not consider sewerage network and tends to predict higher flood extents than reality (Dey and Kamioka, 2007).

In regards to the processes and distinct stages of surcharged sewer systems and urban flooding, simulation models for flood risk analysis are required to accurately describe (Schmitt et. al., 2005):

- The transition from free surface flow to pressure flow in the sewer pipes
- The rise of water level above the ground
- The occurrence of surface flow during surface flooding
- The interaction between surface flow and pressurized sewer flow

Dual drainage modelling has been described by (Djordjević et al., 1999) as an approach to rainfall runoff simulation in which the numerical model takes into account not only the surface flow but also with surcharged sewer systems and its interaction. A dual drainage model consists of double network formed by an upper network (major system) which consists of open channels (street gutters), natural flow paths, retention basins in local depressions or artificial control structures such as brinks and ponds and a lower network (minor system) of closed conduits (sewer pipes) with known stormwater inlets and manholes (Djordjević et. al., 1999; Nasello and Tucciarelli, 2005).

Dual drainage modelling can be illustrated by Figure 2.16 – which shows the interaction between the surface and sewer flow as well as the flow components above and below ground.

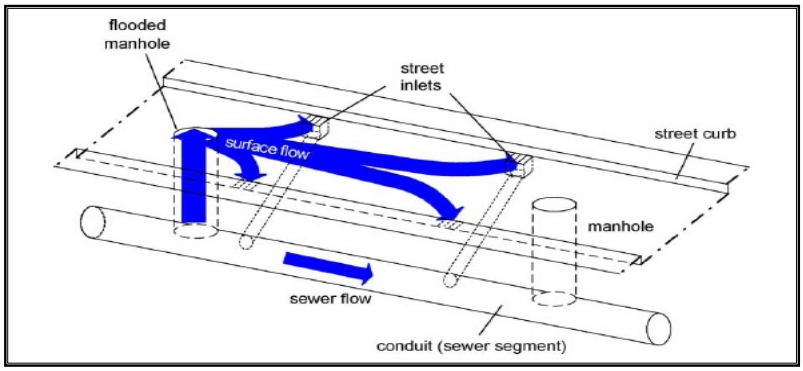

Figure 2.16 – Dual drainage concept showing the interaction between the surface and sewer flow (Schmitt et. al., 2004)

There are three fundamental assumptions with relation to dual urban drainage model according to (Djordjević et. al., 1999). The three assumptions are:

(i) Due to limited capacity of the inlet, the sewer system will not necessarily be able to drain all runoff.
(ii) When a part of the system is pressurised, water in that system is able to go out of the system.
(iii) Surface water that cannot be drained by a sewer system is to be routed further downstream and that the direction of the surface flow can differ from that of the sewer pipes. In this case, the surface flow has to follow the surface flow paths.

It is also often assumed in software modelling that stormwater inlet intercepts all of the surface runoff computed to reach the designated inlet. However, in reality this is usually not the case. The amount of runoff intercepted by an inlet are governed by many factors mainly the design of the inlet and the characteristics of the catchment area such as the crossfall and longitudinal slope of the road. Normally, under design conditions of heavy storms, only a part of the surface runoff at an inlet site gets into the inlet and the rest bypasses the inlet and adds to the downstream surface runoff. Only for light storms can an inlet intercept all of the intended runoff. Thus, most models do not simulate the real

inlet inflow hydrograph and consequently the flow in the sewer system. This error is more critical for larger storms as the by-passed flow is larger (Woo, 1984). Therefore, the understanding of the performance of stormwater inlets is essential for flood prediction purposes.

Water from the pipe system may flow into the streets through gullies when surface flooding takes place. On the other hand, when water in the pipe system is drained, surface-flooding water in the street system can flow through the gullies into the sewer system. In urban flood models, gullies are usually modelled as a broad-crested weir, where the length of the weir is represented by the perimeter of the gully and the weir crest is set at the bottom of the road level. Discharges through the gully are described using the common weir equation, which can represent both the free and submerged flows. The use of a weir to describe the connection between the pipes and the street systems ensures that a restriction applies for both, water from the streets entering the pipe system as well as for the water flowing from the pipes into the streets.

When the sewer system becomes fully surcharged, it is more accurate to use an orifice equation instead of the weir equation. This is because in a fully surcharged condition, the driving head is the difference in head between the pressure in the sewer and the water level on the surface. However, this equation is not really accurate in cases where the orifice is not full flowing (Mark et. al., 2004).

In the process of modelling and managing the inflow of stormwater into sewer systems and infiltration into sanitary sewers, it is necessary to predict the flow rate into the sewers. This flow will depend on whether or not these flow devices are operating under a ponding situation or are subjected to a flowing state (Mustaffa et. al., 2006). A study by Mustaffa et. al., (2006) attempted to determine the usefulness and practicality of describing the flow through stormwater inlets which were used in the City of Edmonton by using the orifice type equation when the gratings are submerged, and the effect of the flow on the discharge coefficient.

2.8 HYDRAULIC PERFORMANCE OF GULLY INLETS

There are 3 types of linkages considered for applying the discharge equations. The three linkages are as below (Chen et. al., 2007):

- **Free weir linkage**

The free weir equation is adopted when the crest elevation (z_{crest}) is between the values of the upstream water level (h_u) and downstream water level (h_D).

$$h_u < z_{crest} < h_D \qquad \text{hence} \quad Q = -/+ [h_{mh} - h_{2d}] C_w w\sqrt{2g} (h_u - z_{crest})^{3/2}$$

[Equation 2.20]

- **Submerged weir linkage**

The submerged weir equation is used when both water levels at manhole and overland grid are greater than the crest elevation and the upstream water depth above the crest ($h_u - z_{crest}$) is less than A_{mh}/w, where A_{mh} is the manhole area (m^2).

$$(h_u - z_{crest}) \leq A_{mh}/w \quad \text{hence} \quad Q = -/+ [h_{mh} - h_{2d}] C_w w\sqrt{2g} (h_u - z_{crest})(h_u - h_D)^{1/2}$$

[Equation 2.21]

- **Orifice linkage**

The orifice equation is used when the manhole is considered to be fully submerged. This occurs when the upstream weir depth above the crest ($h_u - z_{crest}$) is greater than the A_{mh}/w.

$$(h_u - z_{crest}) > A_{mh}/w \quad \text{hence} \quad Q = -/+ [h_{mh} - h_{2d}] C_o A_{mh}\sqrt{2g} (h_u - h_D)^{1/2}$$

[Equation 2.22]

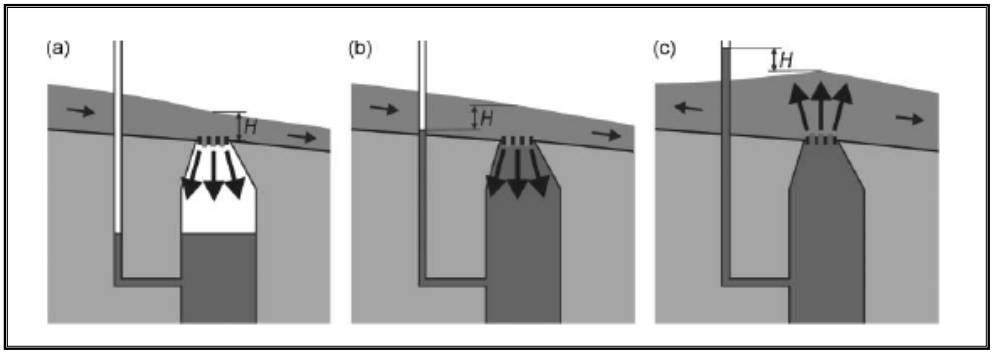

Figure 2.17 The types of linkages – (a) free weir linkage, (b) submerged weir linkage and (c) orifice-type linkage (Djordjevic et. al., 2005)

In this case, it is assumed that the crest level is the street bottom level whereas the head is defined by the gully water level. If submerged, then a reduction coefficient is applied to the discharge depending on the surface water level (Bettez et. al., 2001). On the other hand, when the gully is fully surcharged, the difference between the pressurized gully and the surface water level is taken as the driving head. The above review has highlighted that there has been considerable research to assess the performance of gully systems and to provide design guidance. However, there is still a concise lack of information on the correct C_d and the interaction between the above and below ground drainage systems. Hence, an experimental study has been set up to address this issue. The results of this study will be the need to improve understanding of the discharge coefficients in these equations.

A study by Mark et. al., (2004) identified some of the technical requirements in an urban flood model based on the physical processes involved in urban flooding. The requirements are listed as below:

- Dynamic flow description

In instances when urban flooding occurs, surface water can flow in both street and pipe systems with flow exchange between these two systems. This means that simulation of backwater effects is needed in modelling of urban flooding. By using a dynamic wave model, the model includes backwater effects and surcharge from manhole including rapid change of water level.

- Parallel flow routing

While surface flooding takes place, water from the pipe systems flow through gullies into the streets. Flows along the streets can be in either direction, which is along the gradient of the street or against it. It is not necessary that the flow direction in the street have to be the same as the flow direction in the pipe systems.

- GIS interface

GIS is an important tool for simulation of urban flooding. It provides input data and displays simulation results. By application of GIS with DEM of the study area, surface storage can be computed for the purpose of simulating inundation.

2.9 OTHER DEVELOPMENTS

Many studies have been made to improve the existing dual urban drainage model. Boonya-aroonnet et. al., (2007) raised concerns on how to realistically model overland flow that takes place during heavy storms when water can flow freely into and from the underground sewer network, along streets which urban catchment which has different preferential paths from the streets.

Other advancement of the inundation models include the development of GIS based pathway model for surface flooding and interfaced with surcharged sewer model (Boonya-aroonnet et al., 2007), the study of effects of micro-topography with the flooding potential associated with the failure of a number of inlets in the system (Aronica and Lanza, 2005), the study of the hydraulic behaviour of stormwater to improve the design of drainage inlet systems due to the lack of inlet (Russo et al., 2005), and many others. Amongst recent efforts to describe flooding process more accurately was attempted by Chen et. al., (2010) where the SIPSON/UIM model, an integrated 1D sewer and 2D overland flow was applied to numerical modelling in order to analyse the impact caused by both pluvial and fluvial flooding. Pluvial and fluvial flooding is often considered separately therefore this was an attempt to predict the extent of the surface flooding and identify the worst scenario of the studied catchment taking into consideration the combined effect of both fluvial and pluvial flooding. Another study by

Leandro et. al., (2011) attempted to resolve the absence of field data for the calibration/validation of 1D/1D models using the results of a 1D/2D models. This study was successful in calibrating a faster 1D/1D models and was able to map the 1D/2D flood maximum extent well.

In terms of recent developments with regards to stormwater inlets, studies of retrofitted inserts as well as decentralized inlet-filtration-systems (INNOLET) have proven to be effective and useful as a guide to further develop and improvise on the existing stormwater inlet technologies. A study by Lau et. al., (2001) defines catch basins inserts as devices that can be placed into a catch basin or stormwater inlets which has been designed to reduce pollutant discharge to the receiving water. Although there have been many catch basin inserts which has been marketed, the performance of the inserts to determine the efficiency of pollutant removal has not yet been properly evaluated.

Decentralized inlet-filtration-systems – INNOLET (Sommer et al., 2008) are also one of the currently developed retrofitting methods for reducing the high pollution of runoff from heavily frequented streets and highways. It is a retrofit method, which is able to retain a considerable amount of load – Total Suspended Solid (TSS) mainly from the sewer system. Other studies are the design of grates using decay functions which converts a single grate clogging factor into a multiple-grate clogging factor (Guo, 2000), design of kerb opening inlets using a decay-based clogging factor (Guo, 2006).
The above review has highlighted that there has been considerable research to assess the performance of gully systems and to provide design guidance. In respect of practice there is a need to incorporate this performance understanding into models and this generally requires an accurate value of C_d. The review has highlighted that there is still a concise lack of information on the correct C_d to be used and that this is especially so when the interaction between above and below ground drainage systems is considered. Hence an experimental study has been set up to address these issues and is presented in the following chapter.

CHAPTER 3
LABORATORY SYSTEM

3.1 LABORATORY DESCRIPTION

For the purpose of this experimental programme, a full-scale laboratory system was designed to mimic the hydraulic interaction between the above and below ground drainage system via gully inlets. This system was designed with a small catchment area. The laboratory system consists of a testing platform that is connected to a smaller tank on both left and right hand side of the platform [Figure 3.1 and 3.3] to serve as an inlet/outlet tank depending on the system to be tested. This point forward – these tanks will be referred to as inlet or outlet tanks accordingly in order to avoid confusion. The aforementioned systems will be discussed further in the sections below [3.1.1 – 3.1.3].

The testing platform is a rectangular platform 4.27m (L) x 1.83m (W) and drains a total area of 7.814 m^2. The dimension for the inlet and outlet tank itself is 0.61m (L) x 2.44m (W). Both of these tanks are each equipped with a sluice gate to allow control of the hydraulic depth on the testing platform. Both the outlet tank and the outflow from the gully system itself are each connected to a measuring tank, which allows manual measurements of flowrate to be taken. Each of the concrete measuring tank have the internal dimensions of 2m (L) x 1.25m (W) x 0.75m (D) and was an existing feature in the hydraulic laboratory (Unwin, 2008). Both of the measuring tanks are situated at the lower level of the hydraulic laboratory where the overall testing rig was built on.

The flow for the entire system is provided by an overhead tank and is circulated through the entire system before being transferred into a sump to be pumped back to the overhead tank again. The sump is also of concrete material and have an internal dimension of 2.5m (L) x 2m (W) x 1m (D) and was already an existing feature in the hydraulic laboratory (Unwin, 2008).

Figure 3.1 shows the basic dimensions of the testing platform and connections to the laboratory rig.

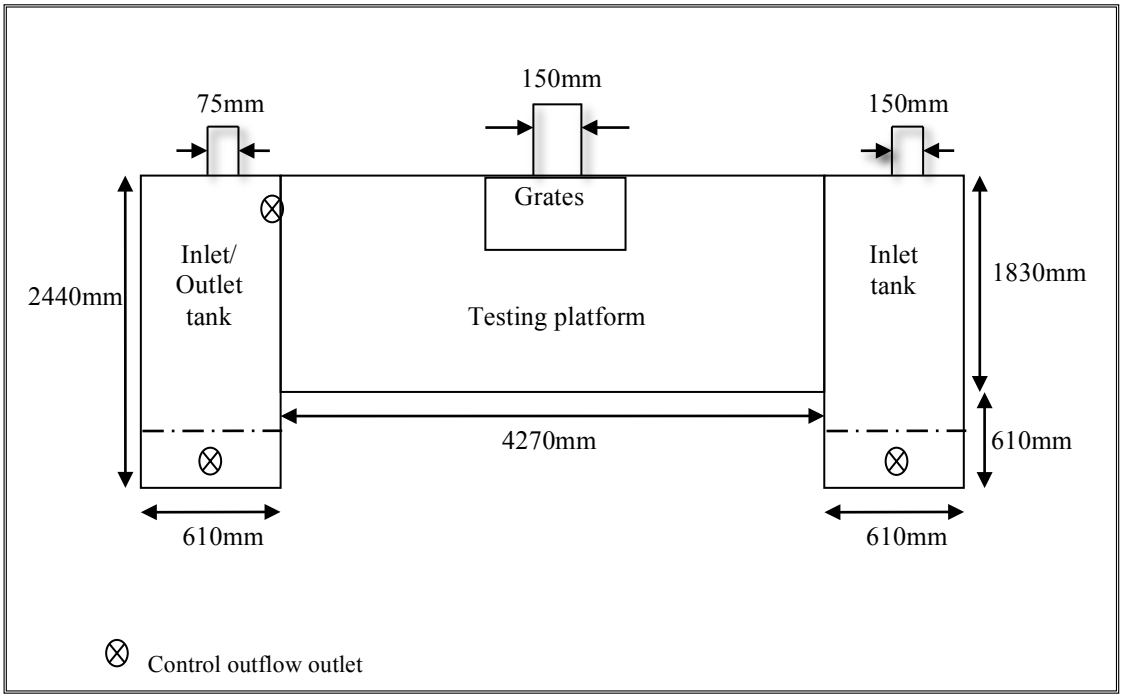

Figure 3.1 – Dimensions of the laboratory rig

The testing platform of the rig was initially designed as a flatbed to serve as an arbitrary datum. At a later phase of the study, longitudinal slopes were later incorporated to allow different representations of road conditions to be studied. Figure 3.2 shows the overall view of the rig and of the initial testing platform (flat bed).

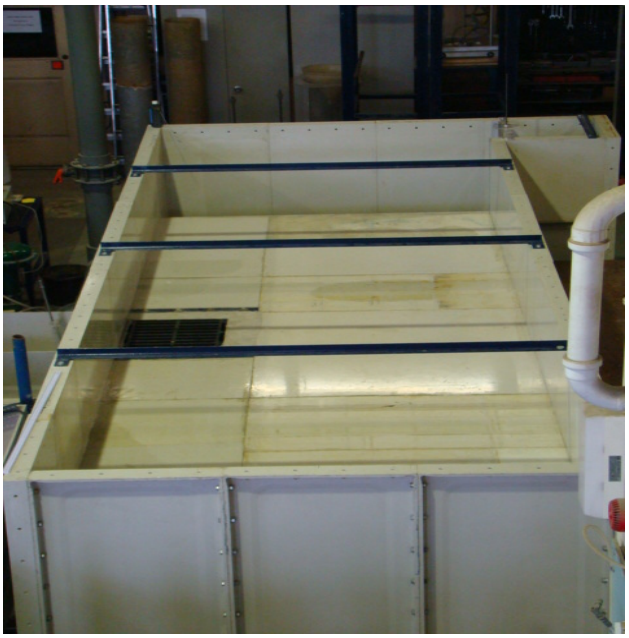

Figure 3.2 – Initial testing platform (Flat bed)

Figure 3.3 and 3.4 show one of the inlet/outlet tanks during a testing session and the sluice gate that is equipped on both the inlet and outlet tank respectively.

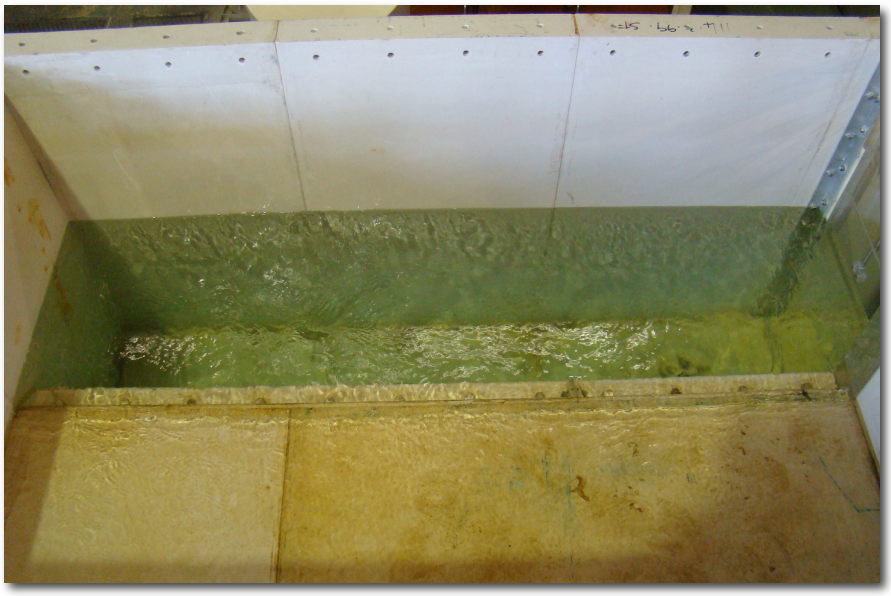

Figure 3.3 – Inlet/outlet tank during a testing session

Figure 3.4 – Sluice gate that was used on both the smaller tanks to enable control of the hydraulic depth on the testing platform.

Three different longitudinal slopes (S_L) were tested – horizontal, 1 in 100 and 1 in 30. The selection of the longitudinal slopes is as justified in Chapter 2 [Section 2.3.6]. Figure 3.5 is a representation of the longitudinal gradient (S_L) that was later incorporated onto the testing platform.

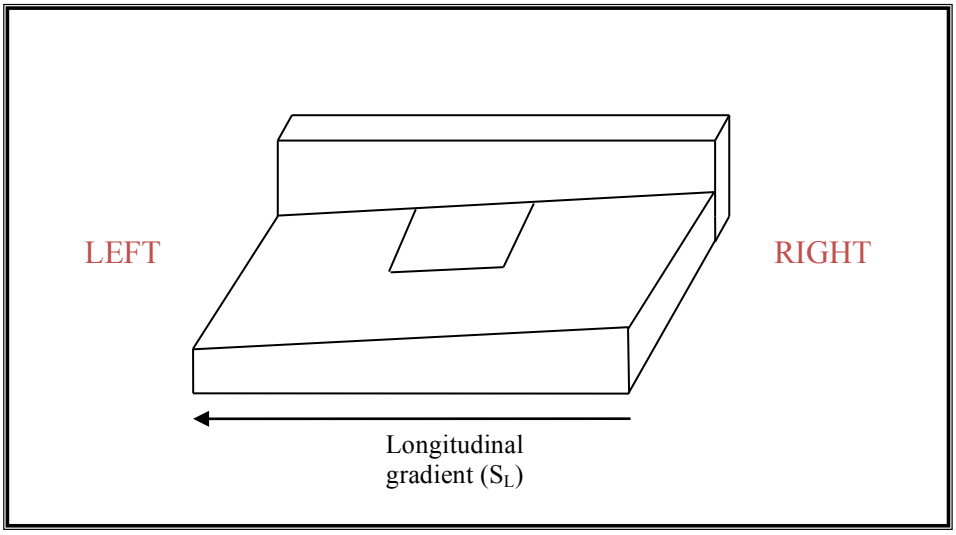

Figure 3.5 – Longitudinal gradient of the testing platform

Due to the walls of the rig, it was not possible to have a cross section view of the slopes on the testing platform itself. Therefore, a glimpse of the sloping platform is given [Figure 3.6 and 3.7] from two different camera angles – plan view and a second camera that focuses more on the flow at the gully grates. The different sloping conditions can easily be differentiated in the pictures since the retrofitted slopes used a slightly different material than the flat bed.

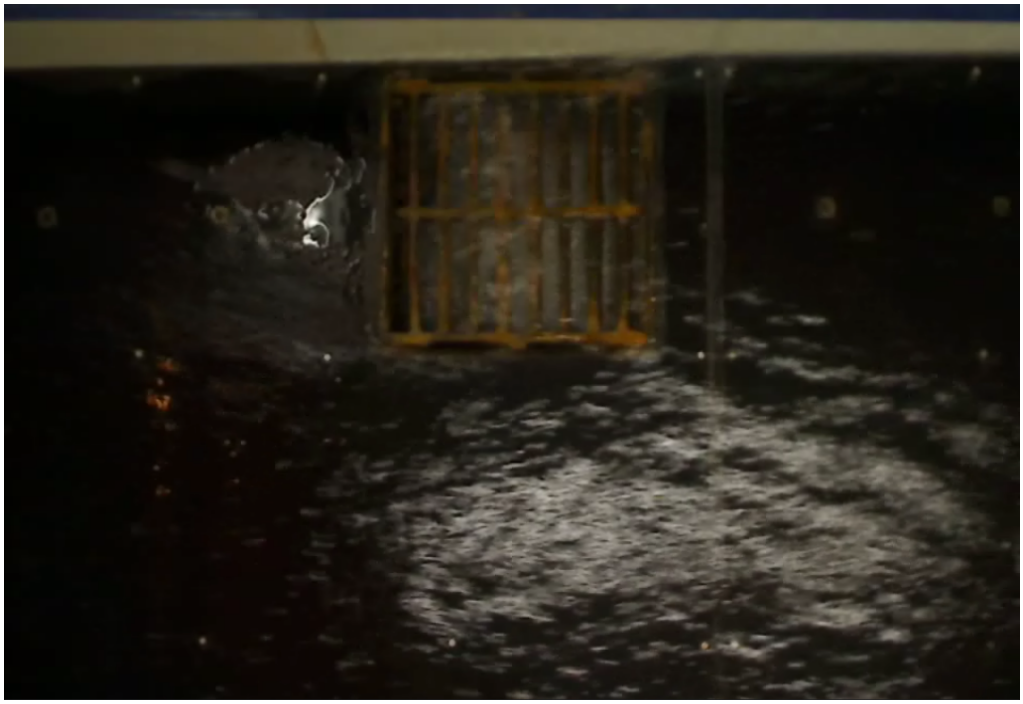

Figure 3.6 – Sloping testing platform (1/30) – plan view

Figure 3.7 – Sloping testing platform (1/30) – detailed view of the flow onto the gully grates

Existing structure in the laboratory allows for two range of flowrate to be supplied to the rig through two different pumps:

- 0 – 40 *l/s* pump
- 0 – 80 *l/s* pump

In the initial set up of the laboratory programme, both of these pumps were used. After much upgrade was retrofitted into the system, the flowrate for this experimental programme was decided to be between 0 – 50 *l*/s due to the limited capacity of the system to hold large amounts of water. This is because the size of the outlet pipe limits the outflow therefore minimising the volume of water that the rig can take at a time. Therefore, in later parts of the experimental programme, only the 0-80 *l/s* pump was used and was calibrated against. Calibration procedures and results will be discussed in the following chapter [Chapter 4].

3.1.1 GULLY SYSTEM

As mentioned previously, this laboratory system can be altered to mimic 3 different gully systems that was the subject of study. The following sections [Section 3.1.1.1 - 3.1.1.3] will attempt to explain these systems further.

3.1.1.1 Terminal system

As mentioned previously [Section 2.2], a terminal system is a system which does not permit any significant amount of flow to past through. Therefore, in this type of system, there is only one outlet in use – which is through the gully. The flow from the overhead tank is transferred into the primary inlet tank and then towards the gully pot underneath the testing platform through the stormwater inlets/gully grates situated on the testing platform [Figure 3.7]. Some of the flow is intercepted by the gully, which then leaves the gully pot via a 150mm diameter outlet pipe into a measuring tank [no.1] whereas the remaining flow will flow into the outlet tank at the far end of the testing rig.

When this type of system is in use, the outflow outlet of the tank at the far end of the testing platform will be manually closed therefore allowing the tank to serve as a retention facility or as a secondary inlet for the system [Figure 3.8 and Figure 3.10]. This is because when the maximum capacity of the outlet tank is filled, it will overflow back onto the testing platform again and will be collected by the gully hence fulfilling the criteria of a terminal gully system whereby all of the approaching flow (Q_a) will solely be intercepted by the gully system.

In this case, the approaching flow (Q_a) will be equivalent to the intercepted flow (Q_i) and some flow that is lost in the system.

$$Q_a = Q_i + Q_{(loss\ in\ the\ system)}$$

[Equation 3.1]

Small differences were observed to occur between the calibrated flowrate and the actual measured flowrate. These small differences were attributed to slight measurement errors. To ensure that these losses were minimised, manual measurements of the intercepted flow were recorded at different intervals of the duration of the test and then compared to the inflow. This resulted in extremely small differences, which were considered insignificant.

Figure 3.8 shows the schematics of a terminal gully and the corresponding pipe connections in use during testing:

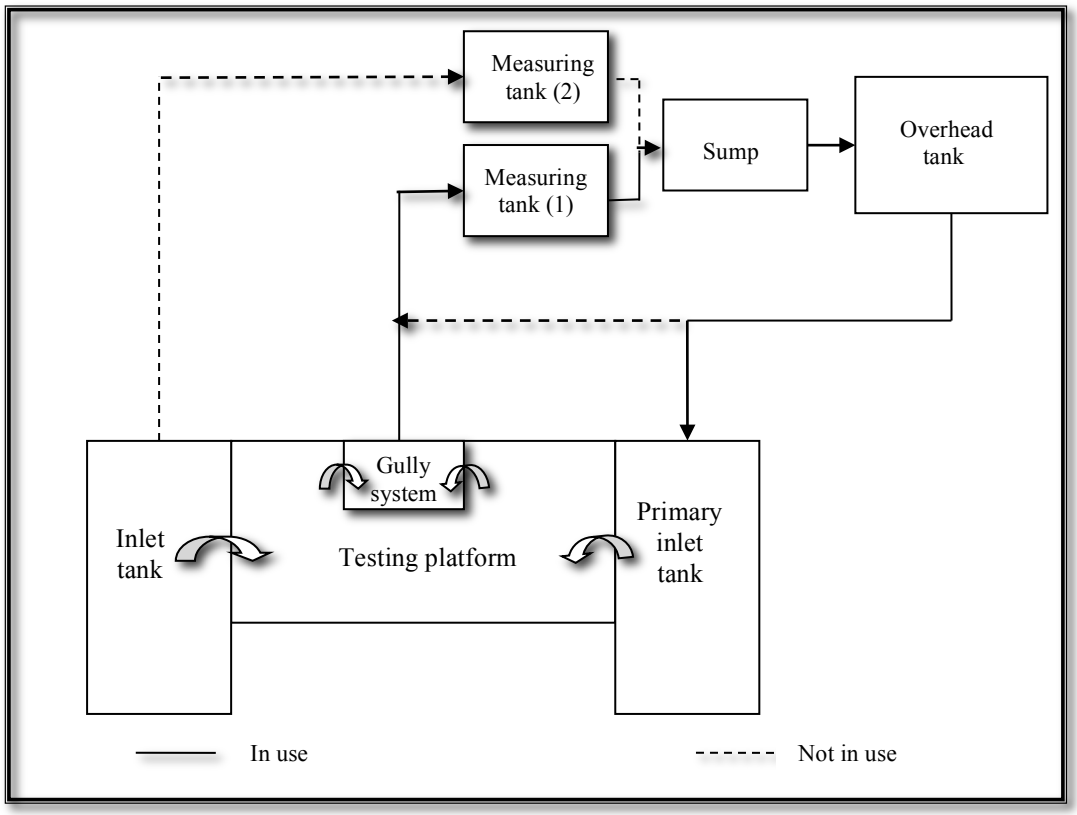

Figure 3.8 – Schematics of a terminal gully system and corresponding pipe connections

Figure 3.9 and 3.10 shows an event during a terminal test – the primary inlet tank and the tank on the left hand side when it serves as a secondary inlet tank.

Figure 3.9 – Primary inlet tank during the terminal tests

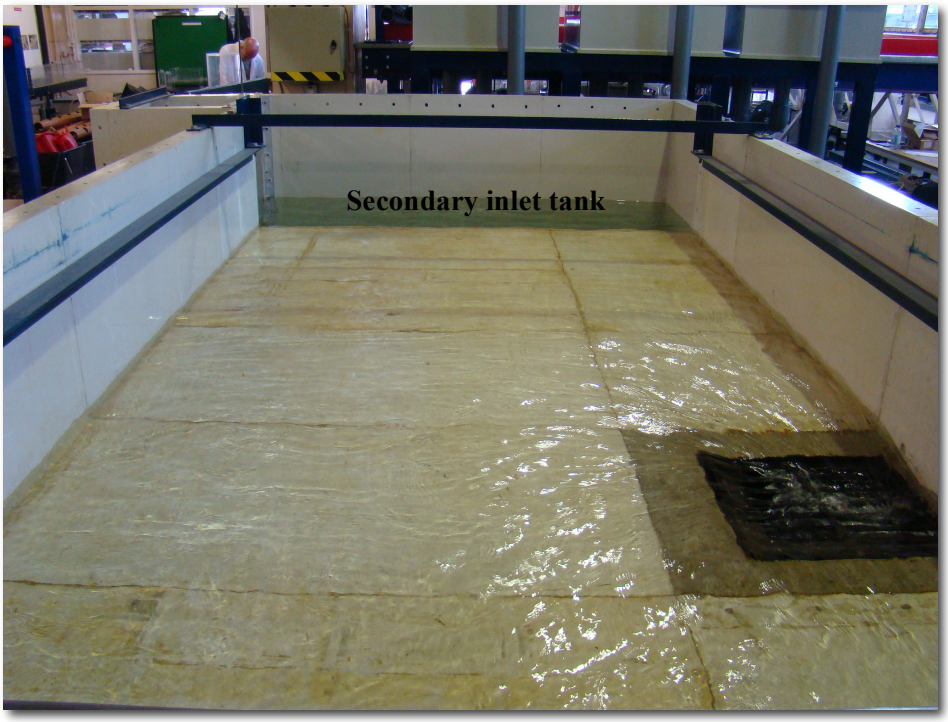

Figure 3.10 – The outlet tank acting as a secondary inlet tank during the terminal test

3.1.1.2 Intermediate system

Intermediate systems are gully system, which permits a portion of the approaching flow to flow past the system and into the next downstream gully. Therefore, in this type of system, there are two consecutive outlets in use. The first would be the gully system itself whereas the second would be the outlet tank at the far end of the testing platform. In this case, the outlet tank acts as a downstream gully system. The fundamental of the system is the same as a terminal system where the only difference is that the bypassed flow is not passed back onto the testing platform. Instead, it is collected separately in the second measuring tank.

In summary, the approaching flow (Q_a) is the total of the intercepted flow (Q_i), bypassed flow (Q_b) and some loss in the system.

$$Q_a = Q_i + Q_b + Q_{(loss\ in\ the\ system)}$$

[Equation 3.2]

Figure 3.11 shows the schematic drawing of the laboratory system, which describes the intermediate gully system.

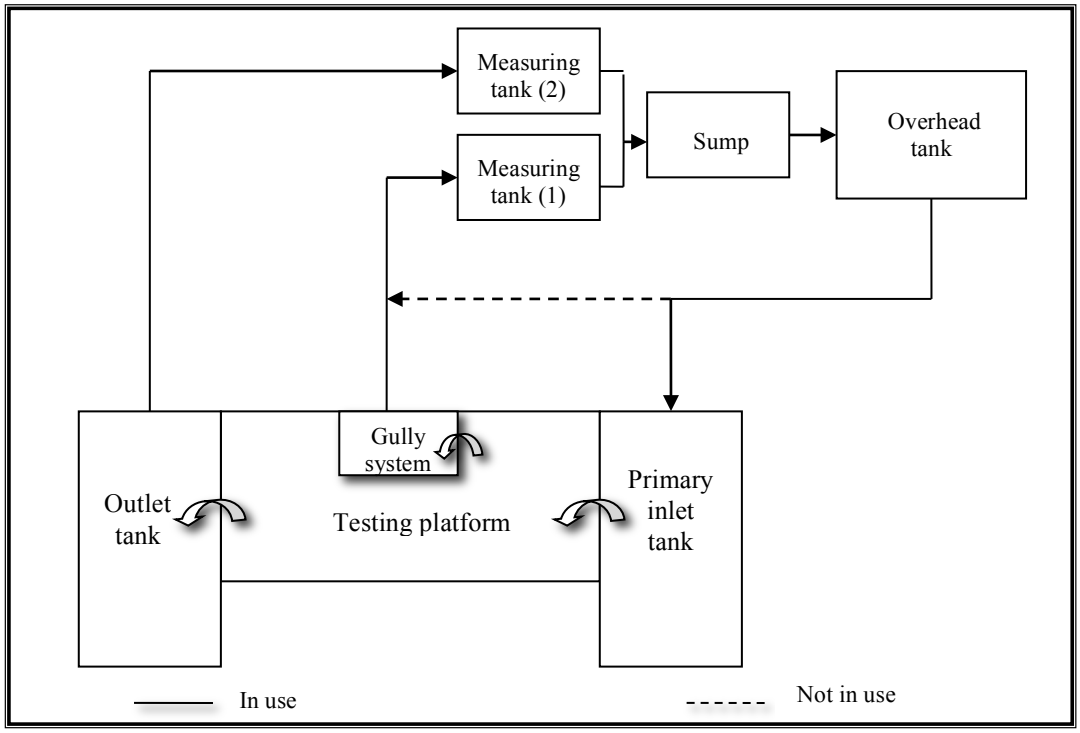

Figure 3.11 – Schematics of an intermediate gully system and corresponding pipe connections

Figure 3.12 shows an event during an intermediate test – where the outlets on the outlet tank (left) are left opened so that the volume can be collected to represent the bypassed flow (Q_b) and therefore mimic a downstream gully system in real life condition.

Figure 3.12 – Outlet tank – mimics a downstream gully system

3.1.1.3 Surcharged system

For the purpose of this experimental programme, surcharged system is a gully system, which has two inlets flow into the laboratory rig. The first is the flow from the primary inlet tank and the other is a secondary flow that comes from the gully system itself. The secondary flow is provided from the overhead tank as well but through a different pipe that is connected directly to the gully pot. During experimental tests for this system – the valve located on the far end of the outlet pipe of the gully pot is set to close so that all of the flow are forced back into the gully pot and hence onto the testing platform. This mimic a surcharge condition in a real gully system – when the drain have reached its capacity and begins to flow onto roads and highways. There is only one allowable outflow from the system – which is through the outlet tank. This outflow is then collected in measuring tank (2) [Figure 3.13].

Figure 3.13 shows the schematic drawing of the laboratory system, which summarises the surcharged gully system.

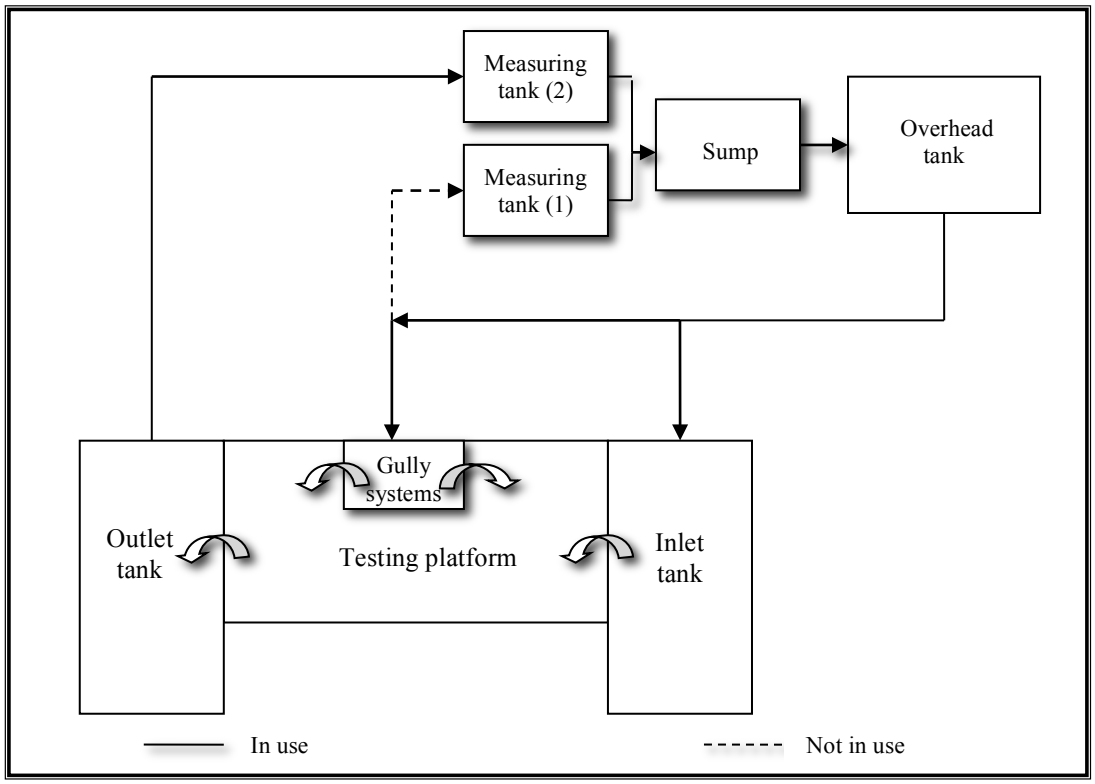

Figure 3.13 – Schematics of a surcharged gully system and the corresponding pipe connections

Figure 3.14 demonstrates a surcharged system during a testing session – when the gully pot has reached its capacity and hence begins to flood the testing platform.

Figure 3.14 – Surcharged system

3.1.2 Gully Pot

In this experimental programme, the gully pot selected is the more commonly used gully type, which is the trapped gully with spigot outlet (BS5911: 2004). Trapped gullies are gullies that are designed to have an outlet that forms a water seal and a rodding eye, which helps to retain oil within the gully pot [Figure 3.15]. Gully pot with the dimension of 375mm in diameter and 750mm in nominal depth was used in this experimental testing. Detailed properties of the gully are as mentioned in Table 3.1. Figure 3.15 and 3.16 shows the gully pot that is used in this experimental programme.

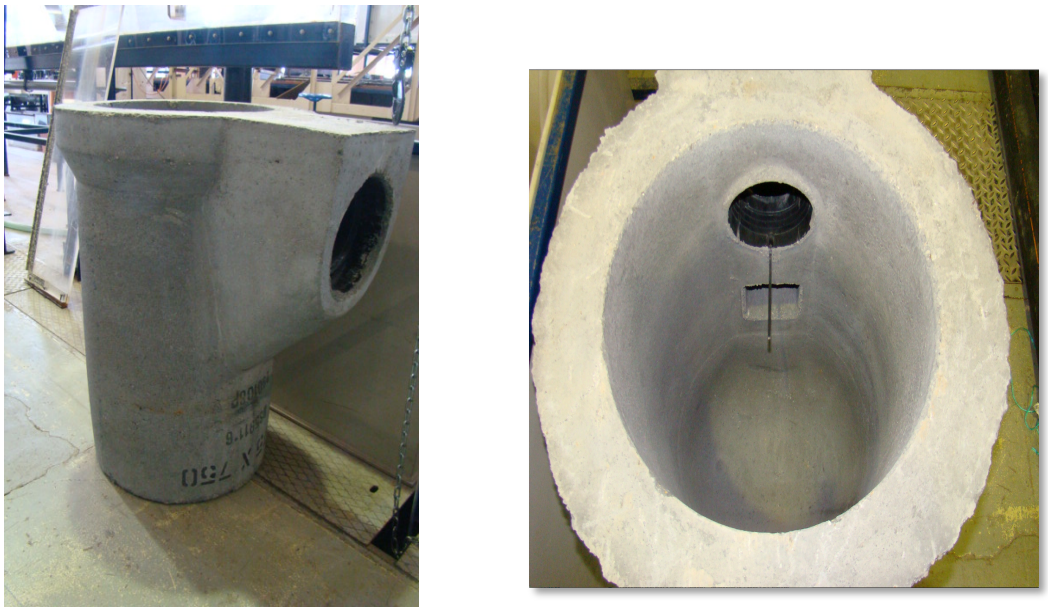

Figure 3.15 - Trapped gully with 150mm diameter outlet

Figure 3.16 shows the outlet (inner and outer view) – that forms the water seal and rodding eye.

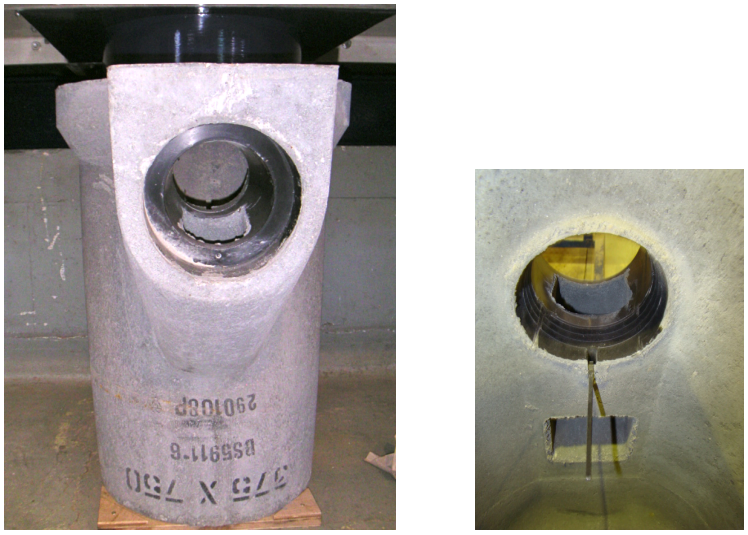

Figure 3.16 – Outlet that forms the water seal and rodding eye

Table 3.1 – Properties of the gully

Internal diameter A (mm)	Internal depth B (mm)	Outlet (mm)	Inside depth to centre of outlet/ rodding eye D (mm)	Outside depth of outlet E (mm)	Dimension of riser F (mm)	Depth of water seal H (mm)	Weight (kg)
375	750	150	148	251	85	85	180

Figure 3.17 is a general representation of the gully as specified by the manufacturer [Milton Precast]. The unit shown is of a 450mm (diameter) x 750mm (nominal depth) gully unit. The gully unit used in this study however is smaller in diameter and its dimensions are as shown in Table 3.1. These dimensions have also been checked against BS5911-6: 2004 and are in accordance to the specifications mentioned. This can also be confirmed with the stamp on the bottom of the gully pot [Figure 3.16]. Actual drawing of the gully and certifications are included in the Appendix section [Appendix 8].

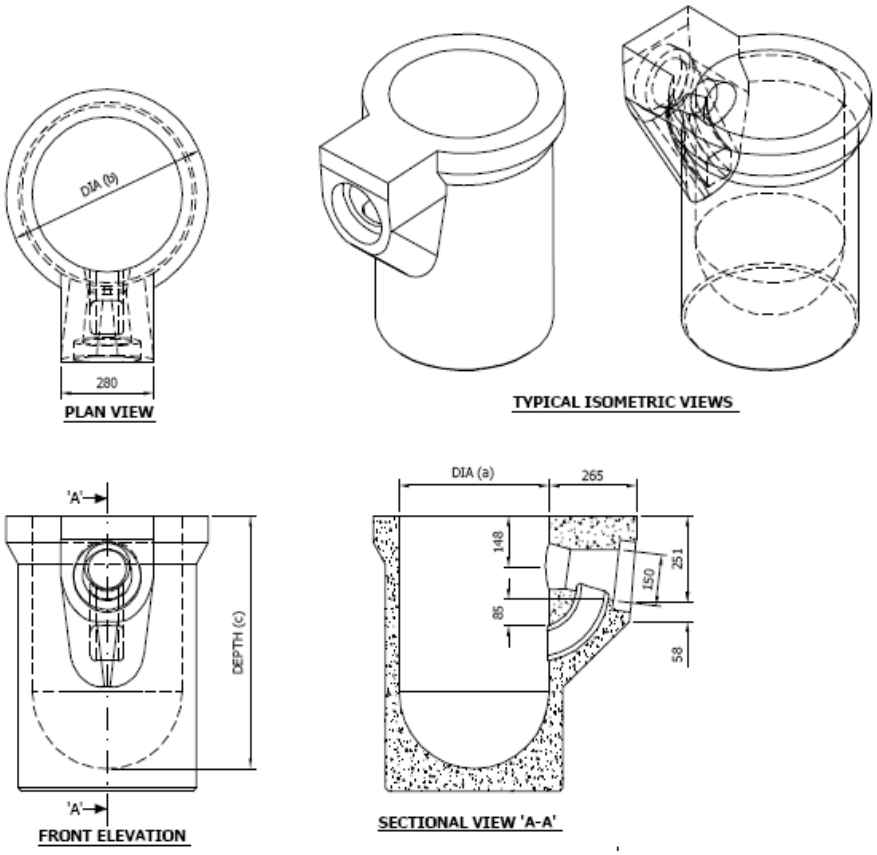

Figure 3.17 – Representations of the properties of the gully system (Milton Precast)

3.1.3 Gully grates

Gully grates according to HA102 are classified based on their hydraulic capacity and are divided to 5 different types which are P, Q, R, S and T [Section 2.3] with their hydraulic capacity decreasing respectively. BS EN 124 has also outlined that in order to ensure a reasonable level of hydraulic capacity, the total waterway area of the slots should not be less than 30% of the clear opening of the grates. The tested grates should also meet the minimum waterway area of 900cm^2 - commonly used in practice in the UK as highlighted in HA 104/02. The loading class selected is for Group 3 (BS EN 124) – C250 that is suitable to be installed in the area of kerbside channels of roads. In the first phase of the study, grate with clear opening of 400mm x 432mm (HA 102 – R) was

used followed by grate with 325mm x 437mm clear opening (HA 102 – S). Refer to Section 2.3 [Chapter 2] for further details regarding the grates.

Figure 3.18 is a representation of the properties of the grates as specified by the manufacturer.

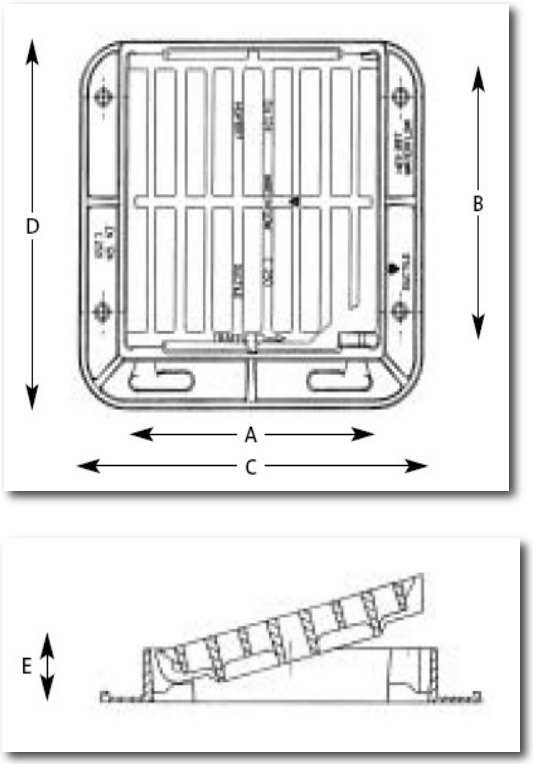

Figure 3.18– Representation of the properties of the grates (St. Gobain Pipelines)

Figure 3.19 and Figure 3.20 shows the grates used in this experimental programme and their properties are as described in Table 3.2.

Table 3.2 – Hydraulic properties of the proposed grates

BS EN 124 loading class	Clear opening A x B (mm)	Over base C x D (mm)	Depth E (mm)	Waterway area (cm^2)	Total mass (kg)	HA 102 reference
C250	325 x 437	475 x 524	75	933	29	S
C250	400 x 432	550 x 530	75	1128	33	R

Figure 3.19 – Grate with 325mm x 437mm clear opening (HA 102 reference – S)

Figure 3.20 – Grate with 400mm x 432mm clear opening (HA 102 reference – R)

3.2 LABORATORY EQUIPMENT

3.2.1 Point- gauge measuring equipment

In the initial stages of the experimental programme, point-gauge measuring equipment was set up in order to measure the depth of water on the bed. The method of measuring the hydraulic depth was later improved with the introduction of pressure transducers which were more accurate and reliable. However, the point gauges were used to calibrate the pressure transducers that were retrofitted at a later stage.

The point-gauge is a commonly used laboratory instrument to measure the depth of a steady state water surface/body during hydraulic testing. It is the simplest method of measuring the liquid surface elevation. The gauge comprises a steel-gauging rod that is lowered to the lowest point of reference (datum) initially and then raised until the point of the gauge just breaks the liquid surface. In using the pointer gauge, the point is lowered until it touches the liquid surface or appears to touch its reflections in the liquid surface. Measurements are then taken by reading from the vernier scale that is attached

to the rod. It is recommended that this method be used in stilling chambers or wells where fluctuations of the liquid surface are much less (Asawa, 2006).

Figure 3.21 shows two different type of the gauging equipment – the hook type and the point type. The latter was opted for this experimental programme due to its availability in the hydraulic laboratory.

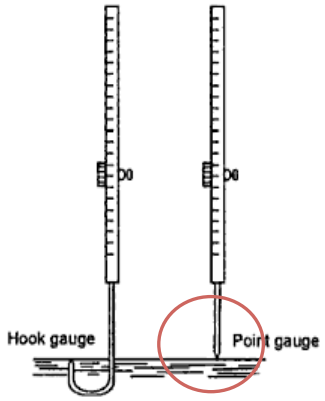

Figure 3.21 – Hook and point-gauge measuring equipment (Asawa, 2006)

For this experimental programme, the same concept applies whereby a stainless steel gauging rod is attached to a vernier scale. This is then mounted on a small square platform with a 4-roller foot. The stainless steel gauging rod is held with a screw-like attachment, which allows the gauging rod to slide up and down over the water surface. This also allows for fine adjustments for accurate reading and can be released for large rapid changes in positions. This gauging rod has a pointed bottom, which allows it to locate the water surface more accurately. The mounted gauge is then set onto a pair of steel embracers also with wheels on either side. This allows for the gauging equipment to be moved to different sections – both horizontally and vertically of the testing platform where measurement needs to be taken.

As mentioned previously, this method was opted as initial measuring equipment and was later used for calibration purposes. This is because there can be numerous human error in taking and reading the measurements especially in high flow rates. This is because due to the high velocity, there are more ripples in the water and reduces the accuracy of the measurement.

Figure 3.22 and 3.23 shows the point-gauge measuring equipment used in this study and the vernier scale attached respectively.

Figure 3.22 – Point-gauge measuring equipment

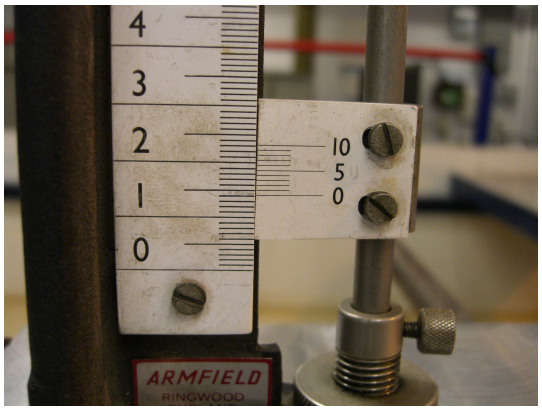

Figure 3.23 – Vernier scale on the point-gauge

Using this experimental setup, a series of tests were conducted in order to establish an understanding of how the water moves across the whole of the platform and therefore obtain an initial collection of data of the water profile for the different hydraulic conditions. This was accomplished by measuring the depth of water at different points of equal intervals across the entire platform. The series of tests were conducted on the flat bed; with a series of increasing flowrate with depth measurements taken at 30 cm intervals horizontally (L) and at 15 cm transversely (W) across the entire platform. The

depth was measured for both the terminal and intermediate system. At this point of the test, the surcharged system was not yet installed.

Figure 3.24 shows the distribution of points where depth measurements were taken in order to obtain an overview of the water depth profile across the whole platform using the point-gauge measuring system.

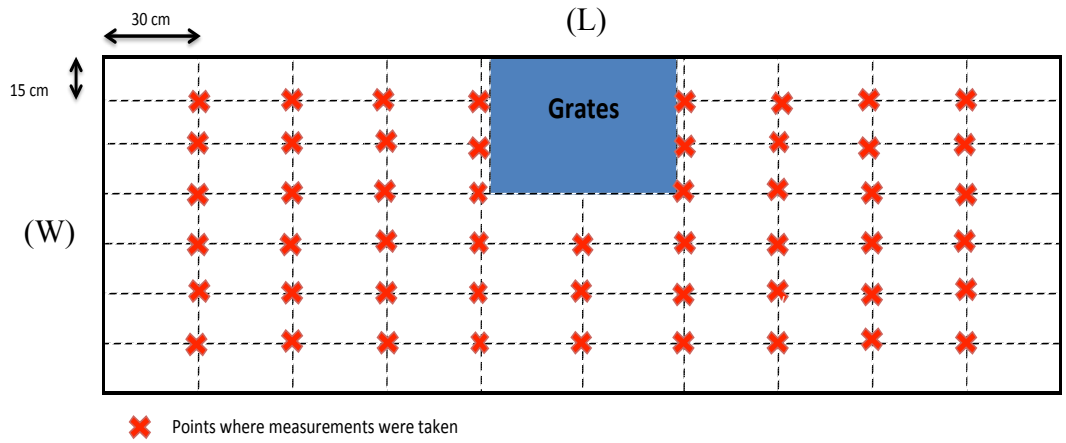

Figure 3.24 – Points of measurement using the point-gauge measuring system

The tests were repeated on at least 3 occasions for each test and the average depth was then used to obtain the depth profile over the plan area of the platform. Using these average depth values typical results of the hydraulic depth profile over the platform are shown in Figures 3.25 – 3.27 for terminal test flowrates of 15.17, 23.80 and 29.76 litres/s respectively. Figure 3.25(a) – Figure 3.27(a) illustrates the depth in the longitudinal direction at different transverse distances across the platform.

Figure 3.25 shows the results when a low flow (15.17 *l/s*) enters the test rig. It can be seen that the highest depth (darkest colour) occurs nearest to the inlet and is mainly uniform throughout the rest of the platform with the exception of locations where there is very low flow due to the presence of the grate. This uniform pattern can be seen more clearly as the flowrate increases [Figure 3.26 and 3.27]. The depth, as expected, decreases gradually as it moves towards the perimeter of the gully as can be seen with the gradual decrease in the colour gradient.

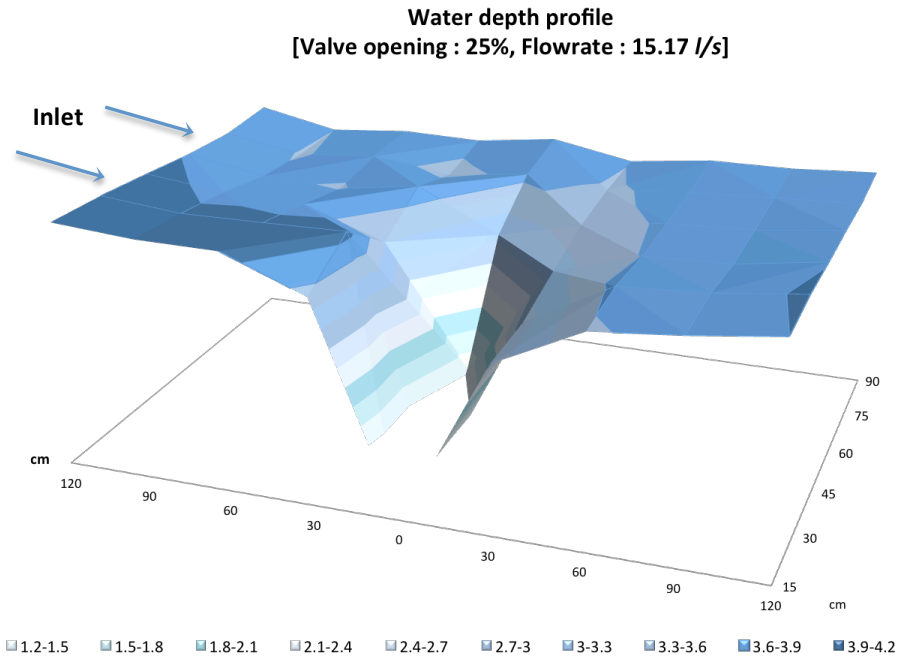

Figure 3.25 – Hydraulic depth profile for flowrate 15.17 litres/s: terminal test

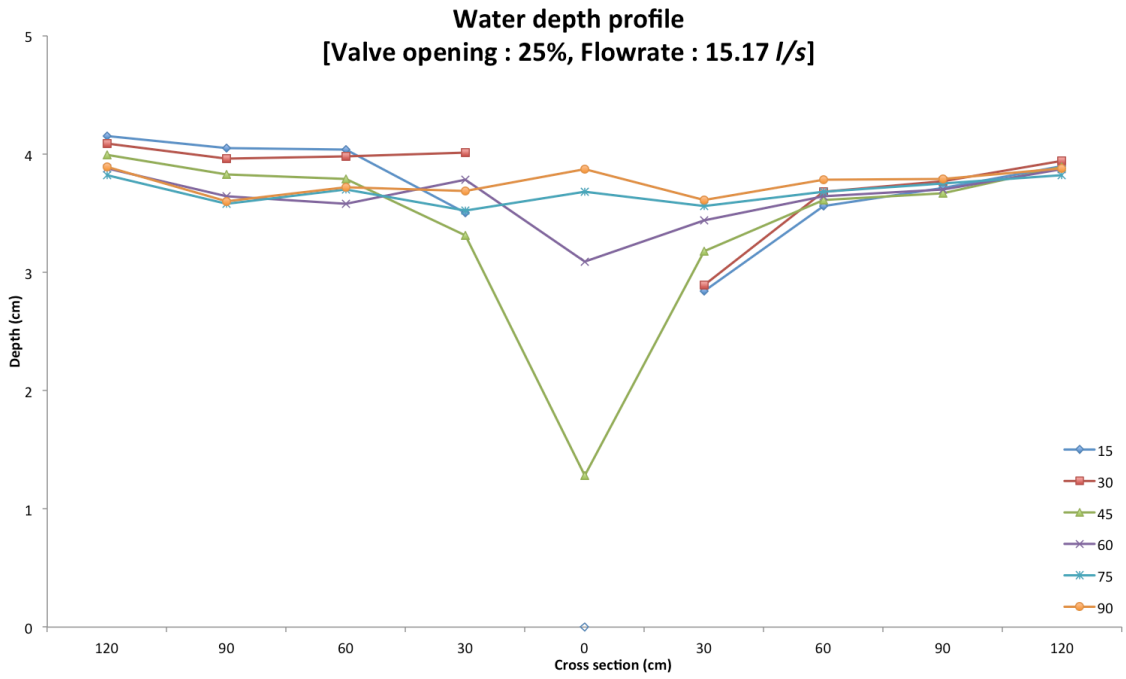

Figure 3.25(a) – Longitudinal depth profiles at different transverse distances across the platform. Flowrate 15.17 litres/s, terminal test.

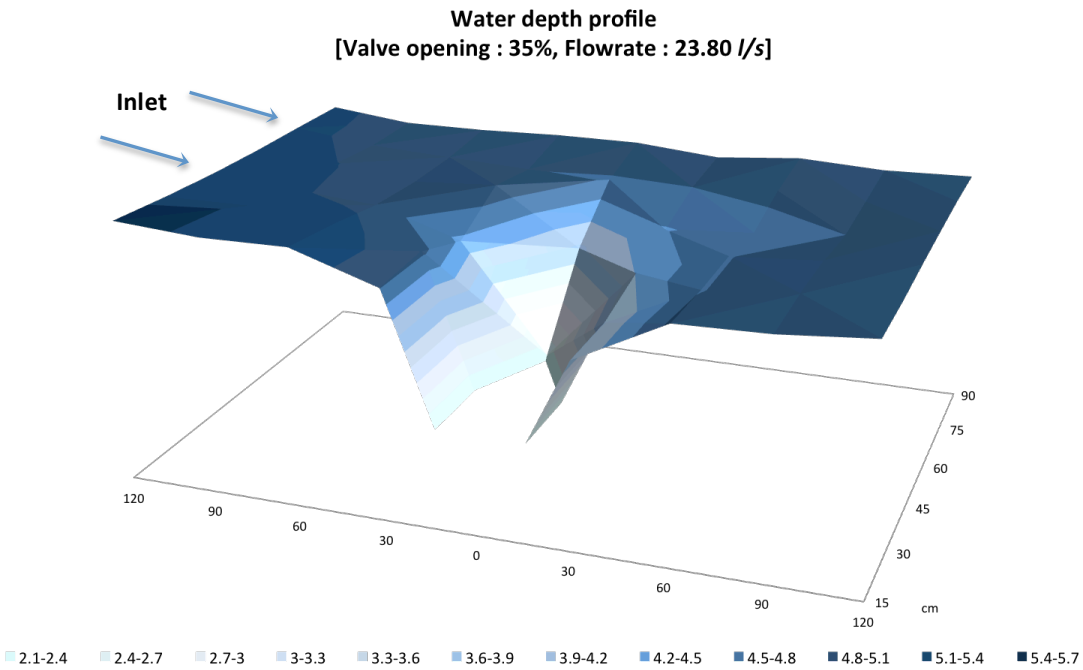

Figure 3.26 – Hydraulic depth profile for flowrate 23.80 litres/s: terminal test

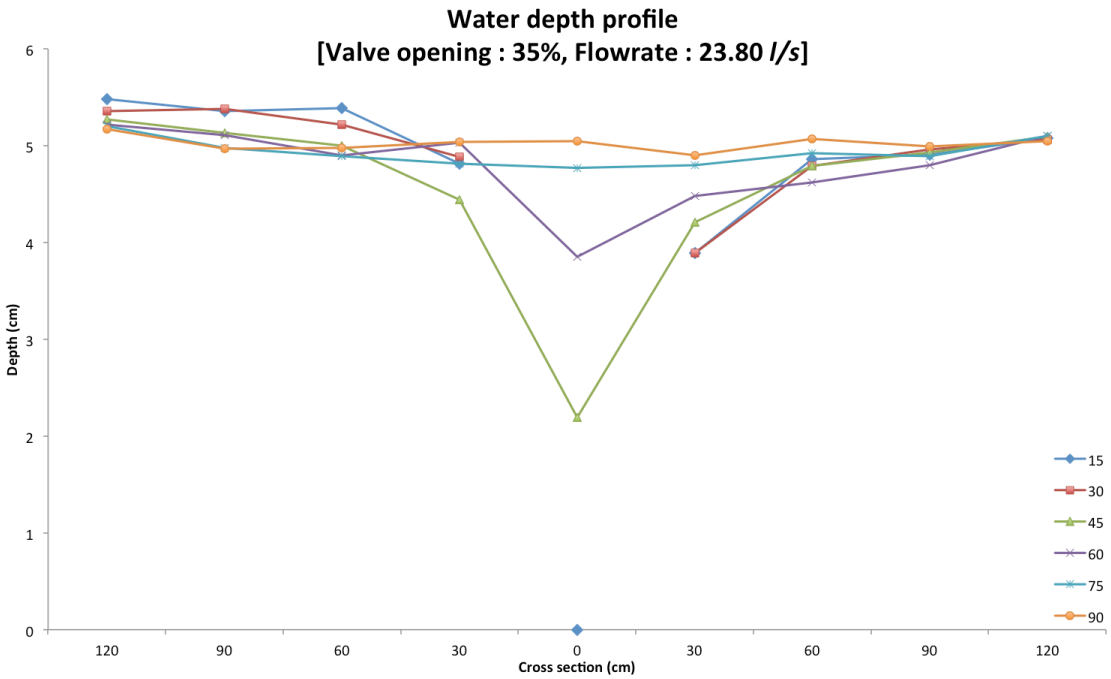

Figure 3.26(a) – Longitudinal depth profiles at different transverse distances across the platform. Flowrate 23.80 litres/s, terminal test.

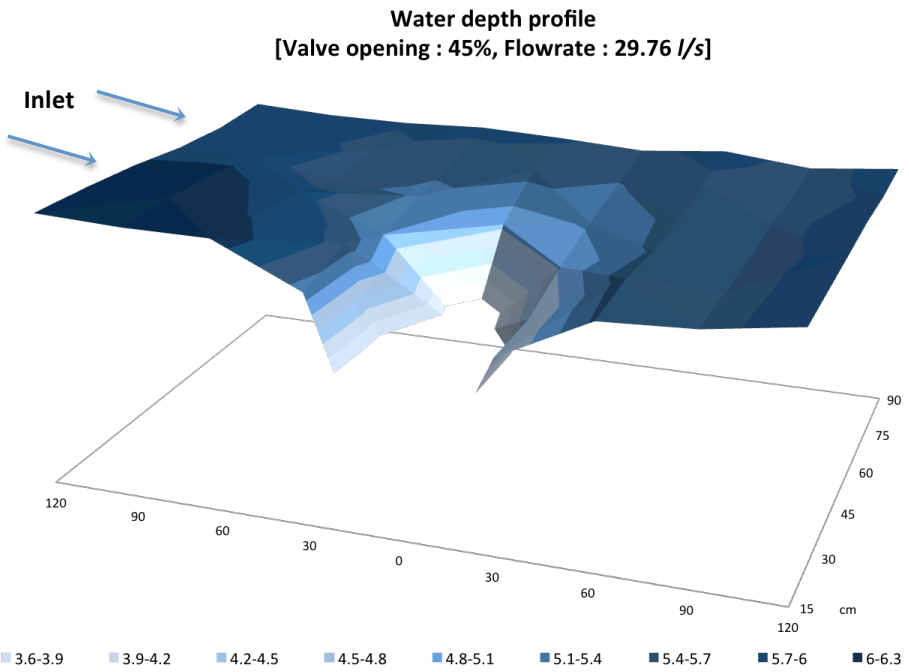

Figure 3.27 – Hydraulic depth profile for flowrate 29.76 litres/s: terminal test

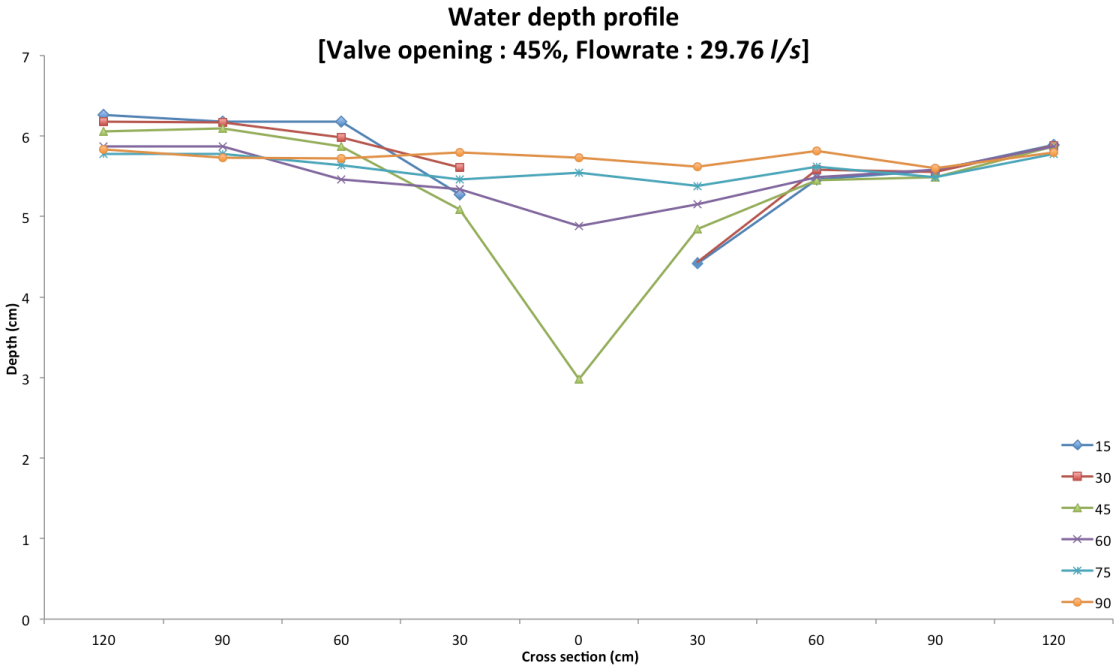

Figure 3.27(a) – Longitudinal depth profiles at different transverse distances across the platform. Flowrate 29.76 litres/s, terminal test.

Tests were completed using the point gauge system and, based on the measurements obtained, the decision was made to use 6 pressure transducers positioned on the bed of

the chamber to record the flow depth to the gully. Based on a review of the point gauge results it was concluded that the transducers should be positioned to record the depth upstream of the grate, along the central axis of the platform in the transverse direction and in the region downstream of the grate. One transducer was also located at the bottom of the gully pot in order to obtain the depth of water in the gully pot itself. Hence seven pressure transducers were used for the experimental programme and the positions of the pressure transducers are shown in Figure 3.28.

Figure 3.28 shows the position of the pressure transducers on the bed of the testing platform. Based on a review of the point gauge results, the transducers were positioned at distances of 300mm equally from the edge of the grate and along the transverse centreline from the grate edge in 3 directions, see Figure 3.28. These positions were selected in order to give an average of hydraulic depth of the flow into the gully grate from all sides. Further details regarding the pressure transducers have been included [Appendix 5].

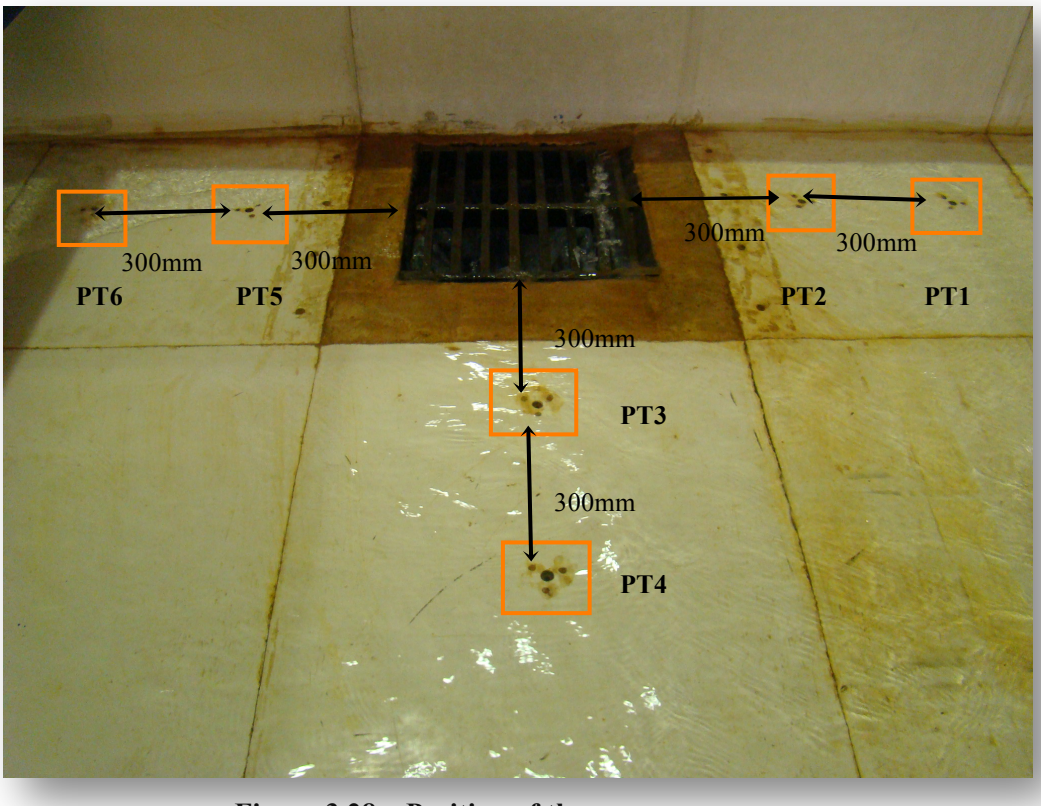

Figure 3.28 – Position of the pressure sensors

3.2.2 Pressure transducers

Pressure transducers are equipment that measures ambient pressure and are often utilised in experimental and real life studies due to its ease of use. Pressure transducer measures the water pressure and because pressure is directly proportional to fluid level, therefore the water pressure can be converted to the height of the water over the transducer.

As have been mentioned previously, pressure transducers were retrofitted into the experimental system as an upgrade to the point-gauge measuring system. This thus enables the implementation of a measuring system that could be automated and allows the procurement of hydraulic depth readings that is more reliable and accurate. However, due to budget concerns, only a limited number of pressure transducers could be implemented as part of the measuring system. From the initial series of tests, it was decided that at least a minimum of seven pressure transducers were needed, in order to obtain a general hydraulic profile of the flow moving from the inlet, across the platform and finally leaving the system either through the outlet tank or the gully system itself. Therefore, the pressure transducers were retrofitted onto the laboratory rig with six on the bed of the platform and one at the bottom of the gully pot. These positions were determined based on the water depth profile obtained using the point gauge method [Figure 3.25 – 3.27].

The pressure transducers used for the experimental programme is the GEMS 5000 series (0-30 mbar) for the bed, and GEMS 5000 series (0-150 mbar) for the gully pot. Both sensors give an output of between 4-20 mA and uses 9-35V of supply power. These pressure transducers have been selected because they have long-term stability and have high accuracy (±0.2%). A series of calibration test were completed to test the accuracy and these are described in Section 4.2.

Figure 3.29 shows an example of the GEMS pressure sensor (5000 series) that was utilised in this experimental programme.

Figure 3.29 – A typical GEMS 5000 series sensor

Details of the calibration of the pressure sensor are given in Section 4.2 and the specification of the pressure transducers is included in the Appendices [Appendix 5].

3.2.3 Flowmeter MAG 910E

The flowmeter utilised in this experimental programme is the inductive flowmeter MAG 910E supplied by Arkon Instruments. The MAG 910E is an instrument designed for measuring, indicating, and totalising the flow of conductive liquids. The flow meter is a highly stable and accurate measuring device. The construction of the flowmeter uses components with long-term, time and temperature stability. Configuration data is backed up and can be recovered after a power failure. This is because the back-up structure enables data recovery even if a partial loss of data occurs (Arkon MAG 910E Data Sheet).

There are two flowmeter utilised in this experimental set up – one on each inlet pipe into the laboratory rig. These flowmeter also comes fully calibrated (manufacturer guaranteed with certificate). Figure 3.30 and 3.31 show the flowmeter and the Electronic Unit display (Front Panel display).

Figure 3.30 - Electromagnetic Flowmeter (MAG 910E)

Figure 3.31 – Electronic Unit display of the Arkon MAG-910E (front panel).

Details of the calibration of these units are given in Section 4.2.2 and the specification is included in the Appendices section [Appendix 6].

3.3 MEASURING TANK

The measuring tanks used in this experimental programme were existing features in the hydraulic laboratory. The mechanism of these measuring tanks are the same as in any hydraulic laboratory where the rise in the liquid level in the measuring tank between two predetermined levels are measured and time required for the rise of liquid noted (Asawa, 2006). The discharge can then be computed since the internal dimensions of the tanks are known. These tanks have been calibrated prior to use. The calibrated volume for each of these tanks is 1.875m^3 or 849.505/s/ft.

Figure 3.32 and 3.33 shows the measuring tanks that were both utilised in this study.

Figure 3.32 – Measuring tank 2

Figure 3.33 – Measuring tank 1

3.4 HARDWARE AND SOFTWARE CONTROL SYSTEM

A set of control system has been assembled in order to give/send signals to the different equipment utilised in the laboratory set up. The control system consists of the following - National Instrument Compact FieldPoint system (NI-cFP) and LabVIEW RealTime (RT) as the hardware system, LabVIEW (version 7.1) and National Instruments Measurement and Automation Explorer (NI MAX) as the programmable controlling software.

3.4.1 Compact FieldPoint System

The control hardware system that was utilised in this experimental programme consists of a single Compact FieldPoint system that is embedded with Real-Time LabVIEW. A Compact FieldPoint system usually consists of one cFP-BP-x backplane, one cFP-20xx controller, one or more I/O modules, and or more connector blocks or accessories. Each of this system can be accessed by an unlimited number of PCs and FieldPoint modules, forming a distributed computing system (NI, 2004).

Compact FieldPoint was designed for industrial control applications that perform advanced embedded control and data logging as well as providing Ethernet connectivity. Due to the nature of some of its components, the Compact Field Point can also perform headless operations when appropriately assembled. Compact FieldPoint, was boasted to be the most rugged and reliable NI platform, and was designed for industrial and mobile environments tolerating high shock, high vibration, and even temperature extremes. FieldPoint is a lower-cost distributed I/O system with a variety of communication options besides Ethernet. It is designed to mount on DIN rails in static applications where the FieldPoint bank is connected to a PC for data collection, analysis, display, and storage.

Figure 3.34 shows an example of a Compact FieldPoint system with multiple set of I/O module and connectors block. Highlighted are the components that make up the Compact FieldPoint system that is utilised in this experimental programme.

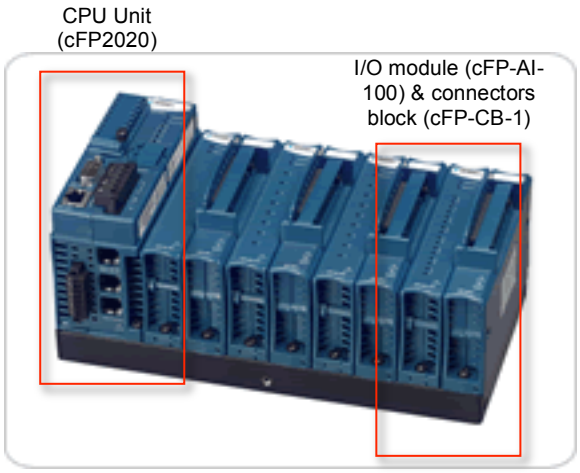

Figure 3.34 – A Compact FieldPoint system (http://www.ni.com/compactfieldpoint/)

Prior to this experimental programme, a Compact FieldPoint system was already available in the hydraulic laboratory for the use of a large-scale interaction network rig. Therefore, in order to reduce the cost of operation, some of the components were shared between a large-scale interaction network rig and this full-scale interaction rig. Other components were later added to complete the set up depending on need. Even so, both the systems are to be considered separately since both cannot run simultaneously.

The components that make up the utilised Compact FieldPoint system for this experimental programme therefore consists of only the following:

- One backplane: cFP-BP-8
- One controller: cFP-2020
- Two I/O module:
  - Analogue Input: cFP-AI-100@6 and
  - Digital Output: cFP-RLY- 421
- One connector block: cFP-BP-1

Figure 3.35 shows all the modules connected to the Compact FieldPoint System as detected by NI MAX.

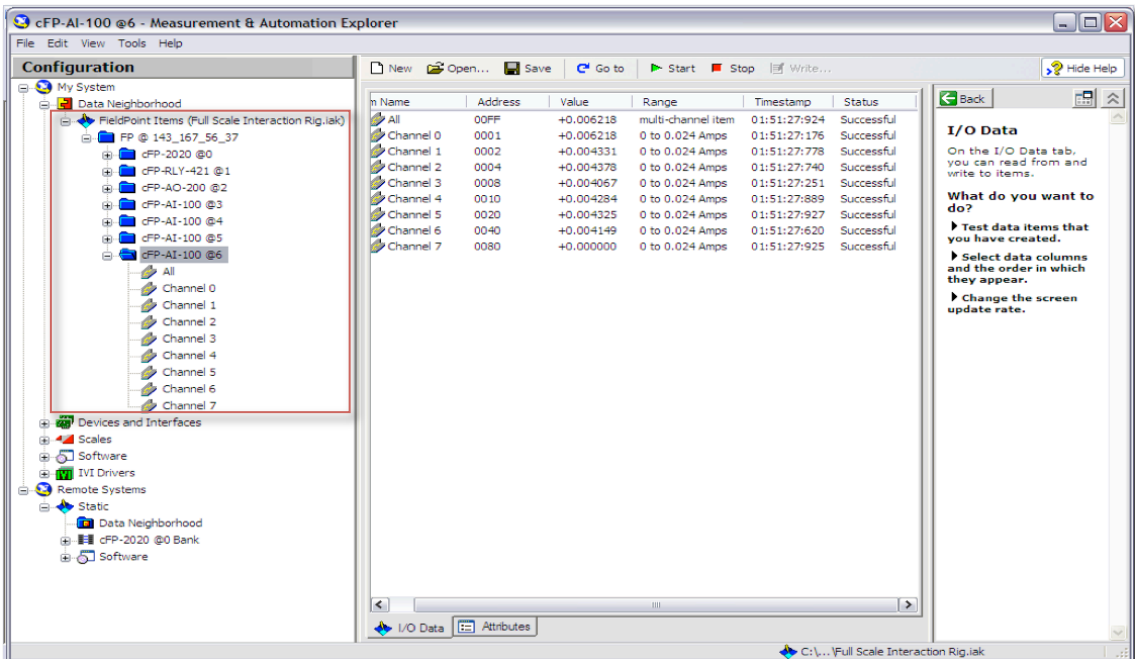

Figure 3.35 – Detected devices on NI MAX settings

3.4.2 Compact FieldPoint Components

The following sections [3.4.2.1 – 3.4.2.3] will introduce each of the components of the Compact FieldPoint system and how the system works together as a controlling hardware for this experimental programme. It will also attempt to cover the basics in constructing a simple Compact FieldPoint system. However, the more complex wiring systems and further details can be found in the user manual supplied by National Instruments.

3.4.2.1 Compact FieldPoint Backplane

National Instruments offers two backplanes for mounting of Compact FieldPoint modules:

- NI cFP-BP-4 (4 slots) and
- NI cFP-BP-8 (8 slots).

In this experimental programme however, the aforementioned readily available backplane is the cFP-BP-8. Therefore, this section will only discuss the used backplane.

NI cFP-BP-8 is a metal backplane that provides a solid mounting surface for the Compact FieldPoint bank and forms the communication bus between the controller module and the I/O modules. The backplanes are constructed of extruded metal with grounding lugs on the bottom, feature screw-down connections for a controller module, eight I/O modules, and 37-pin D-Sub connectors for I/O connections. The backplanes come with a cFP-PM-H horizontal mounting bracket, which provides mounting holes on either side of the backplane so that it can be mounted to a panel (NI data sheet). This backplane is then connected with other Compact FieldPoint modules to create the existing system that was used as part of the experimental programme.

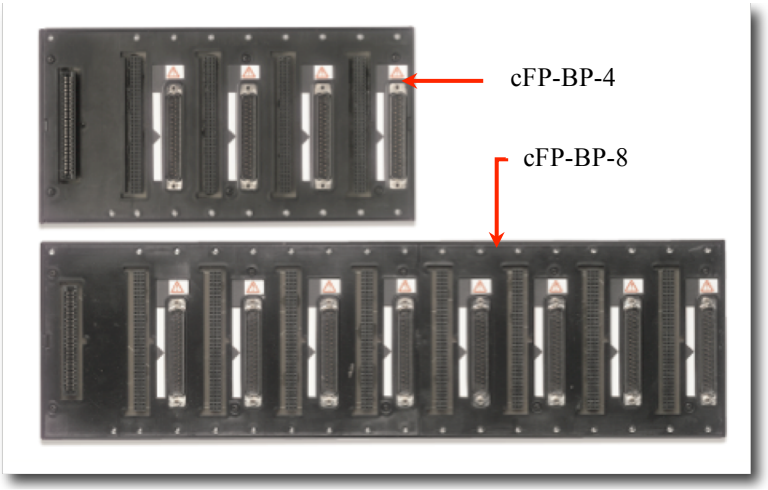

Figure 3.36 – Compact FieldPoint Backplanes (cFP-BP-4 and cFP-BP-8)

3.4.2.2 Compact FieldPoint Controller

In this experimental programme, the selected Controller Interface used as Central Processing Unit (CPU) for the Compact FieldPoint system is the NI cFP-2020. NI cFP-2020 is a programmable automation controller (PAC) and is the primary hardware used in controlling the devices in this laboratory set up. A single NI cFP-2020 controller can manage a bank of up to eight Compact FieldPoint analogue and digital I/O modules (NI, 2004). However, in this experimental setting, only two I/O modules are used with the NI cFP-2020.

The existing NI cFP-2020 also has a 32MB of volatile memory (DRAM) and an additional 64MB of non-volatile memory [Table 3.3]. It also offers both Local Area Network (LAN) and Internet/Ethernet via Virtual Private Network (VPN) connections, which allows users to control the system remotely. This allows for stand-alone programmes to be embedded on the system with removable compact flash storage. The NI cFP-2020 can be operated using Windows 2000/NT/XP.

NI MAX is the included driver software for this controller. NI MAX and the related configuration and settings for the NI cFP-2020 will be discussed in the following sections of this chapter [3.4.3].

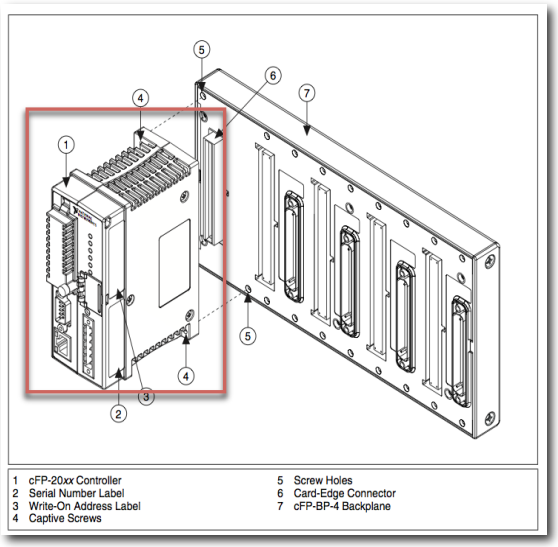

Figure 3.37 – A single Compact FieldPoint controller to be mounted onto the backplane

Table 3.3 – Specifications of the NI cFP-2020 (NI Product Description)

Module	DRAM Memory	Internal Nonvolite Storage	Removable Compact Flash	Ethernet Ports	RS-232 Serial Ports	RS-485 Serial Ports
cFP-2020	32 MB	64 MB	✓	1	3	1
cFP-2010	32 MB	64 MB	–	1	2	0
cFP-2000	16 MB	32 MB	–	1	1	0

3.4.2.3 Compact FieldPoint I/O module

Compact FieldPoint I/O modules are used to control or monitor a range of instrumentation such as pressure transducers and valve openings depending on the signal type. The I/O module utilised in this research is the analogue input I/O - NI cFP-AI-100 and the digital output - NI cFP-RLY-421.

The National Instruments cFP-AI-100 is the module that sends and captures signal in the form of 4-20 (mA) to and from seven pressure transducers. On the other hand, the NIcFP-RLY-42x devices are relay modules that can be used to control digital signals ranging from low voltage to 120 VDC and to 250 VAC. These modules are commonly used to control indicator lights, motors, and power circuits (NI, 2003). In this

experimental programme, the relay type I/O module (cFP RLY-421) is utilised to provide Boolean control (1-on, 0-off) for pumps. The cFP-RLY-421 mounts on a Compact FieldPoint backplane (cFP-BP-8) next to the analogue input module (cFP-AI-100). Again, the selection of this compact FieldPoint module was in order to reduce the cost of operation due to its availability (prior to assembly). Specifications for both the cFP-AI-100 and cFP-RLY-421 can be found in the Appendices section [Appendix 7].

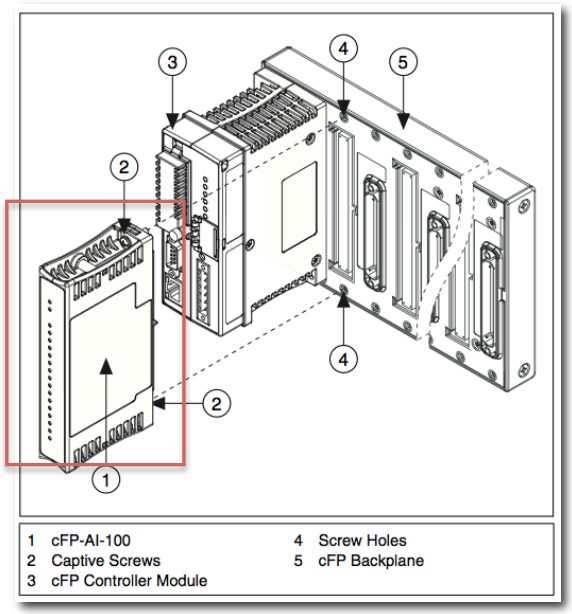

Figure 3.38 – I/O Module (cFP-RLY-421/ cFP-AI-100) to be mounted after the controller

3.4.2.4 Compact FieldPoint connectors block

Connectors block (cFP-CB-1), which was designed for general purpose and hazardous voltage operation with any Compact FieldPoint I/O modules was also utilised. This compact FieldPoint module has been selected for use because it is the recommended connector block compatible especially in handling the high-powered consumption module like cFP-RLY-421.

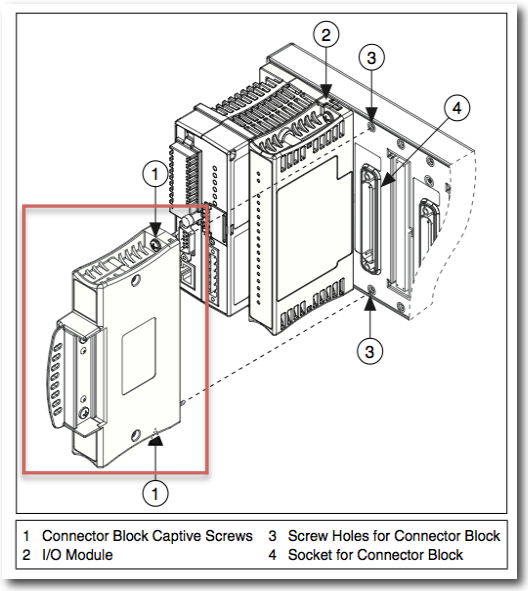

Figure 3.39 – Connectors block (cFP-CB-1) to be mounted after the I/O module

3.4.3 National Instruments Measurement and Automation Explorer (NI MAX)

National Instruments Measurement and Automation Explorer (MAX) is configuration software that is supplied with the Compact FieldPoint hardware. NI MAX is often used with NI application development programme such as LabVIEW to manage the low-level communications, hardware details, as well as simplifying programmatic access to the I/O channels.

For the purpose of this experimental programme, the hardware components for the laboratory system is configured in NI MAX as a remote system which then allowed the author to programmatically design a set of control through Virtual Instruments (VI's) of the LabVIEW interface.

The NI MAX platform simplifies the use and integration of Compact FieldPoint systems with the utilised hardware. This is because it allows configuration of the entire system, including network parameters, module, and I/O settings, and named-channel items to be done in NI MAX itself. NI MAX also detects the Compact FieldPoint as a

remote system, which then allows for wireless configuration and tests of all the associated modules. NI MAX also allows interactive test of I/O modules and channels, viewing input data values, and setting of output values without writing any software code (NI, 2004).

Figure 3.40 shows the item configuration window of the NI cFP-AI-100@6 as seen in NI MAX. This window allows the addition or removal of items/channels of the designated modules.

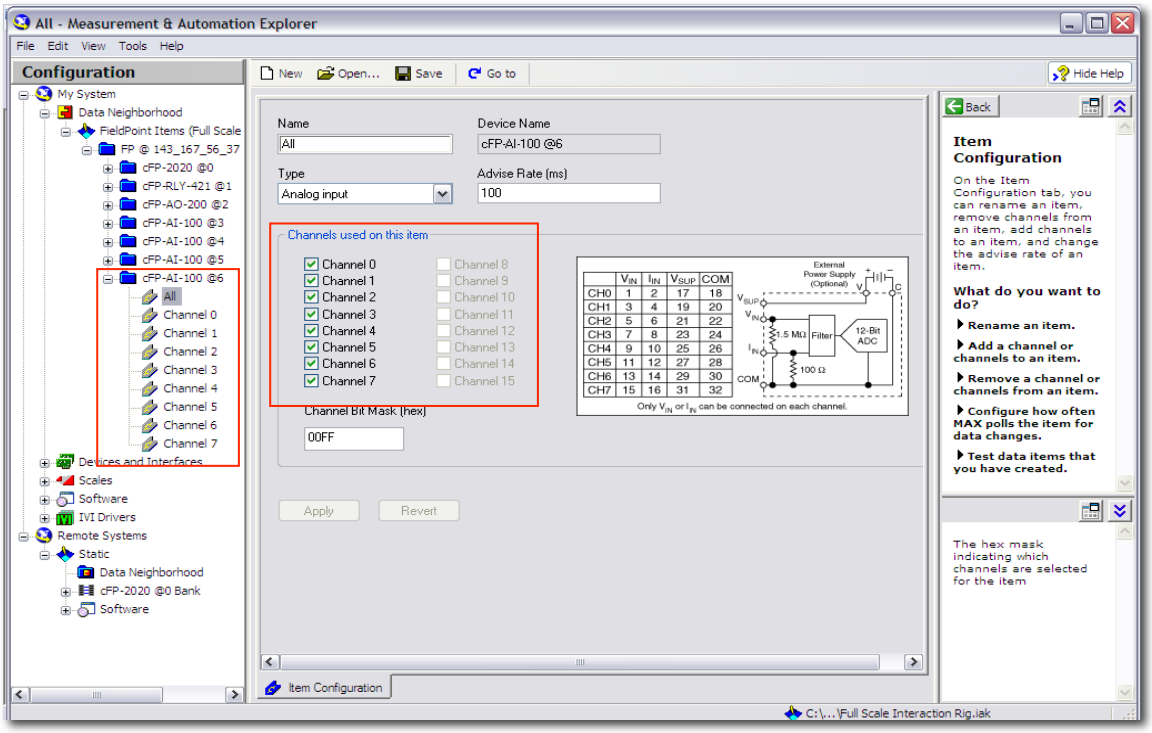

Figure 3.40– Configuration in NI MAX (associated channels and their related ports)

Figure 3.40 shows the seven connected pressure transducers (channel 0-6) that is wired to the analogue I/O module NI cFP-A1-100@6 which gives a signal of between 4-20mA. NI cFP-A1-100@6 (Channel 7) is an empty slot and remains unused throughout the experimental programme. The other I/O modules (cFP-A1-100@3- cFP-A1-100@5) are being utilised by the large-scale interaction network rig and are controlled separately by different sets of VI's.

This I/O Data pane in NI MAX also allows the channels in NI cFP-AI-100@6 bank to test the settings prior to laboratory testing.

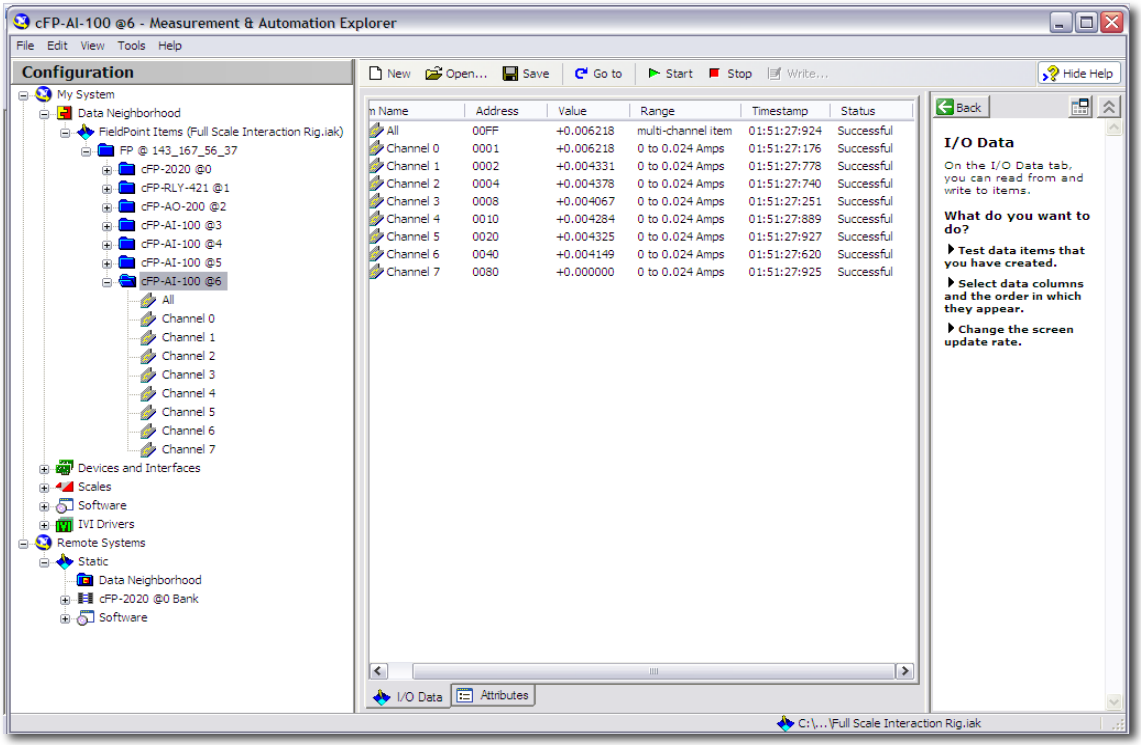

Figure 3.41 – Configuration in NI MAX

Figure 3.42 shows that the entire CFP system being configured to a designated static IP, which allows the host computer to connect to the RT target. This feature is important since it enables other users (with permission/VPN connection) to access and hence programme the same target. It also allows the VI's to be downloaded to the RT target and embedded in the control unit as a stand-alone programme.

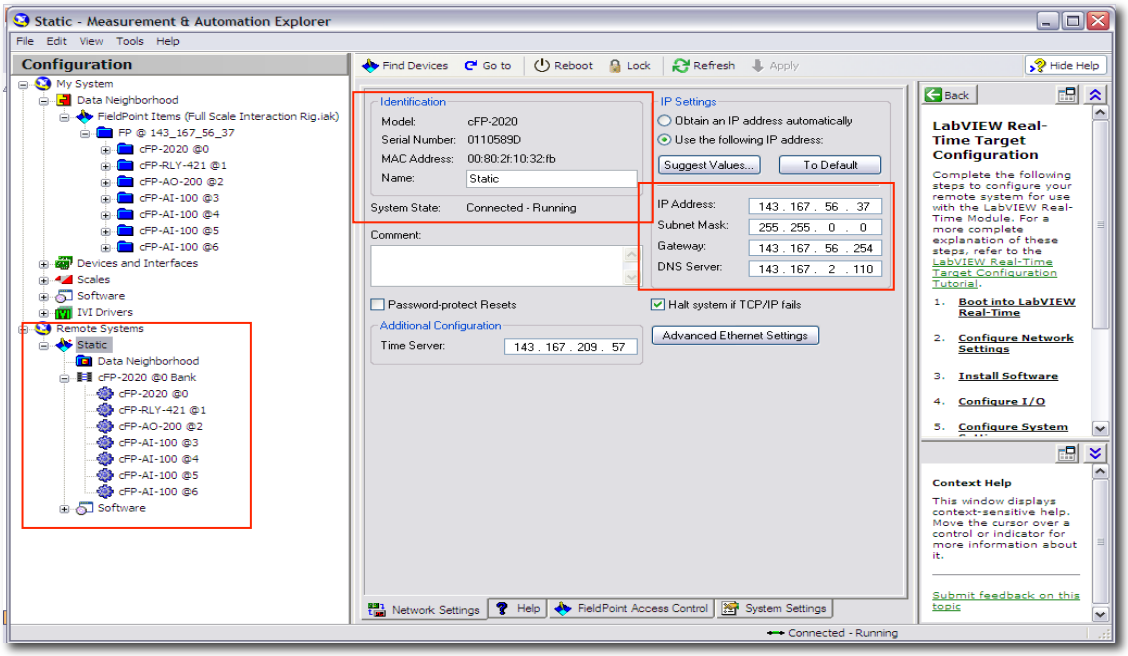

Figure 3.42 – Real-time target IP address

3.4.4 LabVIEW 7.1

The software monitoring system utilised in this experimental programme is the LabVIEW version 7.1. In order to communicate with the hardware, a simple user interface/front panel VI was designed. This VI has the control (knobs, dials, push buttons and etc.) as well as the indicator ability such as graphs, LEDs, and other output displays (LabVIEW manual). Codes are then added in the block diagram VI to control the objects in the front panel VI.

Figure 3.43 and 3.44 show a sample of the front panel VI and block diagram VI constructed to control the system. The front panel VI consists of a graph display as well as a digital display of the measurements and with a stop button function whereas in the block diagram VI [Figure 3.44], a more detailed codes and signals used to control the front panel are shown. In this case, the seven pressure transducers are being told to take measurements after a certain time delay (900s) at a designated time interval (1000ms) and results written to a LabVIEW measurement (.lvm) files. Measurements taken are also sent to the front panel and then displayed as graph and digital display.

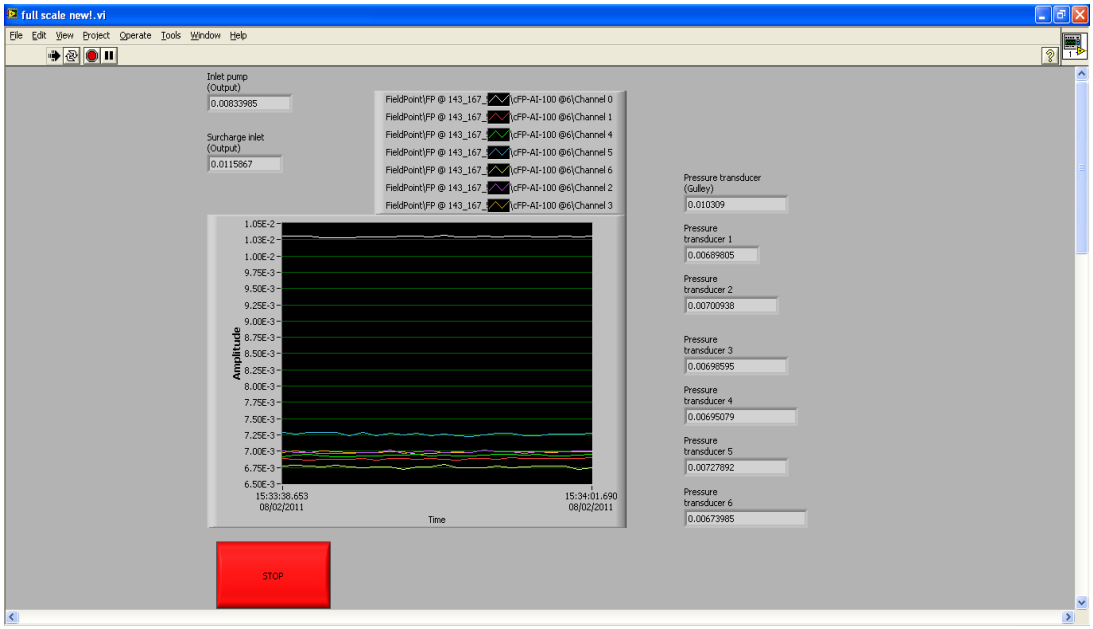

Figure 3.43 – Front panel VI

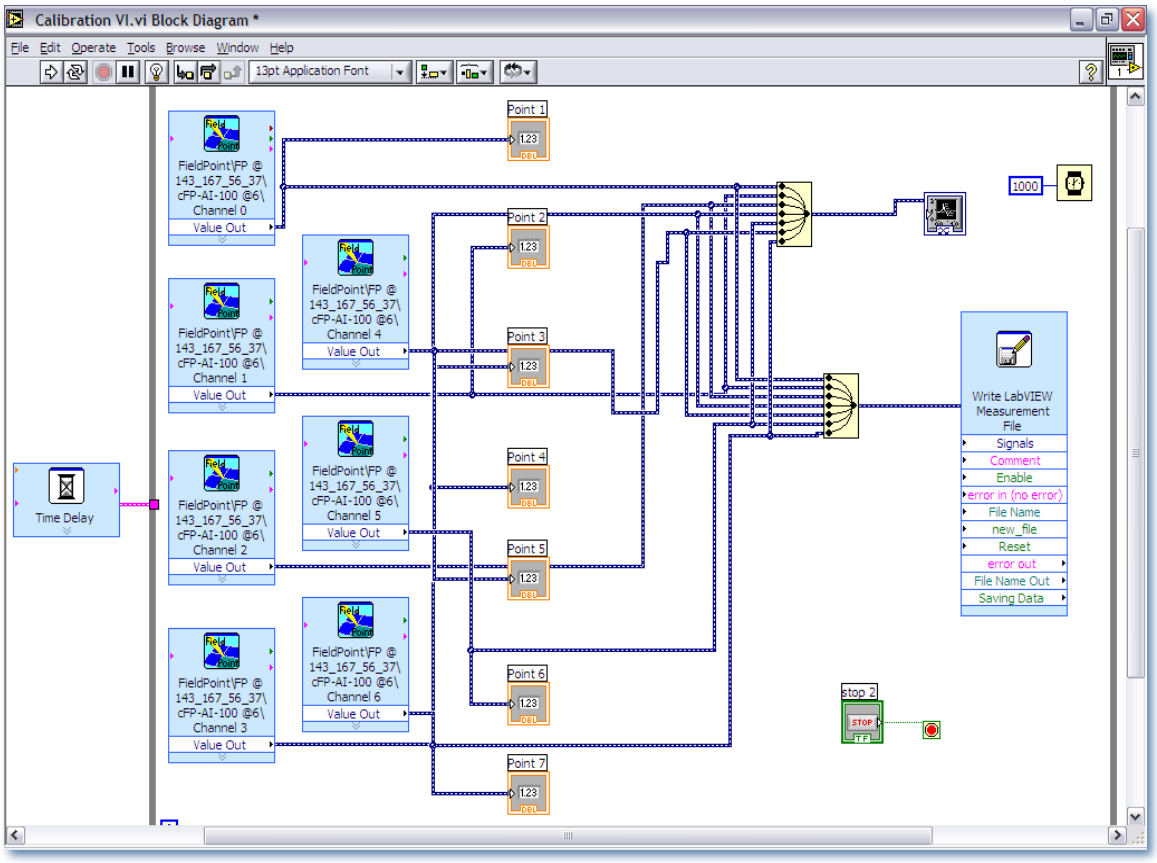

Figure 3.44 – Block diagram VI

The instrumentation and control software and the way that they were used within the experimental programme are presented in Chapter 4.

CHAPTER 4

METHODOLOGY

4.1 CHRONOLOGY OF METHODOLOGY

Figure 4.1 shows the chronology of the methodology adopted for this study.

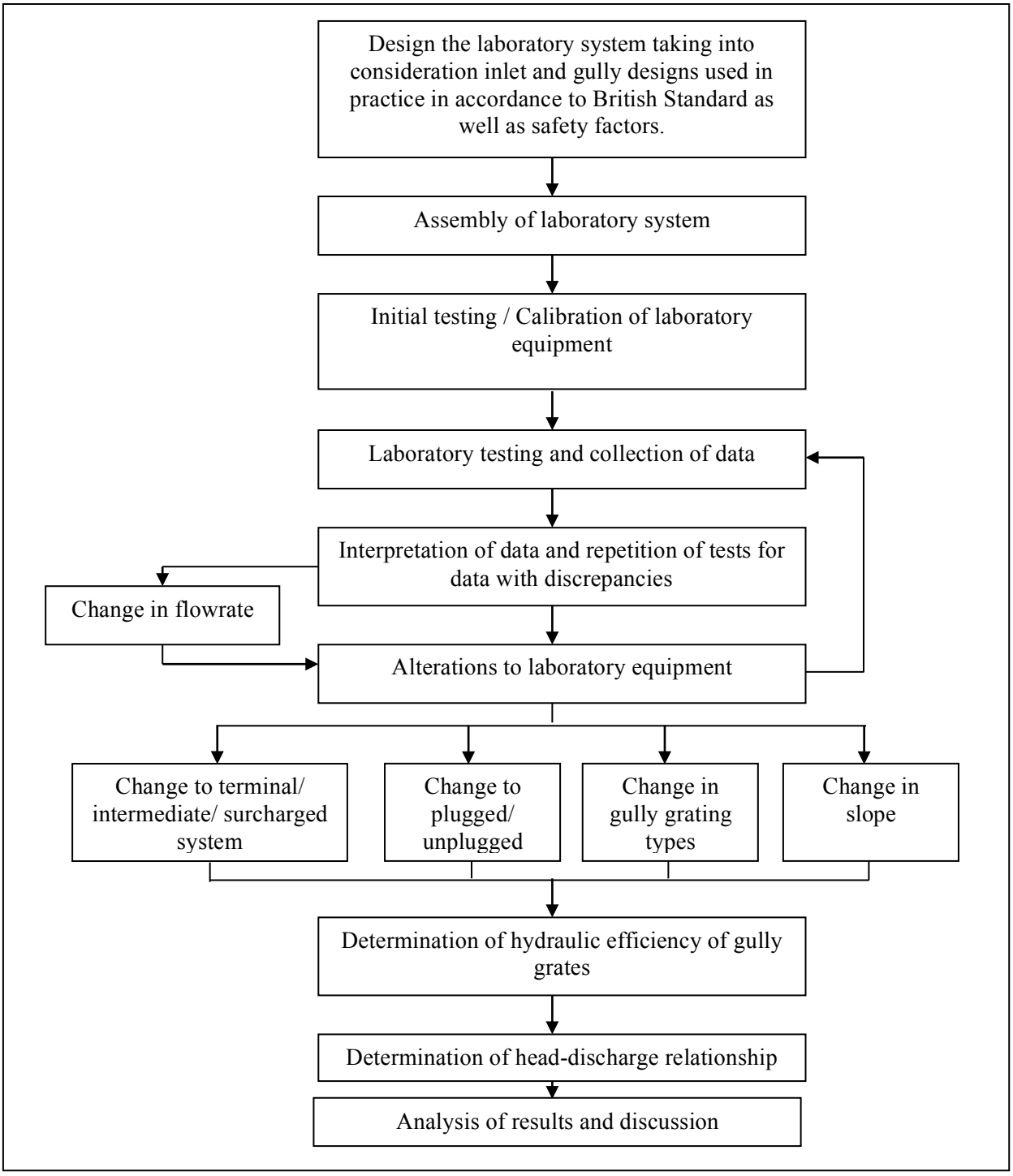

Figure 4.1 – Chronology of methodology

With respect to the design of the laboratory system due consideration was given to the usual UK working practices for gully inlets and pots. The design considerations and justifications of the gully system were discussed and presented in the literature review section [Chapter 2]. Following this, the laboratory rig and measurement system was assembled as discussed in the previous chapter [Chapter 3]. Therefore, only the laboratory testing procedures, collection of data, calibration procedures and results, as well as the interpretation of calibration data have been discussed in the following sections of this chapter. Further analysis to determine the hydraulic efficiency and head discharge relationships for each gully tested are presented in Chapter 5.

4.2 CALIBRATION PROCEDURES AND RESULTS

4.2.1 Calibration of pressure transducers

To check that the pressure transducers gave consistent and repeatable measurements the calibration was completed using two approaches. The initial method was conducted using a measured depth method whereas the second method used a set depth. The calibration methods are explained below:

1) **Measured depth**

Measured depth method involves the use of a simple point gauge measurer. A signal between 6mA – 24mA was sent to the valve in order to achieve a certain flowrate and the resulting hydraulic depths on the platform were then measured using aforementioned point gauge measurer. The hydraulic depths are measured near to each of the pressure transducers and the average of 3 measurements were taken and compared to the average signal of each setting.

2) Set depth

The 'Set Depth' method is a method whereby a certain hydraulic depth on the testing platform is set prior to taking measurements. The initial phase of the calibration process remained the same where an initial measurement of the bed level was taken. Then, the testing platform was flooded to a certain (average) depth and the resulting signal was then taken. For instance, if the (estimated) set depth of 15cm needed to be achieved, the testing platform was then flooded to the designated depth and the resulting reading of the signal was then taken. The estimated depth was checked at random points on the platform (adjacent to the pressure transducers) using a point gauge measurer and the average of 3 measurements are then plotted against the average resulting signal. A minimum of 5 set depths were tested in order to obtain the calibration graph for each sensor.

The calibration results between the measured depth method and set depth method were then compared for each of the pressure transducer in order to give an overview of the results. Included also in the results is the initial calibration conducted manually before the pressure transducers were retrofitted into the laboratory system. The results are presented in Figure 4.2 - 4.7:

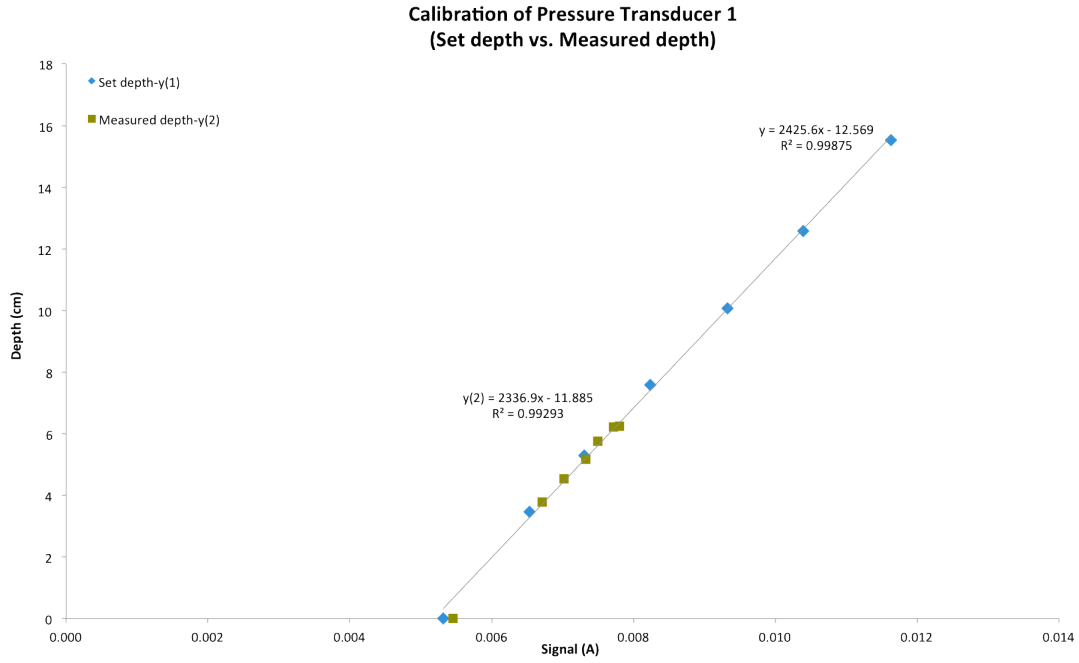

Figure 4.2 – Calibration of Pressure Transducer 1

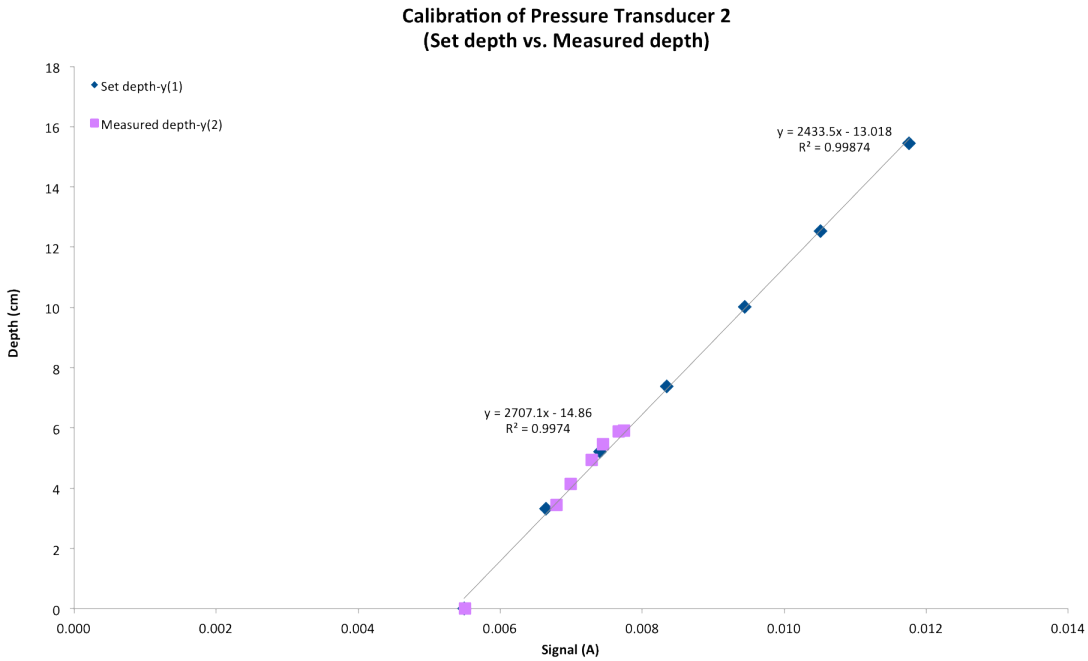

Figure 4.3 – Calibration of Pressure Transducer 2

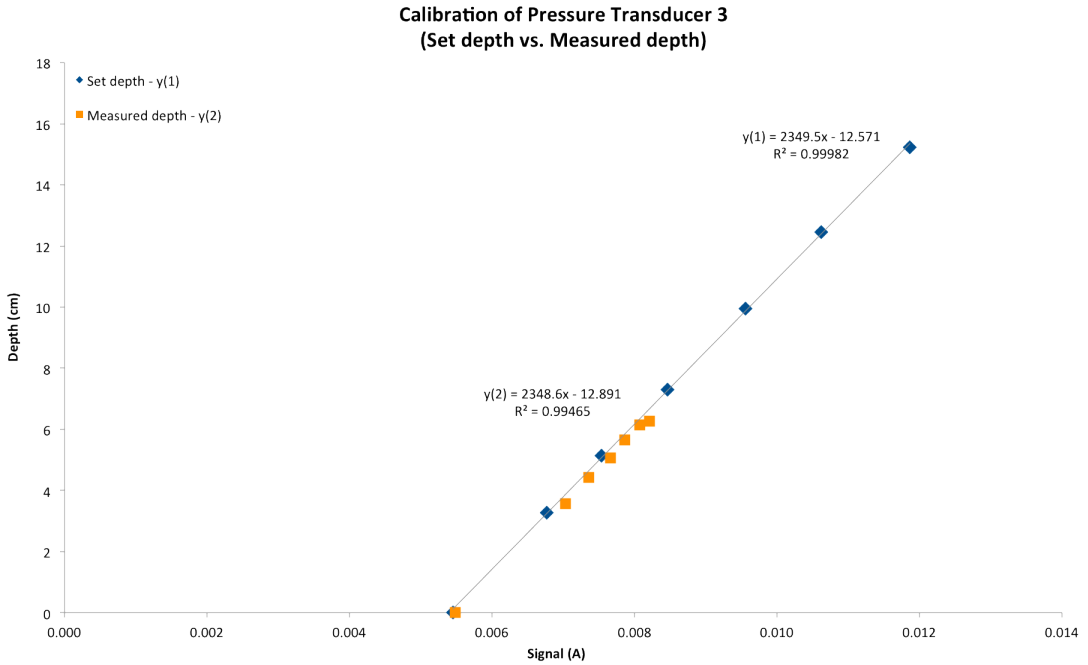

Figure 4.4 – Calibration of Pressure Transducer 3

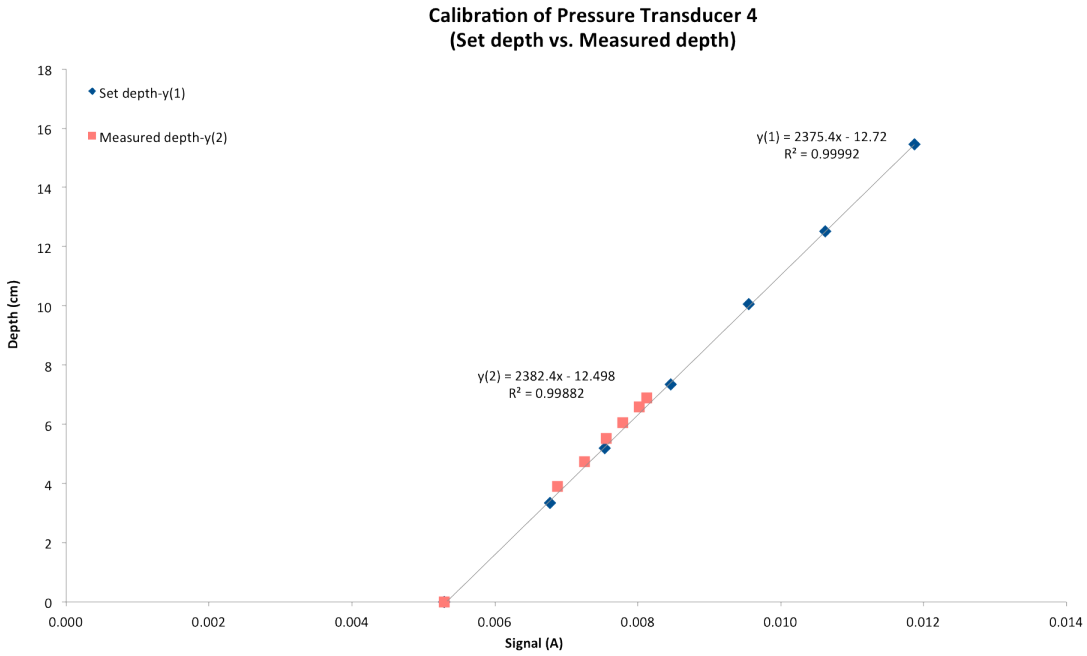

Figure 4.5 – Calibration of Pressure Transducer 4

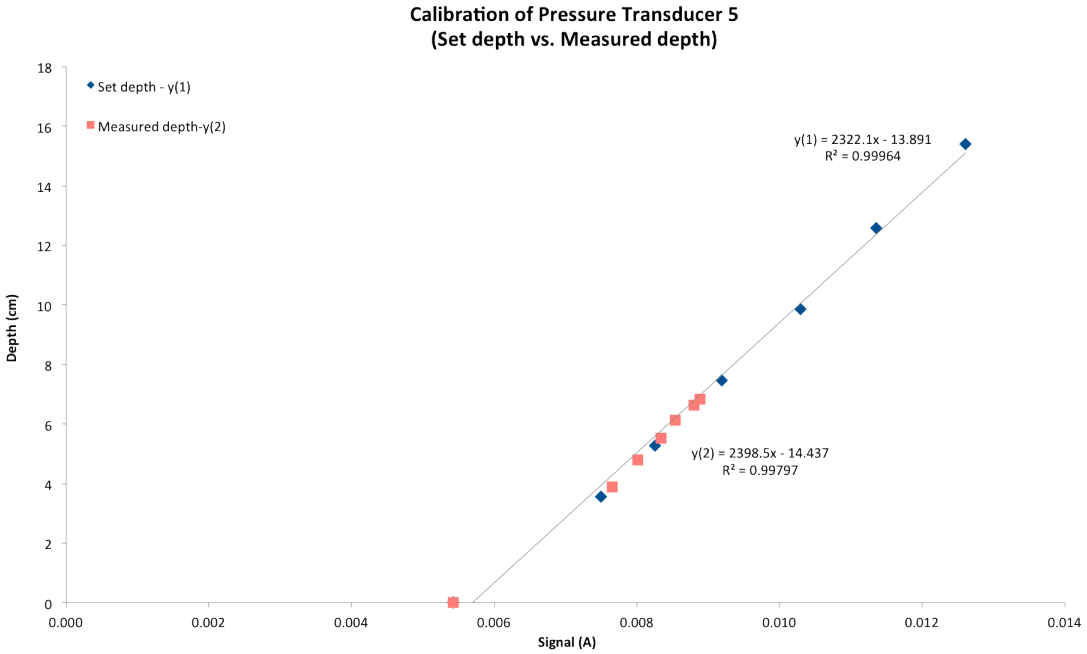

Figure 4.6 – Calibration of Pressure Transducer 5

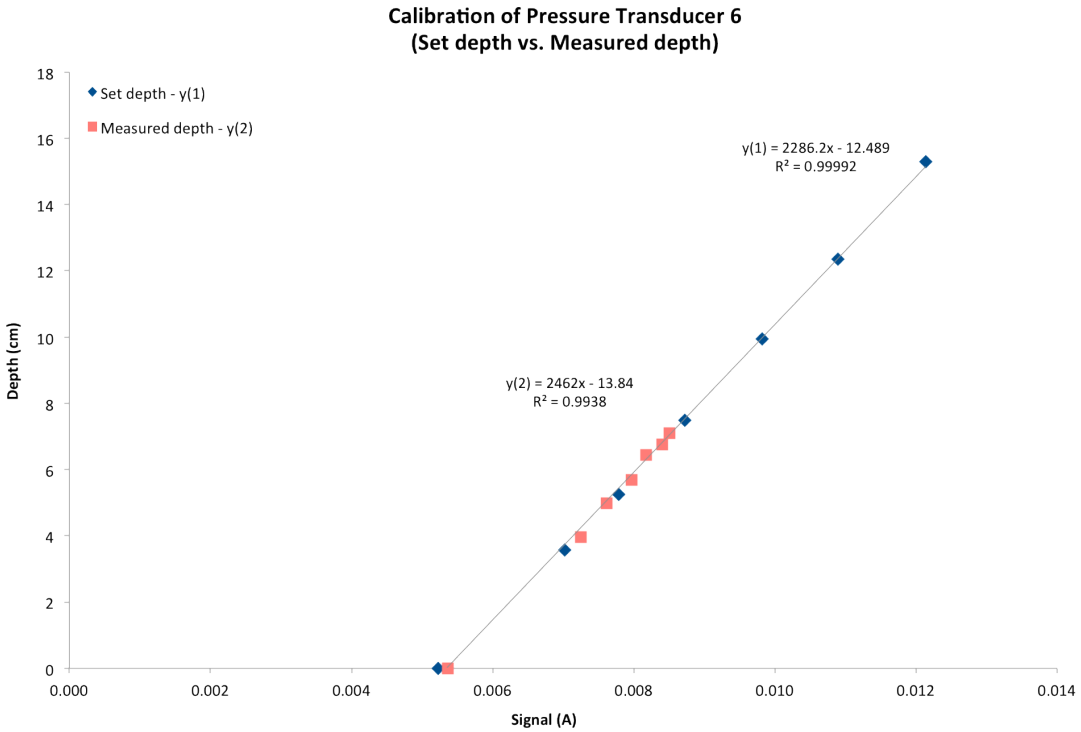

Figure 4.7 – Calibration of Pressure Transducer 6

Based on Figures 4.2 – 4.7, it can be seen that the calibration data obtained from both the set depth and measured depth methods yield similar results with a linear trend of data. There is an extremely good fit between the data and a linear relationship for each transducer with the resulting correlation coefficient, R^2 approaching unity. This is therefore considered an acceptable set of calibration data. Considering the wider set of calibration data obtained using the set depth method, this data was subsequently used in the experimental programme.

Similarly, Figure 4.8 shows an example of the calibration results on a sloped bed.

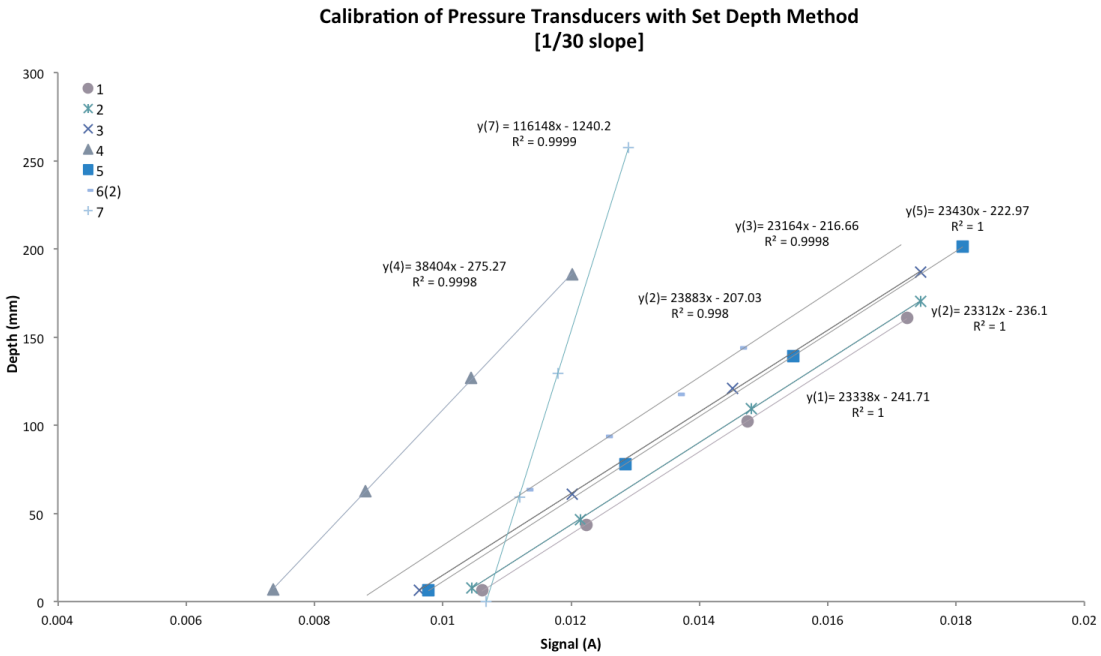

Figure 4.8 – Calibration of Pressure Transducers for the 1/30 slope

Based on Figure 4.8, and the plotted data obtained, it can be seen that the resulting correlation coefficient, R^2 yields an acceptable value approximating to one. Therefore, this is considered an acceptable set of calibration data. Clearly, the pressure transducers provided accurate and repeatable results.

4.2.2 Calibration of Flowmeter - Primary Inlet

Calibration of the flowmeter for the primary inlet was conducted by using the measuring tank that was readily available in the hydraulic laboratory. The calibration of the flowmeter used a simple procedure where the amount of water displaced in the measuring tank was measured against the time taken. The amount of water displaced is measured in terms of height (*ft.*), but because the area of the measuring tank is known, therefore the volume of flow can be computed. The volume is then divided with the time (*s*) taken for the displacement to occur to give the flowrate. Measurements below have been converted into litres. The measured flowrate is also compared to the flowmeter reading (digital reading on the flowmeter display) as well as the derived

flowrate based on the manufacturer supplied equation for the meter. Presented in Figure 4.9 is the calibration result for the primary inlet.

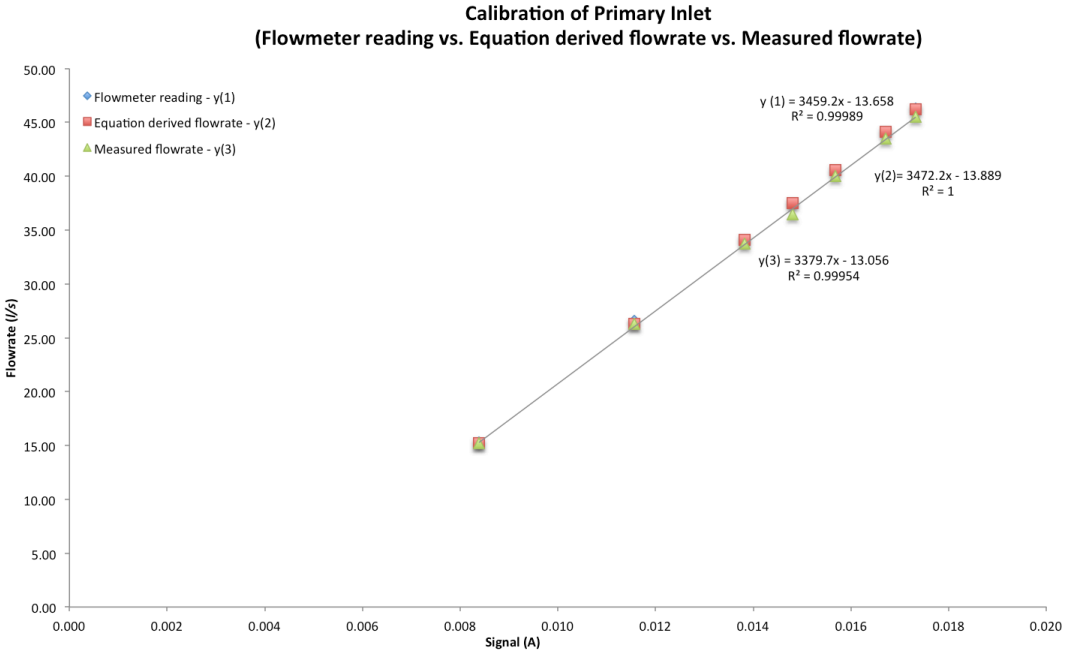

Figure 4.9 – Calibration of Primary Inlet

Based on Figure 4.9 shown, it can be seen that the resulting calibration graph yields a good fit between all the 3 methods discussed above. The obtained determination coefficient, R^2 is approximates to 1 for all the methods of calibration. Therefore, the measured calibration data was considered acceptable and was used for the purpose of this experimental programme.

4.2.3 Calibration of Flowmeter – Surcharged Inlet

Calibration of flowmeter for the surcharged inlet adopted the same method as the calibration for the primary inlet and therefore has not been reiterated. The measured flowrate was also compared to the flowrate obtained from the flowmeter reading and the manufacturer calibration equation. Presented in Figure 4.10 is the calibration results obtained for the surcharged inlet.

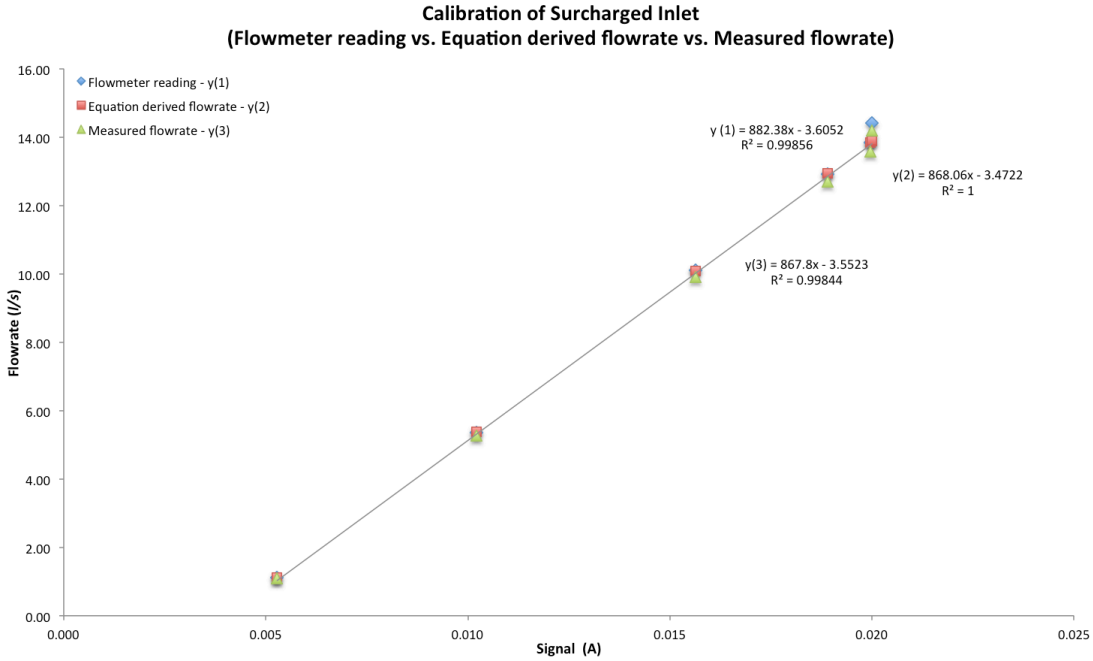

Figure 4.10 – Calibration of Surcharged Inlet

Based on Figure 4.10, it can be seen that the calibration graph obtained from all 3 methods yielded similar results – a linear trend with the R^2 approximating to 1. As with the primary inlet, the measured calibration equation was used to determine the surcharged flow in the subsequent tests.

4.3 LABORATORY TESTING

A total of 486 tests were completed and full details of each test are presented in Appendix 9. The laboratory test protocol was applicable throughout the entire experimental programme. However, before elaborating on the testing protocol that was used in this experimental programme, it is necessary to recognise the philosophy used to decide the order of the tests that were conducted. Following the calibration of all the necessary instruments and sensors, the experimental programme commenced with the testing of Grate A with the flat bed followed by Grate B also with the flat bed, thereby minimising the work required to change the rig. For each grate type, different flow conditions were tested – terminal, intermediate and surcharged conditions with increasing flowrate. The condition of the outlet was also altered from the original unplugged outlet to that of the plugged condition. The maximum flowrate tested depended on the capacity of the laboratory rig of the specific system tested. Hence, the test programme was as follows:

- Flat bed – Grate Type A – **Terminal** - Unplugged
  - Flat bed – Grate Type A – **Intermediate** – Unplugged
    - Flat bed – Grate Type A – **Surcharged** - Unplugged
      - Flat bed – Grate Type A – Terminal - **Plugged**
        - Flat bed – Grate Type A – Intermediate – **Plugged**

Having tested Grate A, the whole set of test were then repeated without the grates in place with the aim to understand impact of grates on the hydraulic performance, whereby:

- Flat bed – **No Grate A** – Terminal - Unplugged
  - Flat bed – **No Grate A** – Intermediate - Unplugged
    - Flat bed – **No Grate A** – Surcharged - Unplugged
      - Flat bed – **No Grate A** – Terminal - Plugged
        - Flat bed – **No Grate A** – Intermediate – Plugged

Following this, Grate Type B was then incorporated into the system and the same set of tests were repeated with Grate B as follows:

- Flat bed – **Grate Type B** – Terminal - Unplugged
  - Flat bed – **Grate Type B** – Intermediate – Unplugged
    - Flat bed – **Grate Type B** – Surcharged - Unplugged
      - Flat bed – **Grate Type B** – Terminal - Plugged
        - Flat bed – **Grate Type B** – Intermediate – Plugged

Upon the completion of tests for the horizontal slope, the tests were repeated for the 1 in 100 slope followed by the 1 in 30 slope. Again, the test programme was as follows:

- **1/100 Slope** – Grate Type A – Terminal - Unplugged
  - **1/100 Slope** – Grate Type A – Intermediate - Unplugged
    - **1/100 Slope** – Grate Type A – Surcharged - Unplugged
      - **1/100 Slope** – Grate Type A – Terminal – Plugged
        - **1/100 Slope** – Grate Type A – Intermediate – Plugged …

The summary of these tests is as given in Appendix 9. Each test was assigned a 'file name' that was used to describe the test that was completed. This was translated as follows:

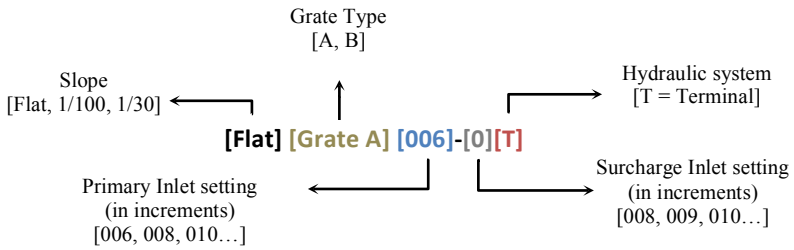

When test were completed with both outlets open, the system is termed 'unplugged'. During test with one outlet plugged by sealing the top outlet, the system is termed 'plugged'. In the case of the plugged/unplugged test, the filename included an additional term. For example:

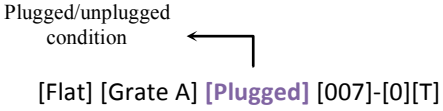

In the absence of any indication of the hydraulic system and the value of the surcharge inlet system is [0], then the tested hydraulic condition would be intermediate. An example of intermediate test file name is:

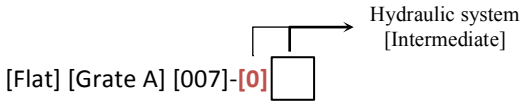

Otherwise, the tested system is surcharged. For example:

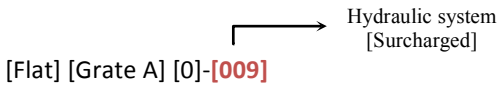

The laboratory tests were completed as a series of stages with a series of changes made to the rig to complete the test programme. Hence it should also be noted that each data set for this experimental programme was unique and calibration tests were conducted before each test programme (after each upgrade), to ensure that the measurement system remained in calibration.

4.3.1 Testing Protocol

As have been discussed earlier [Chapter 3], depending on the type of hydraulic conditions that needed to be achieved (or the type of test conducted) – terminal, intermediate, or surcharged test - the appropriate inlet, and/or outlets were opened or closed. However, the fundamentals of the laboratory testing protocol remained the same and this is summarised below:

1) The pump was primed or fine-tuned by feeding it with water and releasing the trapped air in the pump. This is achieved by turning on the small tap/valve at the pump that is located at the lower basement of the hydraulic laboratory and is an important initial step to ensure the flow that is delivered into the laboratory system is continuous and in a steady manner.
2) The pump was then turned on by switching the green (ON) button for the designated pump.
3) Water was then released from the overhead tank onto the laboratory rig by turning the red lever [Figure 4.11] that acts as a control mechanism of the flow from the overhead tank to the primary inlet.

Figure 4.11 – Control mechanism lever

4) Signals were then sent to the valves from the VI panel of between 0 – 24mA, to achieve the desired flowrate. For a single set of test, only a single flowrate was tested. The tests are then repeated but in increasing flowrates. The range of test conducted, usually begins with the lowest setting of 6mA to the highest achievable flowrate, or the maximum amount of flow that could be contained within the system.
5) A period of 10-15 minutes of settling period was given to the system to allow the flow to reach its steady state conditions before measurements were taken automatically. Once testing commences, all the measurements and data for all 7 pressure transducers were logged on automatically into the system and were written into the designated .lvm file.
6) Intermittently, the flowrates (in the form of outflow) were checked using the measuring tank at random intervals, with a minimum number of 3 measurements taken to ensure that the flow delivered by the inlet was equivalent to the desired flowrate. This was conducted primarily for comparison purposes. In the case of intermediate tests, both the outflow from the two measuring tanks was recorded.
7) The experimental system was left undisturbed to allow continuous measurements to be taken for a minimum of 15 minutes.
8) Once testing was completed, the valve was closed by setting it to 0 mA in the VI panel. The valve can also be shut through the NI MAX window.
9) The pipe that provides water to the pump (at the lower basement) was then turned off.
10) The pump was then turned off by pressing the red (OFF) control button.
11) Finally, the red lever was turned back to its original position to close the gate hence preventing any flow from the overhead tank onto the testing rig.

4.4 COLLECTION OF DATA

Data are automatically written into LabVIEW measurement files, which could be easily differentiated with the .lvm extension at the end of the filename. LabVIEW measurement file format (.lvm) is a text-based file format for one-dimensional data that could be used with the Read LabVIEW Measurement File and Write LabVIEW Measurement File Express VI's (http://www.ni.com). This format was opted because it can easily be imported into a spreadsheet program, such as Microsoft Excel to be processed.

Figure 4.12 shows an example of a written LabVIEW measurement file with its header corresponding to its connections in the NI Max setting.

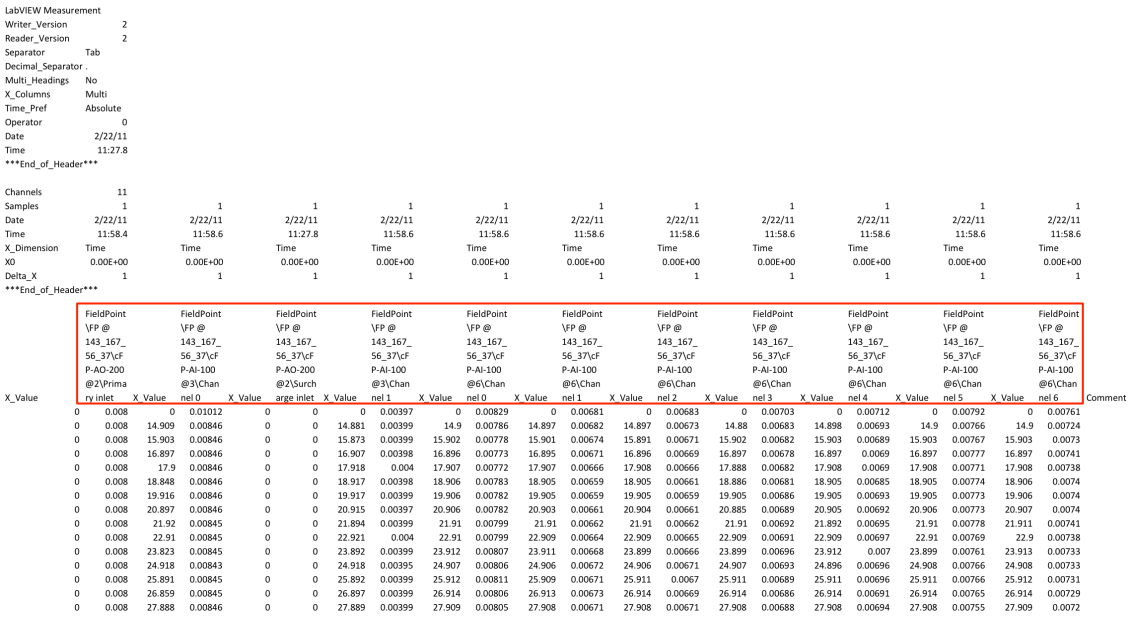

```
LabVIEW Measurement
Writer_Version	2
Reader_Version	2
Separator	Tab
Decimal_Separator	.
Multi_Headings	No
X_Columns	Multi
Time_Pref	Absolute
Operator	0
Date	2/22/11
Time	11:27.8
***End_of_Header***

Channels	11
Samples	1	1	1	1	1	1	1	1	1	1	1
Date	2/22/11	2/22/11	2/22/11	2/22/11	2/22/11	2/22/11	2/22/11	2/22/11	2/22/11	2/22/11	2/22/11
Time	11:58.4	11:58.6	11:27.8	11:58.6	11:58.6	11:58.6	11:58.6	11:58.6	11:58.6	11:58.6	11:58.6
X_Dimension	Time	Time	Time	Time	Time	Time	Time	Time	Time	Time	Time
X0	0.00E+00	0.00E+00	0.00E+00	0.00E+00	0.00E+00	0.00E+00	0.00E+00	0.00E+00	0.00E+00	0.00E+00	0.00E+00
Delta_X	1	1	1	1	1	1	1	1	1	1	1
***End_of_Header***

X_Value	FieldPoint \FP @ 143_167_ 56_37\cF P-AO-200 @2\Primary inlet	X_Value	FieldPoint \FP @ 143_167_ 56_37\cF P-AI-100 @3\Chan nel 0	X_Value	FieldPoint \FP @ 143_167_ 56_37\cF P-AO-200 @2\Surcharge inlet	X_Value	FieldPoint \FP @ 143_167_ 56_37\cF P-AI-100 @3\Chan nel 1	X_Value	FieldPoint \FP @ 143_167_ 56_37\cF P-AI-100 @6\Chan nel 0	X_Value	FieldPoint \FP @ 143_167_ 56_37\cF P-AI-100 @6\Chan nel 1	X_Value	FieldPoint \FP @ 143_167_ 56_37\cF P-AI-100 @6\Chan nel 2	X_Value	FieldPoint \FP @ 143_167_ 56_37\cF P-AI-100 @6\Chan nel 3	X_Value	FieldPoint \FP @ 143_167_ 56_37\cF P-AI-100 @6\Chan nel 4	X_Value	FieldPoint \FP @ 143_167_ 56_37\cF P-AI-100 @6\Chan nel 5	X_Value	FieldPoint \FP @ 143_167_ 56_37\cF P-AI-100 @6\Chan nel 6	Comment
0	0.008	0	0.01012	0	0	0	0.00397	0	0.00829	0	0.00681	0	0.00683	0	0.00703	0	0.00712	0	0.00792	0	0.00761
0	0.008	14.909	0.00846	0	0	14.881	0.00399	14.9	0.00786	14.897	0.00682	14.897	0.00673	14.88	0.00683	14.898	0.00693	14.9	0.00766	14.9	0.00724
0	0.008	15.903	0.00846	0	0	15.873	0.00399	15.902	0.00778	15.901	0.00674	15.891	0.00671	15.902	0.00682	15.903	0.00689	15.903	0.00767	15.903	0.0073
0	0.008	16.897	0.00846	0	0	16.907	0.00398	16.896	0.00773	16.895	0.00671	16.896	0.00669	16.897	0.00678	16.897	0.0069	16.897	0.00777	16.897	0.00741
0	0.008	17.9	0.00846	0	0	17.918	0.004	17.907	0.00772	17.907	0.00666	17.908	0.00666	17.888	0.00682	17.908	0.0069	17.908	0.00771	17.908	0.00738
0	0.008	18.848	0.00846	0	0	18.917	0.00398	18.906	0.00783	18.905	0.00659	18.905	0.00661	18.886	0.00681	18.905	0.00685	18.905	0.00774	18.906	0.0074
0	0.008	19.916	0.00846	0	0	19.917	0.00399	19.906	0.00782	19.905	0.00659	19.905	0.00659	19.905	0.00686	19.905	0.00693	19.905	0.00773	19.906	0.0074
0	0.008	20.897	0.00846	0	0	20.915	0.00397	20.906	0.00782	20.903	0.00661	20.904	0.00661	20.885	0.00689	20.905	0.00692	20.906	0.00773	20.907	0.0074
0	0.008	21.92	0.00845	0	0	21.894	0.00399	21.91	0.00799	21.91	0.00662	21.91	0.00662	21.91	0.00692	21.892	0.00695	21.91	0.00778	21.911	0.00741
0	0.008	22.91	0.00845	0	0	22.921	0.004	22.91	0.00799	22.909	0.00664	22.909	0.00665	22.909	0.00691	22.909	0.00697	22.91	0.00769	22.9	0.00738
0	0.008	23.823	0.00845	0	0	23.892	0.00399	23.912	0.00807	23.911	0.00668	23.899	0.00666	23.899	0.00696	23.912	0.007	23.899	0.00761	23.913	0.00733
0	0.008	24.918	0.00843	0	0	24.918	0.00395	24.907	0.00806	24.906	0.00672	24.906	0.00671	24.907	0.00693	24.896	0.00696	24.908	0.00766	24.908	0.00733
0	0.008	25.891	0.00845	0	0	25.892	0.00399	25.912	0.00811	25.909	0.00671	25.911	0.0067	25.911	0.00689	25.911	0.00696	25.911	0.00766	25.912	0.00731
0	0.008	26.859	0.00845	0	0	26.897	0.00399	26.914	0.00806	26.913	0.00673	26.914	0.00669	26.914	0.00686	26.914	0.00691	26.914	0.00765	26.914	0.00729
0	0.008	27.888	0.00846	0	0	27.889	0.00399	27.909	0.00805	27.908	0.00671	27.908	0.00671	27.908	0.00688	27.908	0.00694	27.908	0.00755	27.909	0.0072
```

Figure 4.12 – Example of a LabVIEW measurement (.lvm) file

The data recorded in each .lvm file was subsequently used in the analysis of data, which is detailed in Section 4.5.

4.5 DATA PROCESSING

This section highlights the step-by-step method undertaken to process the data and of the measures taken to minimise errors and discrepancies in the data. Some of the initial results have been used to illustrate the processes involved, while the remaining results of this experimental programme are further discussed in Chapter 5.

Original data sets in the form of .lvm files were converted to a Microsoft Excel spreadsheet. These data were then processed to find the hydraulic depth and the flowrate into the experimental system using the calibrated equations. The depth of water at each time step was calculated and the overall average for each pressure transducer was then computed. This procedure was applied to both the primary inlet and for the surcharge flow condition. This enabled the flowrate at each time step to be computed, and ultimately an average flowrate for both flows.

Figure 4.13 shows an example of the results that highlights the recorded depth at each pressure transducer over the duration of a 15 minute recording interval – for Grate A in a terminal test. In order to relate the hydraulic depth between the platform surface and that in the gully pot, the gully depth has been added to the existing graph.

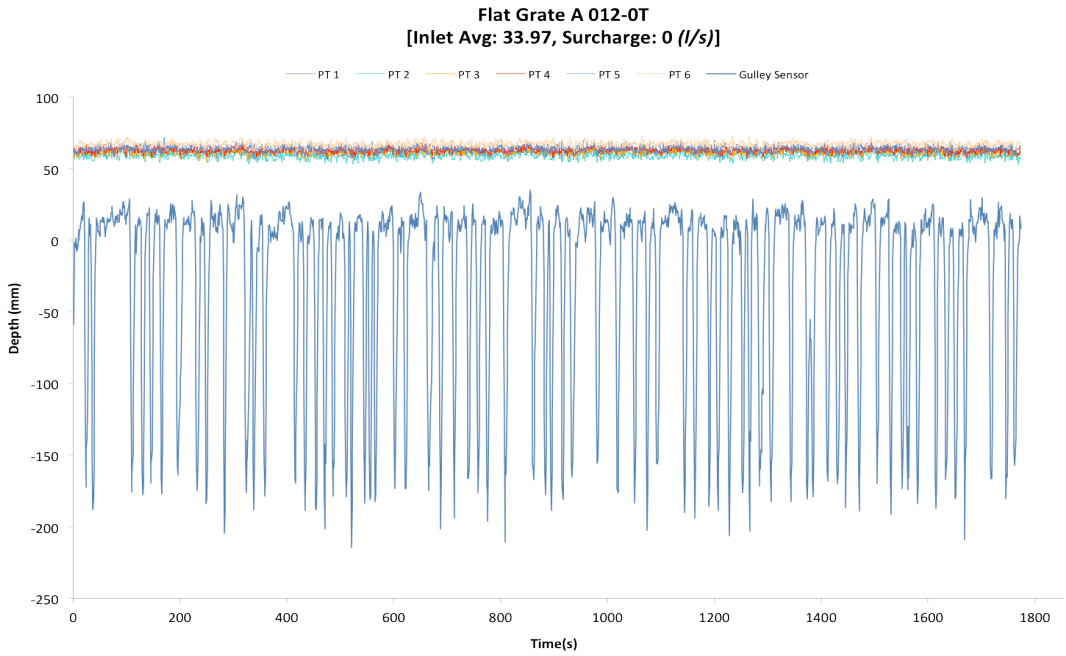

Figure 4.13 – Example of the recorded depth of the pressure transducers

It can be seen that the hydraulic depth on the bed of the platform is quite similar between each of the pressure transducers and the reading of all of the pressure transducers are consistent throughout the test. However, in order to look closely at the depth of a specific point on the bed, the measured depth of a particular pressure transducer could be extracted. An example of this is presented in Figure 4.14, where the hydraulic depth above the pressure transducer closest to the grate from the primary inlet (PT 2) was extracted [Figure 3.24 for specific location]. The depth at a single point was also calculated by taking the average of the entire data set, as highlighted in the figure. The standard deviation, maximum, and minimum reading were also established. Table 4.1 gives a summary of the results for this specific test.

Table 4.1 – Summary of results

	DEPTH (MM)					
	PT1	**PT2**	**PT3**	**PT4**	**PT5**	**PT6**
AVERAGE	62.31	58.88	61.39	62.89	63.77	67.18
STDEV	2.06	2.03	1.71	1.65	2.20	1.91
MAX	68.53	65.73	66.64	68.78	69.95	72.86
MIN	55.10	52.97	55.96	57.12	57.49	61.89

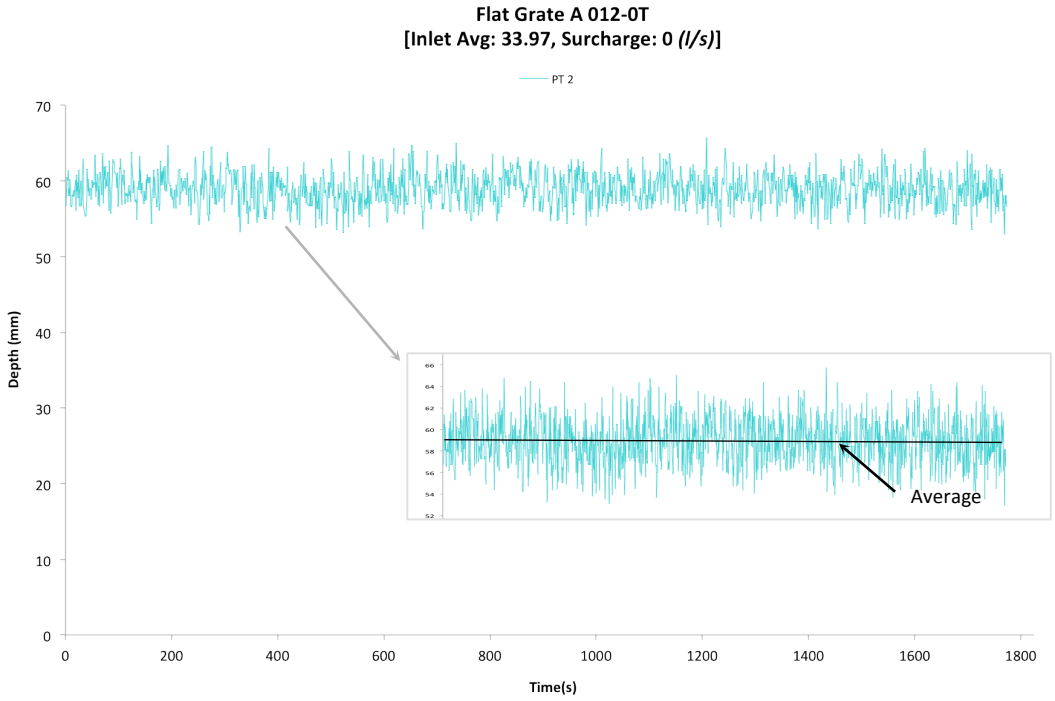

Figure 4.14 – Example of the hydraulic depth for a single pressure transducer

Checks of the data for the rest of the system of the same test are also made. For this particular test, there is only a single flow that enters the experimental system, which is from the primary inlet. The measured flowrate of the primary inlet, as shown in Figure 4.15, highlights that the system fluctuates about a mean value with the following evaluation.

Table 4.2 Summary of the results of the primary inlet

	INLET *(l/s)*
AVERAGE	33.98
STDEV	0.07
MAX	34.24
MIN	33.79

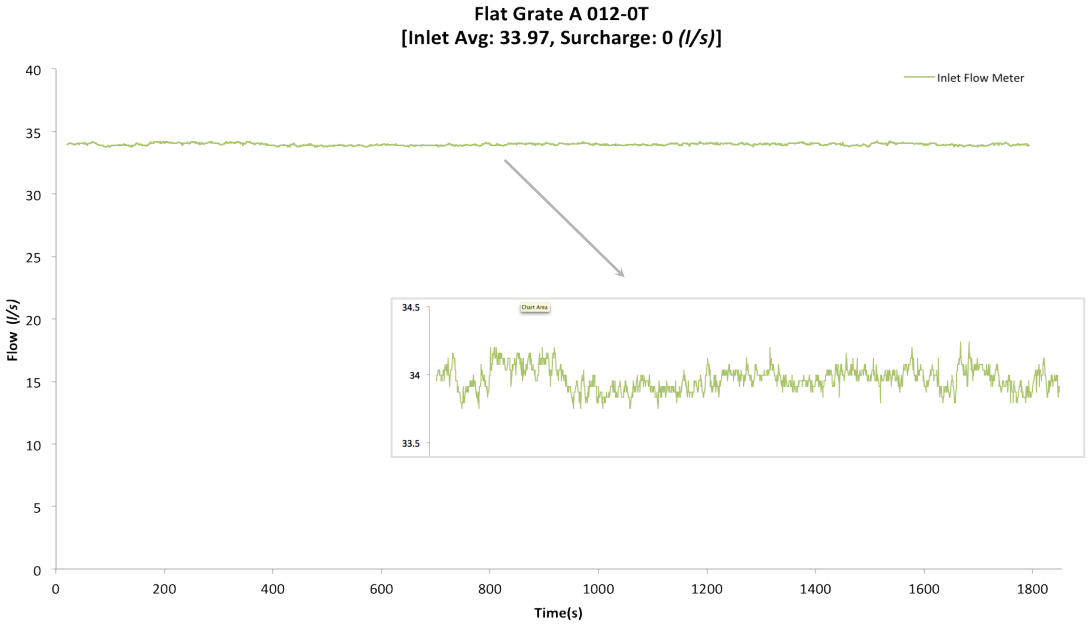

Figure 4.15 – Primary inlet stability

Using these methods, the data obtained from the experimental work was processed and the results are presented in the subsequent chapter.

CHAPTER 5
RESULTS, ANALYSIS AND DISCUSSION

Presented in this chapter are the results, analysis and the discussions of the experimental work. Therefore, the chapter has been split into two subsections: Results (Section 5.1) and Analysis and Discussion of Results (Section 5.2).

5.1 RESULTS

The results are presented as head-discharge relationship and have been presented in a series of chapter sections based on the different types of tests as follows:

- 5.1.1 Terminal tests
- 5.1.2 Intermediate tests
- 5.1.3 Tests with surcharged flow

For the terminal tests, the impact of grates was studied by comparing the effect non-grated inlet on the head-discharge relationship to the grated inlet. The effect of bed slope and plugged/unplugged condition on the head-discharge relationship was also studied and presented. This is presented in Section 5.1.1-5.1.3.

The head-discharge relationship of the terminal tests is then compared to the head-discharge relationship of the intermediate tests. The effect of bed slope on the head-discharge of the intermediate tests was also studied and the efficiency of the grates was also determined. Further detail is presented in Section 5.2.1 and 5.2.2 respectively. For the tests with surcharge flow, the head-discharge relationship was determined for tests with backflow only and for tests with both backflow and approaching flow.

5.1.1 Terminal Tests

As previously explained [3.1.1], a terminal system is a system in which all inflow enters the gully system. Therefore, in this type of system, the approaching flow is comparable to the collected flow.

Presented in Figure 5.1 is the head-discharge relationship of Grate A and Grate B for the Flatbed – Unplugged test. The flow depths are taken as the average of all six pressure transducers to represent the hydraulic depth on the surface. This is because in the case of a terminal test, the depth of water on the testing platform is reasonably constant and the average of all six-pressure transducers therefore provides an appropriate representation of the hydraulic head going into the gully system. Based on this figure, it can be seen that the head-discharge relationship of both Grate A and B displays a similar behaviour throughout the flow range – with a gradual increase of inflow depth as the flowrate increases. The inflow depth for Grate B is often marginally higher as compared to Grate A for the same flowrate. This is a probable indication that Grate A has a higher rate of removal compared to Grate B because the clear opening area of Grate A is larger than Grate B. In addition there is a deviation from a smooth curve at flowrates in the range 34 to 40 litres/s and this has been further explained by reference to the monitored depth of flow in the gully pot as shown in Figure 5.2.

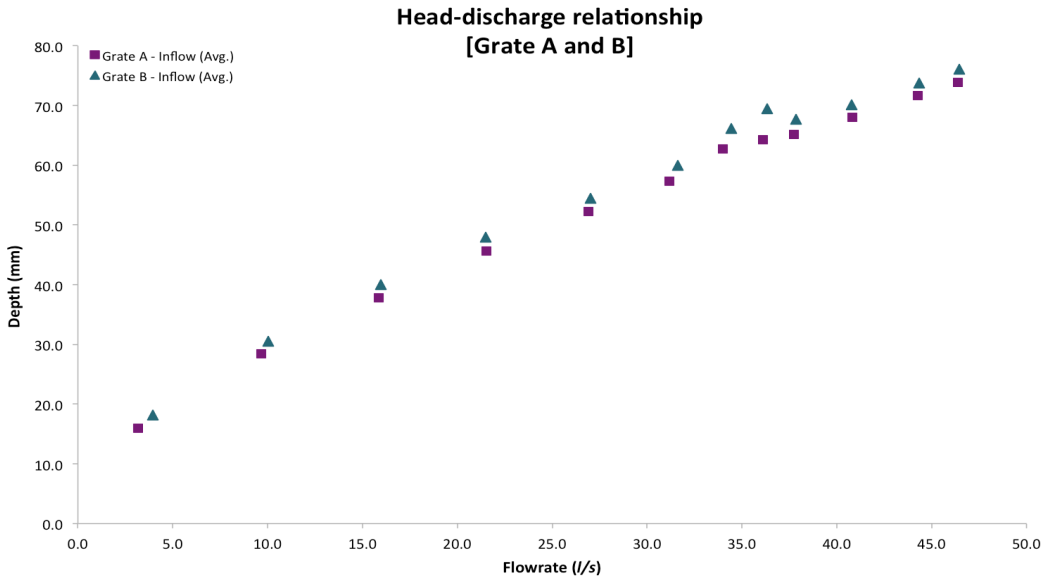

Figure 5.1 – The head-discharge relationship of Grate A and B with a flat bed

The corresponding depth of water in the gully pot is presented for grate (Grate A) and is as shown in Figure 5.2. The gully depth (h_G) has been presented as a negative depth (mm) where 0 mm is the grate surface parallel to the platform surface. Hence a value of -825 mm represents the bottom of the gully -750mm nominal gully depth plus 75mm grate depth, [Figure 3.18, also Table 3.2].

It can be seen that there is a steady increase in gully depth with flowrate. However, after reaching a peak in depth (pt. 2, Fig 5.2) at approximately -25mm and between 30-35 *l/s,* there is a change of depth in the gully. This can be seen by the rapid decline in depth between 34-40 *l/s* followed by a steady increase in depth again. The explanation for this change may be made by reference to the level of the gully pot outlets which become surcharged with pressurised flow. The outlets act like an orifice with pressurised flow with a corresponding increase in the flowrate through the outlet. Subsequently the flow dynamics result in a lowering of the flow depth in the gully pot (as outflow is greater than inflow), which reaches a minimum at pt. 4, Fig 5.2. Subsequently there is a gradual increase in flow depth. A more detailed picture of these changes has been made by reference to captured video images, shown in Figure 5.3. These images have been extracted from a continuous video recording over the duration of the test. The images shown correspond to the key points of change as shown in Figure 5.2.

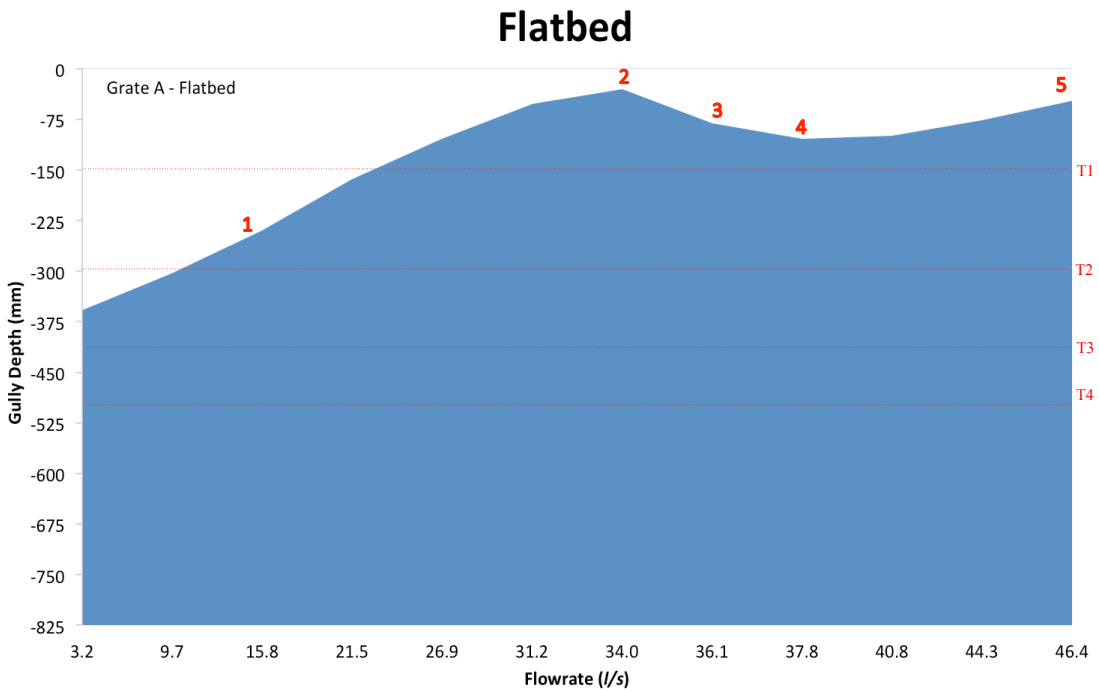

Figure 5.2 – The depth of water in the gully (Grate A) for a range of flowrates with a flat bed

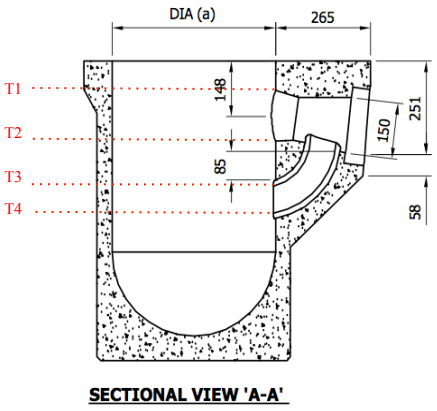

Figure 5.2(a) – The corresponding outlet depth

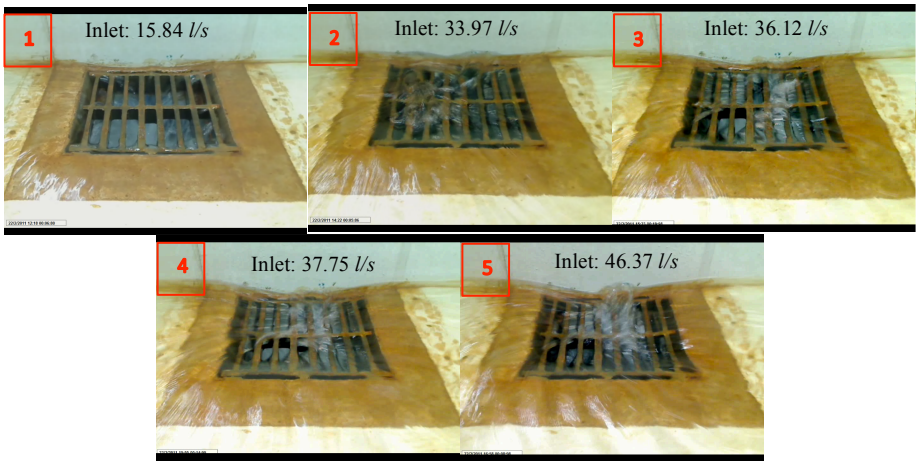

Figure 5.3 – The behaviour of flow at the Grate A inlet at different flowrates

These images highlight the change in surface flow pattern at the grate and from image 1 to image 2 there is a change in flow regime with a transition from an orifice flow to one of a surcharged flow regime. Images 3, 4 and 5 show a gradual return to orifice flow. Hence it is concluded that the flow conditions at the gully are very much a function of the gully pot and that the relationship between flow depth and flowrate is a function of the geometry of each individual grate, the geometry of the gully pot, especially the height of the outlet pipe and the dynamics of the flow that enters the gully.
This conclusion is important and has been reflected in the results presented later.

5.1.1.1 Non-Grated inlets

Tests were also completed with the grates removed, termed Non-Grated tests, where the opening area (AxB) corresponded to the basic frame of the respective grates [Figure 3.18, also Table 3.2]. These tests were conducted to obtain the impact of each of the grate on the efficiency (changes in depth and flowrate) of the surface water removal. Non-Grated tests can also be considered as part of the repeat tests series in order to see if the conditions previously tested were repeatable and yielded similar results.

Figure 5.4 shows the comparison between the Grated and Non-grated tests for both Type A and B grates. It can clearly be seen that the Non-grated inlets – Type A and B shows similar overall characteristics to those recorded for the Grated – Type A and B grates respectively. For low flowrates, the recorded depth is similar for both systems but

in the case of higher flowrates, the inflow depth for the non-grated systems are lower when compared to those for the grated tests (due care being made of the point of surcharge of the gully pot outlet pipe). The difference is slight and highlights that the grate creates a small additional loss due to flow having to pass through the grate openings. Clearly however, the manufacturers have ensured that the design of the grate inlets results in an optimum weir flow (without surcharge). This confirms that the overall design (e.g orientation/size/spacing) of the grates have been devised to perform at its optimal capacity.

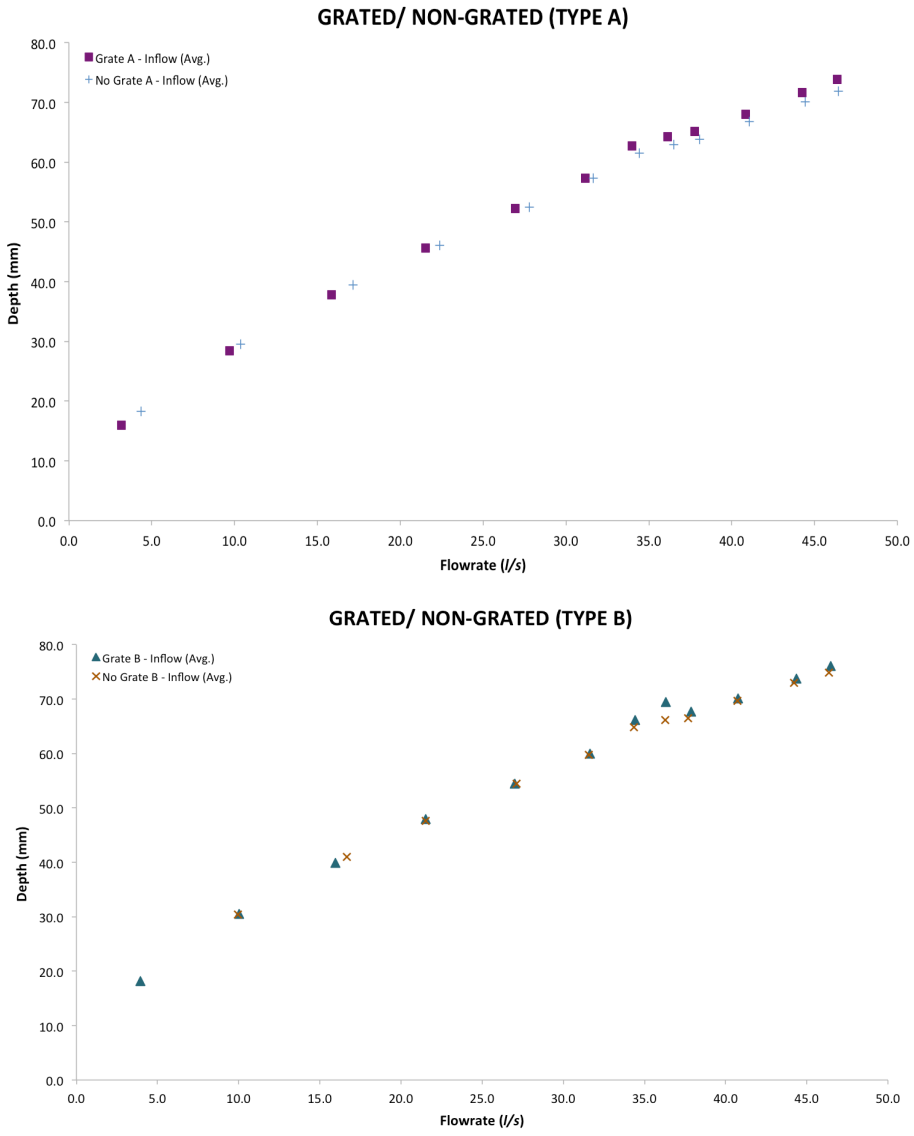

Figure 5.4 – Head discharge comparison between the grated and non-grated inlets

5.1.1.2 Effect of Bed Slope on Head Discharge Relationship

The head-discharge relationship obtained for different sloping conditions is shown in Figure 5.5. The three different longitudinal slopes (S_L) were tested: flatbed, 1 in 100 and 1 in 30. As expected, the results show that the bed slope has a significant impact on the resultant head-discharge relationship for each grate. The effect of slope is more prominent at flows up to 34 litres/s with an increase in depth as the slope is reduced but at flowrates above this value, the relationship between depth and flowrate becomes very similar for the 1 in 100 and 1 in 30 slopes. This is due to the relationship between the gully depth and inflow as previously explained in 5.2, and shown in Figure 5.6. These highlight that the flow depth in the gully pot is similar for the 1 in 100 and 1 in 30 bed slopes thereby confirming the coming together of the relationship between head and discharge.

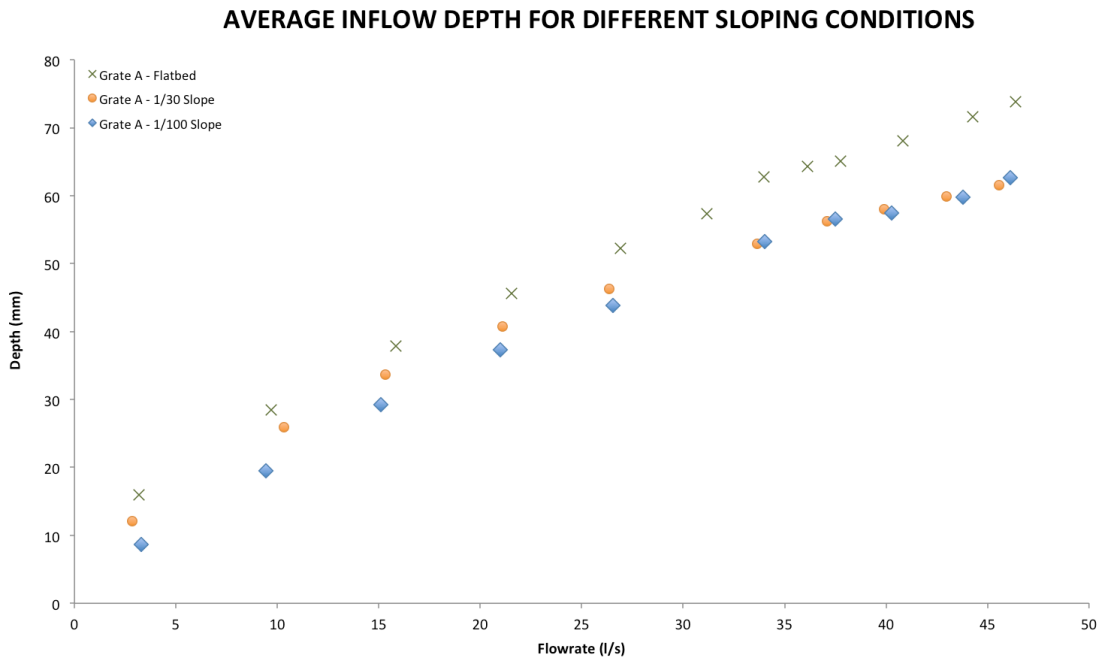

Figure 5.5 – The effect of different sloping conditions on the head-discharge relationship

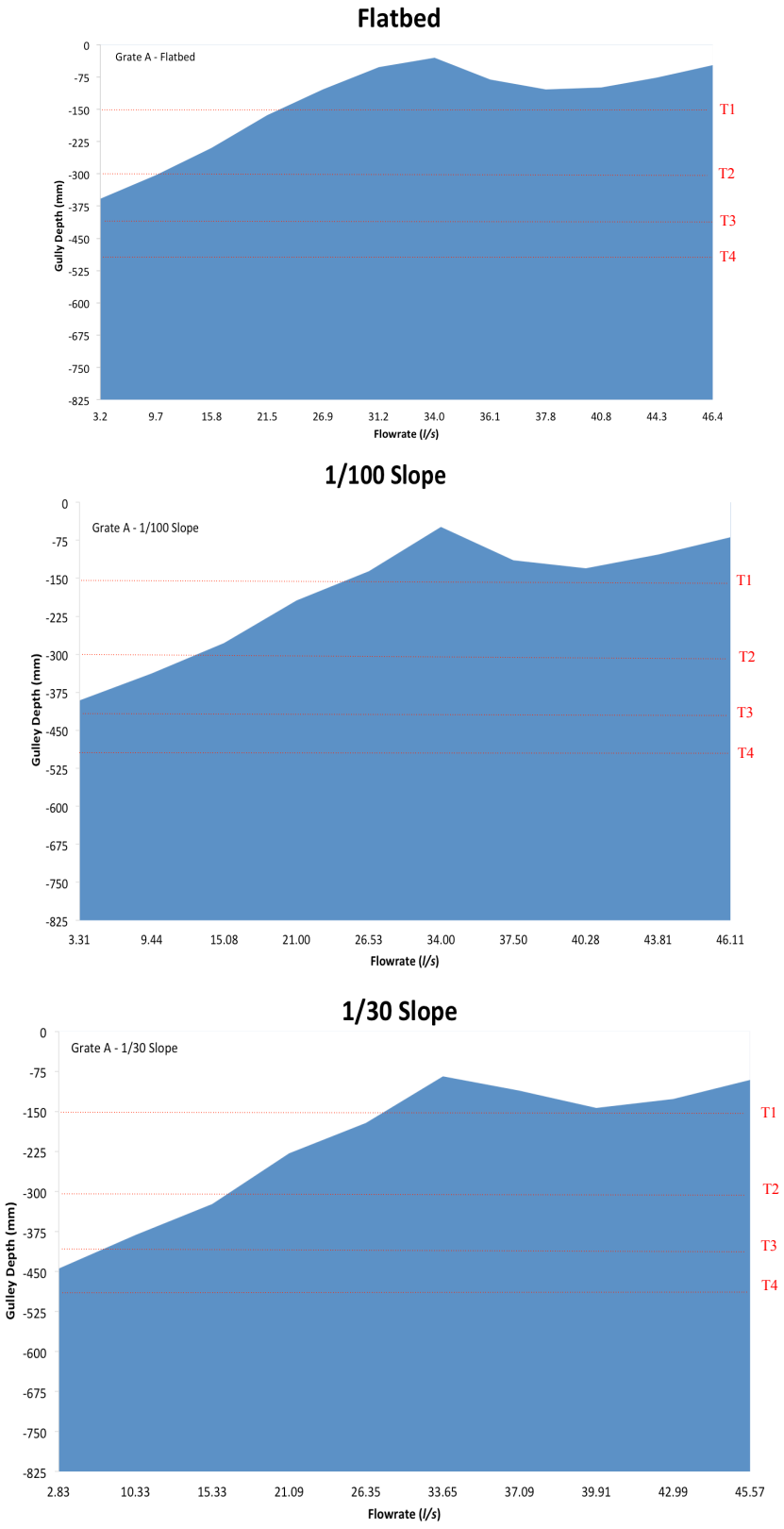

Figure 5.6 – Gully depth for different sloping conditions – flatbed, 1 in 100 and 1 in 30.

5.1.1.3 Plugged/Unplugged tests

In this experimental context, the Plugged system refers to the plugging of the rodding eye and is a condition whereby the capacity of the outflow from the gully pot is reduced. Less flow can leave the system via the gully and the remaining flow has to leave the system from the secondary outlet (downstream outlet tank). Due to the limiting size of the outlet pipes at the (outlet) tank, the tank filled up quickly and caused flooding back onto the surface of the platform. Hence only a limited flow range was used in these tests - between 0 – 22 *l/s* compared to 0 – 50 *l/s* of the unplugged gully tests.

Figure 5.7 shows the comparison of the head-discharge relationship between the plugged/unplugged conditions. It can be seen that the depth of the plugged gulley increased significantly at flowrates above 16 *l/s*. This is because the capacity of the gully pot has been reached. In comparison with the recommendations outlined in HA 102/00, the capacity (maximum flowrate) that can be accepted by a gully pot with a 150mm diameter outlet – without surcharging is approximately 15 *l/s*. Hence the experimental results are in accordance with these design standards. Figure 5.8 shows the effect of the plug on gully depth and it can be seen that with a plugged gully the gully pot is quickly filled, and the depth quickly reaches the surface of the platform and overflows.

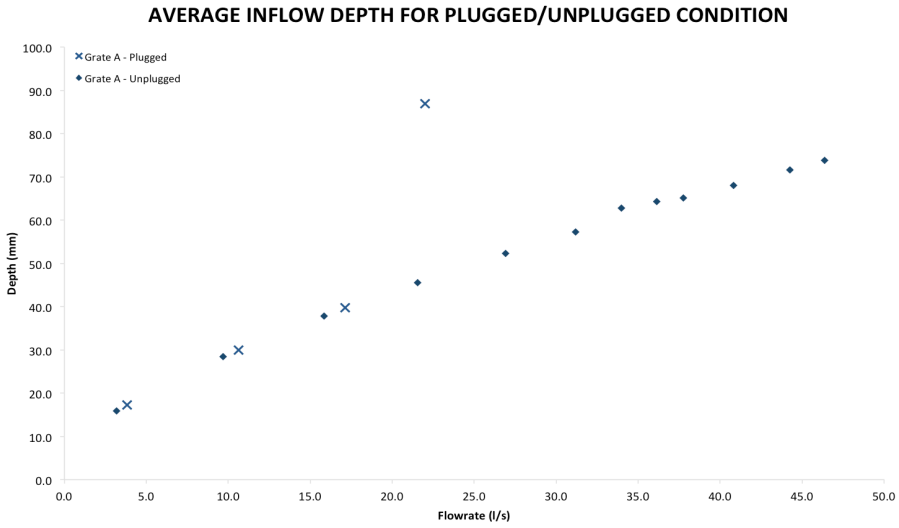

Figure 5.7 – The effect of a gully plug on the head-discharge relationship

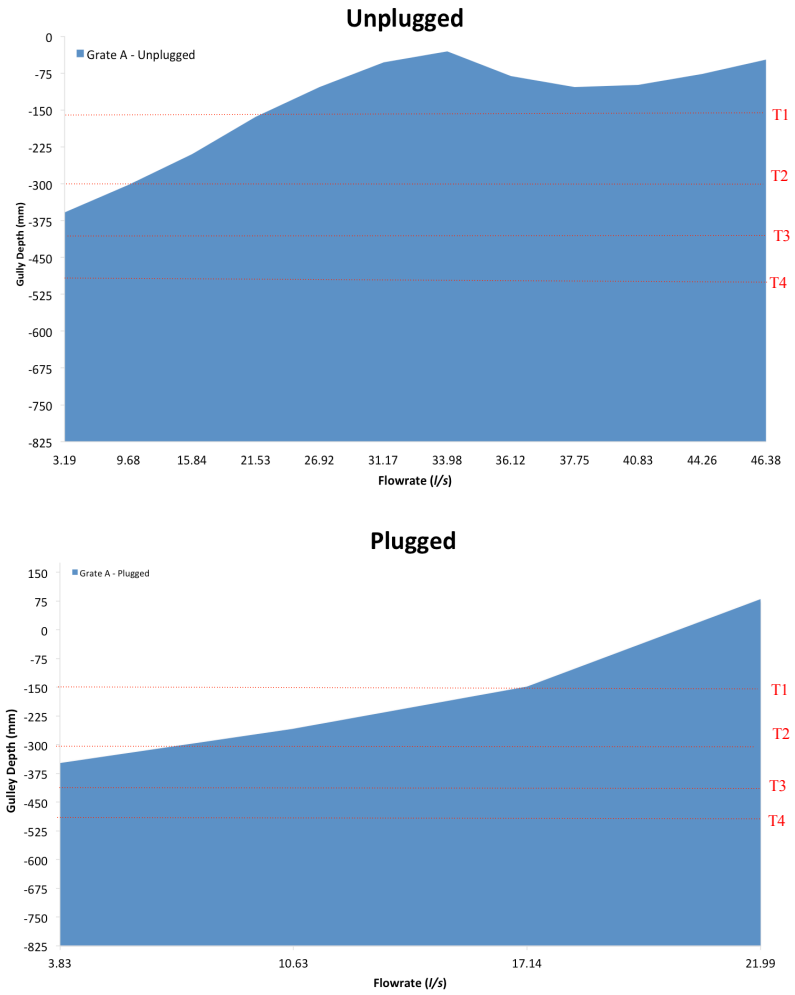

Figure 5.8 – The effect of a plug on the flow depth in the gully

5.1.2 Intermediate Tests

Intermediate systems are gully systems which permit a portion of the approaching flow to flow past the system and onto the next downstream gully. Therefore, in the laboratory system, the amount of flow collected by the gully is termed the 'intercepted' flow and the 'remaining' flow is the bypassed flow. The latter flow was collected in the outlet tank. In the case of the intermediate tests, the head (as presented in this section) is taken as an average of only two pressure transducers (PT1 and PT2) [Figure 3.28] that are situated upstream of the inlet. The reason why these two transducers were selected relates to the flow pattern that occurs over the surface of the platform in the intermediate tests. It was required to have an accurate measurement of the flow depth that was consistent for all tests. Initial measurements showed that the direction of flow to the grate changed with increasing flowrate and as a consequence there was a change in the importance of the different transducers to measure the depth that contributed to the grate flow. For example, the flow paths downstream of the grate sometimes resulted in a swirl motion with a back-flow towards the downstream face of the grate whereas at other flowrates the flow path resulted in a continuous longitudinal flow from the upstream to downstream end of the platform. In contrast, the flow path over the two upstream transducers was always in the same direction and hence these 2 transducers were used in the results analysis. To confirm this decision, a preliminary review of the results was made, whereby the head discharge relationships were established for each pair of transducers (1 & 2, 3 & 4 and 5 &6) and for the average depth of all six transducers. This analysis showed some inconsistencies in the trend of each head discharge relationship but that the expected relationships (based on the terminal tests) were derived from transducers 1 & 2. As a consequence, these 2 transducers were used in the subsequent analysis. Figure 5.9 shows the inconsistencies of the trend between the average depth of all six transducers and the average of a pair of transducer (PT 1 and PT 2).

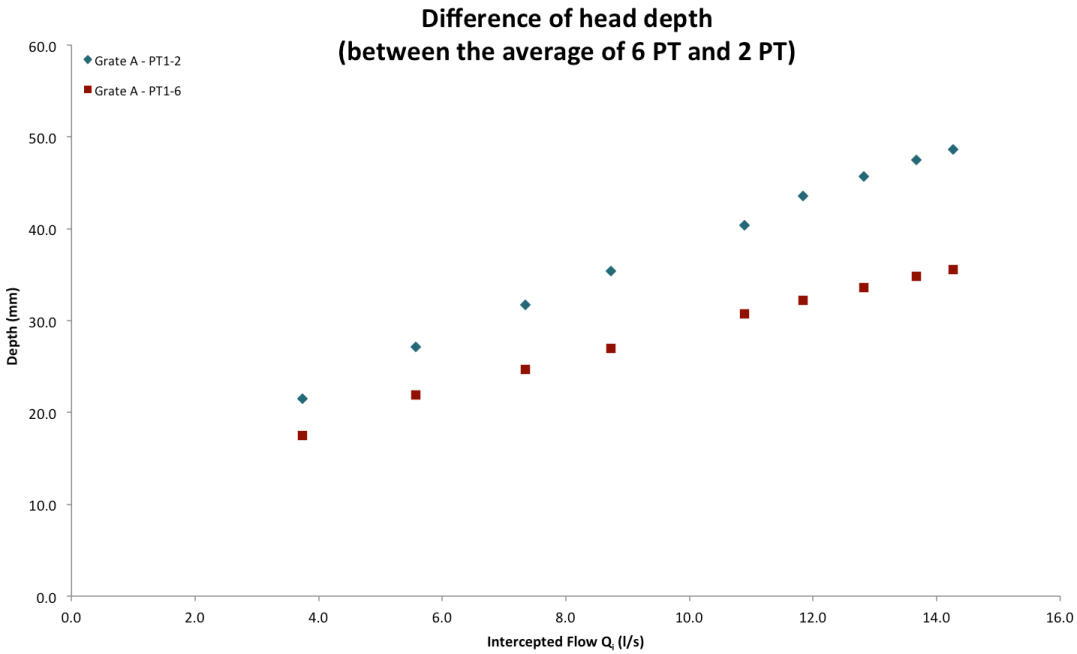

Figure 5.9 – Relationship between depth and intercepted flow (based on the no. of pressure transducers used in the analysis)

Figure 5.10 compares the head between terminal and intermediate system based on different assumptions. The initial assumes that all six pressure transducer carry the same weight in contributing to the average head depth and the second assumes that the more significant pressure transducer are the ones situated at the inlet (PT1 and PT2) – as mentioned earlier. It can be seen that if the average of all six pressure transducers were used to obtain the average head depth, the head depth for the intermediate test would show to be similar to the terminal. If only two of the pressure transducers were considered, then the obtained head depth for the intermediate tests would, as predicted be higher than of the terminal tests. This is because of the position of the pressure transducers – which were situated more closely to the primary inlet as compared to the others.

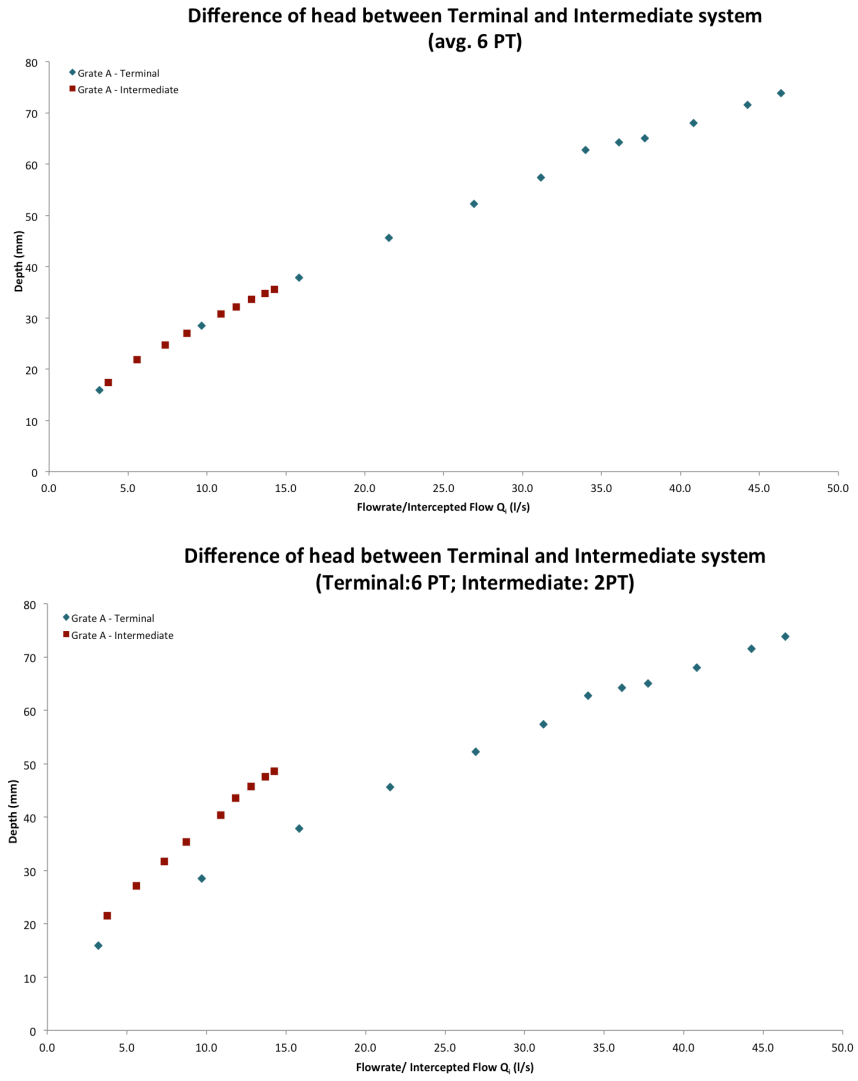

Figure 5.10 – Comparison in terms of head between terminal and intermediate system

Based on the measurements from 2 pressure transducers, Figure 5.11 and 5.12 shows the head-discharge relationship for the intermediate test and the corresponding gully depth respectively, for grates A and B and with no grate, with a flatbed. For the intermediate tests, the intercepted flow Q_i (*l/s*) instead of the total approaching flow, Q_a (*l/s*) as the discharge. This is in order to give an overview of the relationship between the depth and the flow that is passing through the grates. It can be seen that the as the flowrate increases the performance of Grates A and B become more similar. The performance of the grated and non-grated for both type A and B were also similar throughout the entire tested range of flowrates.

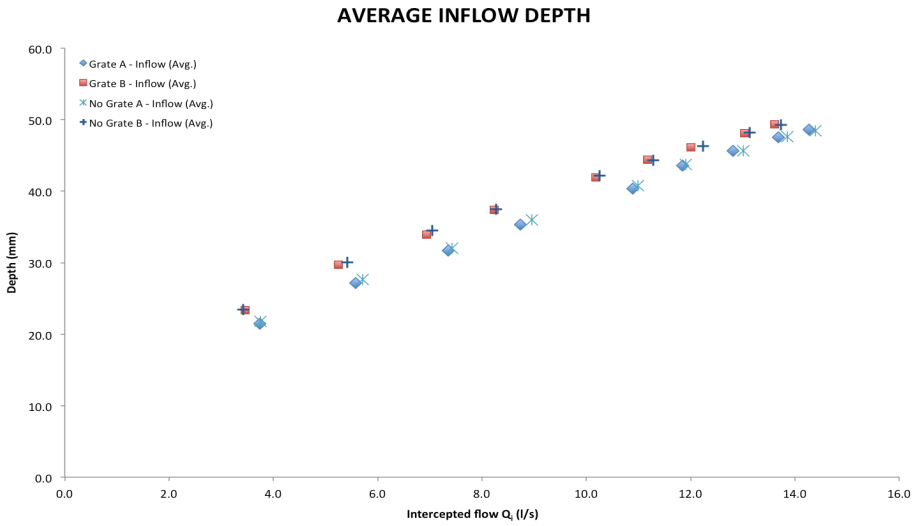

Figure 5.11 – The head-discharge relationship for the intermediate tests with a flatbed and all 3 Grate conditions (A, B and Non-grated)

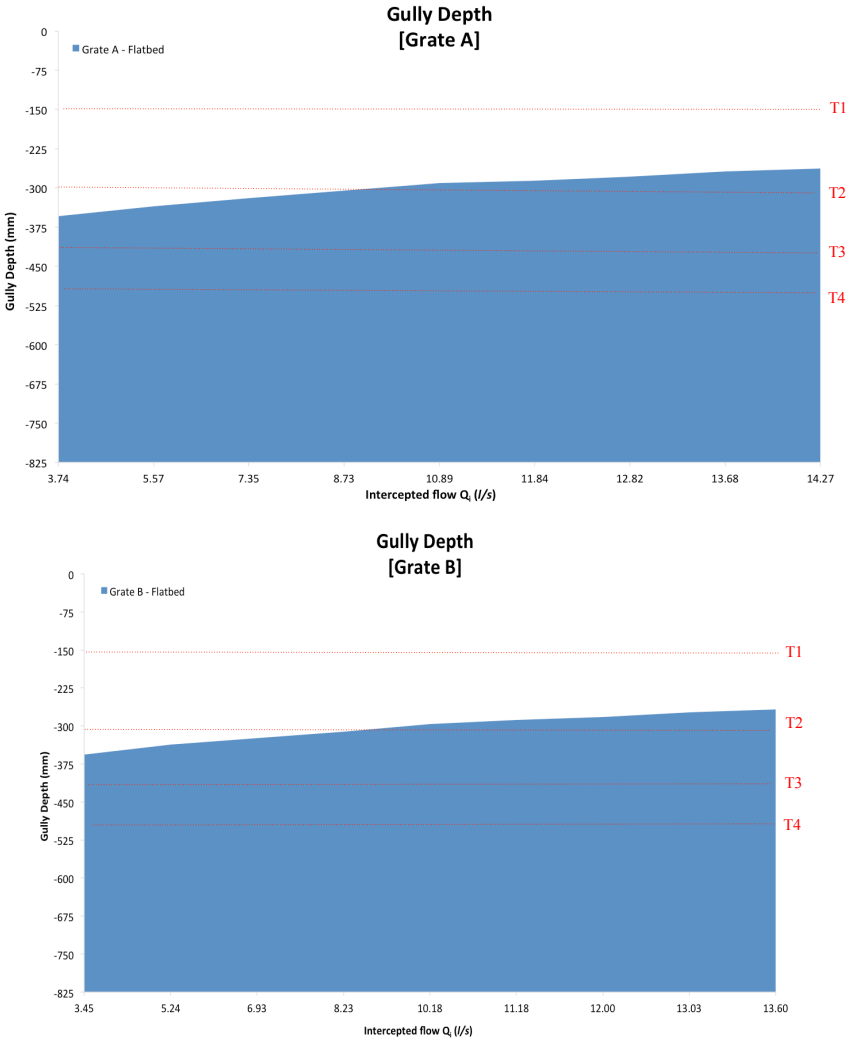

Figure 5.12 – The corresponding gully depth

5.1.2.1 Effect of bed slope on the head-discharge relationship for intermediate tests

Figure 5.13 shows the head-discharge relationship based on the different sloping conditions – flatbed, 1 in 100, and 1 in 30. An initial review of the data showed that a very small average depth was obtained at the 1/30 slope. As a consequence the laboratory rig for the 1/30 slope was narrowed down to half the original width in order to obtain a more significant average depth of the flow. This new setting was termed 1/30N and refers to the narrowed channel of the platform. Figure 5.13 shows the effect of slope on the gully depth (Grate A). In terms of gulley depth, the depth increases as the bed slope increases. However, the intercepted flow decreases as the slope increases. The intercepted flow for the 1/30N tests, as expected, was higher when compared to the 1/30 full width tests but clearly the results suggest that the width of the channel had little impact on the head discharge relationship.

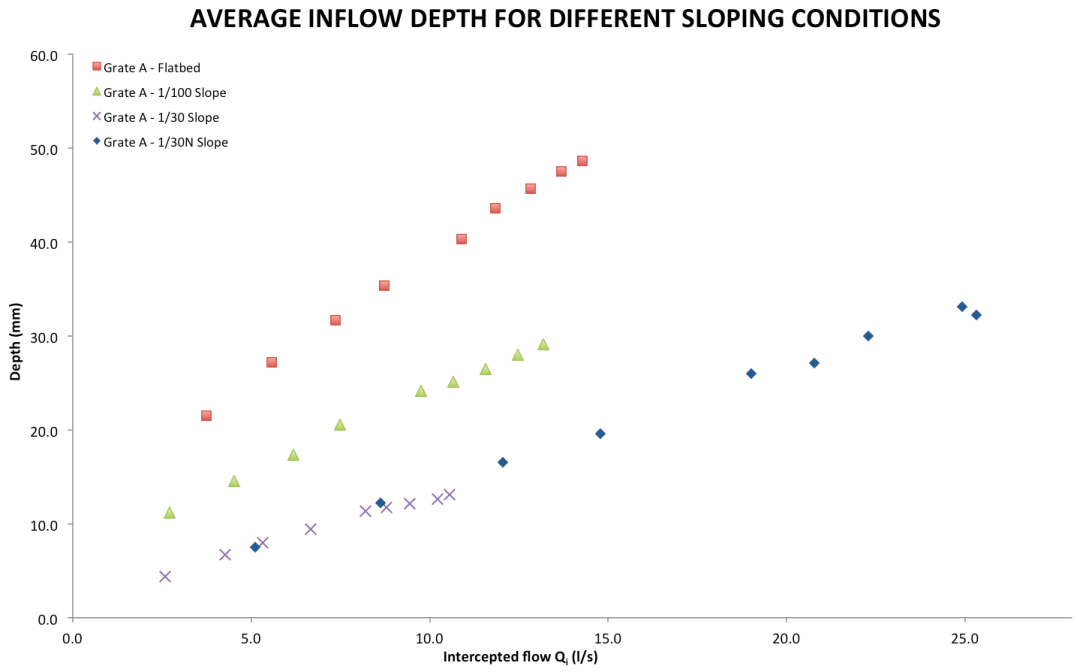

Figure 5.13 – The head-discharge relationship based on the different slopes with Grate A and intermediate tests

As a conclusion, the results clearly show that the width of the channel had little impact on the head-discharge relationship.

5.1.3 Tests with Surcharged Flow

The study completed two forms of tests with surcharge. 1) Backflows through the gully inlet and 2) backflow combined with approaching flow.

5.1.3.1 Backflow only tests

Figure 5.14 shows the head-discharge relationship for the surcharged system with backflows only. The presented results show the head-discharge relationship without considering any other flow (from the primary inlet).

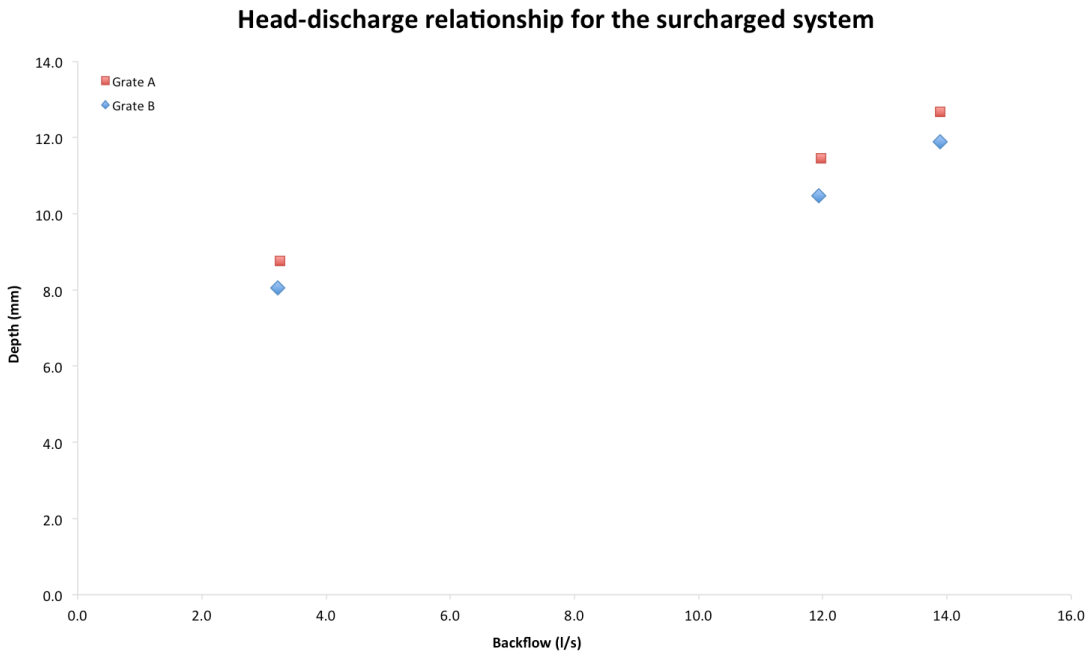

Figure 5.14 – Head-discharge relationship for backflow only through the gully inlet of the surcharged system

Figure 5.14 highlights that as the backflow are increased the depth of flow increases. This is as expected as effectively an orifice flow is converted to a free surface flow governed by Manning's Equation.

5.1.3.2 Backflow with Approaching Flow.

Tests were only possible for the terminal flow condition. The primary data for the combined backflow and the approaching flow (total outflow) is plotted on Figure 5.15. It can be seen that the results obtained are in agreement with the previous tests conducted.

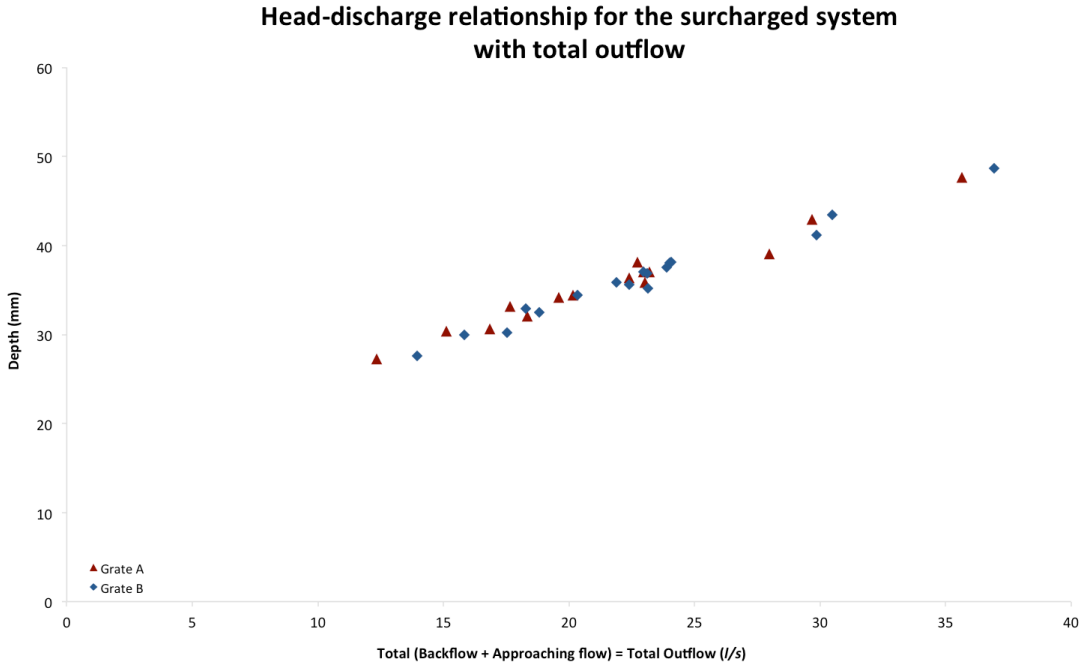

Figure 5.15 – Head-discharge relationship for total outflow (backflow with approaching flow) of the surcharged system

This shows that as the flowrate increases the depth increases but here the relationship is more linear when compared to the backflow only surcharge test.

Based on the head-discharge relationship that were presented in this section [Section 5.1], further analysis have been conducted and is as presented in the following section [Section 5.2].

5.2 ANALYSES AND DISCUSSION OF RESULTS

Analysis and discussion of results section has been split into 3 primary sections: Efficiency [Section 5.2.1], Coefficient of Discharge [Section 5.2.2] and Dimensional Analysis [Section 5.2.3]. The analysis of efficiency was conducted to examine the performance of tested grates with conventional previously published research using two different efficiency equations [Equation 2.3 and 2.5]. The results is as presented in Section 5.2.1.

Based on the head-discharge relationships presented in Section 5.1, it can be concluded that head-discharge relationships are different for each grate and each flow condition. Therefore, a universal relationship is needed. In practice, a C_d value is usually required in order to achieve this. Section 5.2.2 describes the way in which C_d may be defined and a systematic review has been made of the most appropriate equation to be used. The coefficient of discharge, C_d was computed using both the broad crested weir equation and the sharp crested weir equation. It was found that the C_d obtained using the sharp-crested weir equation is closer to the standard C_d for gully inlets in the UK – circa 0.6. Therefore, the following analysis was conducted using the sharp-crested weir equation. This is presented and further discussed in Section 5.2.2. In the case of surcharged flow, orifice equation was used instead to determine the C_d and the results are presented in Section 5.2.2.3.

C_d is known to be a function of many parameters and hence to examine how C_d changes, a dimensional analysis approach has been used [Section 5.2.3]. This has been followed by a review of the application of different types of equations – linear, logarithmic and etc. in an attempt to link the dimensionless terms and hence define a universal equation that describes the performance of the system for a range of conditions. This analysis has resulted in a number of significant findings, which have formed the conclusions to the thesis.

5.2.1 Efficiency of Intermediate tests

The efficiency of an inlet (η) is the ratio of the intercepted flow against the approaching flow towards the gully system. In simple terms, the efficiency of an inlet is given as (Haestad and Durrans, 2003; Despotovic et. al., 2005; Mustaffa et. al., 2006; Valentin and Russo, 2007, Gomez et. al., 2011):

$$Efficiency, \eta = \frac{Q_i}{Q_a}$$

[Equation 2.3]

Figure 5.16 shows the relationship between the approaching flow and the intercepted flow. It can be seen that the effects of slope are more prominent at high flowrates and is less significant during low flows.

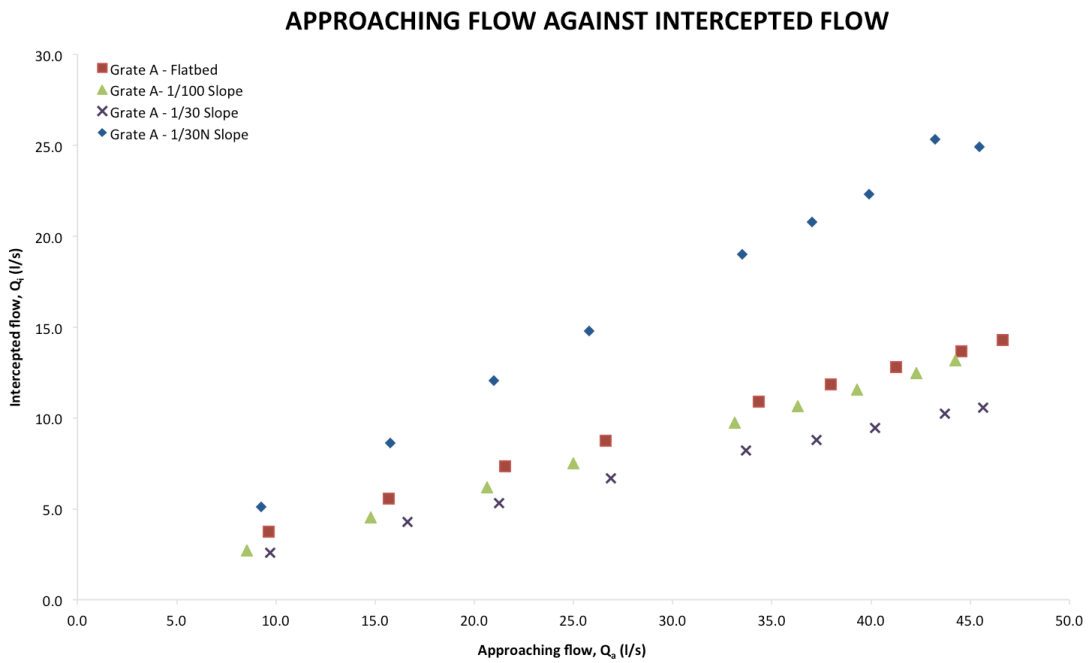

Figure 5.16 – The relationship between the approaching flow and the intercepted flow

There is also another method to describe the capture of the flow by inlets – by using the capture efficiency (η), which is defined as the ratio of the flow captured by the grating, Q_i to the total approaching flow, Q_a (Mustaffa et. al., 2006). Presented in Figure 5.17 is the relationship between the head and the efficiency of the grates (in %) as a function of the flowrate (*l/s*) for the Grate A. The heads are denoted simply with points and correspond to the y-axis whereas efficiency is denoted as points with dashed lines,

which corresponds to the z-axis. It can be seen that as the head increases the efficiency of the grates decreases. This is similar to the results obtained also for Grate B. Figure 5.18 shows the relationship of the head and the efficiency for both Grate A and Grate B.

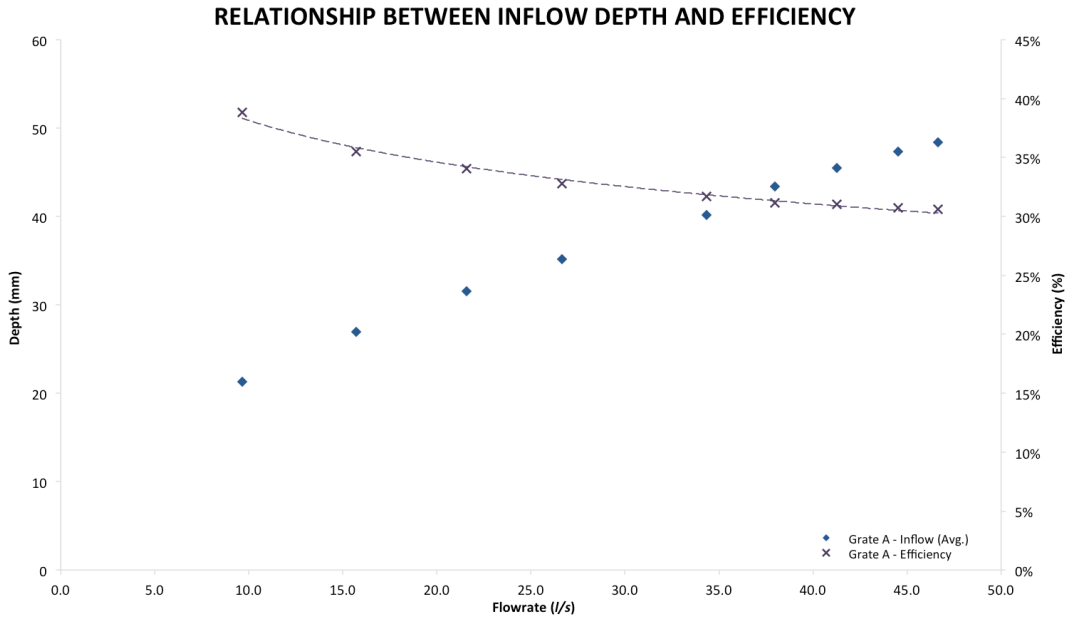

Figure 5.17 – The relationship between inflow depth and efficiency for Grate A

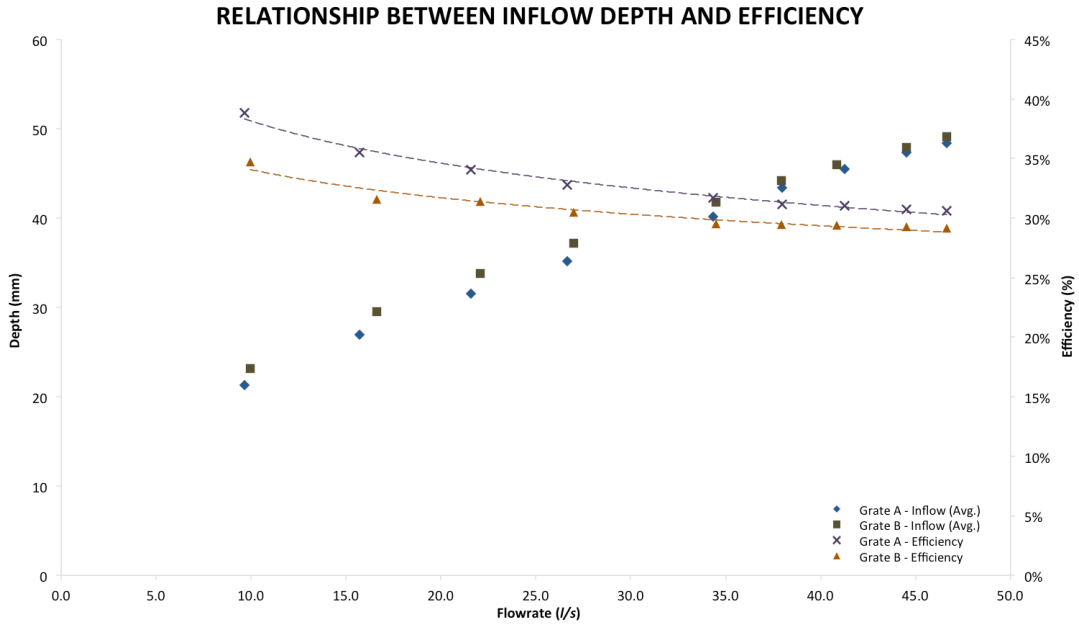

Figure 5.18 – Comparison of flow depth and efficiency for Grate A and B with a flat bed

Figure 5.19 shows the influence of bed slope on the efficiency of Grate A. It can be seen that efficiency of the grated inlets decreases with an increase in flowrate. This is in accordance to HEC 22, where it was concluded that the interception capacity and efficiency would decrease with increased flowrate. This is more prominent in the case of the horizontal slope and the 1 in 30 slope. The efficiency of the 1 in 100 slope is overall very consistent. When the longitudinal slope is increased, water begins to skip or splash over the grate at velocities dependent on the grate configuration (HEC 22). Grated inlets also generally lose capacity with increase in grade (Uyumaz, 1994) and hence the results from this experimental programme highlight similar agreement with the design guides and previous research.

In this study the crossfall (S_c) of the road has not been considered but, based on the results obtained at different longitudinal slopes, it can be deduced that the 1/100 slope is the most efficient since its efficiency is almost consistent for the entire range of the flow. This is in contradiction with the usual practice of assuming greater inlet capacity for steeper longitudinal slope (Despotovic et. al., 2005). It is stressed however that the conclusions drawn from this analysis may not be transferable to all types of grates and situations where there is a crossfall, but that they may be used as inferences for grates with similar physical and hydraulic conditions as those used in the experiments.

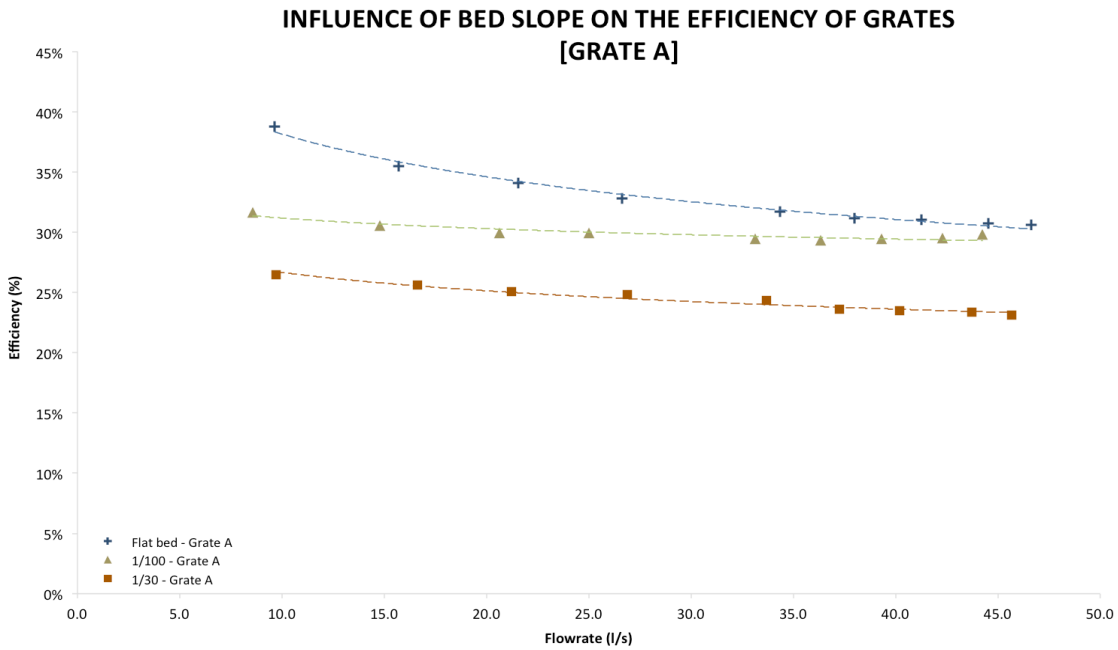

Figure 5.19 – The influence of bed slope on efficiency of Grate A

Figure 5.20 shows the influence of width on efficiency for the 1 in 30 slope. It can be clearly seen that when the width is halved, the efficiency increases immensely, with increased values in the range 50 to 60%.

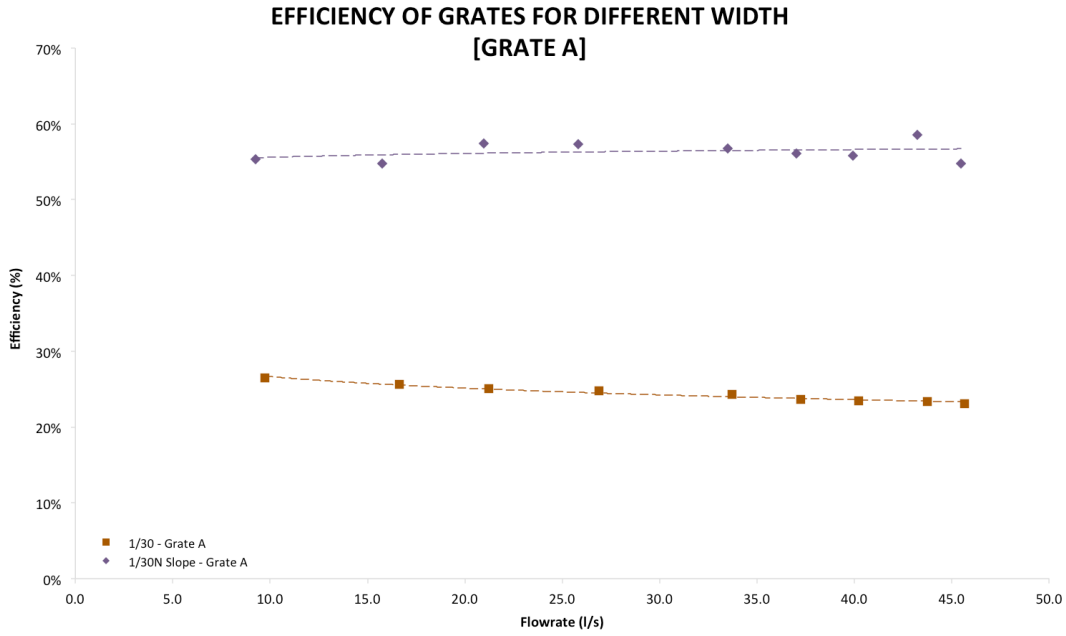

Figure 5.20 – The influence of width on efficiency of Grate A

Figure 5.21 shows the impact of grates on efficiency for the different sloping conditions for both Grate A and Grate B. It can be seen that there is very little difference in terms of efficiency between the grated and non-grated systems across the entire range of the tested flowrate and sloping conditions. Therefore, it can be safely assumed that the overall design (e.g. orientation/size/spacing), of the grates have been devised to perform efficiently.

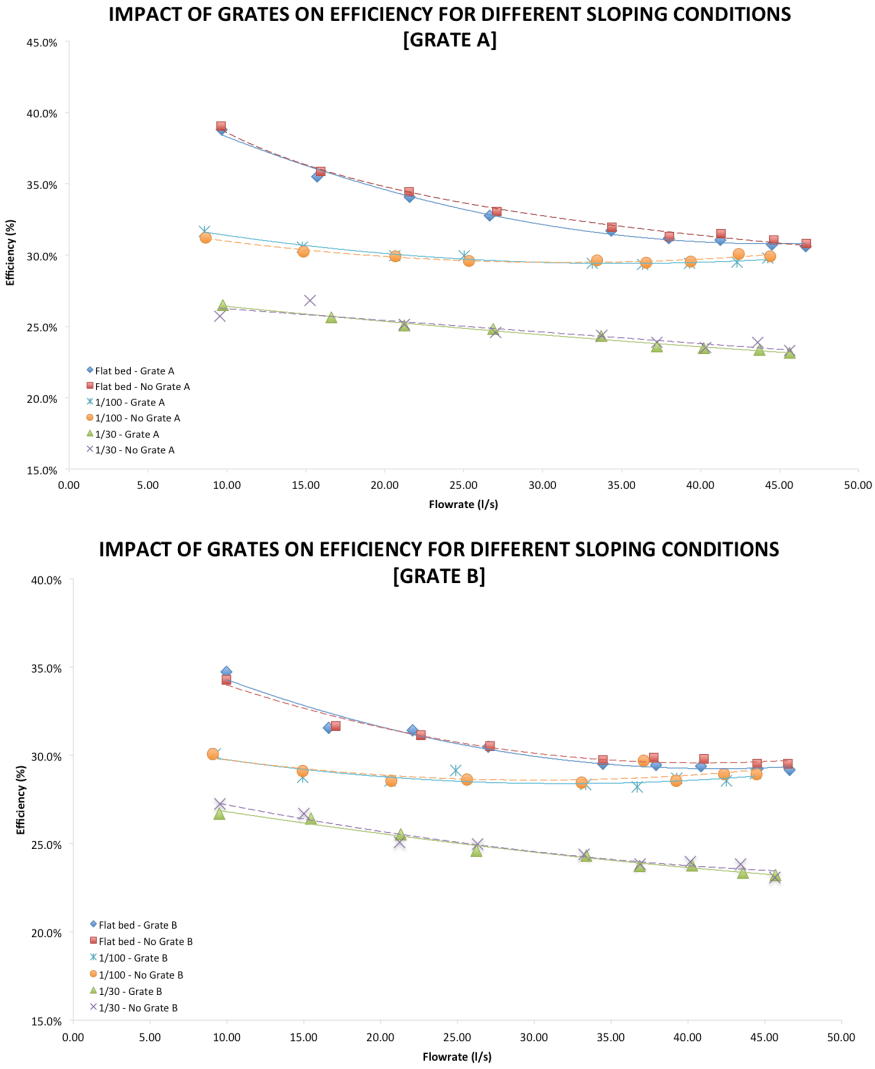

Figure 5.21 – The impact of grates on efficiency for different sloping conditions

Figure 5.22 shows the comparison between Grate A and Grate B in terms of efficiency. It can be seen that the difference in efficiency between Grate A and Grate B decreases as the slope increases. It was shown that the head discharge relationship for Grate A resulted in a lower head for the same flowrate when compared to grate B and hence these results highlight consistency in that, as expected, Grate A is more efficient in capturing flows when compared to Grate B for the flat bed as well as the 1/100 slope. However, it can be said that the efficiency of Grate A and B are similar at higher grade – in this case, the 1/30 slope where both sets of results display a very good agreement of efficiency values with each other.

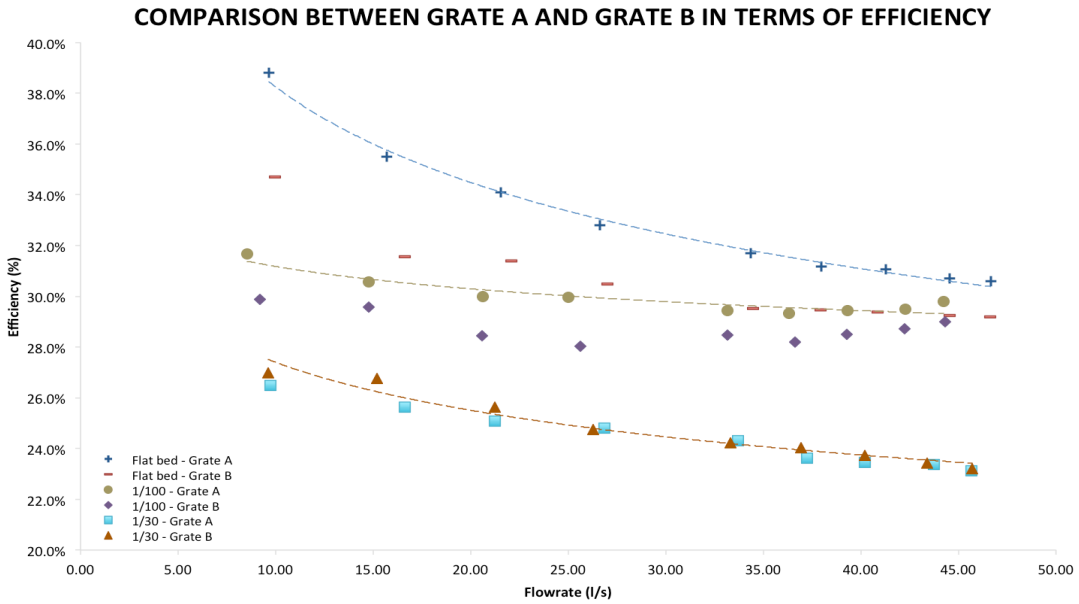

Figure 5.22 – The comparison between Grate A and B in terms of slope and efficiency

Efficiency is often calculated based on the ratio between the intercepted flow and the total approaching flow [Equation 2.3]. However, based on the method as suggested by Design Manual for Road and Bridges (HA 102/00), efficiency can also be calculated using Equation 2.5:

$$Efficiency\ (\eta)\ = 100 -\ G_d \left(\frac{Q}{H}\right)$$

[Equation 2.5]

Using these methods, the resulting efficiency was compared and the results are as shown in Figure 5.23. Based on Figure 5.23, it can be seen that the grating parameter (G_d) significantly affects the resulting efficiency of the grates.

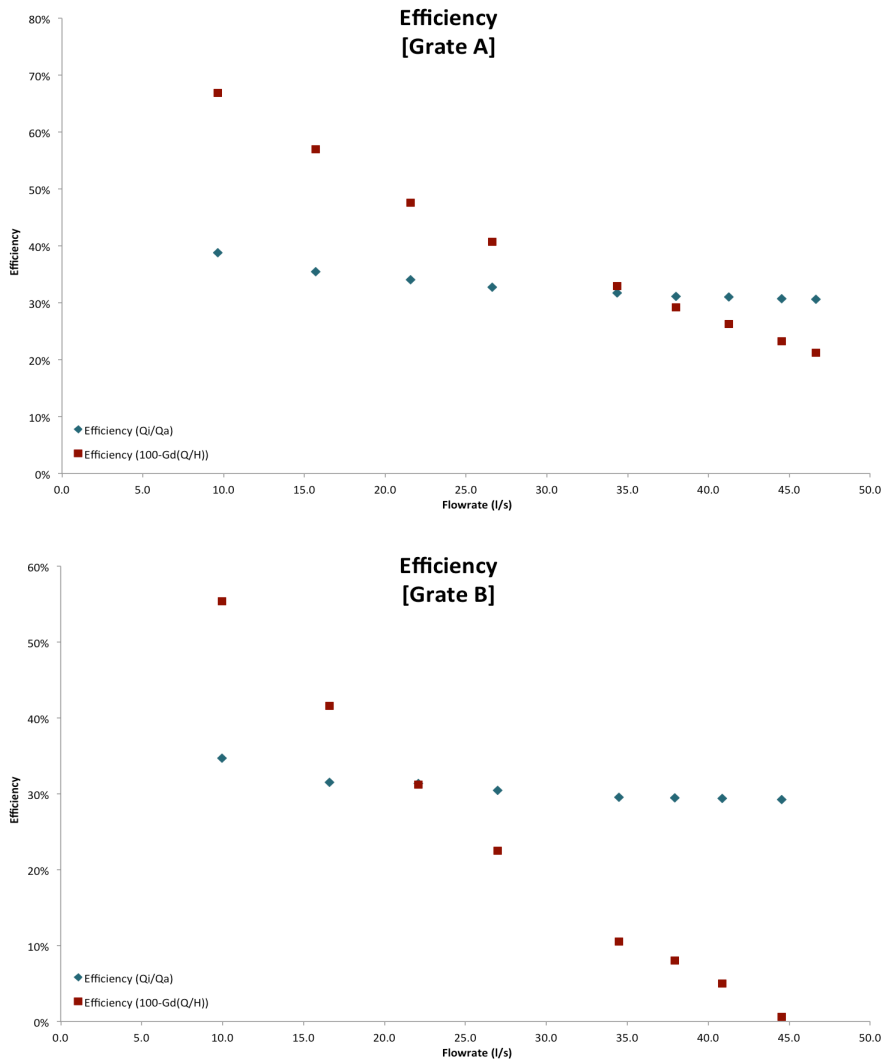

Figure 5.23 – Comparison of efficiency using different equations for both Grate A and Grate B with flatbed

The method suggested by DMRB as mentioned, is very much influenced by the grating parameter, G_d as shown in Figure 5.23. This is because grates are grouped into different types, based on their hydraulic capacity and a certain type of grate actually has a range of G values, but the design value opted, G_d is the maximum value of the range [Table 2.2]. This is not the case with the capture efficiency method, η – where it is only influenced by the captured and approaching flow of the grate only hence the difference in the results. However, it can be said that based on all of the efficiency analysis conducted, it can be concluded the results from this experimental programme highlight similar agreement with the design guides and previous research.

5.2.2 Coefficient of Discharge (C_d)

A primary aim of the thesis was to improve knowledge on the way in which the head-discharge relationships presented in the previous section may be used in practice, a series of coefficients of discharge (C_d) were computed using the sharp crested rectangular weir equation as proposed by the Queensland Urban Drainage Manual (QUDM, 2007) and Leandro (2008):

$$Q = {}^{2}/_{3}\, C_d b \sqrt{2g} H^{\frac{3}{2}}$$

[Equation 5.1]

where,

Q = flowrate (m^3/s)

C_d = coefficient of discharge

b = width of the weir (m)

H = head of the water (m)

g = gravity (m/s^{-2})

However, according to some studies (Fritz and Hager, 1998; Johnson, 2000), the weirs can be categorised according to the effective weir length ratio (or the amount of head associated with the flow passing over the weir), h/L – with 0.1< h/L < 0.3/0.4 (depending on literature) as broad crested weir, 0.3< h/L < 0.6 – as short-crested weir and h/L> 0.6 as sharp crested weir. Taking this into consideration, then based on the average h/L ratio for the entire weir phase, the flow can also be considered as a broad crested weir [Figure 5.31]. Assuming this, the analyses of the C_d have been conducted using both - the sharp-crested and broad-crested weir equation.

The assumption of a sharp crested weir method as suggested by QUDM (2007) and Leandro (2008) was initially assumed because it was more specific for the use of gullies /drainage designs and calculations whereas (Bazin, 1898; Kindsvater, 1964; Fritz and Hager, 1998) is more focused on the C_d for a standard broad crested weir. Figure 5.24 shows the comparison of the obtained C_d using the sharp-crested and broad-crested weir equation respectively.

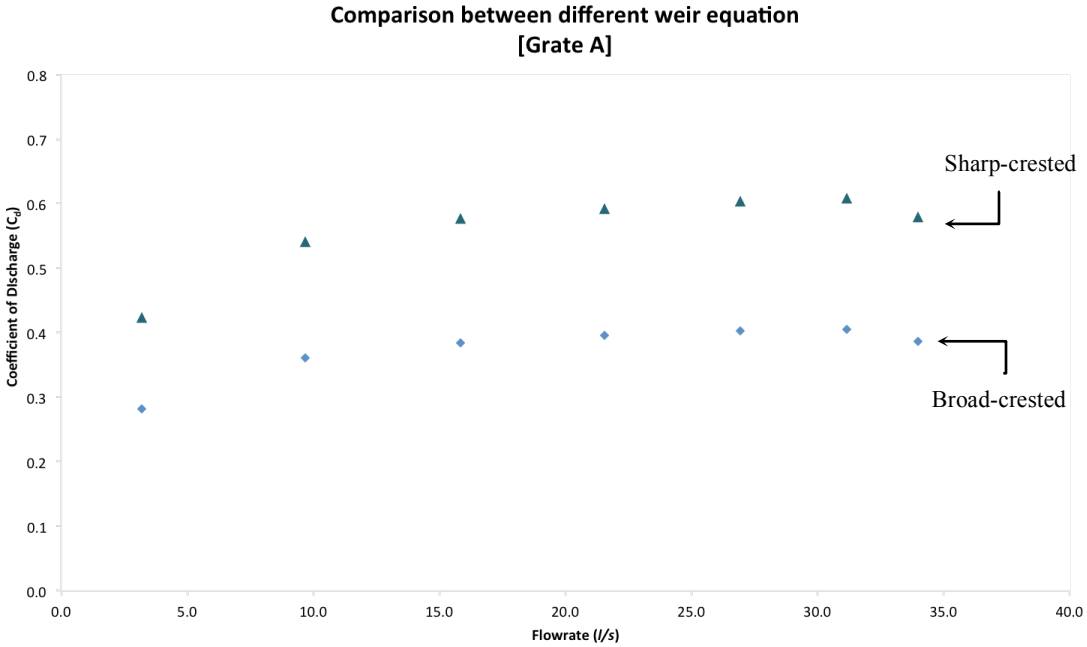

Figure 5.24 – Comparison of coefficient of discharge obtained using different weir equations

Comparing the results obtained from the two different equations, it can be said that the results obtained from both set of analysis yield in results that are comparative to previously conducted studies. The computed (average) C_d for the sharp crested weir is 0.6 (approximate) – and can be compared to the design C_d for gully grates (US Hydraulic Engineering Circular – HEC 22) of 0.67. This is also similar to the standard C_d assumed in the UK of between 0.6- 0.7. The computed (average) C_d for the broad crested weir is 0.3-0.5 (approximate) – and can be compared to the standard C_d for a broad crested weir (Bazin, 1898; Kindsvater, 1964; Nikolov et. al., 1978; Fritz and Hager, 1998) also to be between 0.3 - 0.4 for $0.1 < h/L < 0.3/0.4$ range. It is therefore concluded that because the standard C_d for gully inlets in the UK is circa 0.6, then the initial assumption of a sharp crested weir is to be maintained throughout this study. Therefore, the coefficient of discharge for the following sections has been calculated using the sharp-crested weir equation.

5.2.2.1 Coefficient of discharge - terminal

Figure 5.25 shows the obtained discharge coefficients using the sharp crested weir equation for both Grate A and Grate B for the unplugged, flatbed, terminal test. This is obtained by assuming the entire hydraulic phase is a weir phase. Based on this figure, the computed (average) C_d for Grate A is approximating to 0.6 whereas for Grate B, the computed (average) C_d is just slightly higher than 0.6 for flow conditions between 0-30 *l/s*. Flow conditions between these values best describe the free weir flow. It can be seen that there is a small drop in C_d value between the flowrate of 30 – 35 *l/s* which coincides with the drop in the gully depth after reaching a maximum as presented earlier [Figure 5.2]. This condition applies to both Grate – Type A and B.

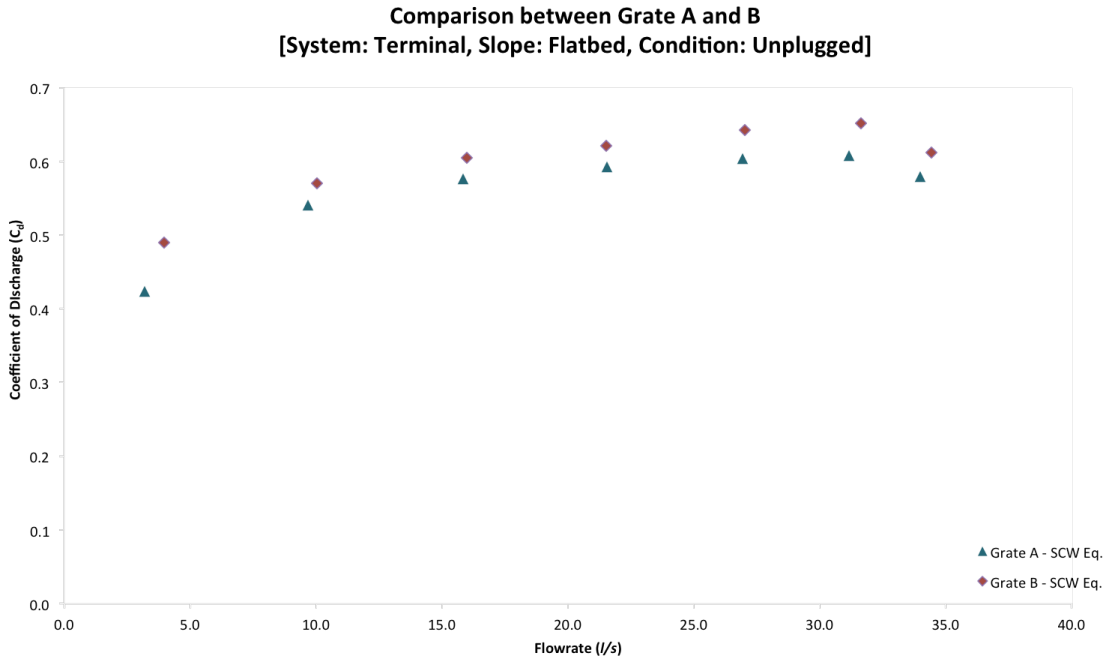

Figure 5.25 – Coefficient of discharge of Grate A and Grate B for the unplugged, flatbed, terminal test

5.2.2.2 Coefficient of discharge - Intermediate

Based on the average depth obtained earlier, a series of coefficient of discharge (C_d) was computed using the sharp-crested rectangular weir equation. This assumption was based on the head-discharge relationship obtained [Figure 5.9], as it shows that grates behave as a free flowing weir for the entire range of the experimented flowrate. Therefore, only the weir equation was used in order to compute the discharge

coefficient for the associated intercepted flow. Presented in Figure 5.26 is the computed C_d against the intercepted flowrate, Q_i (*l/s*) of both Grate A and B.

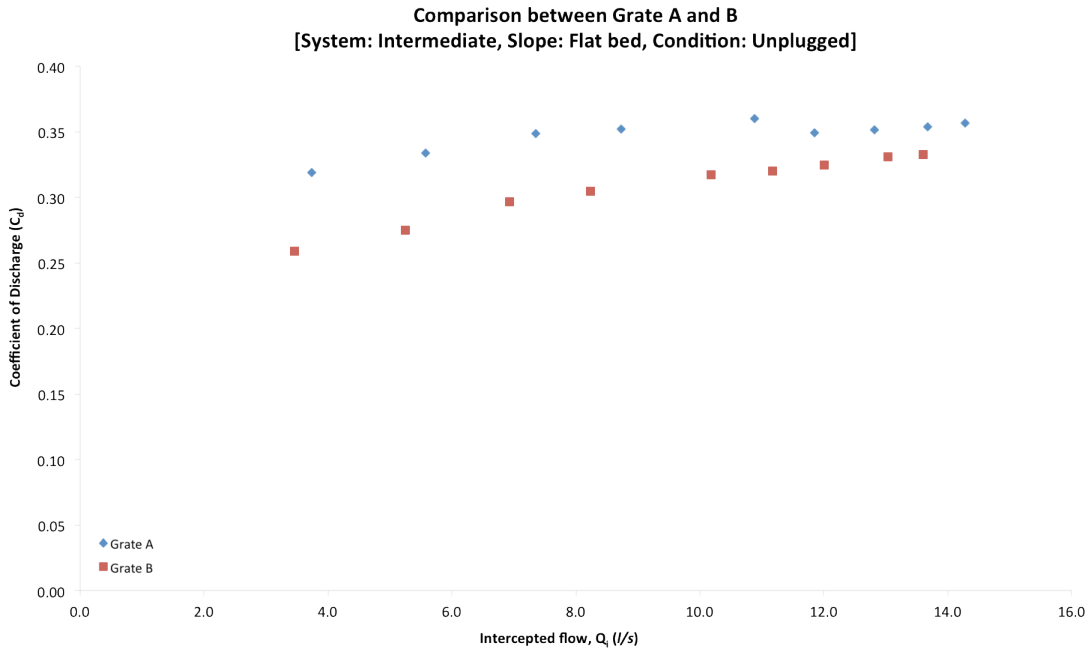

Figure 5.26 – Coefficient of discharge of Grate A and Grate B for the unplugged, flatbed, intermediate test

Figure 5.27 shows the comparison in terms of discharge coefficient between terminal and intermediate test. It can be seen that the discharge coefficient obtained for the intermediate tests are lower when compared to terminal tests. As the head increases, the discharge coefficient decreases.

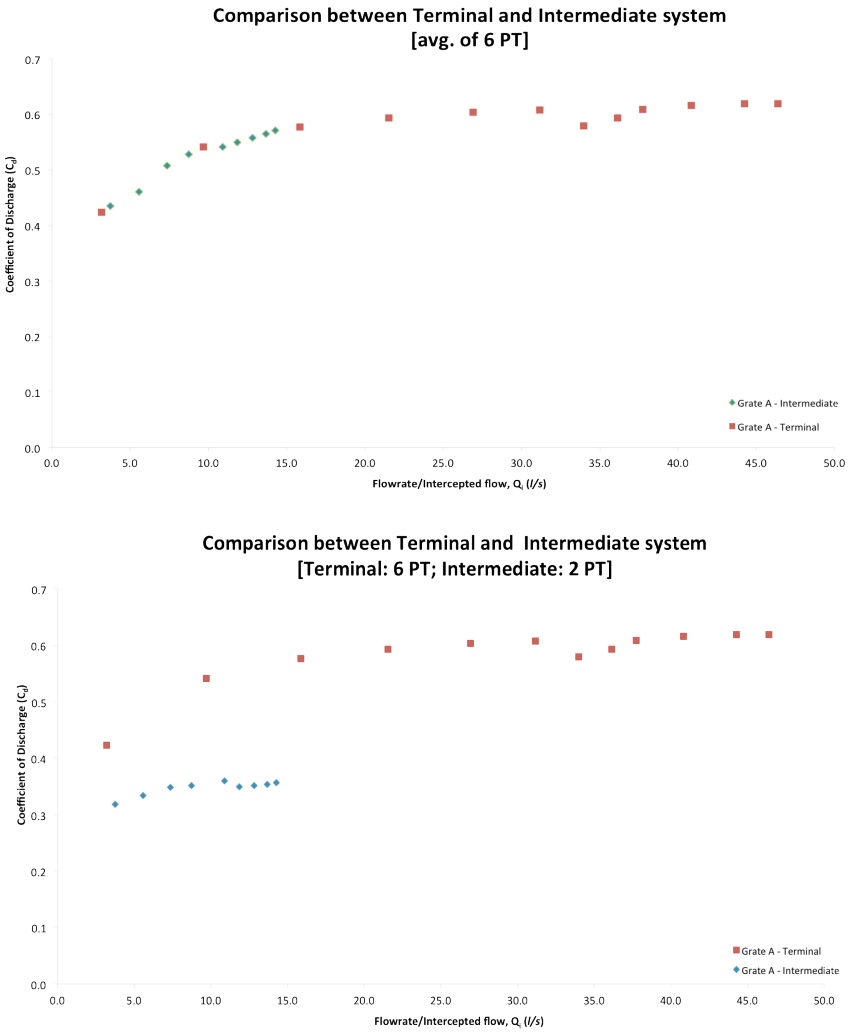

Figure 5.27 – Comparison of C_d between terminal and intermediate system based on the no. of pressure transducers used in the analysis

5.2.2.3 Coefficient of discharge – Surcharged

5.2.2.3(1) Surcharge with backflow only

Figure 5.28 shows the discharge coefficient as a function of surcharge with backflow only. Based on the figure, it can be seen that the relationship between C_d and backflow is linear and the resulting C_d is distributed between 0.1-0.3 over the range of backflow for the flatbed. Differentiating between grates, it has been found that for this experimental condition, the resulting discharge coefficient for Grate B is more often higher when compared to Grate A. Note - These C_d values have been computed using the average depth from all of the pressure transducers on the surface platform as the driving head in the orifice equation.

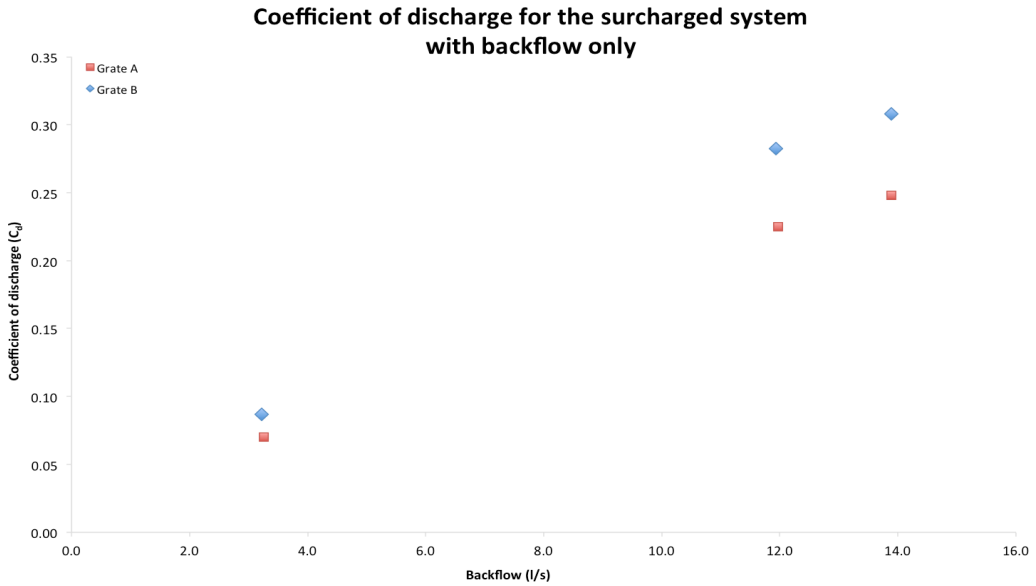

Figure 5.28 – Coefficient of discharge of Grate A and Grate B for the surcharged system with backflow only

5.2.2.3(2) C_d - Surcharge with backflow and approaching flow

Figure 5.29 shows the C_d obtained for Grate A and Grate B for the surcharged system with total outflow. Based on this figure, it can be seen that the relationship between C_d and total outflow is just as linear as the relationship between C_d and backflow only.

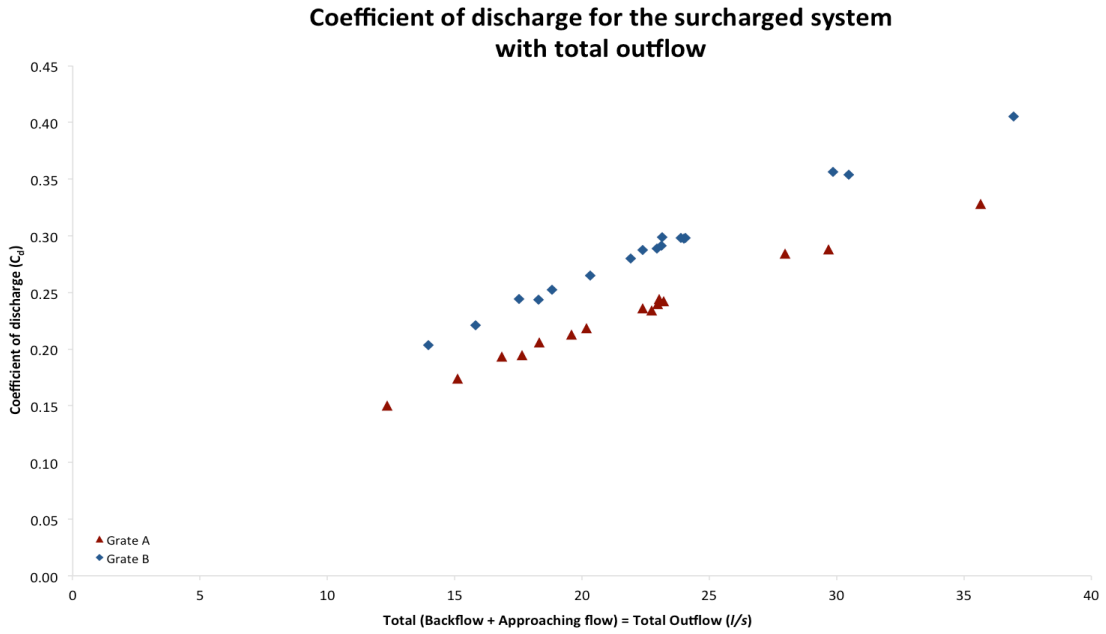

Figure 5.29 – Coefficient of discharge of Grate A and Grate B for the surcharged system with total outflow

The C_d presented so far have been calculated based on the assumption that average depth from all of the pressure transducers on the surface platform is the driving head in the orifice equation. The assumed head for the orifice equation based on the works of Chen et. al., (2007) however, is the difference between the pressurised gully and the surface water level. Assuming this, the C_d was recalculated and the outcome is as presented in Figure 5.30.

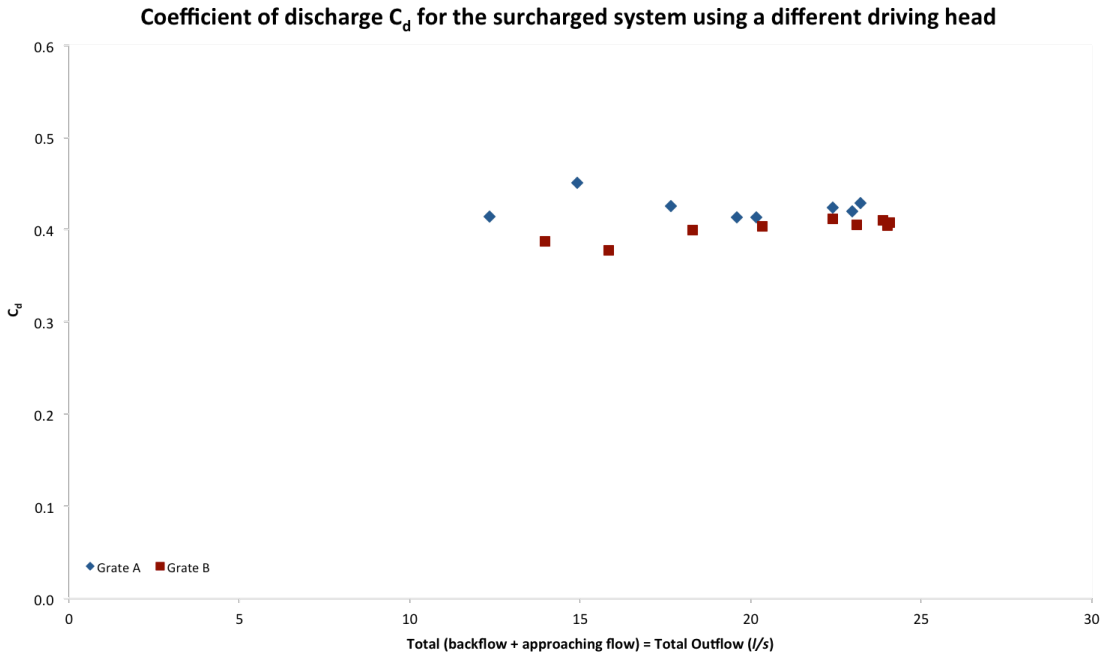

Figure 5.30 – C_d using the difference between the pressurised gully and the surface water level as the driving head

Figure 5.30 shows the resulting C_d computed using the difference between the pressurised gully and the surface water level as the driving head. Using average depth as head in the orifice equation [Figure 5.29] - the (average) C_d obtained is between 0.15-0.30 (approximate). This relates to a previous study by Gomez and Russo (2011). In the experimental testing for a Grate Type 2, the C_d obtained was between 0.14 - 0.16. The grate used in that experimental testing has similar physical attributes to the one tested in this experimental programme – but with a slightly different dimension. The experimented grate has a slightly smaller waterway area and was tested on a longitudinal slope of 1% and crossfall of 0%. However, based on the analysis conducted using the difference between the pressurised gully and the surface water level as the driving head in the orifice equation however, the (average) C_d obtained was between

0.40-0.50 (approximate). This is in comparison closer in terms of value to the standard C_d for an orifice of 0.6 or 0.616 or 0.65 (Guo et. al., 2009).

As a conclusion, the coefficient of discharge obtained from this experimental work is in accordance to previous literature and studies conducted. As mentioned previously, C_d is a function of many parameters and hence to examine how C_d changes, a dimensional analysis approach has been used and is presented in the following section.

5.2.3 DIMENSIONAL ANALYSIS

Experimental data obtained from the laboratory has allowed the identification of parameters that affects the coefficient of discharge. It was found that the coefficient of discharge, C_d is a function of a number of parameters based on the properties of the fluid, the geometry of the grate and the approach channel and the dynamics and nature of the flow conditions to the grate. This can be summarised as:

$$C_d = f\ (Q, (\rho, g, \upsilon, \gamma), Y, h, S_L, grate\ characteristics(L, b, w, R, S, G_d, waterway\ area\ etc), plugged/unplugged, \eta, K, \xi\ )$$

[Equation 5.2]

where: flowrate(Q), density(ρ), viscosity(ν), gravity(g), surface tension(γ), uniform depth of flow upstream (Y), head/depth of water(h), longitudinal slope(S_L), length(L), breadth(b), width(w), wetted perimeter(R), road gradient(S), design grating parameter(G_d), submergence coefficient(K), effective weir length(ξ) and efficiency(η).

Using dimensional analysis, each of the above terms may be made dimensionless and may be expressed in the form:

$$C_d = f(R_e, F_r, B_o, \frac{h}{L}, \frac{b}{h}, \frac{w}{h}, \eta, K, \xi)$$

[Equation 5.3]

where: Reynolds number (R_e), Froude Number (F_r) and Bond number (B_o).

Reynolds number (R_e) is the dimensionless term for viscosity, Froude Number (F_r) for gravity and Bond number (B_o) for surface tension. In this study, it is argued that the

gravity term dominates as the flow to the gully has a free surface and hence the Froude number has been used in the subsequent analysis. Froude number is given as:

$$F_r = \frac{V}{\sqrt{gY}} \; and \; Y = \frac{A}{T}$$

[Equation 5.4]

where V is the velocity of approach, g is gravitational acceleration, Y is the uniform depth of flow upstream of the grate, A is the cross sectional area of the upstream flowrate, and T is the top width of the channel.

The relationship between C_d and these geometric parameters has been examined and is further explained in the following sections.

5.2.3.1 Effective weir length

The discharge coefficient is also governed by another parameter - h/L, sometimes also termed as the effective weir length, ξ. This is a dimensionless parameter – where h is the average head of the weir and L is the length of the grates and can be written as:

$$\xi = \frac{h}{L}$$

[Equation 5.5]

Rao and Muralidhar (1963), and Johnson (2000), redefined the length as w, width of the grates. Hence rewriting the Equation 4.3 as *h/w*. In this study however, the approaching flow is not only from one side of the grate therefore; L is taken as the (total) length of the grate that captures flow. This parameter however, neglects the influence of velocity of approach.

Comparing the coefficient of discharge against the effective weir length results in Figure 5.31. This highlights that there is a difference in the C_d values for the 2 different grates and hence the use of the dimensionless effective weir length is insufficient to fully describe and unify the performance of two different grates. A further parameter or parameters need therefore to be considered. The following sections will attempt to look at other parameters.

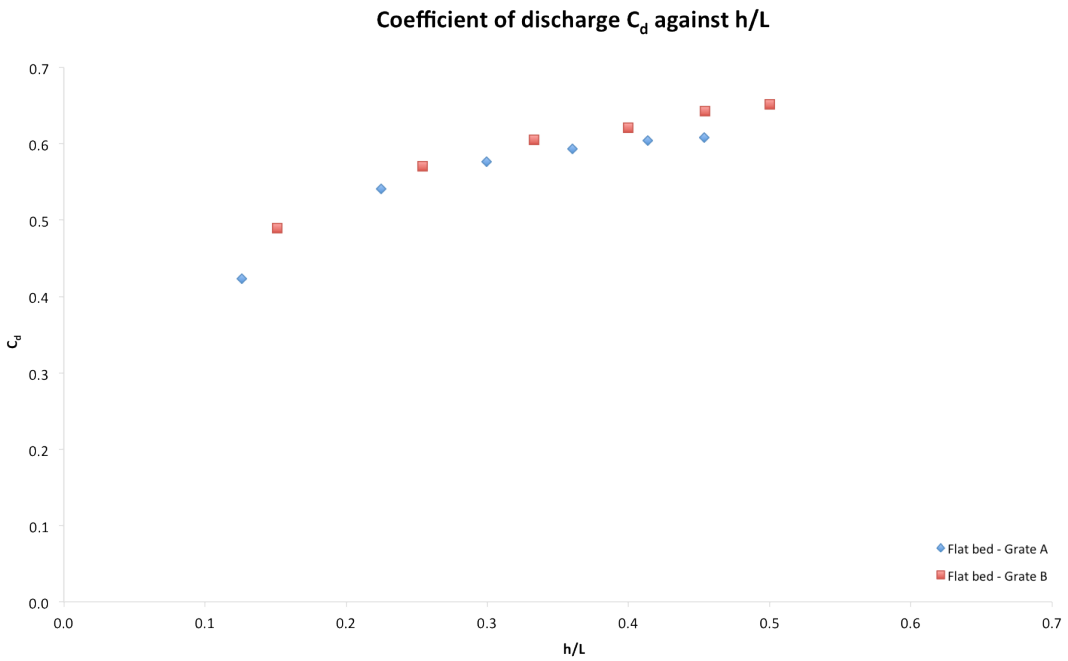

Figure 5.31 – Coefficient of discharge as a function of effective weir length (h/L)

5.2.3.2 Breadth/depth ratio

The relationship between the breadth to depth of water (head) ratio, b/h and C_d is shown in Figure 5.32. In this case, a linear equation has been applied to quantify the data and there is excellent agreement between the measured and the equation with values of R^2 of 0.988 (Grate A) and 0.998 (Grate B). Again each grate yielded an individual relationship but with an almost constant offset at a similar gradient.

In an attempt to analyse the data, a series of equations were established to assess the goodness of fit using different types of regression analysis. The regression analyses tried were the linear, polynomial, logarithmic, exponential and power analysis. The best equation to represent the data was then selected based on the coefficient of determination, R^2 closest to 1. Figure 5.32 – 5.36 shows C_d as a function of b/h using different regression analyses – linear, polynomial, power, exponential and logarithmic respectively.

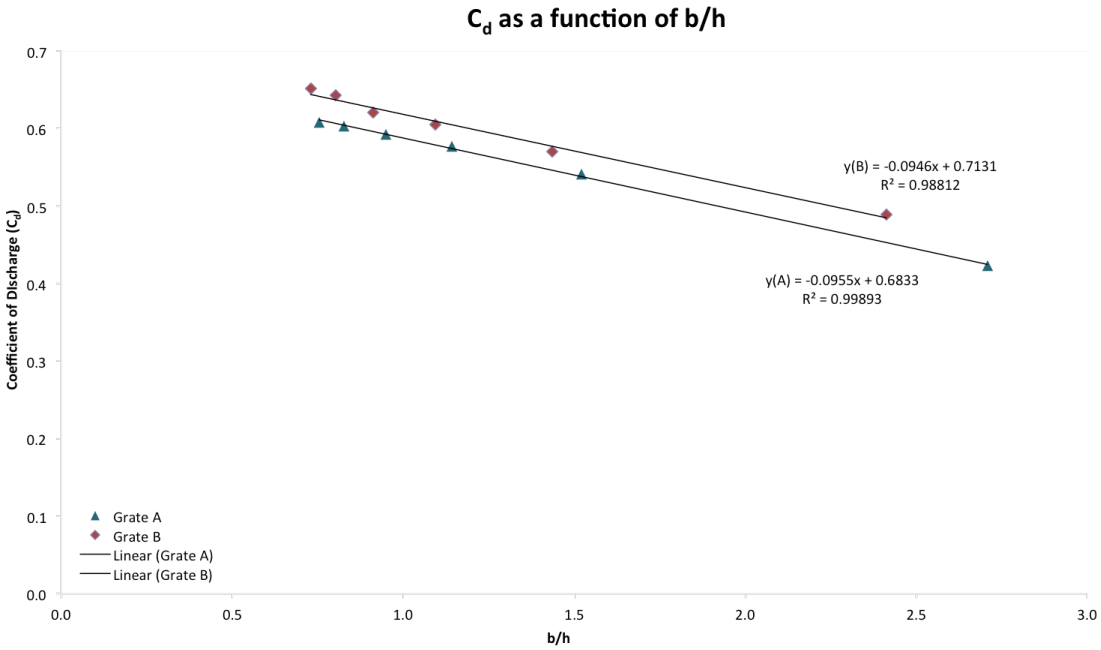

Figure 5.32 – Linear relationship of C_d and b/h

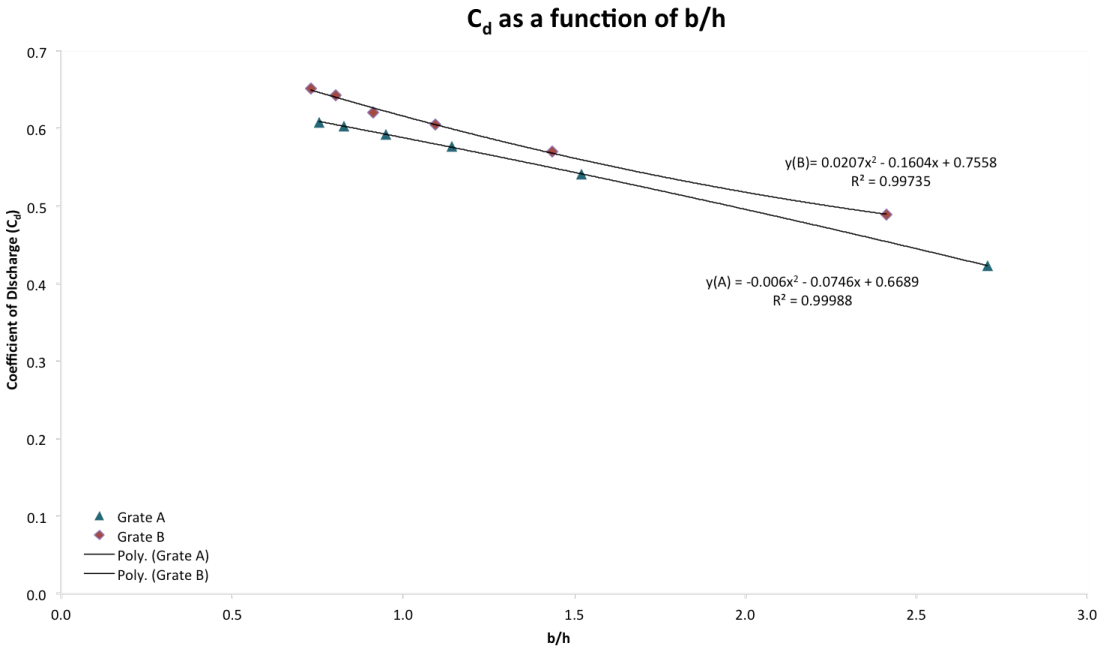

Figure 5.33 – Polynomial relationship of C_d and b/h

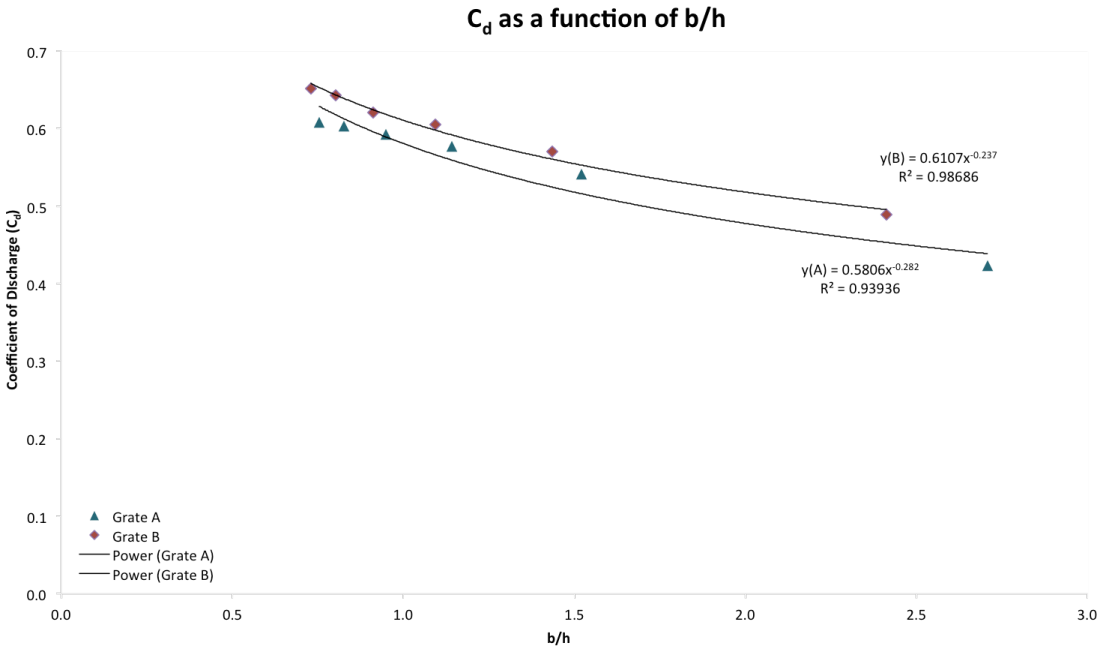

Figure 5.34 – Power relationship of C_d and b/h

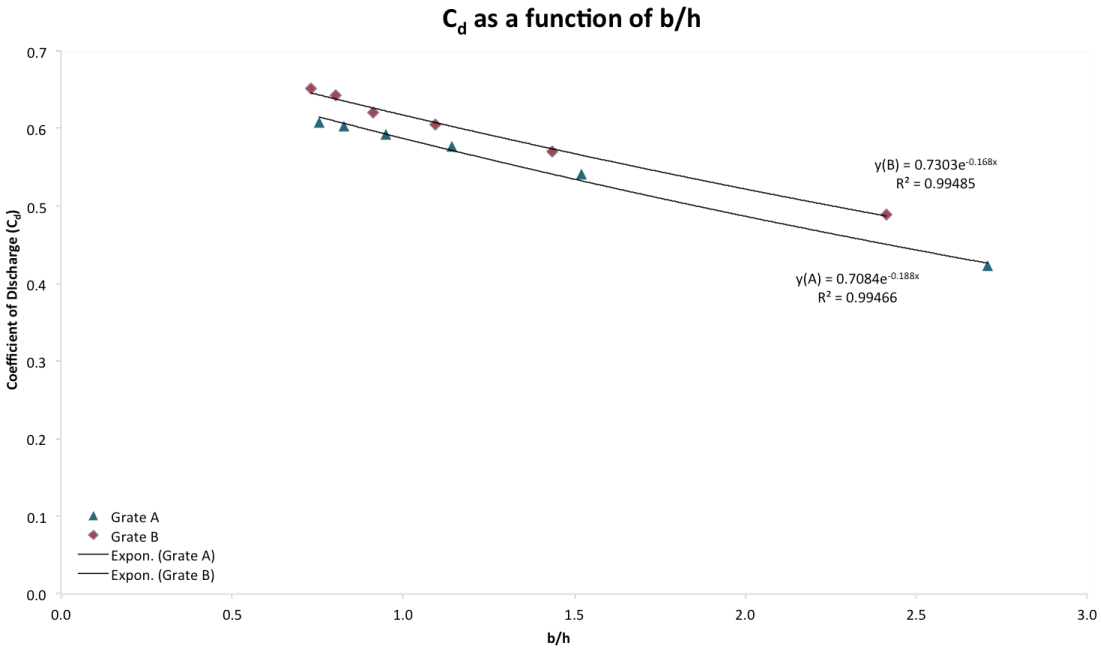

Figure 5.35 – Exponential relationship of C_d and b/h

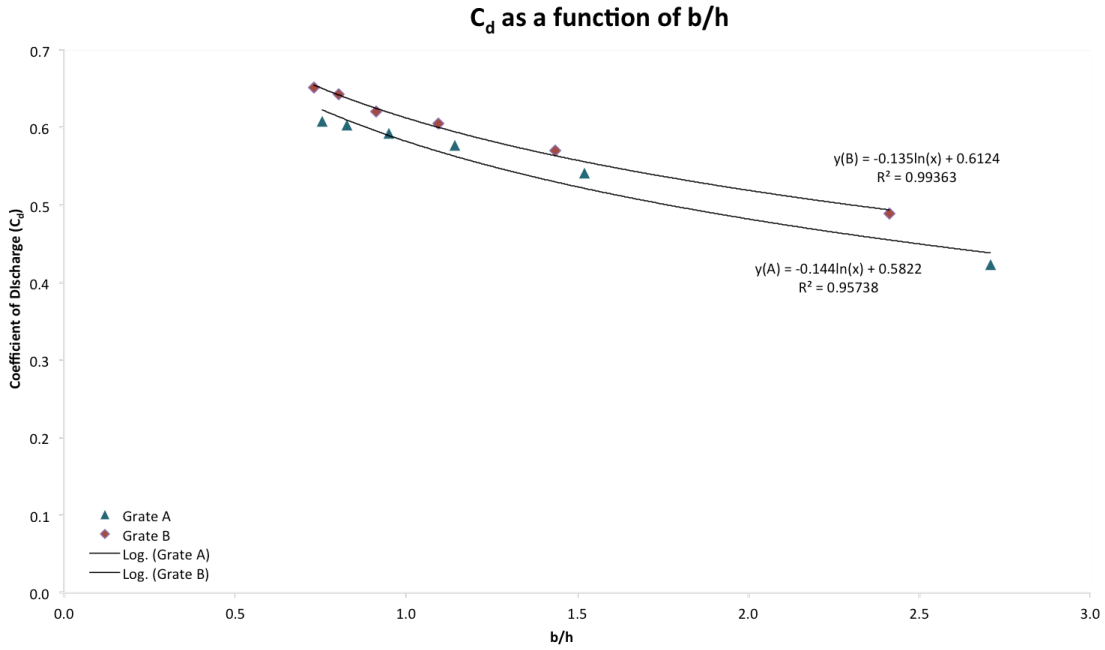

Figure 5.36 – Logarithmic relationship of C_d and b/h

From Figures 5.32 to 5.36 it can clearly be seen that the relationship between C_d and b/h may be defined using a number of relationships each with an R^2 value in excess of 0.95 but with a polynomial relationship yielding the highest values.

The regression analysis was also repeated with other parameters and it was concluded that the relationship between C_d and each parameter might be defined by a number of these equations. For example, the relationship between C_d and b/h is best given by a polynomial relationship. Table 5.1 lists the equation of best fit of C_d and each parameter. Figure 5.37-5.40 shows the relationship between C_d and each parameter – h/L, w/h, mean velocity (v) and F_r respectively.

Table 5.1 – Equation of best fit of C_d and each parameter

Relationship	Equation of best fit	R^2
C_d vs. b/h	$y(A) = -0.006x^2 - 0.0746x + 0.6689$ $y(B) = 0.0207x^2 - 0.1604x + 0.7558$	0.99988 0.99735
C_d vs. h/L	$y(A) = -2.1921x^2 + 1.8059x + 0.2345$ $y(B) = -1.0053x^2 + 1.1041x + 0.3481$	0.99005 0.99329
C_d vs. w/h	$y(A) = -0.007x^2 - 0.0806x + 0.6689$ $y(B) = 0.0375x^2 - 0.2157x + 0.7558$	0.99988 0.99735
C_d vs. V	$y(A) = 0.0816\ln(x) + 0.913$ $y(B) = 0.0776\ln(x) + 0.9309$	0.97209 0.99583
C_d vs. F_r	$y(A) = 1.7282x^2 + 2.1827x + 0.0149$ $y(B) = - -0.5252x^2 + 1.4319x + 0.1997$	0.99985 0.99964

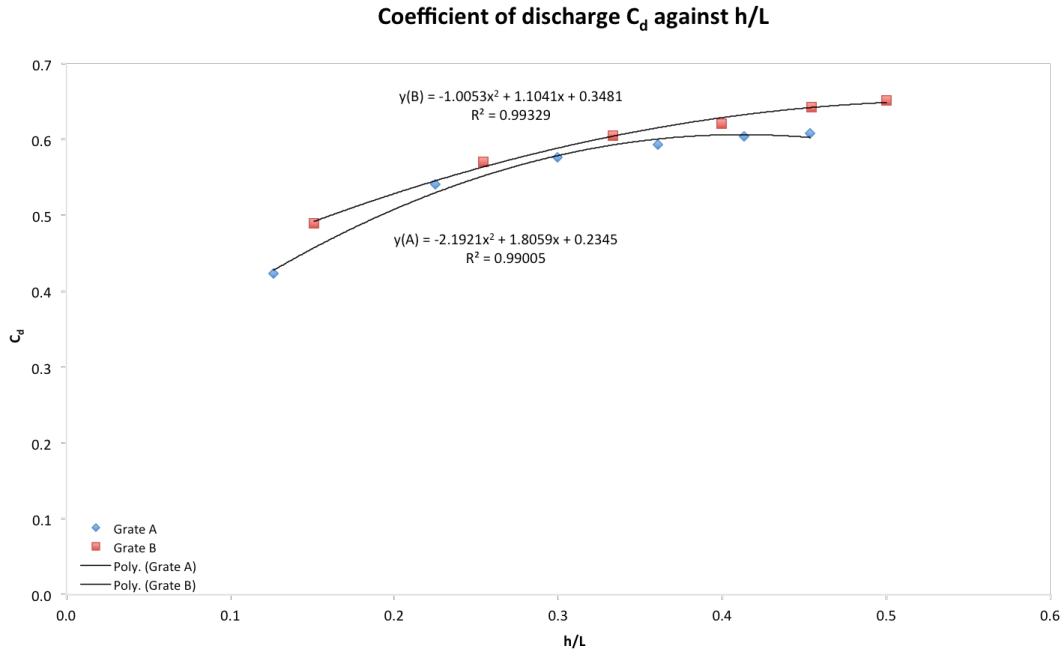

Figure 5.37 – Coefficient of discharge as a function of h/L ratio

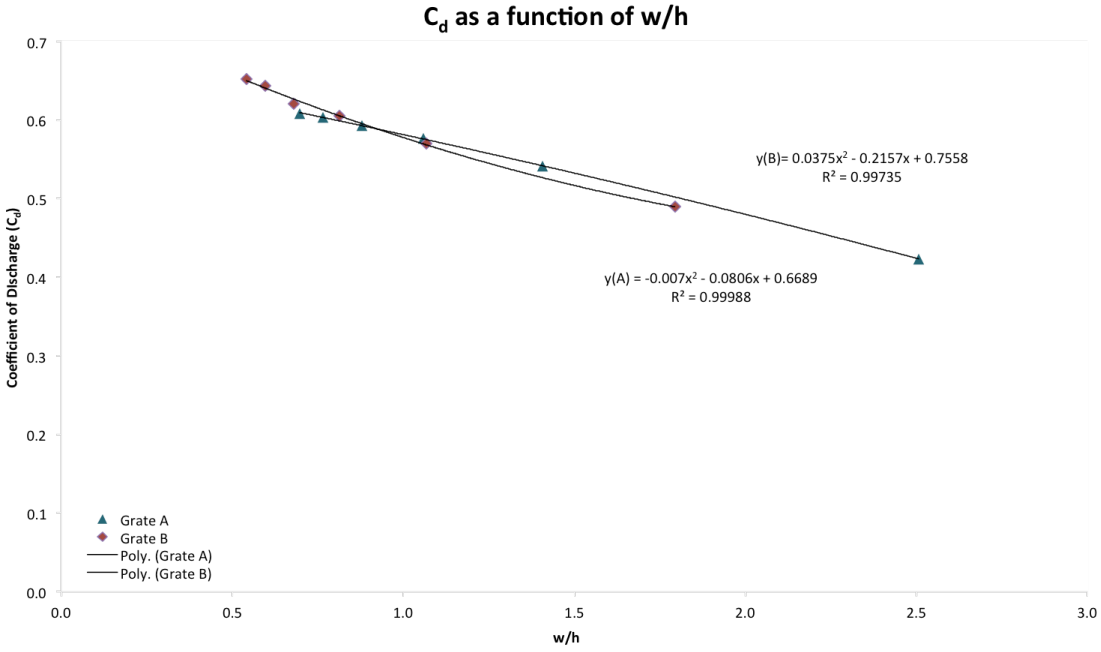

Figure 5.38– Coefficient of discharge as a function of w/h ratio

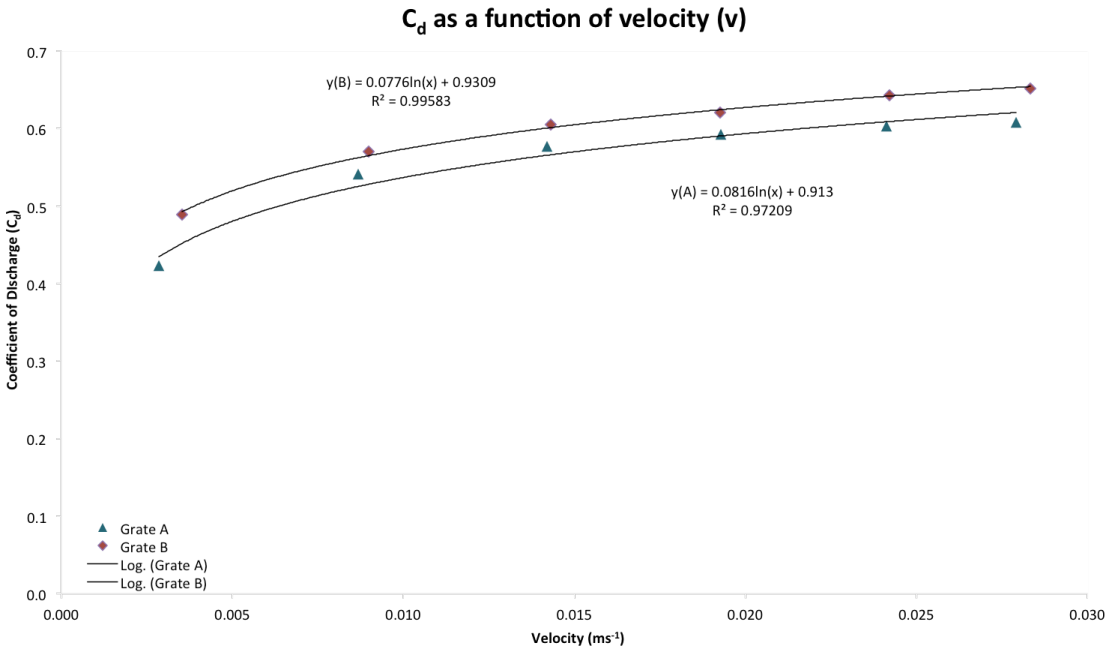

Figure 5.39 – Coefficient of discharge as a function of mean inlet velocity (v)

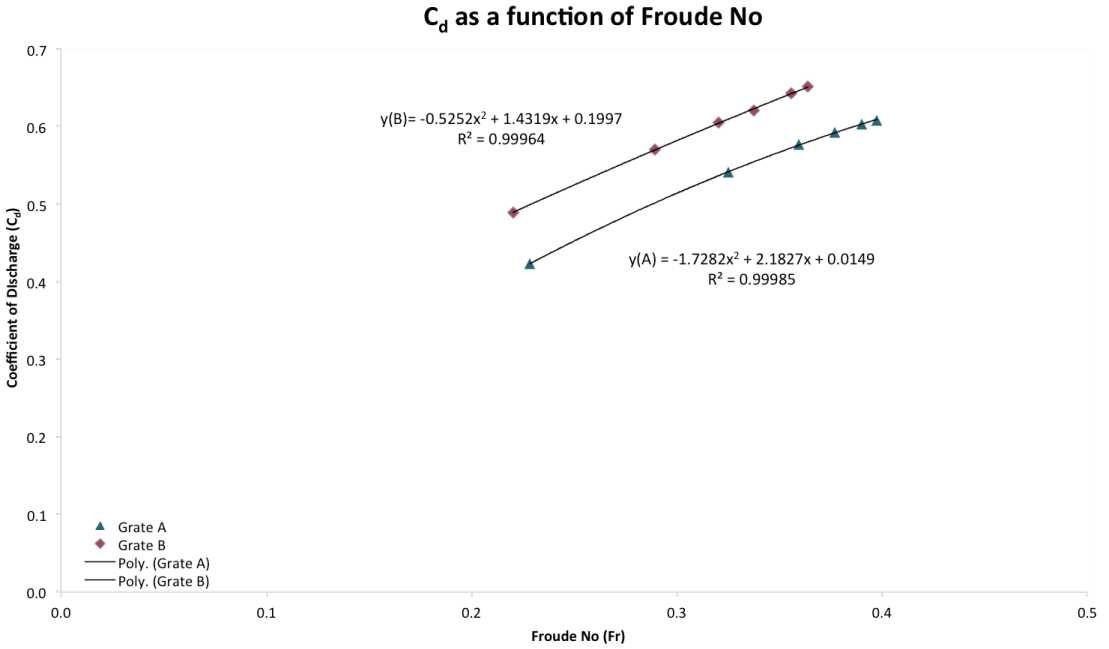

Figure 5.40 – Coefficient of discharge as a function of Froude number (F_r)

5.2.3.3 Froude Number

Comparison was also made between terminal and intermediate system of the resulting C_d in terms of Froude number. Froude number is given as:

$$F_r = \frac{V}{\sqrt{gY}} \; and \; Y = \frac{A}{T}$$

[Equation 5.4]

The result is as shown in Figure 5.41 -5.42 and the corresponding equations are listed in Table 5.2:

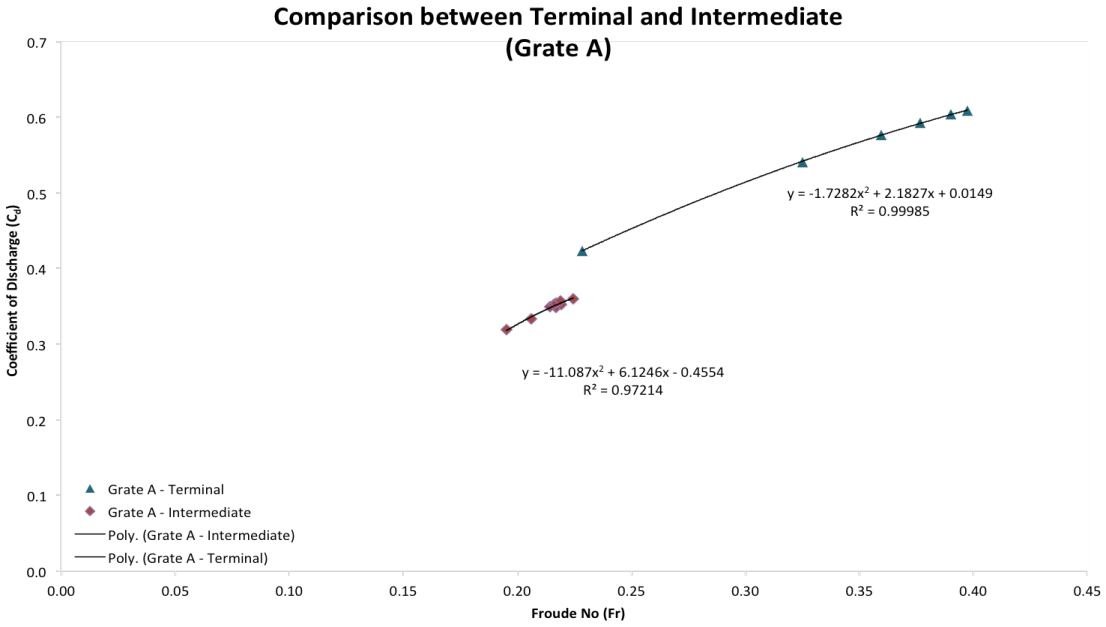

Figure 5.41 – Comparison of the relationship of C_d vs. F_r between terminal and intermediate system for Grate A

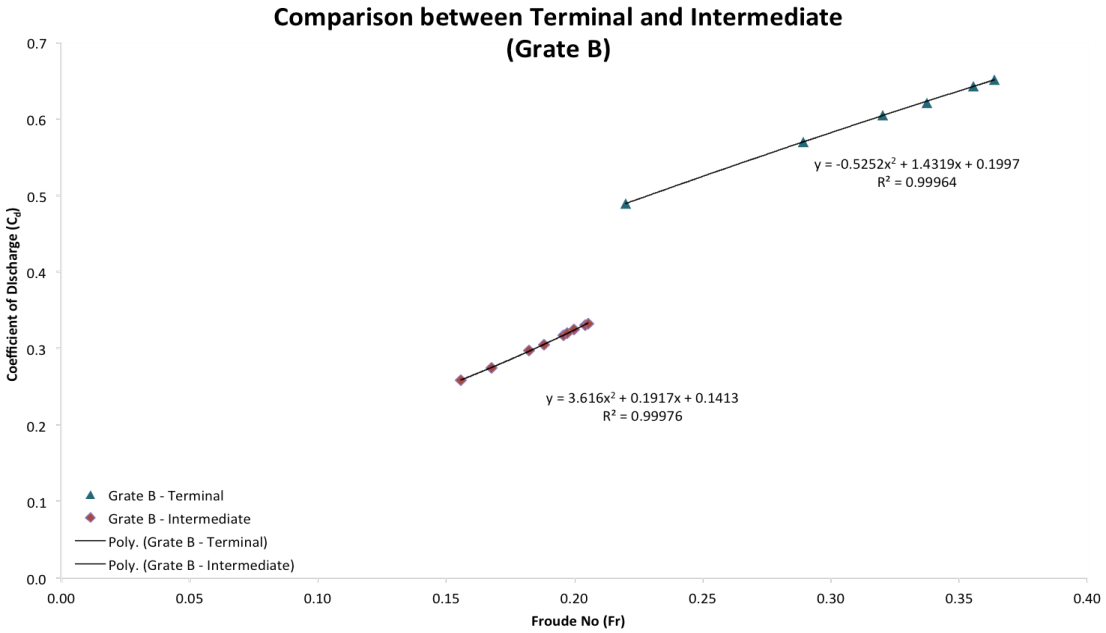

Figure 5.42 – Comparison of the relationship of C_d vs. F_r between terminal and intermediate system for Grate B

Table 5.2 – Equation for C_d vs. F_r for the terminal and intermediate system

	Equation	R^2
Terminal	$y(A) = -1.7282x^2 + 2.1827x + 0.0149$	0.99985
	$y(B) = -0.5252x^2 + 1.4319x + 0.1997$	0.99964
Intermediate	$y(A) = -11.087x^2 + 6.1246x - 0.4554$	0.97214
	$y(B) = 3.616x^2 + 0.1917x + 0.1413$	0.99976

C_d as a function of Froude number can also be compared based on different bed slopes. Analysis based on this was made and the results are presented in Figure 5.43-5.44 and the corresponding equations are listed in Table 5.3.

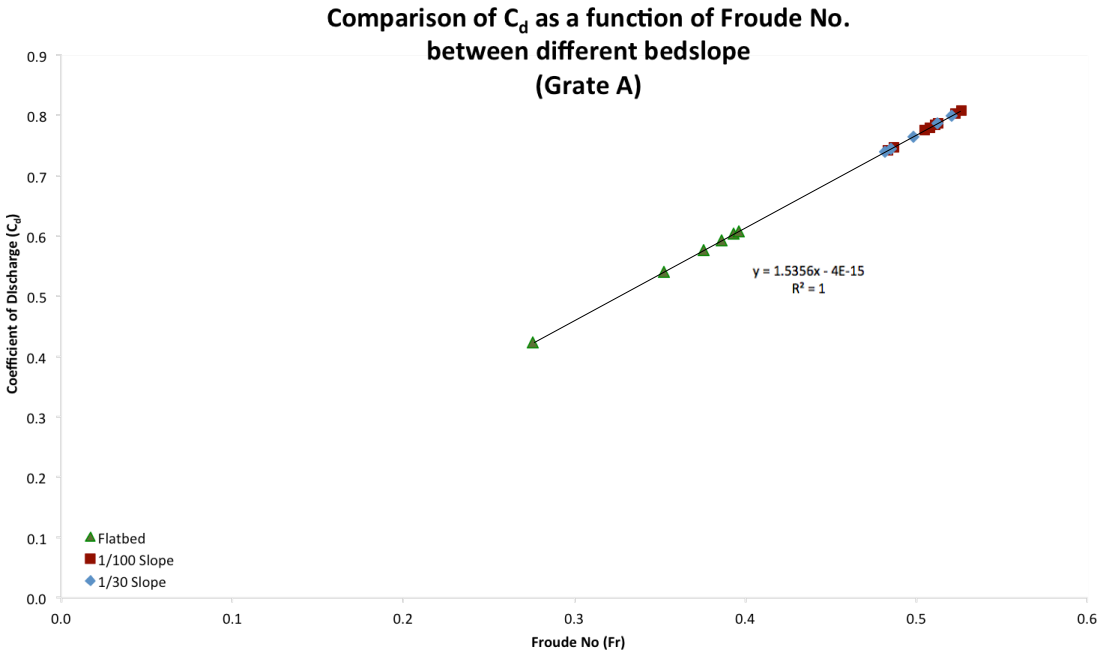

Figure 5.43 – Comparison of C_d vs. F_r between different bed slope (Grate A)

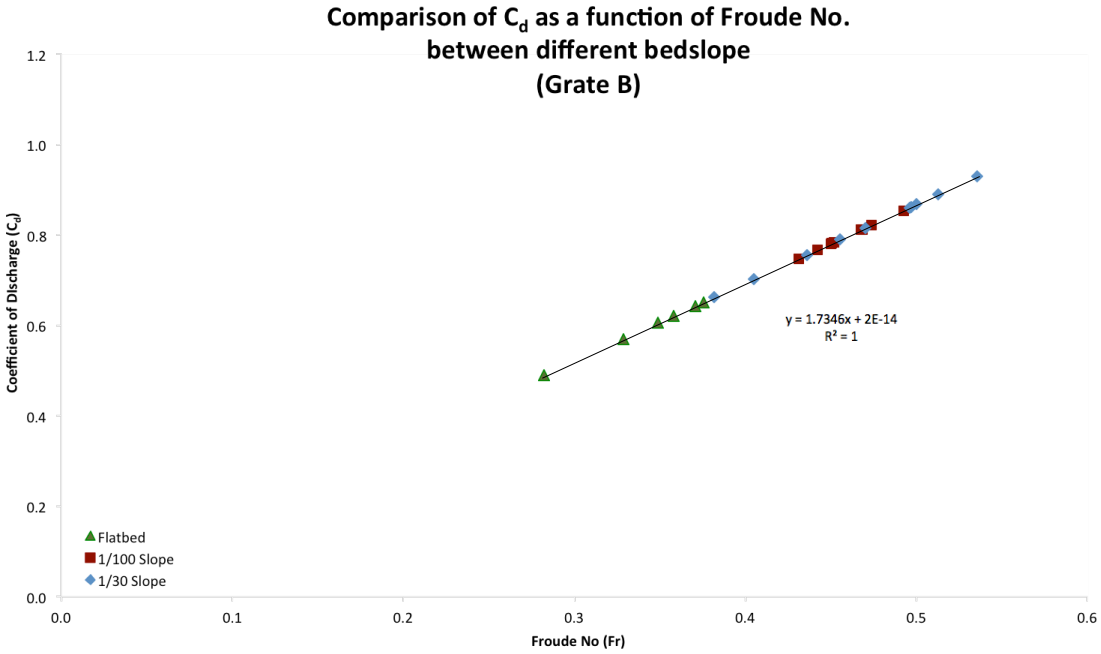

Figure 5.44 – Comparison of C_d vs. F_r between different bed slope (Grate B)

It has been found that the relationship for C_d vs. F_r as a function of slope is as presented in Table 5.3:

Table 5.3 – Equation for C_d vs. F_r as a function of bed slope

	Equation	R^2
Grate A	y = 1.5356x - 4E-15	1
Grate B	y = 1.7346x + 2E-14	1

In an attempt to improve the goodness of fit, a review was made by using dimensional parameters in combination. This is presented in the following section.

5.2.3.4 Combination of parameters

Based on the results presented, a review of dimensional parameters in combination - $F_r(h/L)$, $F_r(b/h)$ and $F_r(w/h)$ were made in an attempt to improve the goodness of fir and the results obtained are shown in Figure 5.45 – 5.46. The equation of best fit is listed in Table 5.4.

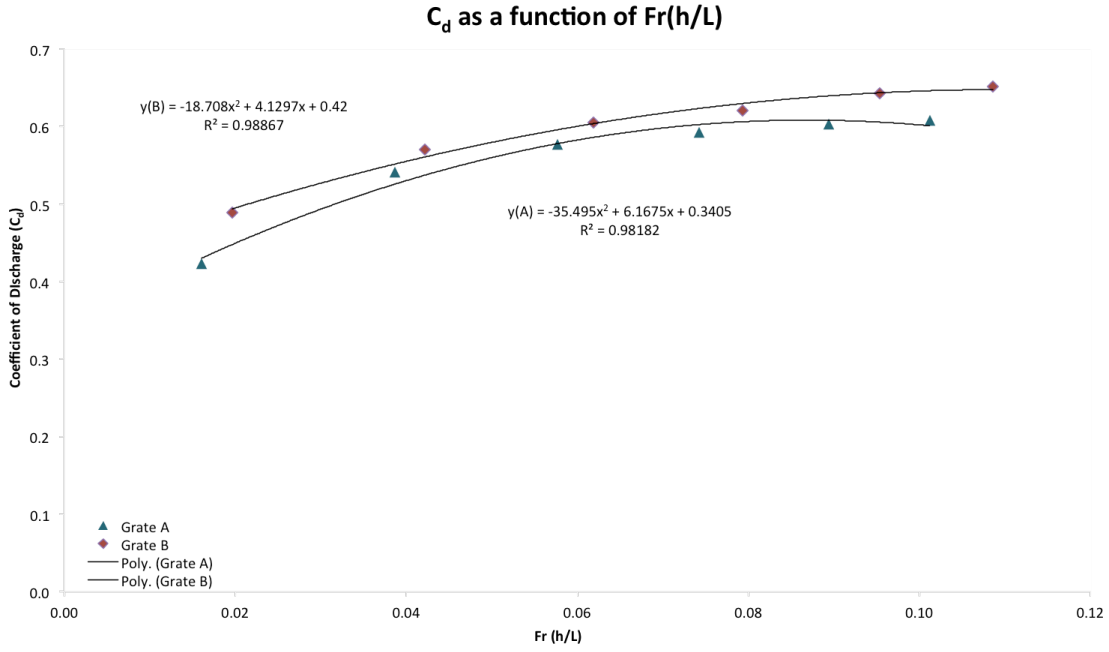

Figure 5.45 – Coefficient of discharge as a function of F_r (h/L)

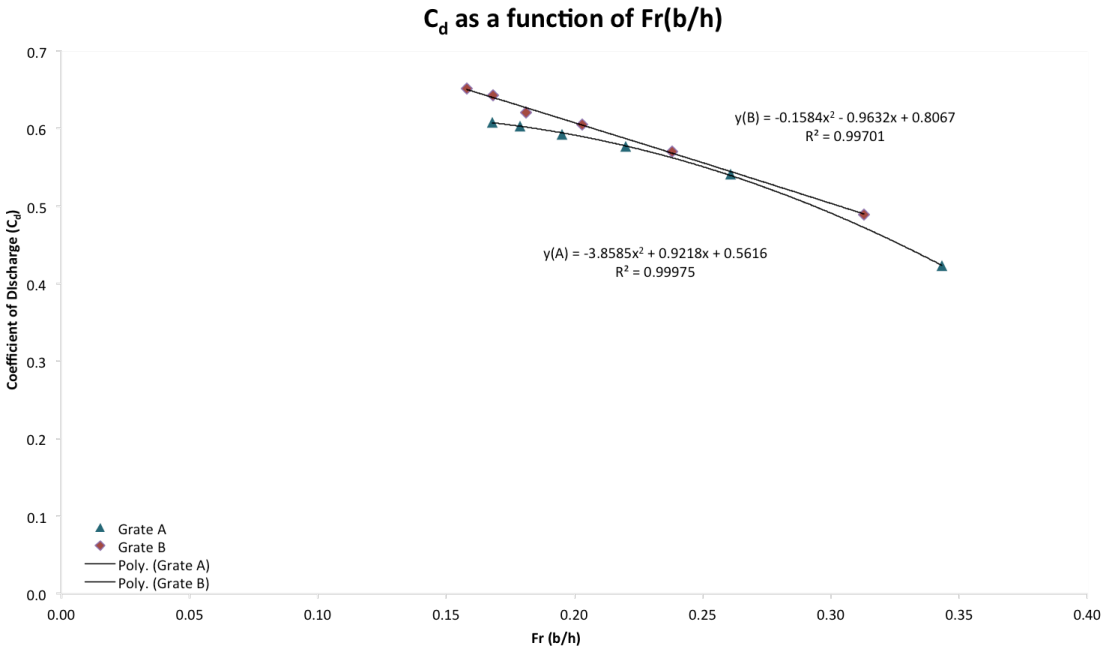

Figure 5.46 – Coefficient of discharge as a function of F_r (b/h)

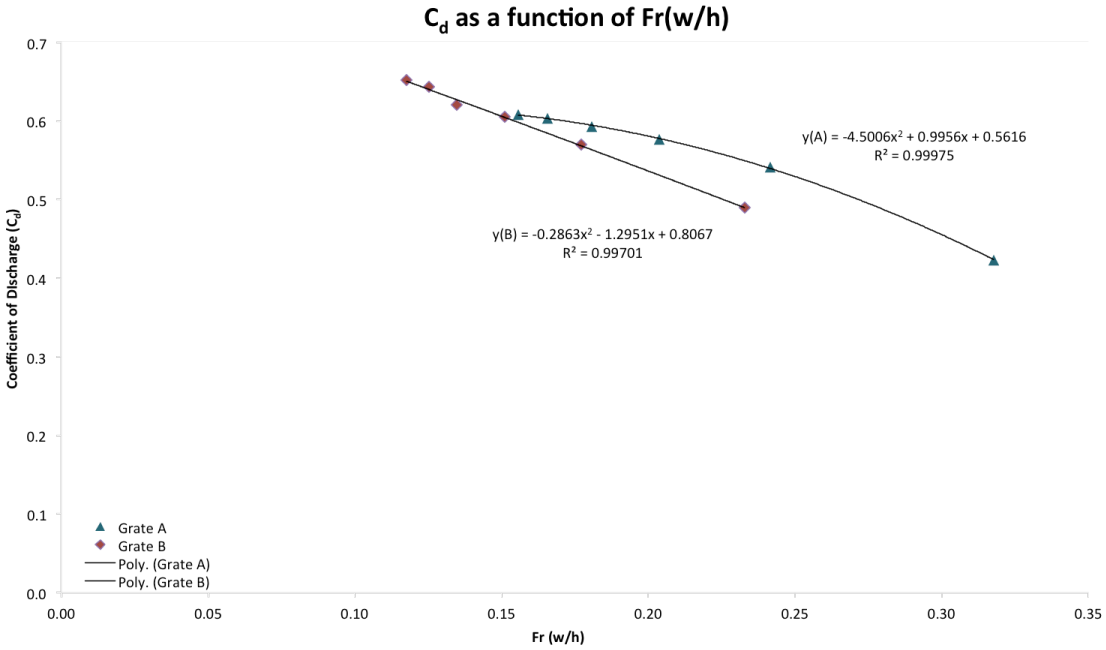

Figure 5.47 – Coefficient of discharge as a function of F_r (w/h)

Table 5.4 – Equation of best fit of C_d against a combination of dimensional parameters

Relationship	Equation of best fit	R^2
C_d vs. F_r (h/L)	y(A) = $-35.495x^2 + 6.1675x + 0.3405$ y(B) = $-18.708x^2 + 4.1297x + 0.42$	0.98182 0.98867
C_d vs. F_r (b/h)	y(A) = $-3.8585x^2 + 0.9218x + 0.5616$ y(B) = $-0.1584x^2 - 0.9632x + 0.8067$	0.99975 0.99701
C_d vs. F_r (w/h)	y(A) = $-4.5006x^2 + 0.9956x + 0.5616$ y(B) = $-0.2863x^2 - 1.2951x + 0.8067$	0.99975 0.99701

These results highlight that the combined dimensionless sets of equations gave no advantage over the single equations in terms of R^2.

5.2.3.5 Submergence coefficient

Submergence coefficient, K is a dimensionless parameter and is taken as the driving head of the submerged gully to the average surface water level.

$$K = \frac{h_G}{h_U}$$

[Equation 5.6]

Figure 5.48 shows the submergence coefficient for the surcharged system with backflow only and Figure 5.49 shows the submergence coefficient for the surcharged system with total outflow.

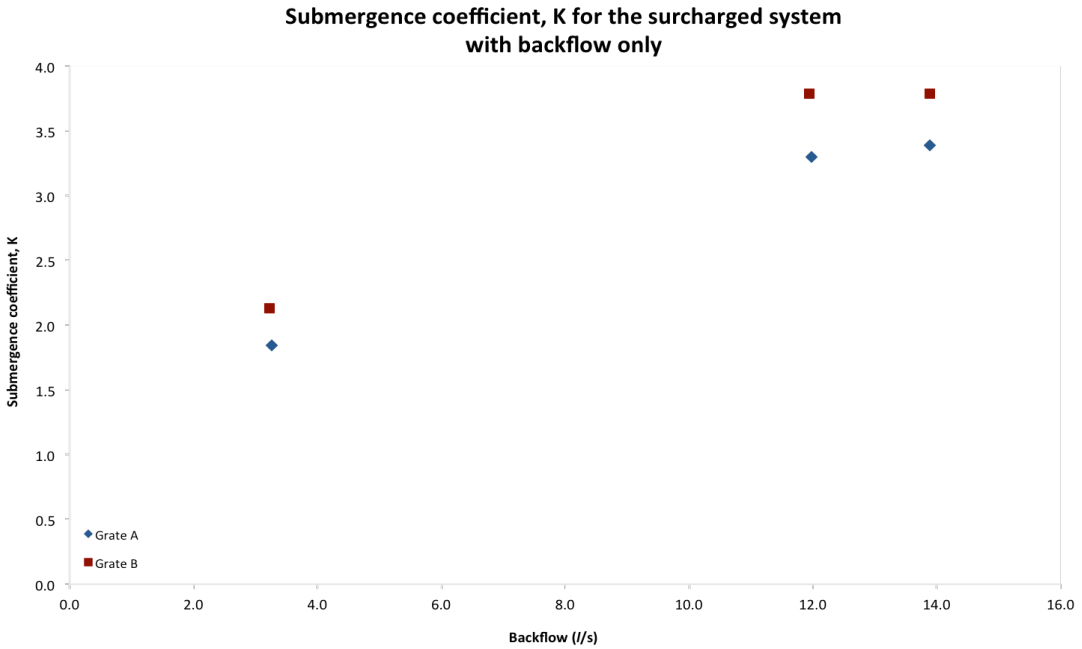

Figure 5.48 – Submergence coefficient, K for the surcharged system with backflow only

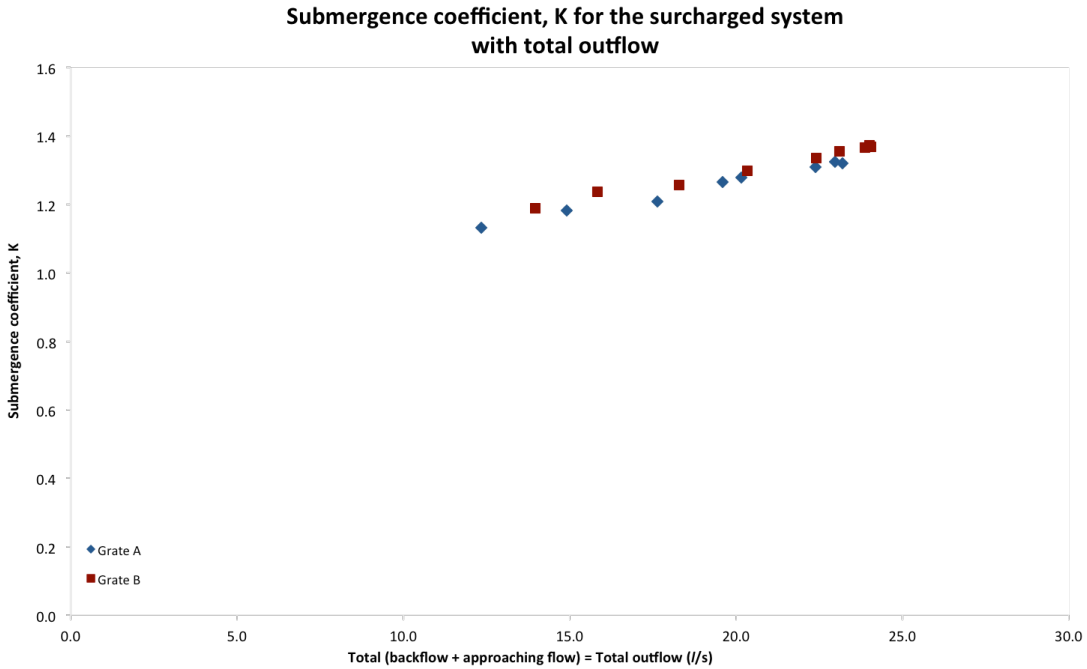

Figure 5.49 – Submergence coefficient, K for the surcharged system with total outflow

From Figure 5.48, it can be seen that Grate B has a higher submergence coefficient as compared to Grate A for the surcharge with backflow only. This reflects the difference in the area of opening of the grates.

In the case of surcharge with both backflow and approaching flow, Figure 5.49, for the same total flow the submergence coefficient reduces for both Grate A and Grate B, when compared to that for surcharged flow only (Fig 5.48). This reflects the impact of the interaction of the free surface flow.

In conclusion, the above analyses has highlighted that it is possible to describe the relationship between C_d and the characteristics of the flow and the geometry of the gully. Individual equations have been derived that link C_d to individual parameters with an excellent goodness of fit but these were grate specific. These equations may take a number of forms - linear, logarithmic, exponential and but they only express the dependency of C_d on the individual parameter i.e. different relationships are derived for different parameters. Attempts to derive a universal relationship were also made by combining two dimensionless groups but these were observed to offer no advantage over the single parameter relationships.

The major finding from the study was that the relationship between C_d and Froude number could be expressed as a single relationship for all bed slopes, albeit for each individual grate. In practice there is a need to relate this finding into design practice and this requires knowledge of a practical value of the hydraulic performance that is used in design. Clearly the most practical parameter is the flowrate to each gully and this may be derived as a function of the area drained to each gully and the corresponding design rainfall (see literature review). Hence, knowing the design flowrate upstream of a gully and the characteristics of the approach channel, it is possible to establish, based on the findings of this research, to determine the value of C_d based on the Froude number of the approaching flow. This value may then subsequently be used to establish the efficiency of gully operation and hence to predict the hydraulic performance. For practical application there is a need to incorporate the C_d value into the appropriate software and this research identifies a way in which the C_d value may be better selected

for a range of flow conditions to an individual grate. Alternatively, if a certain design value of C_d is assumed, then it is possible to predict the optimum design dimensions based on the required efficiency.

CHAPTER 6
CONCLUSION

In conclusion, this research has:

1. Established a system for the measurement of coefficient of discharge, C_d using a full-scale gully experimental facility.
2. Sophisticated instrumentation for the measurement of the C_d.
3. Studied a range of parameters which include:
   – 2 types of grates,
   – 3 bed slopes, and
   – terminal, intermediate and surcharged flows.
4. Completed a total of 486 tests.
5. Completed a series of analyses based on the experimental tests. From the analyses, it can be concluded that:
   - The flow conditions at the gully are very much a function of the outlet capacity of the gully pot. In this study, the pot that was used had two outlets and tests were completed with and without one of these outlets plugged.
   - The relationship between flow depth and flowrate was a function of the geometry of each individual grate but similar trends in the head discharge relationship for each grate were observed. The head discharge relationship for Grate A, in general, resulted in a lower head for the same flowrate when compared to grate B and hence concluding that Grate A is more efficient in capturing flows when compared to Grate B for the flat bed and 1/100 slope, but with similar efficiency at a higher slope.
   - The performance of the system was also tested without the grates in place (i.e. a free inlet to the gully pot). For both the grated and non-grated tests the head discharge relationships were similar throughout the entire tested range of flowrates, and again different curves were established for both type A and B grates. This highlights that the grate has little influence on the flow performance and it was concluded that the overall design (e.g. orientation/size/spacing) of the grates has been devised to perform at its optimal capacity.

- The longitudinal bed slope has a significant impact on the resultant head-discharge relationship for each grate.
- In terms of gulley depth, the depth increases as the bed slope increases. However, the intercepted flow decreases as the slope increases.
- At a bed slope of 1 in 30, the width of the channel had little impact on the head discharge relationship.
- The performance of the grated and non-grated for both type A and B were also similar throughout the entire tested range of flowrates.
- In terms of gulley depth, the depth increases as the bed slope increases. However, the intercepted flow decreases as the slope increases.
- For application in practice, the data was used to establish the coefficient of discharge of each grate and an examination was made of the way in which this coefficient changed for the different testing conditions. Comparing the results obtained from the application of the sharp-crested and broad-crested weir equations highlighted C_d values in the range 0.4 to 0.6 for the sharp-crested weir and 0.3 to 0.5 for the broad-crested weir. The results obtained were of comparable value to those reported in previously conducted studies. To align the results from the experimental programme with the generally accepted C_d value for gully inlets in the UK of circa 0.6, the results from the application of a sharp-crested weir equation was used. Hence, the use of the sharp-crested weir equation was maintained in all subsequent analysis. The coefficient of discharge obtained for the intermediate tests are lower when compared to terminal tests. As the head increases, the C_d decreases.

- Dimensional analysis was used to further examine the way in which the C_d value changes with other parameters. C_d was reported to be a function of many parameters – h/L, b/h, w/h, v, F_r, and K.
- A systematic review using a series of linear, exponential, logarithmic, polynomial and regression equations were used in an attempt to best fit the data. In summary, the equation of best fit for each parameter is summarised below:

Relationship	Equation of best fit	R^2
C_d vs. b/h	$y(A) = -0.006x^2 - 0.0746x + 0.6689$ $y(B) = 0.0207x^2 - 0.1604x + 0.7558$	0.99988 0.99735
C_d vs. h/L	$y(A) = -2.1921x^2 + 1.8059x + 0.2345$ $y(B) = -1.0053x^2 + 1.1041x + 0.3481$	0.99005 0.99329
C_d vs. w/h	$y(A) = -0.007x^2 - 0.0806x + 0.6689$ $y(B) = 0.0375x^2 - 0.2157x + 0.7558$	0.99988 0.99735
C_d vs. V	$y(A) = 0.0816\ln(x) + 0.913$ $y(B) = 0.0776\ln(x) + 0.9309$	0.97209 0.99583
C_d vs. F_r	$y(A) = 1.7282x^2 + 2.1827x + 0.0149$ $y(B) = - -0.5252x^2 + 1.4319x + 0.1997$	0.99985 0.99964

- For practical purposes, it was argued that the Froude number of the approaching flowrate was the most appropriate parameter to use in the subsequent analysis.
- The relationship for C_d vs. F_r as a function of bed slope was established as:

	Equation	R^2
Grate A	y = 1.5356x - 4E-15	1
Grate B	y = 1.7346x + 2E-14	1

- The relationship for C_d vs. F_r for both Grate A and Grate B, for both the terminal and intermediate system was established as:

	Equation	R^2
Terminal	$y(A) = -1.7282x^2 + 2.1827x + 0.0149$ $y(B) = -0.5252x^2 + 1.4319x + 0.1997$	0.99985 0.99964
Intermediate	$y(A) = -11.087x^2 + 6.1246x - 0.4554$ $y(B) = 3.616x^2 + 0.1917x + 0.1413$	0.97214 0.99976

The above results highlight that it is feasible to describe the performance of individual grates using a number of different equations, each with an excellent correlation between the measured and predicted values of C_d.

Primary finding showed that, for an individual grate (Grate A or Grate B), the relationship between C_d and Froude number could be described by a single relationship for all the bed slopes tested. Hence knowing the Froude number of the upstream flow to the grate, it is possible to use these relationships to find the value of C_d that may be used to establish the efficiency of the grate. Alternatively, if a certain value of C_d is assumed, then the optimum design dimensions can be predicted based on the required efficiency. A proposed methodology to utilise the data has been presented for the individual grates used in the study.

6.2 FUTURE WORK

A continuation of the existing experimental programme is suggested in order to understand the complex relationship between the above ground and below ground drainage system through gully systems. This experimental programme has only looked at the quantitative aspects of the system. The continuation of work is therefore suggested in order to consider both the qualitative and quantitative aspects of the gully system and is as presented below:

- Further experimental programme can be conducted in order to look at clogging factors (Guo, 2006; Almedeij et. al., 2006) such as debris and silt of the inlet.
- Suspended solids trapped in the gully pot can also reduce the efficiency of the gully system as a whole. There is a lack of information on pot performance partly due to the lack of appreciation of the role of the pot in urban drainage (Butler and Karunaratne, 1995). It is therefore suggested for further work to be done to assess this factor.
- Other typical types of gratings used in the UK.
- There is an opportunity to complete much further analysis of the data, for example, to accommodate the actual partial area of gulley opening, into the governing equations.
- Other parameters can also be studied such as the effects of crossfall on the discharge coefficient.

R E F E R E N C E S

British Standard: Concrete pipes and ancillary concrete products - Part 6: Specification for road gullies and gully cover slabs. **BS 5911-6:2004**.

British Standard: Gully tops and manhole tops for vehicular and pedestrian areas - Design requirements, type testing, marking, quality control. **BS EN 124:1994**.

British Standard: Selection and use of gully tops and manhole covers for installation within the highway. **BS 7903:1997**.

Design Manual for Roads and Bridges: Part 2 - Surface drainage of wide carriageways. **(TA 80/99)**.

Design Manual for Road and Bridges: Part 3 - Spacing of road gullies. **HA102/00**.

Design Manual for Road and Bridges: Part 3 - Sumpless gullies. **HA 105/04**.

Design Manual for Road and Bridges: Part 5 - Chamber tops and gully tops for road drainage and services: Installation and maintenance. **HA104/02**.

Design Manual for Roads and Bridges: Part 1 - Highway link design. **TD 9/93**.

Design Manual for Roads and Bridges: Part 3 - Surface and Sub-surface drainage systems for highways. **HD 33/06 Volume 4: Geotechnics and Drainage**.

Design Manual for Roads and Bridges: Part 4 - Hydraulic design of road edge surface water channels. **HA 37/97**.

Department of Natural Resources & Water Australia, Institute of Public Works Engineering Australia (2007). Queensland Urban Drainage Manual. (**QUDM).**

US Department of Transportation: Hydraulic Engineering Circular No 12 - Drainage of Highway Pavements (HEC 12).

US Department of Transportation: Hydraulic Engineering Circular No 22 - Urban Drainage Design Manual (HEC 22).

Akan, A. O. (1984). A physics-based approach to determine inlet concentration times. Third International Conference on Urban Storm Drainage, Goteborg, Sweden.

Almedeij, J., Alsulaili A., and Alhomoud J. (2006). "Assessment of grate sag inlets in a residential area based on return period and clogging factor." *Journal of Environmental Management* **79**: 38-42.

Argue, J. R. and Pezzaniti, D. (1996). "How reliable are inlet (hydraulic) models at representing stormwater flow?" *The Science of the Total Environment* **189/190**: 355-359.

Aronica, G. T., and Lanza, L. G. (2005). "Drainage efficiency in urban areas: a case study." *Hydrological Processes* **19**: 1105-1119.

Asawa, G. L. (2006). Laboratory Work in Hydraulic Engineering. New Age International.

Aydin I., Altan-Sakarya, A.B., and Sisman, C. (2011). "Discharge formula for rectangular sharp-crested weirs. *Elsevier. Flow measurement and Instrumentation* **(22)**: 144-151.

Bartlett, R. E. (1981). Surface water sewerage, Applied Science Publishers Ltd.

Bazin, H. (1898). "Experiences nouvelles sur 1'écoulement en déversoir (6e article)." Annales des Ponts et Chaussées, 68(2), 151-265 (in French).

Bettez, J., Townsend, R. D., Comeau, A. (2001). "Scale model testing and calibration of City of Ottawa sewer weirs." *NRC Research Press. Canadian Journal of Civil Engineering* (**28)**: 627-639

Boonya-aroonnet S., Maksimović, C., Prodanović, D. and Djordjević, S. (2007). Urban pluvial flooding: development of GIS based pathway model for surface flooding and interface with surcharged sewer model. Sustainable Techniques and

Strategies in Urban Water Management (6th International Conference), Lyon, France.

Butler, D. and Karunaratne, S. H. P. G. (1995). "The suspended solids trap efficiency of the roadside gully pot." *Water Resources* **29**(2): 719-729.

Butler, D. and Memon, F. A. (1999). "Dynamic modelling of roadside gully pots during wet weather." *Water Resources* **33**(15): 3364-3372.

Chen, A. S., Djordjevic S., Leandro J. and Savić, D. (2007). The urban inundation model with bidirectional flow interaction between 2D overland surface and 1D sewer networks. Sustainable Techniques and Strategies in Urban Water Management (6th International Conference), Lyon, France.

Chen, A. S., Djordjevic S., Leandro, J. and Savić, D. (2010). "An analysis of the combined consequences of pluvial and fluvial flooding." Water Science and Technology 62.7: 1491-1498

Clarke, W.P., Strods, P.J. and Argue, J.R. (1981). Gutter pavement flow relationships for roadway channels of moderate or steep grade. Proceeding I.E. Australia First National Local Government Conference, Adelaide, 130–137.

Davis, A., Jacob R. P., and Ellett, B. (1996). "A review of road-gully spacing methods." Water and Environmental Management **10**: 118-122.

Deletic, A., R. Ashley, and Rest, D. (2000). "Modelling input of fine granular sediment into drainage systems via gully pots." *Water Resources* **34**(15): 3836-3844.

Despotovic, J., Plavsic, J., Stefanovic, N., and Paviovic, D. (2005). "Inefficiency of stormwater inlets as a source of urban floods." *Water Science and Technology* **51**(2): 139-145.

Dey, A. K. and Kamioka, S. (2007). "An integrated modelling approach to predict flooding on urban basin." *Water Science and Technology* **55**(4): 19-29.

Djordjevic, S., Prodanovic, D., and Maksimović, C. (1999). "An approach to simulation of dual drainage." *Water Science and Technology* **39**(9): 95-103.

Djordjevic, S., Prodanovic, D., Maksimović, Č., Ivetić, M., and Savić, D. (2005). "SIPSON - Simulation of interaction between pipe flow and surface overland flow in networks." *Water Science and Technology* **52**(5): 275-283.

Ellis, J. B. and Harrop, D. O. (1984). "Variations in solid loadings to roadside gully pots." *The Science of the Total Environment.* **33:** 203-211.

Ellis, J. B., D. O. Harrop, and Revitt, D. M. (1986). "Hydrological controls of pollutant removal from highway surfaces." *Water Research.* **20**(5): 589-595.

Eskenazi, E. (1984). Laboratory study of absorbed runoff flow by different gully grating systems. Third International Conference on Urban Storm Drainage, Goteborg, Sweden.

Fritz, H. M., and Hager W. H (1998). "Hydraulics of Embankment Weirs." *Journal of Hydraulic Engineering.* **124**: 963-971

Gomez, M., Macchione, F. and Russo, B. (2006). Comparative analysis among different hydrological models to study the hydraulic behaviour of urban streets. The 7th International Conference on Hydroscience and Engineering, Philadelphia, USA.

Gomez, M., and Russo, B. (2007). Hydraulic efficiency of macro-inlets. Sustainable techniques and strategies in urban water management, 6th International Conference - Lyon, France.

Gomez, M. and B. Russo (2011). "Methodology to estimate hydraulic efficiency of drain inlets." Proceedings of the Institution of Civil Engineers. *Water Management.* **164**: 81-90.

Gomez, M., Macchione, F., and Russo, B. (2011). "Methodologies to study surface hydraulic behaviours of urban catchments during storm events." *Water Science and Technology.* **63**(11): 2666-2673.

Grottker, M. (1990). "Pollutant removal by gully pots in different catchment basin." *The Science of the Total Environment* **93**: 515-522.

Guo, J. C. Y. (2000). "Design of grate inlets with clogging factor." *Advances in Environmental Research* **4**: 181-186.

Guo, J. C. Y. (2000). "Street storm water conveyance capacity." *Journal of Irrigation and Drainage Engineering* **126**(2): 119-123.

Guo, J. C. Y. (2006). "Design of street curb opening inlets using a decay-based clogging factor." *Journal of Hydraulic Engineering* **132**(11): 1237-1241.

Guo, J. C. Y., MacKenzie K.A., Mommandi, A. (2009). "Design of street sump inlets." *Journal of Hydraulic Engineering* **135**(11): 1000-1004.

Haestad, M. and S. R. Durrans (2003). Stormwater Conveyance Modelling and Design, Haestad Press.

HR Wallingford. Infoworks CS Technical Review.

Hydraulics Research (1981). Design and analysis of urban storm drainage: The Wallingford Procedure. HR Wallingford.

Hydraulics Research (1983). Design and analysis of urban storm drainage: The Wallingford Procedure. HR Wallingford.

Johnson, M.C (2000). "Discharge coefficient analysis for flat-topped and sharp crested weir." *Irrigation Science* **19:** 133-137.

Kidd, C. H. R. and Helliwell, P. R. (1977). "Simulation of the inlet hydrograph for urban catchments." *Journal of Hydrology* **35**(1-2): 159-172

Kindsvater, C. E. (1964). Discharge characteristics of embankment- shaped weirs. Geological Survey Water Supply Paper I6J7-A, U.S. Government Printing Office, Washington, D.C.

Lau, S.-L., Khan, E., & Stenstrom, M. K. (2001). "Catch basin inserts to reduce pollution from stormwater." *Water Science and Technology* **44**(7): 23-34.

Leandro, J. (2008). Advanced Modelling of Flooding in Urban Areas Integrated 1D/1D and 1D/2D Models. PhD Thesis, University of Exeter.

Leandro, J. (2008). A dynamic-objective- function algorithm to calibrate a 1D/1D coupled hydraulic model versus a 1D/2D model. 11th International Conference on Urban Drainage, Edinburgh, Scotland.

Leandro, J., Djordjević, S., Chen, A. S., Savić, D. A., and Stanić, M. (2011). "Calibration of a 1D/1D urban flood model using 1D/2D model results in the absence of field data." *Water Science and Technology* **64.5**:1016-1024

Mark, O., Weesakul, S., Apirumanekul, C., Aroonet, S. B. and Djordjević, S. (2004). "Potential and limitations of 1D modelling of urban flooding." *Journal of Hydrology* **299**: 284-299.

Martínez, P. and Gómez, M. (2000). "Estudio de eficiencia de la captación de rejas", XIX Congreso Latinoamericano de Hidráulica, Córdoba, Argentina.

Memon, F. A. and D. Butler (2002). "Identification and modelling of dry weather processes in gully pots." *Water Research* **36**: 1351-1359.

Mustaffa, Z., Rajaratnam, N. and Zhu, D. Z. (2006). "An experimental study of inflow into orifices and grating inlets on streets." *Canadian Journal of Civil Engineering*. **33**: 837-845.

Nasello, C. and Tucciarelli, T. (2005). "Dual multilevel urban drainage model." *Journal of Hydraulic Engineering* **131**(9): 748-754.

National Instruments (2003). LabVIEW User Manual.

National Instruments (2004). LabVIEW Real-Time Module User Manual.

Nikolov, N. A, Minkov, I. N., Dimitrov, D. K., Mincheva, S. K. and Mirchev, M. A. (1978). "Hydraulic calculation of a submerged broad-crested weir." Translated from Gidrotekhnicheskoe Stroitel'stvo **6**: 54-56

Pezzaniti, D., Loughlin, G. G. O., and Argue, J. R. (2005). General characteristics of pit inlet capacity relationships. 10th International Conference on Urban Drainage, Copenhagen, Denmark.

Pitt, S. M. (2007). Learning lessons from the 2007 floods: An independent review by Sir Michael Pitt.

Pratt, C. J. (1984). "Design limits on pollution." *The Science of the Total Environment* **33**: 161-170.

Pratt, C. J. and Adams, J. R. W. (1984). "Sediment supply and transmissions via roadside gully pots." *The Science of the Total Environment* **33**: 213-224.

Rao, G. N. S and Muralidhar, D. (1963). " Discharge characteristics of weirs of finite-crest width." *La Houille Blanche* **5**:537-545

Russo, B., Gomez, M., Martinez, P., and Sanchez, H. (2005). Methodology to study the surface runoff in urban streets and the design of drainage inlet systems. Application in a real case study. 10th International Conference on Urban Drainage, Copenhagen, Denmark.

Russo, B., Gomez, M. and Martinez, P. (2006). A simple hydrological approach to design inlet systems in urban areas according to risk criteria. The 7th International Conference on Hydroscience and Engineering, Philadelphia, USA.

Schmitt, T. G., Thomas, M., Ettrich, N. (2004). "Analysis and modelling of urban flooding in urban drainage systems." *Journal of Hydrology* **299**: 300-311.

Schmitt, T. G., Thomas, M., Ettrich, N. (2005). "Assessment of urban flooding by dual drainage simulation model RisUrSim." *Water Science and Technology* **52**(5): 257-264.

Sommer, H., Sieker, H., and Post, M. (2008). Experiences with decentralized inlet-infiltration-systems on highly frequented roads. 11th International Conference on Urban Drainage, Edinburgh, Scotland.

Stephenson, D. (1981). Stormwater hydrology and drainage, Elsevier Scientific.

Unwin, D. M. (2008) "Development of Control Algorithms to Describe Flow Discharge Reduction and Energy Loss at a Manhole Junction." PhD Thesis, University of Sheffield.

Uyumaz, A. (1994). "Highway storm drainage with kerb-opening inlets." *The Science of the Total Environment* **146/147**: 471-478

Valentin, M. G. and Russo, B. (2007). Hydraulic efficiency of macro-inlets. Sustainable Techniques and Strategies in Urban Water Management (6th International Conference), Lyon, France.

Watson, J. (1994). Highway Construction & Maintenance, Longman Group Ltd.

Wong, T. S. W. (1994). "Kinematic wave method for determination of road drainage inlet spacing." *Advances in Water Resources* **17**: 329-336

Wong, T. S. W. and Moh, W. H. (1997). "Effect of maximum flood width on road drainage inlet spacing." *Water Science and Technology* **36**(8-9): 241-246.

Woo, D. C. (1984). Inlets in stormwater modelling. Third International Conference on Urban Storm Drainage, Goteborg, Sweden.

APPENDICES

Appendix 1 – Details of the gully pot

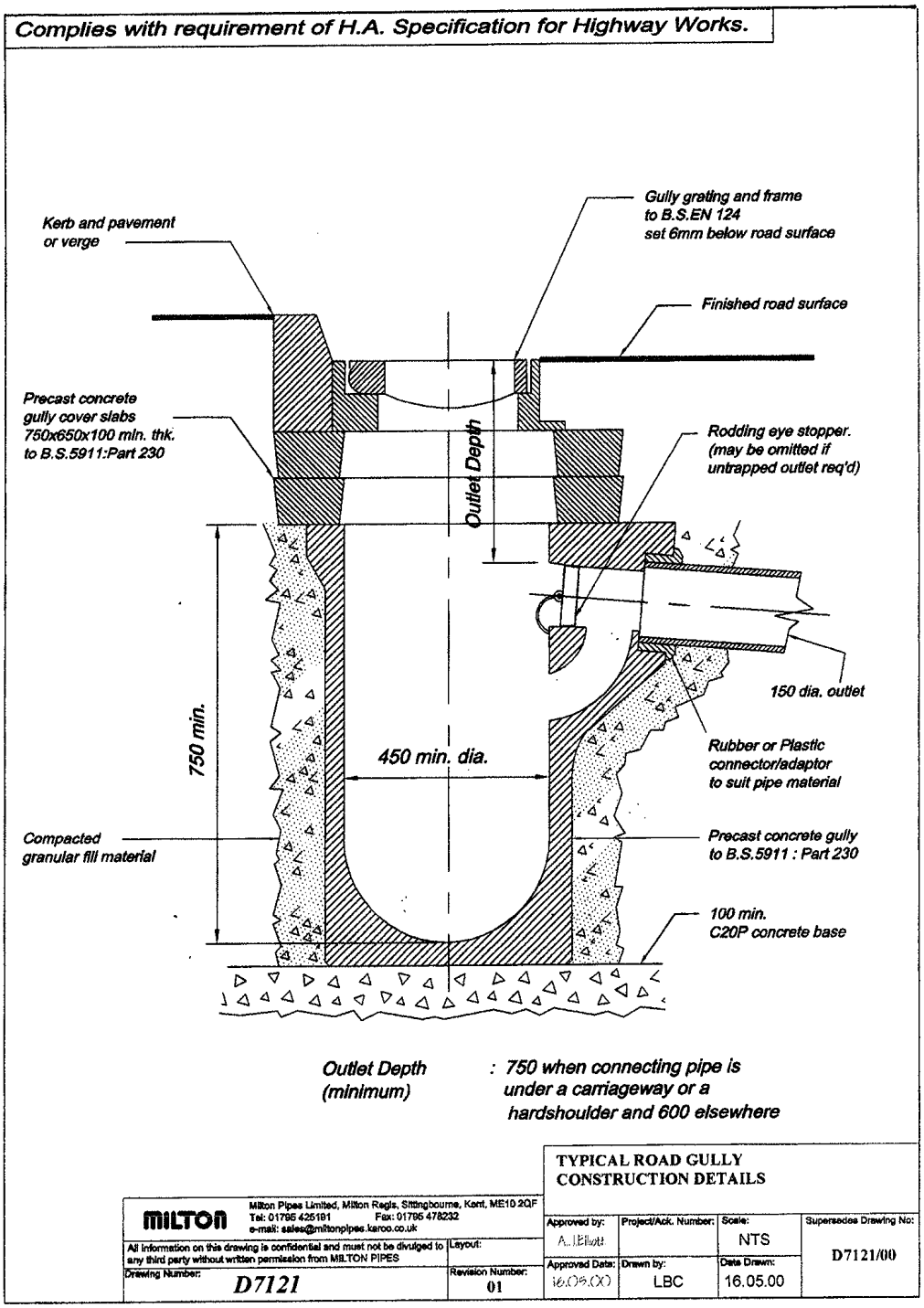

Appendix 2 – Tables C2 – C6

Table C2: TYPE P

Drained area of road in m^2 under a rainfall intensity of 50mm/h and collection efficiency in % (in brackets)

Crossfall (S_c)	**Gradient** (S_L)	**Flow width (B in m)**							
		0.5		0.75		1		1.5	
1/60	1/300	13	*(99)*	38	*(99)*	81	*(98)*	234	*(96)*
	1/150	18	*(99)*	53	*(98)*	114	*(97)*	325	*(94)*
	1/100	22	*(99)*	65	*(98)*	138	*(96)*	393	*(93)*
	1/80	25	*(99)*	73	*(98)*	154	*(96)*	436	*(92)*
	1/60	29	*(99)*	84	*(97)*	177	*(95)*	496	*(91)*
	1/50	31	*(98)*	91	*(97)*	193	*(95)*	539	*(90)*
	1/40	35	*(98)*	102	*(96)*	214	*(94)*	594	*(94)*
	1/30	40	*(98)*	117	*(96)*	245	*(93)*	673	*(87)*
	1/20	49	*(97)*	142	*(95)*	295	*(92)*	797	*(84)*
	1/15	57	*(97)*	162	*(94)*	336	*(91)*	893	*(82)*
1/50	1/300	18	*(99)*	51	*(99)*	109	*(98)*	315	*(95)*
	1/150	25	*(99)*	72	*(98)*	153	*(97)*	437	*(94)*
	1/100	30	*(99)*	88	*(97)*	186	*(96)*	526	*(92)*
	1/80	34	*(99)*	98	*(97)*	207	*(95)*	583	*(91)*
	1/60	39	*(98)*	113	*(97)*	237	*(95)*	663	*(90)*
	1/50	42	*(98)*	123	*(96)*	259	*(94)*	718	*(89)*
	1/40	47	*(98)*	137	*(96)*	287	*(94)*	791	*(87)*
	1/30	54	*(98)*	157	*(95)*	328	*(93)*	893	*(85)*
	1/20	66	*(97)*	190	*(94)*	395	*(91)*	1052	*(82)*
	1/15	76	*(97)*	218	*(94)*	449	*(90)*	1174	*(79)*
1/40	1/300	25	*(99)*	74	*(98)*	158	*(97)*	452	*(95)*
	1/150	36	*(99)*	104	*(98)*	220	*(96)*	624	*(92)*
	1/100	44	*(99)*	126	*(97)*	267	*(95)*	751	*(91)*
	1/80	49	*(98)*	141	*(97)*	297	*(95)*	829	*(90)*
	1/60	56	*(98)*	162	*(96)*	340	*(94)*	941	*(88)*
	1/50	61	*(98)*	177	*(96)*	370	*(93)*	1017	*(87)*
	1/40	68	*(98)*	196	*(95)*	411	*(93)*	1117	*(85)*
	1/30	78	*(97)*	225	*(95)*	468	*(91)*	1256	*(83)*
	1/20	96	*(97)*	272	*(94)*	562	*(90)*	1469	*(79)*
	1/15	110	*(96)*	311	*(93)*	637	*(88)*	1628	*(76)*

Manning's coefficient is n = 0.017
For others values of rainfall intensity I, multiply the area by (50/I)

Table C2 (cont.): TYPE P

Drained area of road in m^2 under a rainfall intensity of 50mm/h and collection efficiency in % (in brackets)

Crossfall (S_c)	Gradient (S_L)	Flow width (B in m)							
		0.5		0.75		1		1.5	
1/30	1/300	41	*(99)*	118	*(98)*	252	*(97)*	718	*(94)*
	1/150	57	*(99)*	166	*(97)*	351	*(95)*	986	*(91)*
	1/100	70	*(98)*	202	*(97)*	425	*(94)*	1181	*(89)*
	1/80	78	*(98)*	225	*(96)*	472	*(94)*	1301	*(88)*
	1/60	89	*(98)*	258	*(95)*	539	*(93)*	1470	*(86)*
	1/50	98	*(97)*	281	*(95)*	586	*(92)*	1584	*(84)*
	1/40	109	*(97)*	312	*(94)*	649	*(91)*	1732	*(83)*
	1/30	125	*(97)*	358	*(94)*	738	*(90)*	1935	*(80)*
	1/20	152	*(96)*	431	*(92)*	880	*(87)*	2235	*(75)*
	1/15	175	*(95)*	491	*(91)*	994	*(85)*	2449	*(71)*
1/25	1/300	55	*(99)*	159	*(98)*	338	*(96)*	960	*(93)*
	1/150	77	*(98)*	223	*(97)*	471	*(95)*	1314	*(90)*
	1/100	94	*(98)*	271	*(96)*	569	*(94)*	1569	*(88)*
	1/80	105	*(98)*	302	*(96)*	631	*(93)*	1725	*(86)*
	1/60	120	*(97)*	346	*(95)*	720	*(92)*	1942	*(84)*
	1/50	132	*(97)*	377	*(94)*	782	*(91)*	2088	*(82)*
	1/40	147	*(97)*	419	*(94)*	865	*(90)*	2276	*(80)*
	1/30	168	*(96)*	478	*(93)*	981	*(88)*	2528	*(77)*
	1/20	204	*(96)*	576	*(91)*	1167	*(86)*	2892	*(72)*
	1/15	234	*(95)*	655	*(90)*	1313	*(84)*	3140	*(68)*
1/20	1/300	79	*(99)*	229	*(97)*	484	*(96)*	1367	*(92)*
	1/150	110	*(98)*	320	*(96)*	672	*(94)*	1861	*(88)*
	1/100	135	*(98)*	388	*(95)*	812	*(93)*	2211	*(86)*
	1/80	150	*(97)*	432	*(95)*	899	*(92)*	2423	*(84)*
	1/60	173	*(97)*	494	*(94)*	1024	*(91)*	2716	*(81)*
	1/50	189	*(97)*	538	*(94)*	1111	*(90)*	2910	*(80)*
	1/40	210	*(96)*	597	*(93)*	1225	*(88)*	3156	*(77)*
	1/30	241	*(96)*	681	*(92)*	1386	*(87)*	3479	*(74)*
	1/20	293	*(95)*	817	*(90)*	1638	*(84)*	3921	*(68)*
	1/15	335	*(94)*	927	*(88)*	1835	*(81)*	4197	*(63)*
1/15	1/300	125	*(98)*	363	*(97)*	767	*(95)*	2145	*(90)*
	1/150	176	*(98)*	507	*(96)*	1061	*(93)*	2895	*(86)*
	1/100	214	*(97)*	614	*(95)*	1276	*(91)*	3415	*(83)*
	1/80	239	*(97)*	682	*(94)*	1411	*(90)*	3725	*(81)*
	1/60	274	*(96)*	780	*(93)*	1602	*(89)*	4143	*(78)*
	1/50	299	*(96)*	848	*(92)*	1734	*(88)*	4415	*(76)*
	1/40	333	*(96)*	939	*(91)*	1906	*(86)*	4749	*(73)*
	1/30	382	*(95)*	1069	*(90)*	2146	*(84)*	5167	*(69)*
	1/20	462	*(94)*	1276	*(88)*	2516	*(80)*	5678	*(62)*
	1/15	528	*(93)*	1443	*(86)*	2796	*(77)*	5924	*(56)*

Manning's coefficient is n = 0.017
For other values of rainfall intensity I, multiply the area by (50/I)

Table C3: TYPE Q

Drained area of road in m^2 under a rainfall intensity of 50mm/h and collection efficiency in % (in brackets)

Crossfall (S_c)	**Gradient (S_L)**	**Flow width (B in m)**							
		0.5		0.75		1		1.5	
1/60	1/300	13	*(99)*	38	*(98)*	80	*(97)*	229	*(94)*
	1/150	18	*(99)*	53	*(97)*	112	*(96)*	316	*(91)*
	1/100	22	*(98)*	64	*(97)*	136	*(95)*	378	*(89)*
	1/80	25	*(98)*	72	*(96)*	151	*(94)*	417	*(88)*
	1/60	29	*(98)*	82	*(96)*	172	*(93)*	472	*(86)*
	1/50	31	*(98)*	90	*(95)*	187	*(92)*	509	*(85)*
	1/40	35	*(97)*	100	*(95)*	208	*(91)*	557	*(83)*
	1/30	40	*(97)*	114	*(94)*	236	*(90)*	623	*(81)*
	1/20	49	*(96)*	138	*(93)*	282	*(88)*	722	*(76)*
	1/15	56	*(96)*	157	*(91)*	319	*(86)*	794	*(73)*
1/50	1/300	17	*(99)*	51	*(98)*	108	*(97)*	307	*(93)*
	1/150	25	*(98)*	71	*(97)*	151	*(95)*	422	*(90)*
	1/100	30	*(98)*	87	*(96)*	182	*(94)*	504	*(88)*
	1/80	33	*(98)*	96	*(96)*	202	*(93)*	554	*(87)*
	1/60	38	*(98)*	111	*(95)*	231	*(92)*	625	*(85)*
	1/50	42	*(97)*	121	*(95)*	251	*(91)*	673	*(83)*
	1/40	47	*(97)*	134	*(94)*	277	*(90)*	734	*(81)*
	1/30	54	*(97)*	153	*(93)*	315	*(89)*	817	*(78)*
	1/20	65	*(96)*	185	*(92)*	375	*(86)*	938	*(73)*
	1/15	75	*(95)*	210	*(90)*	422	*(84)*	1022	*(69)*
1/40	1/300	25	*(99)*	73	*(97)*	155	*(96)*	439	*(92)*
	1/150	35	*(98)*	103	*(96)*	216	*(94)*	599	*(89)*
	1/100	43	*(98)*	125	*(96)*	261	*(93)*	713	*(86)*
	1/80	48	*(98)*	139	*(95)*	289	*(92)*	782	*(85)*
	1/60	55	*(97)*	159	*(94)*	329	*(91)*	878	*(82)*
	1/50	61	*(97)*	173	*(94)*	357	*(90)*	941	*(81)*
	1/40	67	*(97)*	192	*(93)*	394	*(89)*	1022	*(78)*
	1/30	77	*(96)*	219	*(92)*	446	*(87)*	1130	*(75)*
	1/20	94	*(95)*	263	*(90)*	529	*(84)*	1279	*(69)*
	1/15	108	*(94)*	299	*(89)*	593	*(82)*	1375	*(64)*

Manning's coefficient is n = 0.017
For other values of rainfall intensity I, multiply the area by (50/I)

Table C3 (cont.): TYPE Q

Drained area of road in m² under a rainfall intensity of 50mm/h and collection efficiency in % (in brackets)

Crossfall (S_c)	**Gradient (S_L)**	**Flow width (B in m)**							
		0.5		0.75		1		1.5	
1/30	1/300	40	*(98)*	117	*(97)*	247	*(95)*	693	*(90)*
	1/150	57	*(98)*	163	*(96)*	342	*(93)*	937	*(86)*
	1/100	69	*(97)*	198	*(95)*	412	*(92)*	1108	*(83)*
	1/80	77	*(97)*	220	*(94)*	456	*(91)*	1209	*(81)*
	1/60	88	*(97)*	252	*(93)*	518	*(89)*	1347	*(79)*
	1/50	97	*(96)*	274	*(93)*	561	*(88)*	1437	*(77)*
	1/40	107	*(96)*	303	*(92)*	617	*(87)*	1549	*(74)*
	1/30	123	*(95)*	345	*(90)*	696	*(85)*	1690	*(70)*
	1/20	149	*(94)*	413	*(88)*	817	*(81)*	1867	*(63)*
	1/15	171	*(93)*	467	*(86)*	909	*(78)*	1959	*(57)*
1/25	1/300	54	*(98)*	157	*(97)*	332	*(95)*	923	*(89)*
	1/150	76	*(98)*	219	*(95)*	458	*(92)*	1240	*(85)*
	1/100	93	*(97)*	266	*(94)*	550	*(91)*	1457	*(81)*
	1/80	103	*(97)*	295	*(93)*	607	*(89)*	1585	*(79)*
	1/60	119	*(96)*	337	*(92)*	688	*(88)*	1756	*(76)*
	1/50	130	*(96)*	366	*(92)*	744	*(87)*	1865	*(74)*
	1/40	144	*(95)*	405	*(91)*	817	*(85)*	1997	*(70)*
	1/30	165	*(95)*	460	*(89)*	917	*(83)*	2157	*(66)*
	1/20	200	*(93)*	548	*(87)*	1070	*(79)*	2334	*(58)*
	1/15	228	*(92)*	618	*(85)*	1184	*(75)*	2397	*(52)*
1/20	1/300	78	*(98)*	226	*(96)*	474	*(94)*	1305	*(88)*
	1/150	109	*(97)*	314	*(94)*	651	*(91)*	1738	*(82)*
	1/100	133	*(97)*	379	*(93)*	780	*(89)*	2026	*(78)*
	1/80	148	*(96)*	420	*(92)*	859	*(88)*	2192	*(76)*
	1/60	170	*(96)*	479	*(91)*	971	*(86)*	2407	*(72)*
	1/50	186	*(95)*	520	*(90)*	1047	*(85)*	2540	*(70)*
	1/40	206	*(95)*	574	*(89)*	1145	*(83)*	2693	*(66)*
	1/30	236	*(94)*	650	*(88)*	1279	*(80)*	2862	*(61)*
	1/20	285	*(92)*	771	*(85)*	1479	*(76)*	2996	*(52)*
	1/15	324	*(91)*	866	*(83)*	1622	*(72)*	Not eff.	*(44)*
1/15	1/300	124	*(98)*	357	*(95)*	746	*(92)*	2027	*(85)*
	1/150	174	*(97)*	496	*(93)*	1020	*(89)*	2659	*(79)*
	1/100	211	*(96)*	597	*(92)*	1215	*(87)*	3061	*(74)*
	1/80	235	*(95)*	660	*(91)*	1335	*(85)*	3282	*(71)*
	1/60	269	*(95)*	751	*(90)*	1500	*(83)*	3552	*(67)*
	1/50	293	*(94)*	813	*(89)*	1611	*(81)*	3706	*(64)*
	1/40	326	*(93)*	895	*(87)*	1753	*(79)*	3863	*(59)*
	1/30	372	*(92)*	1010	*(85)*	1942	*(76)*	3986	*(53)*
	1/20	447	*(91)*	1189	*(82)*	2211	*(71)*	Not eff.	*(42)*
	1/15	508	*(89)*	1325	*(79)*	2389	*(66)*		

Manning's coefficient is n = 0.017
For other values of rainfall intensity I, multiply the area by (50/I)

Table C4: TYPE R

Drained area of road in m^2 under a rainfall intensity of 50mm/h and collection efficiency in % (in brackets)

Crossfall (S_c)	**Gradient (S_L)**	**Flow width (B in m)**							
		0.5		0.75		1		1.5	
1/60	1/300	13	*(99)*	37	*(97)*	79	*(96)*	224	*(92)*
	1/150	18	*(98)*	52	*(96)*	110	*(94)*	306	*(88)*
	1/100	22	*(98)*	64	*(96)*	133	*(93)*	363	*(86)*
	1/80	25	*(97)*	71	*(95)*	148	*(92)*	398	*(84)*
	1/60	28	*(97)*	81	*(94)*	168	*(91)*	447	*(82)*
	1/50	31	*(97)*	88	*(94)*	182	*(90)*	479	*(80)*
	1/40	34	*(96)*	98	*(93)*	201	*(89)*	520	*(78)*
	1/30	40	*(96)*	112	*(92)*	228	*(87)*	573	*(74)*
	1/20	48	*(95)*	134	*(90)*	269	*(84)*	648	*(68)*
	1/15	55	*(94)*	152	*(89)*	302	*(81)*	695	*(64)*
1/50	1/300	17	*(99)*	51	*(97)*	107	*(95)*	300	*(91)*
	1/150	24	*(98)*	71	*(96)*	148	*(93)*	406	*(87)*
	1/100	30	*(97)*	86	*(95)*	178	*(92)*	481	*(84)*
	1/80	33	*(97)*	95	*(94)*	197	*(91)*	526	*(82)*
	1/60	38	*(97)*	109	*(94)*	224	*(90)*	587	*(79)*
	1/50	42	*(96)*	118	*(93)*	243	*(89)*	627	*(78)*
	1/40	46	*(96)*	131	*(92)*	268	*(87)*	677	*(75)*
	1/30	53	*(95)*	149	*(91)*	302	*(85)*	741	*(71)*
	1/20	64	*(94)*	179	*(89)*	355	*(82)*	825	*(64)*
	1/15	74	*(93)*	203	*(87)*	396	*(79)*	871	*(59)*
1/40	1/300	25	*(98)*	73	*(97)*	153	*(95)*	427	*(89)*
	1/150	35	*(98)*	101	*(95)*	211	*(92)*	574	*(85)*
	1/100	43	*(97)*	123	*(94)*	254	*(91)*	675	*(82)*
	1/80	48	*(97)*	136	*(94)*	281	*(90)*	735	*(79)*
	1/60	55	*(96)*	156	*(93)*	318	*(88)*	814	*(76)*
	1/50	60	*(96)*	169	*(92)*	344	*(87)*	865	*(74)*
	1/40	67	*(95)*	187	*(91)*	378	*(85)*	928	*(71)*
	1/30	76	*(95)*	213	*(89)*	425	*(83)*	1003	*(66)*
	1/20	92	*(93)*	253	*(87)*	496	*(79)*	1089	*(59)*
	1/15	105	*(92)*	286	*(85)*	549	*(76)*	1122	*(53)*

Manning's coefficient is n = 0.017
For other values of rainfall intensity I, multiply the area by (50/I)

Table C4 (cont.): TYPE R

Drained area of road in m^2 under a rainfall intensity of 50mm/h and collection efficiency in % (in brackets)

Crossfall (S_c)	**Gradient (S_L)**	**Flow width (B in m)**							
		0.5		0.75		1		1.5	
1/30	1/300	40	*(98)*	116	*(96)*	243	*(93)*	669	*(87)*
	1/150	56	*(97)*	161	*(94)*	334	*(91)*	888	*(82)*
	1/100	68	*(96)*	195	*(93)*	400	*(89)*	1034	*(78)*
	1/80	76	*(96)*	216	*(92)*	440	*(87)*	1117	*(75)*
	1/60	87	*(95)*	246	*(91)*	497	*(85)*	1225	*(71)*
	1/50	95	*(95)*	267	*(90)*	536	*(84)*	1290	*(69)*
	1/40	106	*(94)*	294	*(89)*	585	*(82)*	1365	*(65)*
	1/30	121	*(94)*	333	*(87)*	653	*(79)*	1445	*(60)*
	1/20	146	*(92)*	395	*(84)*	754	*(75)*	1500	*(51)*
	1/15	166	*(91)*	443	*(82)*	825	*(71)*	Not eff.	*(43)*
1/25	1/300	54	*(98)*	156	*(95)*	325	*(93)*	886	*(86)*
	1/150	76	*(97)*	216	*(94)*	445	*(90)*	1166	*(80)*
	1/100	92	*(96)*	260	*(92)*	531	*(87)*	1346	*(75)*
	1/80	102	*(96)*	288	*(91)*	583	*(86)*	1446	*(72)*
	1/60	117	*(95)*	327	*(90)*	656	*(84)*	1570	*(68)*
	1/50	128	*(94)*	355	*(89)*	706	*(82)*	1642	*(65)*
	1/40	142	*(94)*	391	*(88)*	769	*(80)*	1718	*(61)*
	1/30	162	*(93)*	441	*(86)*	853	*(77)*	1785	*(55)*
	1/20	195	*(91)*	520	*(82)*	974	*(72)*	Not eff.	*(44)*
	1/15	222	*(90)*	581	*(80)*	1056	*(67)*		
1/20	1/300	78	*(97)*	222	*(95)*	463	*(92)*	1244	*(83)*
	1/150	108	*(96)*	307	*(93)*	630	*(88)*	1614	*(77)*
	1/100	132	*(95)*	370	*(91)*	748	*(85)*	1841	*(71)*
	1/80	146	*(95)*	409	*(90)*	819	*(84)*	1961	*(68)*
	1/60	167	*(94)*	464	*(88)*	917	*(81)*	2099	*(63)*
	1/50	182	*(93)*	502	*(87)*	983	*(79)*	2170	*(59)*
	1/40	202	*(93)*	551	*(86)*	1065	*(77)*	2231	*(55)*
	1/30	231	*(92)*	620	*(84)*	1173	*(73)*	Not eff.	*(48)*
	1/20	277	*(90)*	725	*(80)*	1319	*(67)*		
	1/15	314	*(88)*	805	*(77)*	1409	*(62)*		
1/15	1/300	123	*(97)*	352	*(94)*	726	*(90)*	1909	*(80)*
	1/150	172	*(96)*	483	*(91)*	979	*(86)*	2422	*(72)*
	1/100	208	*(94)*	579	*(89)*	1154	*(83)*	2707	*(66)*
	1/80	231	*(94)*	638	*(88)*	1258	*(80)*	2839	*(62)*
	1/60	264	*(93)*	721	*(86)*	1398	*(77)*	2962	*(56)*
	1/50	287	*(92)*	778	*(85)*	1489	*(75)*	2998	*(51)*
	1/40	318	*(91)*	851	*(83)*	1600	*(72)*	Not eff.	*(46)*
	1/30	362	*(90)*	951	*(80)*	1739	*(68)*		
	1/20	432	*(88)*	1101	*(76)*	1905	*(61)*		
	1/15	488	*(86)*	1208	*(72)*	1981	*(55)*		

Manning's coefficient is n = 0.017
For other values of rainfall intensity I, multiply the area by (50/I)

Table C5: TYPE S

Drained area of road in m^2 under a rainfall intensity of 50mm/h and collection efficiency in % (in brackets)

Crossfall (S_c)	**Gradient (S_L)**	**Flow width (B in m)**							
		0.5		0.75		1		1.5	
1/60	1/300	13	*(98)*	37	*(97)*	78	*(94)*	218	*(89)*
	1/150	18	*(98)*	52	*(95)*	108	*(92)*	292	*(85)*
	1/100	22	*(97)*	63	*(94)*	130	*(90)*	343	*(81)*
	1/80	24	*(97)*	70	*(93)*	143	*(89)*	374	*(79)*
	1/60	28	*(96)*	79	*(92)*	162	*(88)*	414	*(76)*
	1/50	31	*(96)*	86	*(92)*	175	*(86)*	439	*(73)*
	1/40	34	*(95)*	95	*(91)*	193	*(85)*	470	*(70)*
	1/30	39	*(94)*	108	*(89)*	216	*(83)*	507	*(66)*
	1/20	47	*(93)*	129	*(87)*	252	*(79)*	548	*(58)*
	1/15	54	*(92)*	146	*(85)*	279	*(75)*	562	*(51)*
1/50	1/300	17	*(98)*	50	*(96)*	105	*(94)*	290	*(88)*
	1/150	24	*(97)*	70	*(95)*	144	*(91)*	386	*(83)*
	1/100	30	*(97)*	84	*(93)*	173	*(89)*	451	*(79)*
	1/80	33	*(96)*	93	*(93)*	191	*(88)*	488	*(76)*
	1/60	38	*(96)*	106	*(91)*	216	*(86)*	536	*(73)*
	1/50	41	*(95)*	115	*(91)*	233	*(85)*	567	*(70)*
	1/40	46	*(95)*	127	*(89)*	254	*(83)*	601	*(67)*
	1/30	52	*(94)*	144	*(88)*	284	*(80)*	640	*(61)*
	1/20	63	*(92)*	171	*(85)*	329	*(76)*	673	*(53)*
	1/15	72	*(91)*	193	*(83)*	361	*(72)*	Not eff.	*(45)*
1/40	1/300	25	*(98)*	72	*(96)*	150	*(93)*	410	*(86)*
	1/150	35	*(97)*	100	*(94)*	206	*(90)*	540	*(80)*
	1/100	42	*(96)*	120	*(92)*	245	*(88)*	624	*(76)*
	1/80	47	*(96)*	133	*(91)*	270	*(86)*	671	*(73)*
	1/60	54	*(95)*	151	*(90)*	304	*(84)*	730	*(68)*
	1/50	59	*(94)*	164	*(89)*	327	*(82)*	764	*(65)*
	1/40	65	*(94)*	181	*(88)*	356	*(80)*	801	*(61)*
	1/30	75	*(93)*	204	*(86)*	395	*(77)*	834	*(55)*
	1/20	90	*(91)*	241	*(83)*	452	*(72)*	Not eff.	*(45)*
	1/15	102	*(90)*	269	*(80)*	491	*(68)*		

Manning's coefficient is n = 0.017
For other values of rainfall intensity I, multiply the area by (50/I)

Table C5 (cont.): TYPE S

Drained area of road in m^2 under a rainfall intensity of 50mm/h and collection efficiency in % (in brackets)

Crossfall (S_c)	**Gradient (S_L)**	**Flow width (B in m)**							
		0.5		0.75		1		1.5	
1/30	1/300	40	*(97)*	114	*(95)*	238	*(91)*	636	*(83)*
	1/150	56	*(96)*	158	*(92)*	323	*(88)*	823	*(76)*
	1/100	68	*(95)*	190	*(91)*	383	*(85)*	936	*(70)*
	1/80	75	*(95)*	210	*(90)*	419	*(83)*	995	*(67)*
	1/60	86	*(94)*	238	*(88)*	469	*(81)*	1061	*(62)*
	1/50	94	*(93)*	257	*(87)*	502	*(79)*	1094	*(58)*
	1/40	104	*(93)*	282	*(85)*	543	*(76)*	1120	*(53)*
	1/30	118	*(91)*	317	*(83)*	597	*(73)*	Not eff.	*(46)*
	1/20	142	*(89)*	370	*(79)*	669	*(66)*		
	1/15	161	*(88)*	410	*(76)*	712	*(61)*		
1/25	1/300	54	*(97)*	153	*(94)*	317	*(90)*	836	*(81)*
	1/150	75	*(96)*	211	*(91)*	428	*(86)*	1067	*(73)*
	1/100	91	*(95)*	253	*(90)*	505	*(83)*	1197	*(67)*
	1/80	101	*(94)*	279	*(88)*	551	*(81)*	1260	*(63)*
	1/60	115	*(93)*	315	*(87)*	614	*(78)*	1322	*(57)*
	1/50	125	*(92)*	340	*(85)*	654	*(76)*	1345	*(53)*
	1/40	139	*(92)*	372	*(83)*	704	*(73)*	Not eff.	*(48)*
	1/30	158	*(90)*	417	*(81)*	768	*(69)*		
	1/20	189	*(88)*	484	*(77)*	846	*(62)*		
	1/15	213	*(86)*	532	*(73)*	885	*(56)*		
1/20	1/300	77	*(96)*	218	*(93)*	449	*(89)*	1161	*(78)*
	1/150	107	*(95)*	299	*(90)*	601	*(84)*	1450	*(69)*
	1/100	129	*(94)*	358	*(88)*	705	*(81)*	1594	*(62)*
	1/80	144	*(93)*	393	*(87)*	766	*(78)*	1652	*(57)*
	1/60	164	*(92)*	443	*(84)*	846	*(75)*	1687	*(51)*
	1/50	178	*(91)*	477	*(83)*	898	*(72)*	Not eff.	*(46)*
	1/40	197	*(90)*	520	*(81)*	959	*(69)*		
	1/30	224	*(89)*	579	*(78)*	1031	*(64)*		
	1/20	266	*(86)*	664	*(73)*	1106	*(56)*		
	1/15	300	*(84)*	723	*(69)*	Not eff.	*(50)*		
1/15	1/300	122	*(96)*	344	*(92)*	699	*(87)*	1751	*(74)*
	1/150	169	*(94)*	468	*(88)*	925	*(81)*	2107	*(63)*
	1/100	204	*(93)*	556	*(86)*	1073	*(77)*	2234	*(54)*
	1/80	226	*(92)*	609	*(84)*	1156	*(74)*	Not eff.	*(49)*
	1/60	257	*(91)*	682	*(81)*	1262	*(70)*		
	1/50	279	*(90)*	731	*(80)*	1326	*(67)*		
	1/40	308	*(88)*	793	*(77)*	1396	*(63)*		
	1/30	348	*(87)*	873	*(74)*	1467	*(57)*		
	1/20	412	*(84)*	984	*(68)*	Not eff.	*(48)*		
	1/15	461	*(81)*	1052	*(63)*				

Manning's coefficient is n = 0.017
For other values of rainfall intensity I, multiply the area by (50/I)

Table C6: TYPE T

Drained area of road in m^2 under a rainfall intensity of 50mm/h and collection efficiency in % (in brackets)

Crossfall (S_c)	**Gradient (S_L)**	**Flow width (B in m)**							
		0.5		0.75		1		1.5	
1/60	1/300	13	*(98)*	37	*(95)*	77	*(92)*	208	*(85)*
	1/150	18	*(97)*	51	*(93)*	105	*(89)*	272	*(79)*
	1/100	22	*(96)*	61	*(92)*	125	*(87)*	314	*(74)*
	1/80	24	*(95)*	68	*(91)*	137	*(85)*	336	*(71)*
	1/60	28	*(95)*	77	*(89)*	154	*(83)*	364	*(67)*
	1/50	30	*(94)*	83	*(88)*	165	*(81)*	380	*(63)*
	1/40	33	*(93)*	92	*(87)*	180	*(79)*	395	*(59)*
	1/30	38	*(92)*	104	*(85)*	199	*(76)*	408	*(53)*
	1/20	46	*(91)*	122	*(82)*	226	*(71)*	Not eff.	*(42)*
	1/15	52	*(89)*	136	*(79)*	245	*(66)*		
1/50	1/300	17	*(97)*	49	*(95)*	102	*(91)*	275	*(83)*
	1/150	24	*(96)*	68	*(93)*	139	*(88)*	356	*(76)*
	1/100	29	*(95)*	82	*(91)*	165	*(85)*	405	*(71)*
	1/80	32	*(95)*	90	*(90)*	181	*(83)*	431	*(67)*
	1/60	37	*(94)*	103	*(88)*	203	*(81)*	461	*(62)*
	1/50	40	*(93)*	111	*(87)*	217	*(79)*	476	*(59)*
	1/40	45	*(93)*	122	*(85)*	235	*(77)*	488	*(54)*
	1/30	51	*(91)*	137	*(83)*	258	*(73)*	Not eff.	*(47)*
	1/20	61	*(90)*	160	*(79)*	290	*(67)*		
	1/15	69	*(88)*	177	*(76)*	309	*(62)*		
1/40	1/300	25	*(97)*	71	*(94)*	146	*(90)*	385	*(81)*
	1/150	34	*(96)*	97	*(91)*	197	*(86)*	489	*(72)*
	1/100	42	*(95)*	116	*(89)*	232	*(83)*	548	*(66)*
	1/80	46	*(94)*	128	*(88)*	253	*(81)*	576	*(62)*
	1/60	53	*(93)*	145	*(86)*	282	*(78)*	603	*(57)*
	1/50	58	*(92)*	157	*(85)*	300	*(76)*	612	*(52)*
	1/40	64	*(91)*	171	*(83)*	323	*(73)*	Not eff.	*(47)*
	1/30	73	*(90)*	192	*(81)*	352	*(69)*		
	1/20	87	*(88)*	222	*(76)*	387	*(62)*		
	1/15	98	*(86)*	244	*(73)*	404	*(56)*		

Manning's coefficient is n = 0.017
For other values of rainfall intensity I, multiply the area by (50/I)

Table C6 (cont.): TYPE T

Drained area of road in m^2 under a rainfall intensity of 50mm/h and collection efficiency in % (in brackets)

Crossfall (S_c)	**Gradient (S_L)**	**Flow width (B in m)**							
		0.5		0.75		1		1.5	
1/30	1/300	39	*(96)*	112	*(93)*	229	*(88)*	587	*(77)*
	1/150	55	*(95)*	153	*(90)*	306	*(83)*	725	*(67)*
	1/100	66	*(93)*	182	*(87)*	357	*(79)*	789	*(59)*
	1/80	74	*(93)*	200	*(86)*	387	*(77)*	811	*(55)*
	1/60	84	*(92)*	225	*(83)*	427	*(73)*	Not eff.	*(48)*
	1/50	91	*(91)*	242	*(82)*	451	*(71)*		
	1/40	101	*(90)*	264	*(80)*	480	*(67)*		
	1/30	114	*(88)*	293	*(77)*	512	*(62)*		
	1/20	136	*(85)*	334	*(71)*	542	*(54)*		
	1/15	152	*(83)*	362	*(67)*	Not eff.	*(47)*		
1/25	1/300	53	*(96)*	149	*(92)*	304	*(87)*	762	*(74)*
	1/150	73	*(94)*	203	*(88)*	402	*(81)*	918	*(63)*
	1/100	89	*(93)*	242	*(86)*	467	*(77)*	974	*(54)*
	1/80	98	*(92)*	265	*(84)*	503	*(74)*	Not eff.	*(49)*
	1/60	112	*(91)*	297	*(81)*	549	*(70)*		
	1/50	121	*(90)*	318	*(80)*	577	*(67)*		
	1/40	134	*(88)*	345	*(77)*	608	*(63)*		
	1/30	151	*(87)*	380	*(74)*	639	*(58)*		
	1/20	179	*(84)*	428	*(68)*	Not eff.	*(48)*		
	1/15	200	*(81)*	458	*(63)*				
1/20	1/300	76	*(95)*	212	*(90)*	427	*(85)*	1038	*(70)*
	1/150	105	*(93)*	287	*(86)*	559	*(78)*	1203	*(57)*
	1/100	126	*(92)*	339	*(83)*	641	*(73)*	Not eff.	*(47)*
	1/80	140	*(91)*	370	*(81)*	686	*(70)*		
	1/60	159	*(89)*	413	*(79)*	740	*(65)*		
	1/50	172	*(88)*	440	*(77)*	770	*(62)*		
	1/40	189	*(87)*	474	*(74)*	799	*(58)*		
	1/30	213	*(85)*	518	*(70)*	818	*(51)*		
	1/20	250	*(81)*	572	*(63)*	Not eff.	*(40)*		
	1/15	279	*(78)*	601	*(57)*				
1/15	1/300	120	*(94)*	332	*(89)*	658	*(81)*	1515	*(64)*
	1/150	165	*(92)*	444	*(84)*	843	*(74)*	Not eff.	*(49)*
	1/100	198	*(90)*	521	*(80)*	950	*(68)*		
	1/80	218	*(89)*	565	*(78)*	1003	*(64)*		
	1/60	247	*(87)*	624	*(74)*	1058	*(59)*		
	1/50	267	*(86)*	661	*(72)*	1081	*(55)*		
	1/40	293	*(84)*	705	*(69)*	Not eff.	*(49)*		
	1/30	328	*(82)*	756	*(64)*				
	1/20	381	*(77)*	808	*(56)*				
	1/15	420	*(74)*	Not eff.	*(49)*				

Manning's coefficient is n = 0.017
For other values of rainfall intensity I, multiply the area by (50/I)

Appendix 3 - Recommended Runoff Coefficient for Rational Method (HEC22)

Type of Drainage Area	Runoff Coefficient, C*
Business:	
Downtown areas	0.70 - 0.95
Neighborhood areas	0.50 - 0.70
Residential:	
Single-family areas	0.30 - 0.50
Multi-units, detached	0.40 - 0.60
Multi-units, attached	0.60 - 0.75
Suburban	0.25 - 0.40
Apartment dwelling areas	0.50 - 0.70
Industrial:	
Light areas	0.50 - 0.80
Heavy areas	0.60 - 0.90
Parks, cemeteries	0.10 - 0.25
Playgrounds	0.20 - 0.40
Railroad yard areas	0.20 - 0.40
Unimproved areas	0.10 - 0.30
Lawns:	
Sandy soil, flat, 2%	0.05 - 0.10
Sandy soil, average, 2 - 7%	0.10 - 0.15
Sandy soil, steep, 7%	0.15 - 0.20
Heavy soil, flat, 2%	0.13 - 0.17
Heavy soil, average, 2 - 7%	0.18 - 0.22
Heavy soil, steep, 7%	0.25 - 0.35
Streets:	
Asphaltic	0.70 - 0.95
Concrete	0.80 - 0.95
Brick	0.70 - 0.85
Drives and walks	0.75 - 0.85
Roofs	0.75 - 0.95
*Higher values are usually appropriate for steeply sloped areas and longer return periods because infiltration and other losses have a proportionally smaller effect on runoff in these cases.	

Appendix 4 - Values of 2minM5 rainfall depth in the UK (HA 102)

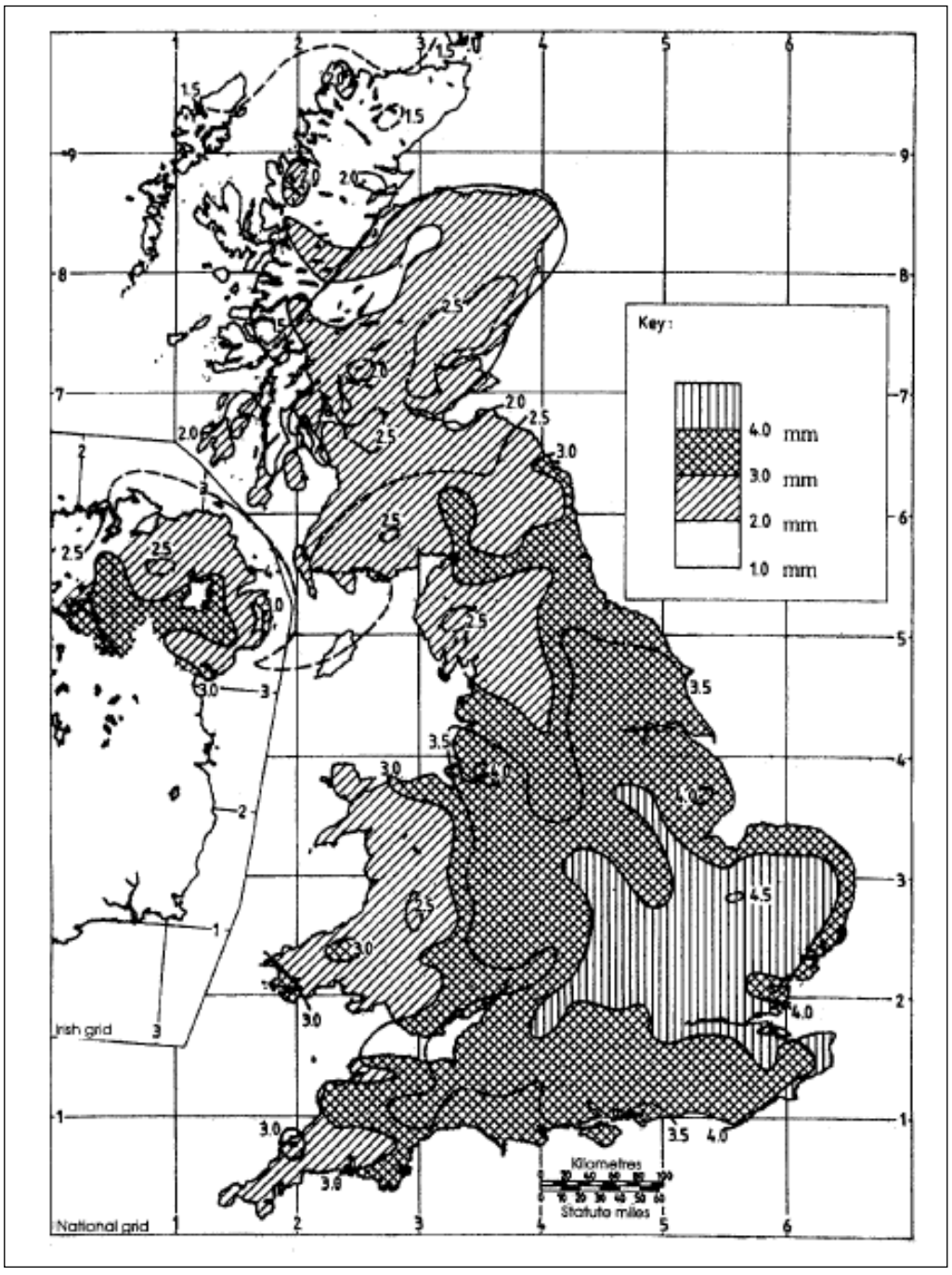

Gems Sensors & Controls

PRESSURE SENSORS

5000 Series Low Range Pressure Transducer

PRESSURE TRANSDUCERS

LOW RANGE

- Immersible and general purpose models
- Open faced for viscous liquids
- High proof pressures

The 5000 Series features a sturdy ceramic diaphragm and precision capacitance technology to detect minute pressure variations, while withstanding large pressure spikes. The tough ceramic sensor is housed in a stainless steel case to ensure performance in the most demanding applications. Both voltage and 4-20mA outputs are available at time of order. A switch and potentiometer can be accessed for field adjustment of range with 3:1 ranging capability.

Ex

CE

Lloyds Register

Specifications

Input	
Pressure Range	0 to 25mb to 0 to 1bar
Proof Pressure	2bar for ranges 200mb and below 4bar for ranges 201mb to 350mb 7bar ranges 351mb to 1bar
Burst Pressure	3bar for 70mb and below 4bar for 71mb to 200mb 6bar for 201mb to 350mb 10bar for bar ranges 351mb to 1bar
Fatigue Life	10 million FS cycles
Performance	
Long Term Stability	.25% span/annum
Accuracy	.2% span max
Thermal Error	2% span max
Compensated Temperatures	-20°C to 60°C (-5° to 140°F)
Operating Temperatures	-25°C to +85°C (-15° to 185°F) Electrical Code G and L -20°C to +50°C (-5° to 120°F) Electrical Code M and 3 -40°C to +100°C (-40° to 212°F) Process media
Zero Tolerance	0.1% span
Span Tolerance	0.1% span
Mounting Effects	.25% span max
Response Time	5ms
Supply Voltage Sensitivity	.01% span/volt
Zero Adjustment	±10% (by potentiometer)
Span Adjustment	±10% (by potentiometer)
Mechanical Configuration	
Pressure Port	(See ordering guide)
***Wetted Parts**	S/S to UNS 31803; Inconel 625, Ceramic & Nitrile
Electrical Connection	(See ordering guide)
Enclosure	Code M IP68 Submersible Code G IP65
Approvals	CE, Lloyds Register ExII 1G, EEx ia IIB T4 (-20<Ta<+75°C)
Weight	330gms (excluding cable)
Individual Specifications	
Voltage Output units	
Output	(See ordering guide)
Supply Voltage (Vs)	8 to 35V Max
Current Output Unit	
Output	4-20mA (2 wire)
Supply Voltage (Vs)	9 to 35Vdc
Max. Loop Resistance	(Vs-9) x 50 ohms

www.gemssensors.com

PLATON
An RM&C Brand

FLOW

Product Data Sheet **DS1601**

Electromagnetic Flowmeter

INDUCTIVE FLOW METER MAG 900

A flowmeter designed to measure, indicate and store both flow rate and total flow of conductive liquids. The MAG 900 records both positive and negative flows. As there are no moving mechanical parts in the flow profile, the device can be applied to measure dirty liquids even with solid particles.

APPLICATIONS

Designed to be used in the chemical industry, water and waste-water industries and all process industries.

FEATURES

- Displays flow rate and total
- High and low alarms
- Bi-directional
- DN10 - DN1000, PN10 - PN25
- Accuracy ± 0.5% of reading
- Frequency, pulse, curent outputs
- Infra-red RS232 communications port
- Configuration data is backed up

DIMENSIONS

Nominal diameter (mm)	Nominal Length DN LN (mm)
10 - 100	200
125 - 150	300
200 - 250	400
300 - 500	500
600	600
700	700
800	800
900	900
1000	1000

RM&C Roxspur Measurement & Control Ltd

FieldPoint™ Operating Instructions

FP-AI-100 and cFP-AI-100

Eight-Channel, 12-Bit Analog Input Modules

These operating instructions describe how to install and use the FP-AI-100 and cFP-AI-100 analog input modules (referred to inclusively as the [c]FP-AI-100). For information about configuring and accessing the [c]FP-AI-100 over a network, refer to the user manual for the FieldPoint network module you are using.

Features

The [c]FP-AI-100 is a FieldPoint analog input module with the following features:

- Eight analog voltage or current input channels
- 11 input ranges: 0–1 V, 0–5 V, 0–15 V, 0–30 V, ±1 V, ±5 V, ±15 V, ±30 V, 0–20 mA, 4–20 mA, and ±20 mA
- 12-bit resolution
- 250 V_{rms} CAT II continuous channel-to-ground isolation, verified by 2,300 V_{rms}, 1 minute dielectric withstand test
- –40 to 70 °C operation
- Hot swappable

Installing the FP-AI-100

The FP-AI-100 mounts on a FieldPoint terminal base (FP-TB-*x*), which provides operating power to the module. Installing the FP-AI-100 onto a powered terminal base does not disrupt the operation of the FieldPoint bank.

NATIONAL INSTRUMENTS

FieldPoint Operating Instructions

cFP-RLY-421

Eight-Channel SPST Relay Module

These operating instructions describe how to install and use the National Instruments cFP-RLY-421 relay module. For details on configuring and accessing the cFP-RLY-421 over a network, refer to the user manual for the FieldPoint network module you are using.

Features

The cFP-RLY-421 is a Compact FieldPoint relay output module with the following features:

- Eight single-pole single-throw (SPST) relay channels
- Switching capacity 1.5 A at 35 VDC or 250 VAC
- LED relay status indicators
- Hot swappable
- –40 to 60 °C operation
- 250 V_{rms} maximum isolation voltage
- 2,300 V_{rms} transient overvoltage protection

Power Requirement

The cFP-RLY-421 is powered by the FieldPoint network module through the backplane bus. The cFP-RLY-421 is a high-power consumption module, which may limit the number of I/O modules that you can connect to a single network module.

323617A-01 *May 2003*

NATIONAL INSTRUMENTS

Appendix 8 – Gully drawing by Milton Precast

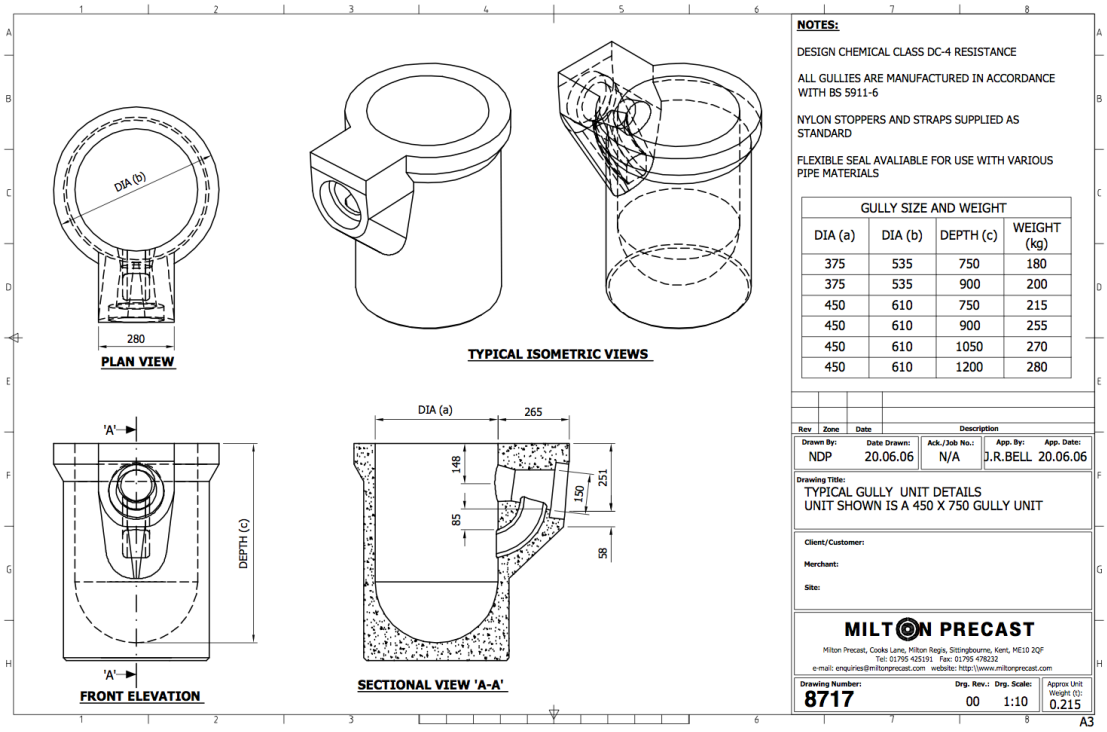

Appendix 9 – Summary of tests

TERMINAL TESTS	
Filename	**Filename**
Flat Grate A 006-0T	Flat Grate B 006-0T
Flat Grate A 007-0T	Flat Grate B 007-0T
Flat Grate A 008-0T	Flat Grate B 008-0T
Flat Grate A 009-0T	Flat Grate B 009-0T
Flat Grate A 010-0T	Flat Grate B 010-0T
Flat Grate A 011-0T	Flat Grate B 011-0T
Flat Grate A 012-0T	Flat Grate B 012-0T
Flat Grate A 013-0T	Flat Grate B 013-0T
Flat Grate A 014-0T	Flat Grate B 014-0T
Flat Grate A 016-0T	Flat Grate B 016-0T
Flat Grate A 018-0T	Flat Grate B 018-0T
Flat Grate A 020-0T	Flat Grate B 020-0T
Flat Grate A Plugged 006-0T	Flat Grate B Plugged 006-0T
Flat Grate A Plugged 007-0T	Flat Grate B Plugged 007-0T
Flat Grate A Plugged 008-0T	Flat Grate B Plugged 008-0T
Flat Grate A Plugged 009-0T	Flat Grate B Plugged 009-0T
Filename	**Filename**
130 Grate A 006 - 0T	130 Grate B 006 - 0T
130 Grate A 007 - 0T	130 Grate B 007 - 0T
130 Grate A 008 - 0T	130 Grate B 008 - 0T
130 Grate A 009 - 0T	130 Grate B 009 - 0T
130 Grate A 010 - 0T	130 Grate B 010 - 0T
130 Grate A 012 - 0T	130 Grate B 012 - 0T
130 Grate A 014 - 0T	130 Grate B 014 - 0T
130 Grate A 016 - 0T	130 Grate B 016 - 0T
130 Grate A 018 - 0T	130 Grate B 018 - 0T
130 Grate A 020 - 0T	130 Grate B 020 - 0T
130 Grate A Plugged 006 - 0T	130 Grate B Plugged 006 - 0T
130 Grate A Plugged 007 - 0T	130 Grate B Plugged 007 - 0T
130 Grate A Plugged 008 - 0T	130 Grate B Plugged 008 - 0T
130 Grate A Plugged 009 - 0T	130 Grate B Plugged 009 - 0T

TERMINAL TESTS	
Filename	**Filename**
100 Grate A 006 - 0T	100 Grate B 006 - 0T
100 Grate A 007 - 0T	100 Grate B 007 - 0T
100 Grate A 008 - 0T	100 Grate B 008 - 0T
100 Grate A 009 - 0T	100 Grate B 009 - 0T
100 Grate A 010 - 0T	100 Grate B 010 - 0T
100 Grate A 012 - 0T	100 Grate B 012 - 0T
100 Grate A 014 - 0T	100 Grate B 014 - 0T
100 Grate A 016 - 0T	100 Grate B 016 - 0T
100 Grate A 018 - 0T	100 Grate B 018 - 0T
100 Grate A 020 - 0T	100 Grate B 020 - 0T
100 Grate A Plugged 006 - 0T	100 Grate B Plugged 006 - 0T
100 Grate A Plugged 007 - 0T	100 Grate B Plugged 007 - 0T
100 Grate A Plugged 008 - 0T	100 Grate B Plugged 008 - 0T
100 Grate A Plugged 009 - 0T	100 Grate B Plugged 009 - 0T
Filename	**Filename**
Flat No Grate A 006-0T	Flat No Grate B 006-0T
Flat No Grate A 007-0T	Flat No Grate B 007-0T
Flat No Grate A 008-0T	Flat No Grate B 008-0T
Flat No Grate A 009-0T	Flat No Grate B 009-0T
Flat No Grate A 010-0T	Flat No Grate B 010-0T
Flat No Grate A 011-0T	Flat No Grate B 011-0T
Flat No Grate A 012-0T	Flat No Grate B 012-0T
Flat No Grate A 013-0T	Flat No Grate B 013-0T
Flat No Grate A 014-0T	Flat No Grate B 014-0T
Flat No Grate A 016-0T	Flat No Grate B 016-0T
Flat No Grate A 018-0T	Flat No Grate B 018-0T
Flat No Grate A 020-0T	Flat No Grate B 020-0T
Flat No Grate A Plugged 006-0T	Flat No Grate B Plugged 006-0T
Flat No Grate A Plugged 007-0T	Flat No Grate B Plugged 007-0T
Flat No Grate A Plugged 008-0T	Flat No Grate B Plugged 008-0T
Flat No Grate A Plugged 009-0T	Flat No Grate B Plugged 009-0T

TERMINAL TESTS	
Filename	**Filename**
100 No Grate A 006 - 0T	100 No Grate B 006 - 0T
100 No Grate A 007 - 0T	100 No Grate B 007 - 0T
100 No Grate A 008 - 0T	100 No Grate B 008 - 0T
100 No Grate A 009 - 0T	100 No Grate B 009 - 0T
100 No Grate A 010 - 0T	100 No Grate B 010 - 0T
100 No Grate A 012 - 0T	100 No Grate B 012 - 0T
100 No Grate A 014 - 0T	100 No Grate B 014 - 0T
100 No Grate A 016 - 0T	100 No Grate B 016 - 0T
100 No Grate A 018 - 0T	100 No Grate B 018 - 0T
100 No Grate A 020 - 0T	100 No Grate B 020 - 0T
100 No Grate A Plugged 006 - 0T	100 No Grate B Plugged 006 - 0T
100 No Grate A Plugged 007 - 0T	100 No Grate B Plugged 007 - 0T
100 No Grate A Plugged 008 - 0T	100 No Grate B Plugged 008 - 0T
100 No Grate A Plugged 009 - 0T	100 No Grate B Plugged 009 - 0T
Filename	**Filename**
130 No Grate A 006 - 0T	130 No Grate B 006 - 0T
130 No Grate A 007 - 0T	130 No Grate B 007 - 0T
130 No Grate A 008 - 0T	130 No Grate B 008 - 0T
130 No Grate A 009 - 0T	130 No Grate B 009 - 0T
130 No Grate A 010 - 0T	130 No Grate B 010 - 0T
130 No Grate A 012 - 0T	130 No Grate B 012 - 0T
130 No Grate A 014 - 0T	130 No Grate B 014 - 0T
130 No Grate A 016 - 0T	130 No Grate B 016 - 0T
130 No Grate A 018 - 0T	130 No Grate B 018 - 0T
130 No Grate A 020 - 0T	130 No Grate B 020 - 0T
130 No Grate A Plugged 006 - 0T	130 No Grate B Plugged 006 - 0T
130 No Grate A Plugged 007 - 0T	130 No Grate B Plugged 007 - 0T
130 No Grate A Plugged 008 - 0T	130 No Grate B Plugged 008 - 0T
130 No Grate A Plugged 009 - 0T	130 No Grate B Plugged 009 - 0T

INTERMEDIATE TESTS	
Filename	**Filename**
Flat Grate A 007-0	Flat Grate B 007-0
Flat Grate A 008-0	Flat Grate B 008-0
Flat Grate A 009-0	Flat Grate B 009-0
Flat Grate A 010-0	Flat Grate B 010-0
Flat Grate A 012-0	Flat Grate B 012-0
Flat Grate A 014-0	Flat Grate B 014-0
Flat Grate A 016-0	Flat Grate B 016-0
Flat Grate A 018-0	Flat Grate B 018-0
Flat Grate A 020-0	Flat Grate B 020-0
Flat Grate A Plugged 007-0	Flat Grate B Plugged 007-0
Flat Grate A Plugged 008-0	Flat Grate B Plugged 008-0
Flat Grate A Plugged 009-0	Flat Grate B Plugged 009-0
Flat Grate A Plugged 010-0	Flat Grate B Plugged 010-0
Flat Grate A Plugged 012-0	Flat Grate B Plugged 012-0
Flat Grate A Plugged 014-0	Flat Grate B Plugged 014-0
Flat Grate A Plugged 016-0	Flat Grate B Plugged 016-0
Flat Grate A Plugged 018-0	Flat Grate B Plugged 018-0
Flat Grate A Plugged 020-0	Flat Grate B Plugged 020-0
Filename	**Filename**
130 Grate A 007 - 0	130N Grate A 007 - 0
130 Grate A 008 - 0	130N Grate A 008- 0
130 Grate A 009 - 0	130N Grate A 009- 0
130 Grate A 010 - 0	130N Grate A 010 - 0
130 Grate A 012 - 0	130N Grate A 012 - 0
130 Grate A 014 - 0	130N Grate A 014 - 0
130 Grate A 016 - 0	130N Grate A 016 - 0
130 Grate A 018 - 0	130N Grate A 018 - 0
130 Grate A 020 - 0	130N Grate A 020 - 0
130 Grate A Plugged 007 - 0	130N Grate A Plugged 007 - 0
130 Grate A Plugged 008 - 0	130N Grate A Plugged 008- 0
130 Grate A Plugged 009 - 0	130N Grate A Plugged 009- 0
130 Grate A Plugged 010 - 0	130N Grate A Plugged 010 - 0
130 Grate A Plugged 012 - 0	130N Grate A Plugged 012 - 0
130 Grate A Plugged 014 - 0	130N Grate A Plugged 014 - 0
130 Grate A Plugged 016 - 0	130N Grate A Plugged 016 - 0
130 Grate A Trapped 018 - 0	130N Grate A Plugged 018 - 0
130 Grate A Trapped 020 - 0	130N Grate A Plugged 020 - 0

INTERMEDIATE TESTS	
Filename	**Filename**
130 Grate B 007 - 0	130N Grate B 007 - 0
130 Grate B 008 - 0	130N Grate B 008 - 0
130 Grate B 009 - 0	130N Grate B 009 - 0
130 Grate B 010 - 0	130N Grate B 010 - 0
130 Grate B 012 - 0	130N Grate B 012 - 0
130 Grate B 014 - 0	130N Grate B 014 - 0
130 Grate B 016 - 0	130N Grate B 016 - 0
130 Grate B 018 - 0	130N Grate B 018 - 0
130 Grate B 020 - 0	130N Grate B 020 - 0
130 Grate B Plugged 007 - 0	130N Grate B Plugged 007 - 0
130 Grate B Plugged 008 - 0	130N Grate B Plugged 008 - 0
130 Grate B Plugged 009 - 0	130N Grate B Plugged 009 - 0
130 Grate B Plugged 010 - 0	130N Grate B Plugged 010 - 0
130 Grate B Plugged 012 - 0	130N Grate B Plugged 012 - 0
130 Grate B Plugged 014 - 0	130N Grate B Plugged 014 - 0
130 Grate B Plugged 016 - 0	130N Grate B Plugged 016 - 0
130 Grate B Plugged 018 - 0	130N Grate B Plugged 018 - 0
130 Grate B Plugged 020 - 0	130N Grate B Plugged 020 - 0
Filename	**Filename**
100 Grate A 007 - 0	100 Grate B 007 - 0
100 Grate A 008 - 0	100 Grate B 008 - 0
100 Grate A 009 - 0	100 Grate B 009 - 0
100 Grate A 010 - 0	100 Grate B 010 - 0
100 Grate A 012 - 0	100 Grate B 012 - 0
100 Grate A 014 - 0	100 Grate B 014 - 0
100 Grate A 016 - 0	100 Grate B 016 - 0
100 Grate A 018 - 0	100 Grate B 018 - 0
100 Grate A 020 - 0	100 Grate B 020 - 0
100 Grate A Plugged 007 - 0	100 Grate B Plugged 007 - 0
100 Grate A Plugged 008 - 0	100 Grate B Plugged 008 - 0
100 Grate A Plugged 009 - 0	100 Grate B Plugged 009 - 0
100 Grate A Plugged 010 - 0	100 Grate B Plugged 010 - 0
100 Grate A Plugged 012 - 0	100 Grate B Plugged 012 - 0
100 Grate A Plugged 014 - 0	100 Grate B Plugged 014 - 0
100 Grate A Plugged 016 - 0	100 Grate B Plugged 016 - 0
100 Grate A Plugged 018 - 0	100 Grate B Plugged 018 - 0
100 Grate A Plugged 020 - 0	100 Grate B Plugged 020 - 0

INTERMEDIATE TESTS	
Filename	**Filename**
Flat No Grate A 007-0	Flat No Grate B 007-0
Flat No Grate A 008-0	Flat No Grate B 008-0
Flat No Grate A 009-0	Flat No Grate B 009-0
Flat No Grate A 010-0	Flat No Grate B 010-0
Flat No Grate A 012-0	Flat No Grate B 012-0
Flat No Grate A 014-0	Flat No Grate B 014-0
Flat No Grate A 016-0	Flat No Grate B 016-0
Flat No Grate A 018-0	Flat No Grate B 018-0
Flat No Grate A 020-0	Flat No Grate B 020-0
Flat No Grate A Plugged 007-0	Flat No Grate B Plugged 007-0
Flat No Grate A Plugged 008-0	Flat No Grate B Plugged 008-0
Flat No Grate A Plugged 009-0	Flat No Grate B Plugged 009-0
Flat No Grate A Plugged 010-0	Flat No Grate B Plugged 010-0
Flat No Grate A Plugged 012-0	Flat No Grate B Plugged 012-0
Flat No Grate A Plugged 014-0	Flat No Grate B Plugged 014-0
Flat No Grate A Plugged 016-0	Flat No Grate B Plugged 016-0
Flat No Grate A Plugged 018-0	Flat No Grate B Plugged 018-0
Flat No Grate A Plugged 020-0	Flat No Grate B Plugged 020-0
Filename	**Filename**
130 No grate A 007 - 0	130 No Grate B 007 - 0
130 No grate A 008 - 0	130 No Grate B 008 - 0
130 No grate A 009 - 0	130 No Grate B 009 - 0
130 No grate A 010 - 0	130 No Grate B 010 - 0
130 No grate A 012 - 0	130 No Grate B 012 - 0
130 No grate A 014 - 0	130 No Grate B 014 - 0
130 No grate A 016 - 0	130 No Grate B 016 - 0
130 No grate A 018 - 0	130 No Grate B 018 - 0
130 No Grate A 020 - 0	130 No Grate B 020 - 0
130 No Grate A Plugged 007 - 0	130 No Grate B Plugged 007 - 0
130 No Grate A Plugged 008 - 0	130 No Grate B Plugged 008 - 0
130 No Grate A Plugged 009 - 0	130 No Grate B Plugged 009 - 0
130 No Grate A Plugged 010 - 0	130 No Grate B Plugged 010 - 0
130 No Grate A Plugged 012 - 0	130 No Grate B Plugged 012 - 0
130 No Grate A Plugged 014 - 0	130 No Grate B Plugged 014 - 0
130 No Grate A Plugged 016 - 0	130 No Grate B Plugged 016 - 0
130 No Grate A Plugged 018 - 0	130 No Grate B Plugged 018 - 0
130 No Grate A Plugged 020 - 0	130 No Grate B Plugged 020 - 0

INTERMEDIATE TESTS	
Filename	**Filename**
100 No Grate A 007 - 0	100 No Grate B 007 - 0
100 No Grate A 008 - 0	100 No Grate B 008 - 0
100 No Grate A 009 - 0	100 No Grate B 009 - 0
100 No Grate A 010 - 0	100 No Grate B 010 - 0
100 No Grate A 012 - 0	100 No Grate B 012 - 0
100 No Grate A 014 - 0	100 No Grate B 014 - 0
100 No Grate A 016 - 0	100 No Grate B 016 - 0
100 No Grate A 018 - 0	100 No Grate B 018 - 0
100 No Grate A 020 - 0	100 No Grate B 020 - 0
100 No Grate A Plugged 007 - 0	100 No Grate B Plugged 007 - 0
100 No Grate A Plugged 008 - 0	100 No Grate B Plugged 008 - 0
100 No Grate A Plugged 009 - 0	100 No Grate B Plugged 009 - 0
100 No Grate A Plugged 010 - 0	100 No Grate B Plugged 010 - 0
100 No Grate A Plugged 012 - 0	100 No Grate B Plugged 012 - 0
100 No Grate A Plugged 014 - 0	100 No Grate B Plugged 014 - 0
100 No Grate A Plugged 016 - 0	100 No Grate B Plugged 016 - 0
100 No Grate A Plugged 018 - 0	100 No Grate B Plugged 018 - 0
100 No Grate A Plugged 020 - 0	100 No Grate B Plugged 020 - 0

Flat bed - Surcharged	
Filename	**Filename**
Flat Grate A 0-009	Flat Grate B 0-009
Flat Grate A 0-013	Flat Grate B 0-013
Flat Grate A 0-018	Flat Grate B 0-018
Filename	**Filename**
Flat Grate A 007-009	Flat Grate B 007-009
Flat Grate A 007-010	Flat Grate B 007-010
Flat Grate A 007-011	Flat Grate B 007-011
Flat Grate A 007-012	Flat Grate B 007-012
Flat Grate A 007-013	Flat Grate B 007-013
Flat Grate A 007-014	Flat Grate B 007-014
Flat Grate A 007-015	Flat Grate B 007-015
Flat Grate A 007-016	Flat Grate B 007-016
Flat Grate A 007-017	Flat Grate B 007-018
Filename	**Filename**
Flat Grate A 008-008	Flat Grate B 008-008
Flat Grate A 008-009	Flat Grate B 008-009
Flat Grate A 008-010	Flat Grate B 008-010
Flat Grate A 008-011	Flat Grate B 008-011
Flat Grate A 008-018	Flat Grate B 008-018
Flat Grate A 009-008	Flat Grate B 009-008
Flat Grate A 009-018	Flat Grate B 009-018
Flat Grate A 010-008	Flat Grate B 010-008

1/100 - Surcharged	
Filename	**Filename**
100 Grate A 0 - 009	100 Grate B 0 - 009
100 Grate A 0 - 013	100 Grate B 0 - 013
100 Grate A 0 - 018	100 Grate B 0 - 018

1/30 - Surcharged	
Filename	**Filename**
130 Grate A 0 - 009	130 Grate B 0 - 009
130 Grate A 0 - 009	130 Grate B 0 - 009
130 Grate A 0 - 013	130 Grate B 0 - 013
130 Grate A 0 - 013	130 Grate B 0 - 013
130 Grate A 0 - 018	130 Grate B 0 - 018
130 Grate A 0 - 018	130 Grate B 0 - 018